The impact of a single nucleotide polymorphism in *fusA1* on biofilm formation and virulence in *Pseudomonas aeruginosa*

Eve A Maunders

September 2018

University of Cambridge
Department of Biochemistry
King's College

This dissertation is submitted for the degree of
Doctor of Philosophy

The impact of a single nucleotide polymorphism in *fusA1* on biofilm formation and virulence in *Pseudomonas aeruginosa*

Eve A Maunders

Summary

Pseudomonas aeruginosa is an opportunistic human pathogen that is now the leading cause of morbidity and mortality in immunocompromised individuals. Those suffering with the genetic disease cystic fibrosis (CF) commonly encounter *P. aeruginosa* infections. *P. aeruginosa* infection can present itself as an acute infection, which is characterised by highly virulent, "free-swimming" bacteria, or as a chronic infection associated with the formation of surface-adhered bacterial communities known as biofilms. The labyrinth of interconnecting signalling networks has meant that the regulatory mechanisms behind biofilm formation and virulence are largely undefined.

In this dissertation, a single nucleotide polymorphism was identified within the gene, *fusA1,* encoding elongation factor G (EF-G). The mutation introduced minor structural changes to the protein which were likely to have functional repercussions in its involvement in protein synthesis. Phenotypic analysis revealed that the mutation conferred changes in both resistance and sensitivity to various antibiotics, as well as changes in motility, exoenzyme production, quorum sensing, metabolism, synthesis of biofilm-associated proteins and exopolysaccharide production. Most notably was the up-regulation of a major virulence determinant, the type three secretion system, typically characteristic of cells comprising an acute infection. Proteomic and transcriptomic profiling of the mutant strain provided an insight into the genetic basis behind these phenotypes, identifying the up-regulation of multidrug efflux systems and modulations to the chemotactic systems. This study also found links between several biological processes that were modulated in the mutant strain, such as crosstalk between sulfur metabolism, iron uptake and the oxidative stress response.

In summary, the work presented in this dissertation highlights the susceptibility of *fusA1* to spontaneous mutation and identifies a novel role for EF-G in bacterial virulence and antibiotic sensitivity, both of which have worrying implications for infection within the CF lung.

Declaration

This dissertation is the result of my own work and includes nothing which is the outcome of work done in collaboration, except as declared in the Preface and specified in the text.

This work has not been submitted for any other degree or qualification at the University of Cambridge or any other University or similar institution. Parts of the work presented in the Introduction chapter of this dissertation have been adapted from a previously published minireview in FEMs Letters; 'Matrix exopolysaccharides; the sticky side of biofilm formation' by E Maunders and M Welch, 2017. This minireview was authored by myself and edited by my supervisor, Dr Martin Welch.

The length of this thesis does not exceed the prescribed word limit stated by the Biology Degree Committee. The work presented in this thesis was conducted under the supervision of Dr Martin Welch at the University of Cambridge, department of Biochemistry between October 2014 and June 2018.

Eve Maunders

Date 4th September 2018

Acknowledgements

A great number of individuals have been pivotal in the progress of my PhD, for which I am extremely grateful. First and foremost, I would like to express my thanks to Dr Martin Welch for his guidance throughout my project and for his endless positivity with each mutagenesis screen. I would like to thank Dr Rita Monson for her advice and her assistance with whole-genome sequencing. Thanks to the MRC for funding this PhD, without whom this thesis would not have been possible, and to King's College and the Cambridge Philosophical society for additional grants throughout my project.

I was extremely lucky to have been surrounded by a great team, making every day entertaining, and so my deepest thanks goes to all the members of the Welch group, past and present. In particular, Emem Ukor-Keefer and Audrey Crousilles, who have come full circle with me, and to Alyssa McVey, Yassmin Abdelhamid, Larry Clarkson, Rory Triniman, Andre Wijaya, Sean Bartlett, Xavier Chee, Suzie Forrest, Stephen Trigg and Tom O'Brien, for all the fun and foolishness. Special thanks to my RNA-saviour, Stephen Dolan, for his advice, insight and for keeping the team alert, good stuff!

For my sanity, I would like to express my relentless gratitude to a wonderful cretin, Katerina Geladaki, and to Dori Szigeti and Heather Wilson, for always placing a smile on my face and a beer in my hand. And finally, I would like to thank my parents for all their support, proofreading, interest and for being a constant source of encouragement (despite all of my apparent stubbornness).

Contents

Chapter 1: Introduction

Chapter 2: Materials and methods

Chapter 3: Identification of a *fusA1* mutation

Chapter 4: Proteomic analysis of FUS443

Chapter 5: Transcriptomic analysis of FUS443

List of Figures

Chapter 1

Chapter 3

Chapter 4

Chapter 5

List of Tables

Chapter 2

Chapter 3

Chapter 4

Chapter 5

Abbreviations

ATP	Adenosine triphosphate
BHL	N-butanoyl-L-homoserine lactone
bp	Base pairs
cAMP	3'-5'-cyclic adenosine monophosphate
Cb^r	Carbenicillin resistance cassette
c-di-GMP	Cyclic di-guanylate
cDNA	complementary DNA
CF	Cystic fibrosis
CFTR	Cystic fibrosis transmembrane conductance regulator
CFU	Colony forming unit
DAPA	2,6-diaminopimelic acid
DGC	Diguanylate cyclase
dH_20	Deionised water
DMSO	Dimethyl sulfoxide
DNA	Deoxynucleic acid
dNTP	Dinucleotide triphosphate
eDNA	Extracellular DNA
EDTA	Ethylenedinitrilo tetra-acetic acid
EF-G	Elongation factor G
FC	Fold change
FPKM	Fragments per kilobase, per million
FRT	Flp-recombinase target sites
gDNA	Genomic DNA
Gm^r	Gentamicin resistance cassette
GTP	Guanosine triphosphate
HSP	Heat shock protein
ICD	Isocitrate dehydrogenase
IS	Iron starvation
kb	Kilobase pairs
kDa	Kilodaltons
Km^r	Kanamycin resistance cassette
LB	Luria broth
LCFA	Long chain fatty acids
LC-MS/MS	Liquid chromatography couple with tandem mass spectrometry
Mbp	Million base pairs
MCS	Muliple cloning site
MDR	Multi-drug resistance
MIC	Minimal inhibitory concentration
NAD	Nicotinamide adenine dinucleotide
NADH	Reduced nicotinamide adenine dinucleotide
NCBI	National Centre for Biotechnology Information
OD	Optical density
OdDHL	N-3-(oxododecanoyl)-L-homoserine lactone
ORF	Open reading frame
PBS	Phosphate buffered saline
PCA	Principal component analysis

P*cdrA*	*cdrA* gene promoter
PCH	Pyochelin
PCR	Polymerase chain reaction
PDE	Diguanylate phosphatase
PQS	Pseudomonas quinolone signal
PVD	Pyoverdine
PVDF	Polyvinylidene fluoride
QS	Quorum sensing
RNA	Ribonucleic acid
ROS	Reactive oxygen species
rpm	Revolutions per minute
rRNA	Ribosomal RNA
SD	Shine-Dalgarno
SDS	Sodium dodecyl sulfate
SDS-PAGE	Sodium dodecyl sulfate polyacrylamide gel electrophoresis
SNP	Single nucleotide polymorphism
T1SS	Type I secretion system
T2SS	Type II secretion system
T3SS	Type III secretion system
T4P	Type IV pili
T6SS	Type VI secretion system
TAE	Tris-acetate EDTA
TCA	Tricarboxylic acid cycle
TEMED	N,N,N',N'-tetramethyl-ethane-1,2-diamine
Trp	Tryptophan
UTR	Untranslated region
v/v	Volume/volume
w/v	Weight/volume
WT	Wild type
X-gal	5-bromo-4-chloro-3 indolyl-B-D-galactopyranoside
λ max	Maximum emission wavelength

Chapter 1

1. Introduction

1.1 *Pseudomonas aeruginosa*

1.1.1 General characteristics

Pseudomonas aeruginosa is a Gram-negative, rod shaped bacterium that can be found ubiquitously within the environment. The name '*aeruginosa*' was coined from the Latin word, *aerūgō*, meaning "copper rust", and refers to its characteristic blue-green colouration (Brown, 1954). Typically, *P. aeruginosa* lives as a relatively harmless microorganism, inhabiting a wide variety of environments, from plants, soil and aquatic areas, to living on nematodes and animals. It is not uncommon for *P. aeruginosa* to inhabit healthy human individuals; however, in these cases the *Pseudomonas* population would be largely outnumbered by other microbial flora. In the case of immunocompromised individuals or patients receiving immunosuppressive drugs, *P. aeruginosa* embodies an opportunistic human pathogen and takes advantage of the subdued immune response. Should the body be unable to clear an infection, it can become severe enough to result in the death of the patient. *P. aeruginosa* is particularly dreaded amongst the clinical community due to its ability to grow on medical equipment such as catheters, stents and ventilators, and has even been isolated from soaps and hydrotherapy pools. This creates a high risk of transmission between patients and has afforded *P. aeruginosa* the dubious accolade of being one of the most common nosocomial infective pathogens (Lister *et al.*, 2009; Pereira *et al.*, 2014).

1.1.2 Infection

The ability of *P. aeruginosa* to adapt and persist in a wide variety of environments can be attributed to its large genome, consisting of 6.3 Mbp and 5,570 predicted open reading frames (ORFs) (Stover *et al.*, 2000). Having one of the largest and most complex bacterial genomes allows this organism to have a flexible metabolism and simple nutritional requirements. For this reason, *P. aeruginosa* can colonise numerous areas of

the body and is often isolated from burn wounds, and the respiratory, gastrointestinal and urinary tracts.

In acute burn wounds the protective layers of the skin are destroyed and the immune system is suppressed, making the exposed tissue open to colonisation. *P. aeruginosa* proliferates within the damaged tissue and, in some severe infections, the bacteria can spread into the circulatory system causing bacteraemia and septic shock (Liu *et al.*, 2014). *P. aeruginosa* is also implicated in the development of swimmers ear, a bacterial infection of the external ear canal, causing inflammation and temporarily hearing impairment (Reid *et al.*, 1981). As well as this, for individuals who wear contact lenses, *P. aeruginosa* is the most common cause of corneal infection and the development of sight-threatening corneal ulcers. This is due to its ability to survive on the lens, within storage solution and thrives within the ocular environment (Stapleton *et al.*, 2012). However, most notably, *P. aeruginosa* is currently the leading cause of morbidity and mortality in immunocompromised patients with, for example, ventilator-associated pneumonia or cystic fibrosis (CF). This is because it causes irreversible damage to the lung tissue, reducing lung function and leading to accelerated lung failure (McCarthy *et al.*, 2014; Raineri *et al.*, 2014).

1.1.3 Resistance and treatment

The 20th century became the golden age for medical advancement and antibiotic discovery. However, almost no new antibiotics have been identified in the last 30 years and infections that were once easily treated are once again becoming a serious threat to modern healthcare. Over-prescribing and the use of antibiotics in the farming industry have led to a surge in antimicrobial resistance. In hospitals, the intense selection pressures, and availability of susceptible patients, provides the perfect environment for cultivating antimicrobial resistant 'super-bugs'. When combined with the large growth in the immunocompromised population, that has occurred in the last decade, resistance is progressively becoming a huge health and economic burden (Lister *et al.*, 2009; Taylor *et al.*, 2014).

Amongst the growing number of antibiotic resistant bacteria, the World Health Organisation ranked *P. aeruginosa* the number two priority pathogen for which new

antibiotics are urgently needed, only out-matched by the carbapenem-resistant, *Acinetobacter baumannii* (Kahlmeter *et al.*, 2017). Treatment options for *P. aeruginosa* infection are therefore limited as not only is antibiotic treatment often ineffective but it can worsen the condition by killing off competing microorganisms and allowing the population of *P. aeruginosa* to expand.

Antibiotic resistance can spread amongst bacterial populations on mobile genetic elements or can occur through the spontaneous mutation of genes encoding resistance mechanisms. *P. aeruginosa* already confers a high level of intrinsic resistance due to the production of antibiotic inactivating enzymes that target a diverse range of antibiotics and reduce their effectivity. Inactivation of aminoglycosides, for example, involves chemical modification of the drug by either phosphorylation, acetylation or adenylation. This means that numerous modifying enzymes, encoded by *P. aeruginosa*, are effective at rendering a single antibiotic useless and consequently result in high levels of resistance to that drug (Poole, 2005).

In addition to modifying enzymes, *P. aeruginosa* encodes several multi-drug resistance (MDR) efflux pumps which reduce susceptibility to antibiotics by translocating drugs out of the cell. Not only do efflux pumps export antibiotics, but they also remove toxic substances, metabolites and quorum sensing molecules to assist environmental adaptation and communication between bacteria. Four efflux systems have been studied extensively in *P. aeruginosa*; MexAB-OprM, MexCD-OprJ, MexEF-OprN and MexXY-OprM (Soto, 2013). These are composed of a proton motive force-driven antiporter pump (MexB, D, F and Y), which lies within the cytoplasmic membrane, a gated outer membrane channel (OprM, J and N) and a linker lipoprotein (MexA, C, E and X) (Livermore, 2002). The first pump to be identified was the MexAB-OprM efflux pump, which remains to be one of the most highly expressed efflux systems. This pump also has the broadest range of antimicrobial targets, including fluoroquinolones, tetracyclines, chloramphenicols and β-lactams. The other efflux systems have a narrower range of substrates but can be equally important in antibiotic resistance, particularly during infection when a number of these systems exhibit increased activity (Aeschlimann, 2003, Terzi, Kulah and Ciftci, 2014).

1.2 Biofilms

1.2.1 Life cycle and formation

P. aeruginosa is one of the most highly studied and clinically-significant organisms in relation to biofilm formation (Müsken *et al.*, 2010). Biofilms are surface-associated bacterial communities embedded within a self-made, extracellular polymeric matrix. These communities exhibit increased antibiotic resistance, increased immune evasion, and can prove to be extremely persistent during antimicrobial treatment (Alhede *et al.*, 2009).

A number of technological advances have catalysed insight into the development of bacterial biofilms. In particular, the development of flow cell biofilm chambers, which can be monitored using laser scanning confocal microscopy, has revealed the temporal changes which accompany biofilm formation *in vitro*. These studies have revealed that biofilm formation follows a sequential process of attachment, growth, maturation and dispersal, and high-throughput screening has aided in the discovery of many of the fundamental genetic factors required for biofilm formation. Moreover, details of the physical and chemical communication systems and "social interactions" within the biofilm are now being unearthed (Klausen *et al.*, 2003; Müsken *et al.*, 2010).

The transition from 'free-swimming' planktonic growth to biofilm formation involves several distinct steps. In 1998, O'Toole and Kolter published the first global genetic screen aimed at identifying *P. aeruginosa* mutants that are defective in biofilm formation; an approach that highlighted the importance of Surface Attachment Defective (*sad*) genes. Several *sad* genes are required for flagellar synthesis, and the functional disruption of these genes blocks biofilm formation at a very early stage; surface attachment. This is because the flagellum is involved in overcoming surface repulsion at the liquid-surface interface, thereby enabling temporary surface attachment during the first stage of biofilm formation. Temporary surface attachment is followed by exploration of the surrounding surface via type IV pili (T4P)-dependent twitching motility (Müsken *et al.*, 2010). This way, the surface associated bacteria come together to form microcolonies (Figure 1.1).

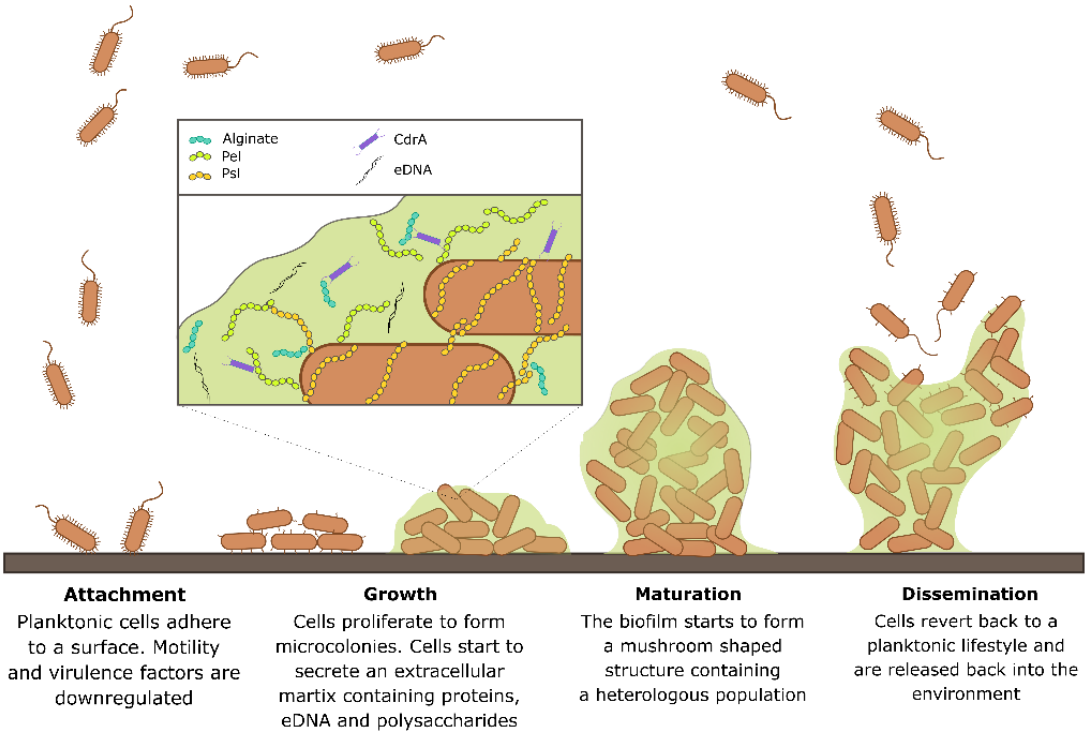

Figure 1.1. Biofilm formation begins when highly motile planktonic cells adhere to a surface. The cells undergo physical changes that involve down-regulation of motility apparatus and virulence factors whilst up regulating the production of an exopolysaccharide-rich extracellular matrix. The community matures into mushroom-shaped structures. In response to inducing conditions, cells become motile once again and disseminate to colonise new ecological niches.

Microcolony formation is accompanied by a reduction in motility and virulence gene expression (Klausen *et al.*, 2003). Concomitant with this, the microcolonies grow in size to form larger cellular aggregates (Landry *et al.*, 2006) and secrete large volumes of characteristic extracellular matrix. The majority of the matrix is made from a viscous mixture of extracellular polysaccharides, principally Psl, Pel and alginate. Proteins such as CdrA act as 'spars' between matrix components, adding strength to the structural scaffold, and extracellular DNA (eDNA) is present in the matrix, providing further structural rigidity. In continuous flow biofilms, the colonies eventually develop into protruding mushroom-shaped structures. However, when conditions require it, the cells on the periphery of the structure are capable of reverting to a planktonic phenotype where they begin to produce enzymes which cleave the matrix components, thereby

allowing cells to disseminate into the surrounding environment and colonise new niches (O'Toole *et al.*, 1998; Fazli *et al.*, 2014).

1.2.2 The extracellular matrix

1.2.2.1 Exopolysaccharides

Of the three exopolysaccharides (Psl, Pel and alginate) secreted by *P. aeruginosa*, alginate is responsible for the mucoid phenotype which is essentially pathognomic of CF. Alginate is a capsule-like exopolysaccharide composed of α-D-mannuronic acid and glucuronic acid, producing a negatively charged copolymer (Pulcrano *et al.*, 2012). In contrast, Psl and Pel polysaccharides monopolise the matrix in non-mucoid strains, such as environmental and domestic laboratory strains. Pel is a glucose-rich polysaccharide with a particular role in pellicle formation; a 'floating biofilm' which forms at a liquid-air interface. A pellicle provides the colony access to high concentrations of oxygen and nutrients, and can be seen on the surface of standing cultures (Friedman and Kolter, 2004a). The second non-mucoid polysaccharide, Psl, forms fibrous structures around *P. aeruginosa* cells creating a mesh-like scaffold to which neighbouring cells can bind (Wang *et al.*, 2015). Overexpressing Psl results in cell aggregation when grown in liquid culture, demonstrating its role in cell-cell interactions, and causes increased adhesion of cells to microtitre wells during *in vivo* biofilm plate assays verifying its role in cell-surface interactions (Ma *et al.*, 2006; Borlee *et al.*, 2010). Together, the secreted exopolysaccharides play a range of roles in the matrix, by providing structure, protection and adhesion.

1.2.2.2 CdrA

The protein CdrA was first identified through a screen for genes transcriptionally induced by c-di-GMP. Here, its function as a protein component of the biofilm matrix was determined and it was predicted to be a rod-shaped adhesin that acts as a stabilising crossbar between matrix components to increase the structural integrity of the biofilm. *CdrA* is found within a two gene operon with *cdrB*, forming a two-partner secretion

system, consisting of a secreted adhesin (CdrA) and its transporter (CdrB). The over-expression of *cdrA* leads to cell aggregation in liquid culture, which has been attributed to CdrA binding to Psl exopolysaccharides. *CdrA* mutants form weak biofilms in which Psl is no longer tightly associated with the cells, suggesting that CdrA cross-links Psl polysaccharides or tethers Psl to cell membranes. In doing so, this increases the stability of the matrix and promotes cell aggregation and microcolony formation. Strains defective in Psl synthesis also exhibit reduced cell-associated CdrA levels and therefore produce less robust biofilms (Borlee *et al.*, 2010).

1.2.3 Antibiotic resistance and targeting biofilms

Biofilm cells are linked to enhanced antimicrobial defences, including the restriction of drug uptake, increasing efflux pump activity, altering drug targets, or directly inactivating the drug. This is thought to be due to changes in gene expression, as cells move from planktonic growth into biofilm development (Lambert, 2002; Breidenstein *et al.*, 2011; Liao *et al.*, 2012). The biofilm is also composed of a heterologous population, exhibiting mutational changes and variations in transcriptional activity. For example, subpopulations will often display differential tolerance levels to antimicrobial compounds, which makes finding an antibiotic treatment that is effective on the whole biofilm extremely difficult (L. Yang *et al.*, 2007).

The tight colony structure of the biofilm also contributes to antimicrobial resistance forming a diffusion barrier so that only cells within the surface layers are exposed to lethal concentrations of the drug. Within the surface layers, antimicrobials can be consumed or deactivated to prevent their toxic effects disturbing the rest of the microcolony (Mulcahy *et al.*, 2014; Baker *et al.*, 2015). Studies have suggested that the exopolysaccharides play an important role in this process, as they act as a protective capsule that effectively delays the penetration of antimicrobial agents. Through a similar mechanism, they assist in the evasion of the host immune system by reducing the penetration of antibodies, reducing macrophage induced phagocytosis and limiting the migration of neutrophils (Horsman *et al.*, 2012). Therefore, it is becoming of increasing interest to directly target components of the biofilm matrix. Disrupting biofilm formation, using polysaccharide lyases and digestive enzymes, leaves the bacteria vulnerable to

antimicrobials and can improve the effectiveness of antibiotic treatment. Preventative methods could also involve targeting adhesins to inhibit initial cell attachment and arrest the establishment of a biofilm (Wei *et al.*, 2013).

1.2.4 Regulation of biofilm formation

Biofilm formation is a highly regulated process which is finely tuned by a cascade of signals and interconnecting regulatory networks. The composition of the extracellular environment is most likely to be the initial catalyst for the progression of planktonic cells into a biofilm lifestyle (O'Toole and Kolter, 1998), although many of the downstream effectors remain elusive and, in most instances, the environmental cues are also unknown (Mulcahy *et al.*, 2011).

Bis-(3'-5')-cyclic dimeric guanosine monophosphate (c-di-GMP) is a signalling molecule produced by bacteria to control a whole consort of biological processes. At high intracellular concentrations, c-di-GMP is the key regulator in activating biofilm growth. Intracellular pools of c-di-GMP are modulated by diguanylate cyclases (DGC), which synthesise the molecule, and c-di-GMP phosphodiesterases (PDE), which catabolise it. However, it is very difficult to predict effectors of c-di-GMP, and the signalling molecule affects a very diverse range of proteins (Römling *et al.*, 2013). One such group of proteins are those involved in flagellar motility, which become down-regulated by c-di-GMP, thereby forcing the bacteria into a sessile mode of growth. Concomitant with this, the production of matrix components, including exopolysaccharides, adhesive pili, eDNA and adhesins, become up-regulated by increased c-di-GMP levels (Römling, Galperin and Gomelsky, 2013).

Whilst c-di-GMP has been recognised as the main regulator of the biofilm lifestyle, several other pathways impact its development, including the Gac/Rsm pathway which is vital in balancing the expression of biofilm-associated genes with planktonic-associated genes. In a similar manner, quorum sensing (QS) plays a role in the expression of exopolysaccharides, eDNA and the biosynthesis of rhamnolipids, a glycolipid biosurfactant which helps maintain the channelling systems that run throughout the biofilm (Davey *et al.*, 2003; Sakuragi *et al.*, 2007).

1.3 *P. aeruginosa* and cystic fibrosis

1.3.1 Cystic fibrosis

CF is the most prevalent lethal autosomal recessive disorder amongst the Caucasian population (McCarthy *et al.*, 2014), and is caused by mutations in the cystic fibrosis transmembrane conductance regulator, *CFTR*, gene, which encodes a chloride channel. CFTR is essential for maintaining periciliary liquid volume and efficient mucociliary clearance within the lung. As a result, *CFTR* mutation causes mucus to accumulate in the airways and inhaled microbes are not cleared effectively, leading to recurrent infection by pathogens. It is this recurrent infection which aggravates the airways causing chronic inflammation and damage to the lung tissue. The lungs become severely scarred as a result and eventually, function can only be recovered through radical procedures such as transplantation. Loss of lung function due to bacterial infection is therefore one of the most significant causes of deterioration in CF patients (Ratjen *et al.*, 2003; McCarthy *et al.*, 2014; Trinh *et al.*, 2015).

1.3.2 The CF lung

The CF lung provides an idyllic environment for colonising bacteria as the thick mucus layer provides a protective and nutritious home for microbial communities. This abnormally high accumulation of mucus occurs from hyper-reabsorption of water in the lung due to the faulty chloride channel, CFTR (Maiuri *et al.*, 2017). The CFTR channel is also involved in bicarbonate secretion which interacts with mucins and affects their composition. In the CF lung, dysfunctional CFTR channels reduce bicarbonate secretion, causing the mucins to become thick and dense. This is due to bicarbonate-free mucins adhering very strongly to the surface of the airways which prevents clearance of the mucus and any trapped particles. Because of this, pathogens can survive in the airways without risk of mucociliary clearance. The reduction in bicarbonate also causes the liquid of the CF lung to be more acidic than in non-CF patients. A low pH deactivates many antimicrobial peptides and therefore reduces the effectiveness of bacterial killing during treatment (Cantin *et al.*, 2015).

Embedded within the mucus layer are a variety of inflammatory substances, including polymorphonuclear leukocytes, dead host cells, serum, and bacterial products from the thriving microbial population. It is this complex mix, collectively known as sputum, that is the main nutritional resource supporting the diverse range of microbes in the lung (Turner *et al.*, 2015).

Counter-intuitively, the CF lung is in fact an oxygen-limited environment. *P. aeruginosa* is well adapted to a micro-aerobic lifestyle and thrives under these conditions (Ratjen and Döring, 2003). The accumulation of mucus in the CF lung reduces the transfer of oxygen from the lungs into the bloodstream and can result in stabilisation of the hypoxia inducible factor-1, a transcription factor that promotes inflammation. Whilst the inflammatory response can help to clear out bacteria, having an active immune system is not always beneficial; polymorphonuclear leukocytes recruited to infection sites secrete proteases which can cleave immune receptors, such as T-cell receptors, and host extracellular matrix, impeding bacterial cell recognition and damaging the surrounding host tissue (Cantin *et al.*, 2015). Because of this, even the presence of sessile and low virulent biofilms have extremely damaging effects on the lung.

1.3.3 Progression of a CF infection

Alongside *P. aeruginosa*, the CF airways are colonised by a variety of other microorganisms, such as *Staphylococcus aureus* and *Haemophilus influenzae* (Figure 1.2). Colonisation of the lung occurs during infancy but the abundances of each microorganism fluctuates throughout the individual's lifetime. The increased prevalence of *P. aeruginosa* in the lung coincided with the introduction of CF specialised centres in the 1960s, leading to an increase in the level of patient to patient transmission. Nowadays, contact between CF patients is minimised but still, by the age of 20, *P. aeruginosa* commonly dominates the microbial community of the lung and often remains with the patient for the rest of their life (Langton Hewer *et al.*, 1996; Lyczak *et al.*, 2002).

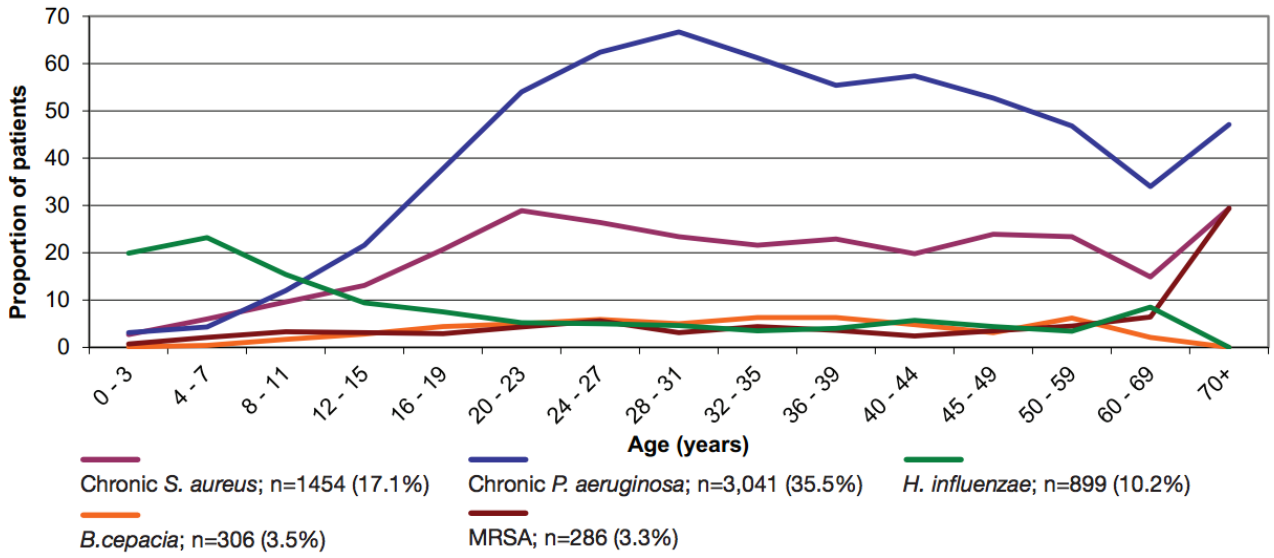

Figure 1.2. Prevalence of respiratory organisms in CF patients throughout their life (taken from the UK Cystic Fibrosis Registry annual data report 2012 (Owen and Bilton, 2013)).

There are distinct structural abnormalities of the CF lung that are present at birth which can affect lung function, but at this early stage there is minimal inflammation. It is only after accumulating a high titre of bacteria in the lungs that the immune system is activated, and begins to cause damage to the host tissue (Cantin *et al.*, 2015, Alhede *et al.*, 2009). During infection, *P. aeruginosa* grows to high densities of 10^7-10^9 colony forming units (CFU)/mL in the CF lung, more than enough to activate the host immune response (Turner *et al.*, 2015). In principle, these infections can be divided into two broad types; acute infections, which are associated with highly-virulent planktonic cells, that are extremely invasive and cause substantial tissue damage, and chronic infections, which are commonly-associated with biofilm formation (Alhede *et al.*, 2009). Infection exacerbates the CF respiratory condition and causes a relapsing cycle of infection, inflammation and airway obstruction. This cycle produces prolonged tissue damage and scarring, leading to progressive lung failure (Høiby *et al.*, 2010; Mulcahy *et al.*, 2014).

1.3.4 From acute infection to chronic infection

P. aeruginosa initially infect the CF airways as planktonic cells, where being highly motile and equipped with multiple toxin secretion systems, enables the pathogen to overcome host defences and bacterial competition. This stage is often associated with acute infection due to the considerable level of damage caused by the high activity of virulence factors and pathogenicity (Bhagirath *et al.*, 2016). One such virulence factor, is the type three secretion system (T3SS), which injects multiple exotoxins into host cells, resulting in cytotoxicity. During respiratory infection, strains expressing the T3SS have been found to cause up to six-fold higher mortality (Anantharajah *et al.*, 2016).

Acute infection causes rapid decline in lung function, but *P. aeruginosa* can go on to establish a chronic infection through the formation of biofilms on the lung epithelium. With chronic infection comes pulmonary exacerbations; worsening of CF symptoms, including increased sputum, coughing, weight loss and adventitious sounds during examination of the lung (Smyth *et al.*, 2008). So far it remains unclear exactly what triggers the transition from a planktonic lifestyle to biofilm growth. The lung presents a distinctly different environment to that outside of the body and bacteria need to overcome the nutrient- and oxygen-limitation, oxidative stresses and host immune defences. These challenges may be the first cues to influence gene expression and activate biofilm formation. (McCarthy *et al.*, 2014).

1.3.4 Treatment of CF infections

CF treatment and survival rates have improved in recent years, however, over 80% of patients still die from pulmonary obstruction, microbial lung infection and lung tissue damage resulting in lung failure (Milla *et al.*, 2014). Current treatment regimes involve aggressive use of high dose antibiotics and combination therapy which helps improve lung function and survival of the patient. Diversity within the *P. aeruginosa* population creates a reservoir of antibiotic-resistant mutants, so although treatment often temporarily improves lung function, it is rarely effective in eradicating chronic infections (Mowat *et al.*, 2011; Milla *et al.*, 2014). Furthermore, treatment can be a long and repetitive process, and can potentially worsen the condition by selecting for resistant

cells that develop throughout the course of treatment. These resistant cells readily recolonise the CF airways following treatment and leads to recurrent infection, which drastically extends the length of patient hospitalisation (J. K. Miller *et al.*, 2014). In addition to antibiotics, anti-inflammatory drugs can be used to slow host-inflicted lung damage and the rate of decline in lung function (Cantin *et al.*, 2015).

1.4 Virulence

1.4.1 Virulence determinants

Bacterial virulence is vital for the survival of pathogenic bacteria and transmission of infectious diseases. Virulence genes control motility, cytotoxicity and the production of virulence factors (Breidenstein *et al.*, 2011). Virulence in *P. aeruginosa* is at its highest during planktonic growth to assist invasion and help establish an acute infection in new host tissue. Many mechanisms in the cell contribute to bacterial virulence, such as motility apparatus in the form of flagella and T4P which are thought to play a role in adhesion and movement across the lung substratum. Similarly, lectins enhance adhesion to epithelial cells and also reduce ciliary function in the respiratory tract (Khalifa *et al.*, 2011; Grishin *et al.*, 2015).

Numerous virulence factors are secreted into the extracellular environment, such as elastases which have high proteolytic activity, allowing for the deactivation of antibodies and cytokines, and degradation of elastin found within the pulmonary epithelium (Kida *et al.*, 2008; Khalifa *et al.*, 2011). Pyocyanin, a blue pigment contributing to *P. aeruginosa*'s colouration, is also secreted and contributes to oxidative stress in the host cells, disrupts calcium homeostasis, and inhibits cell respiration and growth (Lau *et al.*, 2004). Alkaline protease is secreted by the T1SS and degrades complement components of the immune system, as well as cytokines and chemokines, preventing phagocytosis (Kida *et al.*, 2008). Whilst exotoxin A, is a toxin secreted by the T2SS which inhibits protein synthesis to induce cell death in neighbouring host cells. Other virulence factors associated with acute infection include, lipopolysaccharides, which help to protect against serum-induced lysis, and rhamnolipids, which are extracellular glycoproteins that disrupt mucociliary transport, inhibit phagocytosis and are involved in motility and

biofilm formation (Khalifa *et al.*, 2011). Finally, the T3SS is a major virulence factor that allows bacteria to inject toxins directly into neighbouring host cells and induce cell death by necrosis (Khalifa *et al.*, 2011).

Once the bacteria have become established, acute virulence factors are down-regulated and the infection progresses to a chronic stage. During the chronic stage of growth, the bacteria develop immune-evasive strategies, promote the expression of antibiotic resistance mechanisms and form protected biofilm communities. Virulence determinants that are associated with chronic growth include the production of siderophores for iron acquisition and the secretion of a polysaccharide-rich matrix (Khalifa *et al.*, 2011; Balasubramanian *et al.*, 2013).

1.4.2 Quorum sensing

QS plays a central role in the regulation of virulence. It is a density-dependent bacterial communication system that regulates gene expression in response to critical thresholds of signalling molecules. These signals are small diffusible molecules that are secreted into the environment and are taken up by neighbouring cells where they bind to their cognate receptors. As the bacterial population grows, the concentration of accumulated QS signal molecules exceed a critical threshold and trigger the coordinated expression of a wide range of genes, most notably virulence-associated genes (Arevalo-Ferro *et al.*, 2003; Davenport *et al.*, 2015). Paradoxically, QS also enhances biofilm formation. The mechanism by which this occurs is not known but it is postulated to work through the up-regulation of the *psl* operon (Diggle *et al.*, 2003; Irie *et al.*, 2010).

P. aeruginosa utilises four QS systems, the N-acyl-homoserine lactone based systems (*las* and *rhl*), the alkyquinolone system (*pqs*), and the recently-identified integrated quorum sensing system (IQS) which responds to phosphate limitation (Jones *et al.*, 1993; Ochsner *et al.*, 1995; Kirisits *et al.*, 2006; Lee *et al.*, 2013). These interlink in a hierarchical manner with the *rhl* and *pqs* systems under the control of the *las* system (Figure 1.3) (Lee *et al.*, 2015). The *las* pathway leads to the production of OdDHL, which complexes with the LasR receptor. This complex then multimerises to induce transcription of *lasI*, encoding the OdDHL synthase, and the *rhl* and *pqs* systems. The *rhl* system induces the production of N-butanoyl-L-homoserine lactone (BHL) which goes on

to bind RhlR and activates transcription of the BHL synthase encoding gene, *rhlI*. LasR-OdDHL also upregulates *pqsR* expression, which in turn, upregulates the *Pseudomonas* quinolone signal (PQS) biosynthesis genes, *pqsABCD* and *pqsH*. PQS feeds back by promoting transcription of *rhlI*, whereas RhlR-BHL inhibits the *pqs* system. The IQS system is not as defined as the other pathways but IQS is thought to be a byproduct from the biosynthesis of the siderophore pyochelin, and its corresponding receptor has yet to be identified (Ye *et al.*, 2014; Sun *et al.*, 2016).

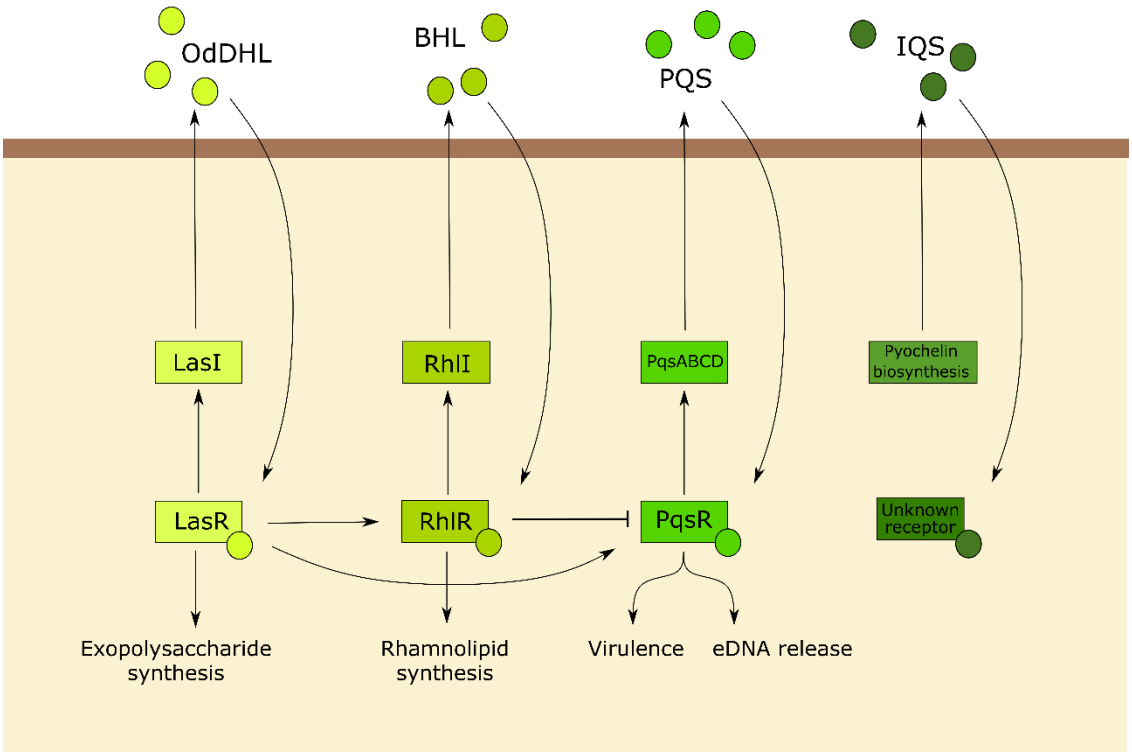

Figure 1.3. The intertwined quorum sensing systems of *P. aeruginosa* which regulate gene expression *via* autoinducer synthases, receptor proteins and feedback regulation.

Numerous environmental factors affect the activity of the QS network, for example, phosphate or iron depletion sees a rise in *pqs* and *rhl* activity (Bains *et al.*, 2012; Lee *et al.*, 2015), oxygen limitation is linked to the *las* system (Kim *et al.*, 2005), and nutrient starvation sees a spike in BHL synthesis (Baysse *et al.*, 2005). Using QS to respond to a diverse range of environmental stimuli allows *P. aeruginosa* to quickly

respond and adapt to changes in its surroundings. The *las* system controls the expression of various proteases, such as elastase, LasA protease and alkaline protease, as well as the T2SS effector protein, exotoxin A (Nouwens *et al.*, 2003). The *rhl* system was named after its regulation of rhamnolipid production but is also required for regulation of elastase and LasA protease, along with the production of hydrogen cyanide, siderophores, lectin, and the pigmented virulence factor pyocyanin (Diggle *et al.*, 2003; Chen *et al.*, 2004). The *pqs* system regulates elastase and pyocyanin production but is also linked to iron chelation and pro-oxidant activities (Reen *et al.*, 2011). QS, in particular the *rhl* system, negatively regulates T3S without affecting the T3S master regulatory genes, *exsCEBAD* (Bleves *et al.*, 2005; Yahr *et al.*, 2006).

1.4.3 The type III secretion system

In *P. aeruginosa*, the T3SS creates a direct link between the bacterial and host cytoplasm through which four effector proteins are translocated. These effector proteins generate pathogenic effects by disrupting the host cell cytoskeleton to promote apoptosis or by disrupting signalling cascades to inhibit phagocytosis (Yahr *et al.*, 2006; Chung *et al.*, 2013; Banerjee *et al.*, 2014)

The T3SS is encoded by over 40 genes, across 5 operons, which constitute the translocation apparatus, regulatory proteins, chaperones and effector proteins (Figure 1.4) (Brutinel *et al.*, 2010). The syringe-like machinery is an evolutionary development from the bacterial flagellum. The needle complex of the T3SS is a hollow structure that spans both bacterial membranes and the peptidoglycan layer, transporting effector proteins from the cytosol to the translocation apparatus at the tip of the needle. The translocation apparatus comprises a translocation pore, formed by PopB and PopD, and a secreted protein, PcrV, which is important in pore assembly. PopB/D interact with the host cell membrane to deliver the effector proteins into the host cytosol (Hauser, 2009; Izoré *et al.*, 2011; Anantharajah *et al.*, 2016).

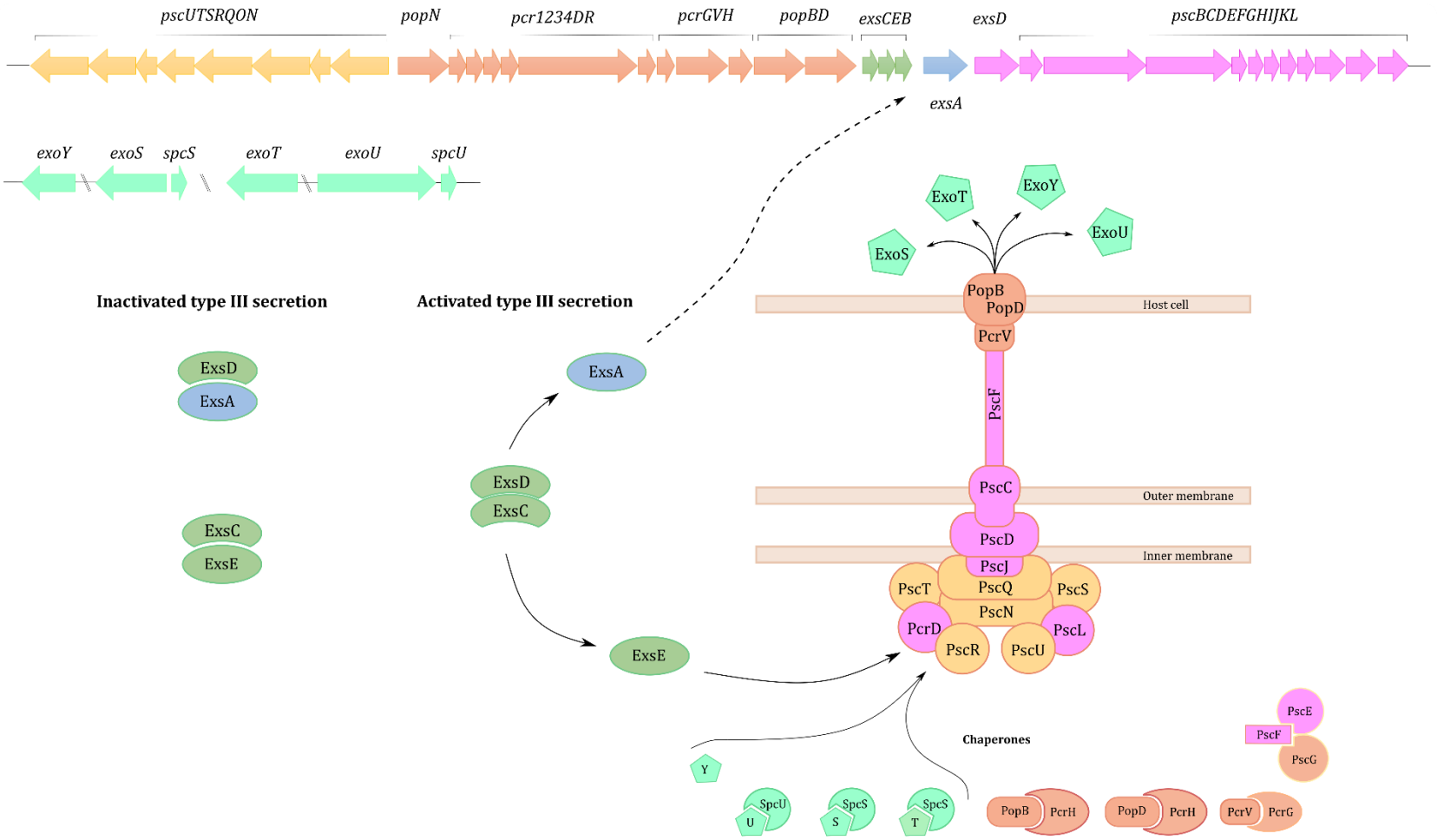

Figure 1.4. The type III secretion system of *P. aeruginosa.* The translocation of numerous exoenzymes, which induce cytotoxicity in host cells, through the type III secretion apparatus is controlled by the ExsACDE regulatory cascade, which also controls the transcription of over 40 T3SS genes.

There are at least four effectors that are secreted by this system, ExoS, ExoU, ExoT and ExoY (Anantharajah *et al.*, 2016). At the base of the injectosome, the ATPase activity of the basal body separates effector proteins from their chaperones and translocates them through the needle complex. ExoS and ExoT share the chaperone, SpcS, whilst chaperone, SpcU, interacts with ExoU. Thus far, no chaperones have been identified for ExoY. Chaperone proteins are also required for several of the T3S apparatus, including PopB and PopD, the structural needle protein, PscF, and regulatory protein ExsE (Hauser, 2009; Anantharajah *et al.*, 2016).

ExoS and ExoT are GTPase-activating proteins (GAPs) that disrupt organisation of the actin cytoskeleton by targeting small GTPases within the host cell. This prevents the cell from migrating or phagocytosing and instead induces cell rounding and detachment from neighbouring cells. In addition to their GAP activity, ExoS and ExoT also possess ADP-ribosyltransferase domains. In ExoS, this domain inhibits DNA synthesis, affects vesicular trafficking, and causes cytotoxicity and apoptosis. ExoS is a major cause of pulmonary damage as it disrupts the pulmonary-vascular barrier. The ADP-ribosyltransferase and GAP domains of ExoT work together to impair phagocytic activity and delay wound healing which promotes bacterial invasion (Hauser, 2009; Anantharajah, Mingeot-Leclercq and Van Bambeke, 2016). ExoY influences the production of numerous cyclic nucleotides, including cyclic adenosine monophosphate (cAMP). In doing so, the actin cytoskeleton is disrupted leading to cell necrosis (Yahr *et al.*, 1998). And finally, considered a major exotoxin, ExoU has intrinsic phospholipase activity, disrupting host cell membranes and promoting necrotic cell death of epithelial cells, macrophages and neutrophils. ExoU can also trigger an inflammatory response and is associated with acute lung injury and sepsis (Hauser, 2009; Anantharajah, Mingeot-Leclercq and Van Bambeke, 2016).

1.4.4 Regulation of type III secretion

The master regulator of T3S is the AraC family transcriptional regulator, ExsA, which binds to and promotes transcription of T3SS genes, including the regulation of its own expression. Expression of the T3SS is also coupled with secretion of ExsE, and involves a partner-switching mechanism between proteins, ExsA, ExsC, ExsD and ExsE

(Figure 1.4). Under non-inducing conditions, the binding of these proteins favours inhibitory complexes that prevent ExsA-induced transcription of T3SS genes. ExsA is bound by the anti-activator ExsD, and ExsE is sequestered by its binding partner ExsC. Injectosomes are still expressed at low levels under non-inducing conditions but become rapidly up-regulated upon incoming inducing signals. When T3S is activated, ExsE is secreted from the cell, releasing its partner ExsC. ExsD then favourably binds the newly-freed ExsC, which displaces ExsA. In its unbound state, ExsA directly binds T3SS gene promoters and initiates transcription (Brutinel *et al.*, 2010).

There are 10 transcriptional units within the T3SS operons and genes, all of which are ExsA-dependent. Activation by ExsA is thought to arise via the monomer assembly model, whereby an initial ExsA monomer binds to the promoter at one site and recruits a second monomer to a neighbouring second site. The ExsA proteins recruit RNA polymerase to the promoter to initiate transcription of T3SS genes, although it is unclear whether just one monomer, or both, are responsible for this (Diaz *et al.*, 2011).

Host cell contact and calcium limitation are highly studied inducers of T3SS expression, however the way in which these environmental cues influence T3SS genes is poorly understood. So far, besides ExsA, only one other transcription factor, PsrA, has been found to regulate T3S. PsrA also regulates motility, polysaccharide production and metabolism, and is influenced by the presence of long chain fatty acids (Diaz, King and Yahr, 2011). Other biological and environmental changes, such as DNA damage, high salt and metabolic stress, have also been associated with the up-regulation of T3S. Unfortunately, the way in which these stimuli activate the secretory mechanism is still poorly understood (Balasubramanian *et al.*, 2013).

Virulence factor regulator (Vfr) is a global regulator of virulence gene expression, including regulation of T3S, and works in conjunction with its co-regulator, cAMP. Two adenylate cyclases, CyaA and CyaB, and the cAMP phosphodiesterase, CpdA, all work to modulate the levels of cAMP available to Vfr. Activated Vfr binds the *exsA* promoter to initiate transcription and so there is a positive correlation between T3SS activity and intracellular levels of cAMP (Diaz *et al.*, 2011; Marsden *et al.*, 2016). Calcium limitation and high salt conditions stimulate the production of cAMP to promote T3S (Diaz, King and Yahr, 2011). Interestingly, the biofilm promoting nucleotide, c-di-GMP, has been found to reduce virulence-associated phenotypes by interfering with cAMP production (Almblad

et al., 2015), and in some *Pseudomonas* species c-di-GMP regulates secretion systems directly via the injectosome ATPase (Trampari *et al.*, 2015). Although the precise mechanism behind c-di-GMP interference remains undefined, it provides further evidence for the tightly regulated, inverse relationship between virulent, planktonic growth and biofilm formation.

1.4.5 The T3SS *versus* biofilm formation

The inverse expression profile of the T3SS and biofilm genes is well established. These two processes are meticulously regulated to meet the bacterias needs at different stages of colony growth. One pathway implicated in this cross-regulation is the Gac/Rsm system. The Gac/Rsm pathway is based on a two-component system in which a sensor histidine kinase, GacS, modulates the phosphorylation level of its cognate response regulator, GacA (Figure 1.5). The signalling activity of GacS is controlled by two sensor kinases, RetS and LadS, which work antagonistically to control GacS kinase activity. Phospho-GacA upregulates the transcription of two small RNAs, *rsmY* and *rsmZ*. Each of these RNA molecules can bind multiple copies of the small RNA-binding protein RsmA, thereby reducing the concentration of "free" (unbound) RsmA in the cell (Moscoso *et al.*, 2014).

Free-RsmA can function as a repressor by binding directly to mRNA 5'UTR regions, promoting their degradation by RNases; for example, the T6SS is thought to be down-regulated in this way (Frangipani *et al.*, 2014). Repression of the *pslA* transcript is more complex, as RsmA binds to and stabilises a stem-loop structure in which the Shine-Dalgarno (SD) sequence is made unavailable through base-pairing with an anti-SD sequence, thus preventing access by the ribosome (Irie *et al.*, 2010). RsmA can also function as an activator, and upregulates motility apparatus and virulence factors, including the T3SS. The mechanism behind this is poorly understood but may involve mRNA stabilization (Intile *et al.*, 2014). RsmA also regulates rhamnolipid production, lipase production, quorum sensing and pyocyanin production, and is vital for balancing virulence and planktonic growth with T6S and biofilm formation (Moscoso *et al.*, 2011).

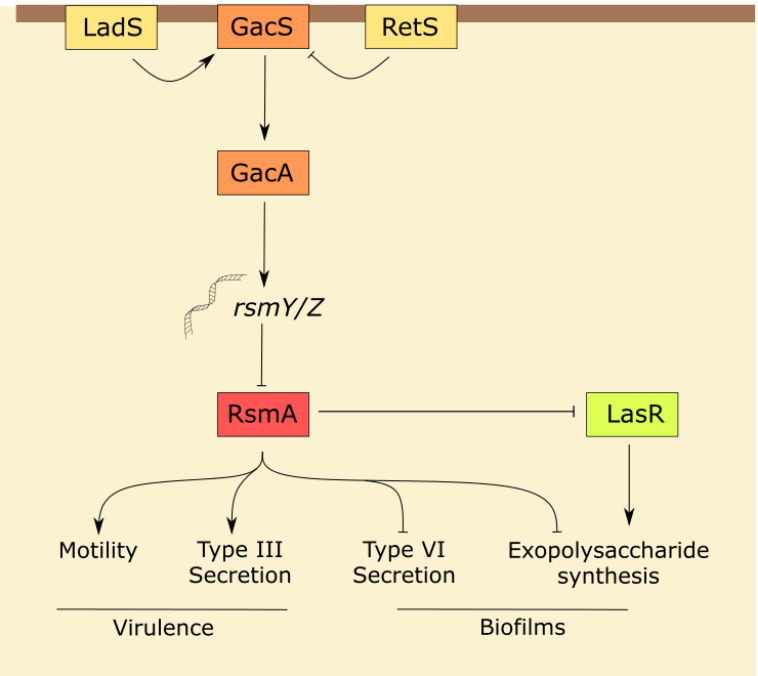

Figure 1.5. The Gac/Rsm pathway of *P. aeruginosa* mediates the inverse regulation of virulence factors and biofilm-forming genes in response to unknown signals received by two sensor kinases, LadS and RetS.

Activation of the Gac/Rsm system is dependent on incoming stimuli detected by RetS and LadS. These triggering stimuli are still largely uncharacterised; however, recently calcium has been found to bind to the periplasmic domain (DISMED2) of LadS activating its kinase activity and ultimately promoting biofilm formation (Broder *et al.*, 2016). This provides a mechanism by which an external stimulus can reciprocally affect the expression of biofilm genes as well as the T3SS. RetS also contains a DISMED2 domain but so far the only known environmental stimuli that activate RetS comes from neighbouring lysed cells. It is thought that these lysing cells release danger signals which bind to RetS and disrupt it's inhibition of GacS, leading to the de-repression of the T6SS (LeRoux *et al.*, 2015).

1.5 Siderophores

1.5.1 Iron and cell survival

Another component of the *P. aeruginosa* virulence system is the production of siderophores. Iron is essential for almost all of the biological processes that occur in bacteria, from metabolic activity and nucleic acid synthesis to electron transfer and redox reactions. In the environment, bioavailability of useful iron (Fe^{2+}) is limited due to the formation of insoluble ferric oxide-hydroxides (Fe^{3+}). In mammals, Fe^{3+} is toxic even at low levels, and so Fe^{3+} is sequestered by the iron transport protein, transferrin (Johnstone *et al.*, 2015). Withholding iron supplies also serves as a defence mechanism against microbial colonisation, and is known as nutritional immunity (Lopez-Medina *et al.*, 2015). Therefore, microbes develop specialised mechanisms to acquire iron within these iron-limited environments, and so not surprisingly, iron acquisition has been correlated with disease severity (Heinrichs *et al.*, 1991).

In order to obtain iron, bacteria produce small molecules known as siderophores. Siderophores are iron chelators that are synthesised in response to iron limitation. With a high affinity for iron, siderophores can effectively scavenge ferric ions, even in extremely iron-depleted environments. They solubilise Fe^{3+} and transport it back into the bacterial cell making the it available for use (Brandel *et al.*, 2012; Balasubramanian *et al.*, 2013).

1.5.2 Pyochelin and pyoverdine

P. aeruginosa synthesises two major siderophores, pyochelin and pyoverdine, which specifically chelate Fe^{3+}. These siderophores have distinct structural characteristics; pyoverdine is a peptide-based fluorescent siderophore, with two hydroxamic groups and an Fe^{3+} binding dihydroxyquinoline chromophore. Pyochelin, however, is a smaller, salicylate-based siderophore that possesses a lower affinity for iron (Figure 1.6) (Minandri *et al.*, 2016).

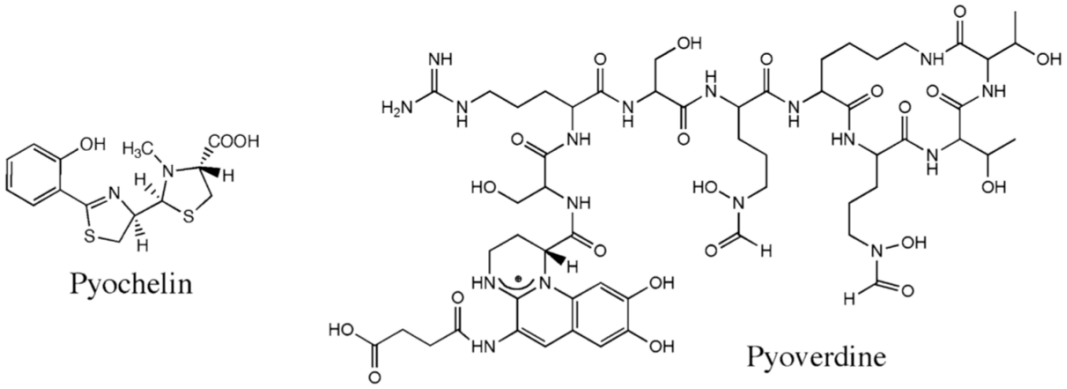

Figure 1.6. Siderophores, pyochelin and pyoverdine, produced by *P. aeruginosa* (image taken from Hoegy *et al*., 2014).

A pyoverdine precursor is synthesised in the cytoplasm via a siderosome, a non-ribosomal peptide synthesis unit. The precursor is exported to the periplasm where it matures and is secreted from the cell by the PvdR-OpmQ efflux pump. Pyoverdine chelates iron with a stoichiometry of 1:1, at which point the ferric-bound pyoverdine binds the outer membrane receptor, FpvA, and is transported back into the periplasm. The Fe^{3+} is not chaperoned straight through to the cytosol, but is instead reduced to Fe^{2+} in the periplasm and is internalised, independently of pyoverdine (Figure 1.7). Iron-free pyoverdine is recycled back out of the cell to sequester more Fe^{3+} ions (Bouvier *et al.*, 2015; Paulen *et al.*, 2017). As pyoverdine has a much higher affinity for Fe^{3+} than pyochelin it is considered the dominant siderophore for iron acquisition (Hare *et al.*, 2012a).

Pyochelin is a much smaller and less complex molecule than pyoverdine. Biosynthesis of pyochelin occurs in the cytosol, by proteins encoded on two divergent operons, *pchDCBA* and *pchEFGHI*. The pyochelin uptake operon, *fptABCX*, is also clustered nearby, along with the regulatory gene, *pchR*. Pyochelin chelates iron with a stoichiometry of 2:1, PCH:Fe and is transported into the cell using the outer membrane receptor FptA. Unlike pyoverdine, pyochelin carries iron all the way into the cytosol, crossing the inner membrane via the permease, FptX. In the cell, ferric-pyochelin activates the PchR regulator, which initiates a positive feedback loop and induces expression of pyochelin biosynthesis genes (Youard *et al.*, 2011). Although the

biosynthesis and uptake of pyochelin has been studied extensively, the mechanism behind its secretion still remains unknown, as is the mechanism of PCH:Fe dissociation and siderophore recycling, which occurs in the cytoplasm (Paulen *et al.*, 2017).

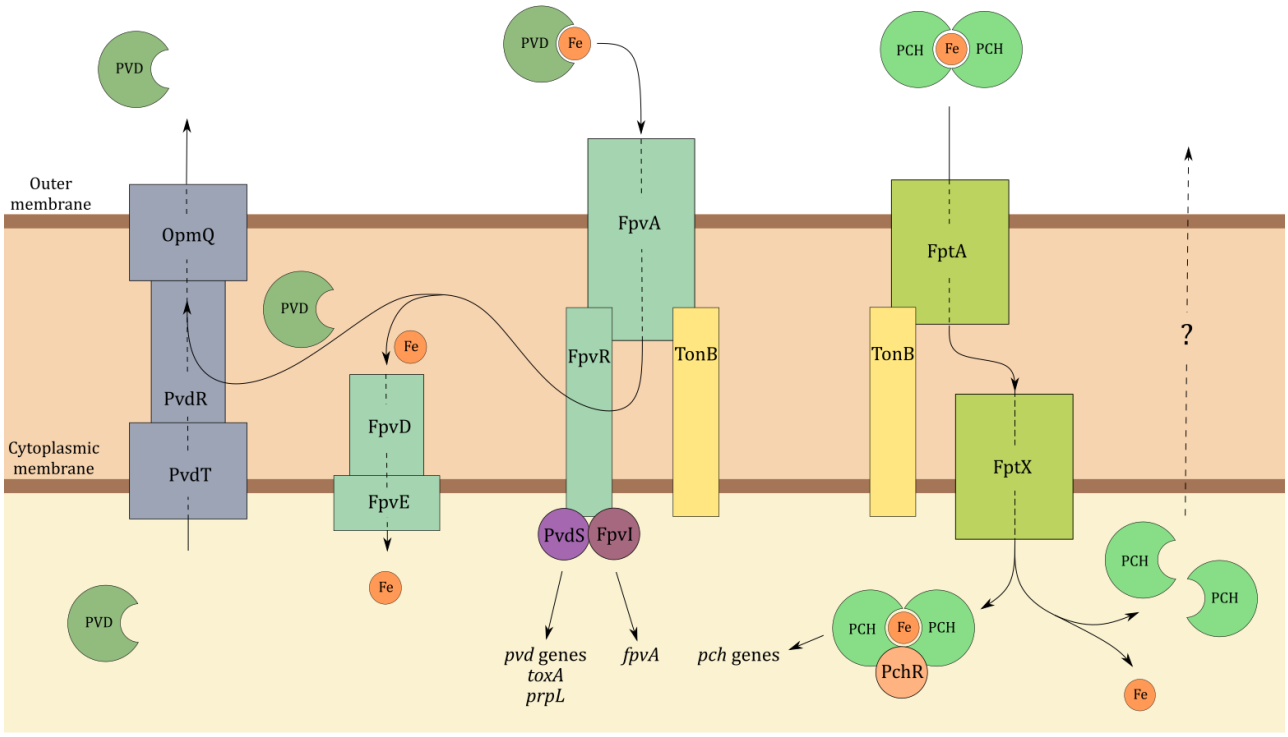

Figure 1.7. Pyoverdine (PVD) and pyochelin (PCH) secretion and uptake pathways in *P. aeruginosa.*

Translocation of ferrisiderophores into the cell by their respective outer membrane receptors is dependent on the TonB protein. TonB proteins complex with two inner membrane proteins, ExsB and ExsD, which use the proton-motive force to provide the energy required for active transport of siderophores across the outer membrane. *P. aeruginosa* encodes over 30 TonB-dependent outer membrane receptors, many of which play a central role in iron uptake and three TonB proteins with low protein similarity (between 30% to 40% amino acid identity). TonB1 is considered to be the primary TonB protein but mutants can be partially complemented by TonB2 (Shirley *et al.*, 2009; Bouvier *et al.*, 2015).

1.5.3 Regulation of iron uptake

Excess free iron in the cell can lead to the formation of toxic reactive oxygen species, and so iron uptake must be tightly regulated. Fur, the ferric uptake regulator, is a DNA binding protein and key regulator in maintaining iron homeostasis. In iron-rich environments, Fur binds ferric iron within the cell and functions as a transcriptional repressor of iron uptake genes by blocking transcription, thus preventing a build-up of excess iron. Fur also represses the expression of iron-containing respiratory enzymes, anti-oxidant enzymes and the small RNA, *prrF*, which affects the expression of over 50 iron-storage genes (Nguyen *et al.*, 2014). Fur-boxes are present in the promoters of all siderophore biosynthesis-, regulatory- and uptake-genes. In the case of pyochelin, iron-limited conditions cause Fur to be released from the promoter of pyochelin biosynthesis genes allowing expression to occur at a basal level. At this point, ferric-pyochelin activates the regulator, PchR, and together they rapidly promote the up-regulation of the pyochelin biosynthesis operons (Youard *et al.*, 2011).

1.5.4 Siderophores and virulence

The role of siderophores and iron acquisition in infection and virulence has been documented across many bacterial species. In *P. aeruginosa*, Fe^{3+} uptake is essential for infection in mouse pneumonia models, and mutants defective in pyoverdine, pyochelin and TonB all exhibit lower levels of virulence (Minandri *et al.*, 2016). Binding of ferric-pyoverdine to the membrane receptor, FpvA, initiates a signalling cascade from the cell surface into the cytoplasm via FpvR, an anti-sigma factor. This cascade induces the activation of FvpI and PvdS sigma factors (Figure 1.7). FvpI specifically promotes expression of the *fvpA* receptor gene, whereas PvdS coordinates the expression of numerous genes involved in pyoverdine biosynthesis and transport, and also controls two virulence factors, PrpL and exotoxin A (Minandri *et al.*, 2016). PrpL is an extracellular endoprotease and can degrade host iron-binding proteins, such as lactoferrin and transferrin, and exotoxin A inhibits protein synthesis (Wilderman *et al.*, 2001). The role of siderophores in virulence make them a major influence in acute infection. However, they appear to be far less important during chronic infection with one

study finding that one-third of *P. aeruginosa* isolates from the CF lung no longer produce pyoverdine (De Vos *et al.*, 2001).

Fur-mediated regulation of the T3SS and T6SS, has been demonstrated in *Bordetella pertussis*, *B. bronchiseptica*, *E. coli* and *Edwarsiella tarda*, where iron starvation leads to the repression of T6SS genes and the up-regulation of T3SS genes. This highlights that iron depletion can act as a nutritional stressor which triggers the expression of virulence determinants and promotes bacterial pathogenicity. Due to the conservation of the T3SS and T6SS across bacterial species this activation may also occur in *P. aeruginosa* (Brickman *et al.*, 2011; Brunet *et al.*, 2011; Chakraborty *et al.*, 2011; Kurushima *et al.*, 2012).

Manipulation of siderophores has recently opened up a new method for targeting bacteria with antimicrobial agents. *P. aeruginosa* can bind siderophores from other *Pseudomonas* species, allowing them to 'piggy-back' off these strains and reduce their own energy costs. Because of this promiscuity in the outer membrane receptors, antibiotic-siderophore conjugates are being tested as potential vectors to deliver antibiotics into the cell via the bacteria's own translocation machinery, aptly named the Trojan Horse strategy (Bouvier *et al.*, 2015; Paulen *et al.*, 2017).

1.6 Elongation factor G

1.6.1 Ribosomal translation

Cell growth and survival relies almost entirely on efficient protein synthesis. At the centre of protein synthesis is the ribosome, where amino acids are bonded together to form polypeptide chains in relation to an mRNA transcript. In *P. aeruginosa*, the ribosome is made up of 57 highly conserved ribosomal proteins and 3 ribosomal RNAs (rRNAs); 23S, 16S, and 5S (Wilson, 2014; Valot *et al.*, 2015). Together these comprise the 70S ribosome, which can be further divided into the small (30S) and large (50S) subunits (Wilson, 2014).

Four main processes occur during protein synthesis; initiation, elongation, termination and recycling. Firstly, with the assistance of three initiation factors, the ribosome binds to an mRNA transcript and positions the start codon and an initiator tRNA

within the P-site of the ribosome. The P-site is one of 3 binding pockets that accommodate tRNA within the ribosome. Following the initiator tRNA, the relevant, charged tRNA, that corresponds to the mRNA codon sequence, is positioned in the A-site (Aminoacyl-tRNA binding site), and progressively moves to the P-site (Peptidyl-tRNA binding site) and finally into the E-site (tRNA Exit site) before being released from the ribosome (Figure 1.8) (Zhou *et al.*, 2014). Elongation factor Tu (EF-Tu) helps to incorporate aminoacylated-tRNA into the A-site of the ribosome in a template-dependent manner through base-pairing between the tRNA and mRNA transcript. A peptide bond is formed between the neighbouring amino acids within the A- and P-sites, at which point, elongation factor G (EF-G) orchestrates the translocation of tRNAs from the A- to P-site and from the P-site to E-site of the ribosome. This process is repeated and the polypeptide chain elongates through an exit tunnel located within the large subunit. The mRNA is also moved through the ribosome until a stop codon is encountered; at which point release factors hydrolyse the peptidyl-tRNA bond and the polypeptide chain is released. The ribosomal units then dissociate and are recycled for further translational initiation (Wilson, 2014, Zhou *et al.*, 2014).

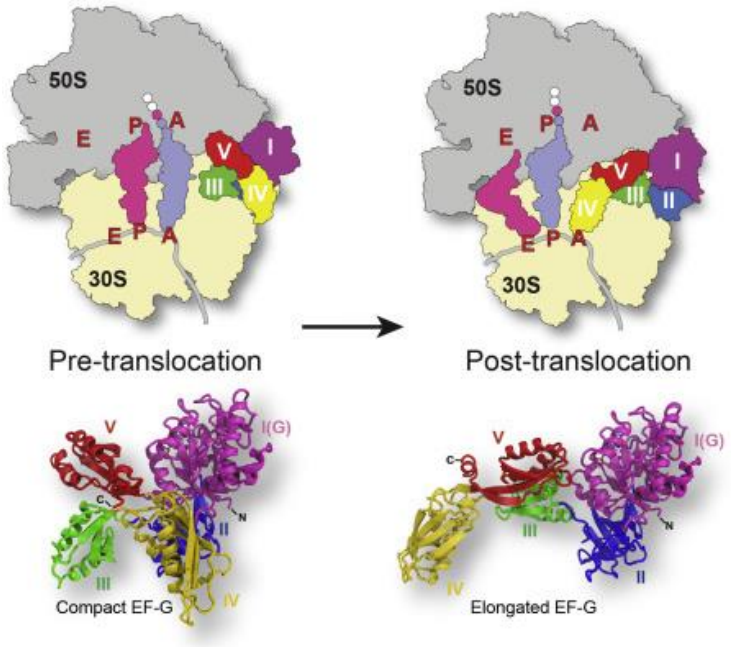

Figure 1.8. Structural conformation of elongation factor G when bound to the ribosome and during translocation of aminoacyl-tRNA from the A-site to the P-site of the ribosome (image taken from Lin *et al.*, 2015).

EF-G is essential for protein synthesis. The precise mechanism by which EF-G catalyses tRNA translocation is still not fully understood but the top of the aminoacyl-tRNA is predicted to move first, followed by subsequent movement of the anticodon end of the tRNA, coupled with mRNA translocation in the small ribosomal subunit. During the elongation steps the ribosome undergoes several conformational changes to accommodate these dynamic movements and EF-G also experiences its own structural rearrangements which mediate binding, GTPase activity and disassociation from the ribosome (Salsi *et al.*, 2015).

1.6.2 Elongation factor G

EF-G is comprised of five domains; domain I is the site for GTP binding and hydrolysis and domain IV docks into the A-site of the ribosome where it interacts with the mRNA transcript promoting translocation (Salsi *et al.*, 2014). In its cytosolic form, EF-G adopts a compacted structure where domains I and V are folded closely to one another. EF-G binds the ribosome in its compact form but during translocation it subsequently undergoes inter-domain rearrangements to take on an elongated conformation, thought to aid positioning of domain IV within A-site of the ribosome (Figure 1.8) (Connell *et al.*, 2007; Lin *et al.*, 2015).

P. aeruginosa synthesises two paralogous EF-G proteins which are encoded by two distinct genes, *fusA1* and *fusA2*, positioned separately within the genome (4.77 Mbp and 2.27 Mbp, respectively) (Winsor *et al.*, 2016). The amino acid sequence of the two paralogues is highly conserved, with a shared identity of 84%, however it is likely that these two proteins have distinct roles. EF-G1B, encoded by *fusA2*, is predicted to have greater involvement in elongation and polypeptide synthesis than EF-G1A, encoded by *fusA1*. However, EF-G1A is predicted to have a more dominant role in ribosomal recycling and association with ribosomal recycling factors (Palmer *et al.*, 2013).

FusA was named after EF-G's ability to bind fusidic acid and the observed resistance resulting from *fusA* mutation. Fusidic acid is a steroid-like antibiotic which inhibits protein synthesis by disrupting peptide elongation. It typically has a low affinity for EF-G, but when EF-G is bound to the ribosome fusidic acid forms a strong complex with the protein. Once bound, fusidic acid locks EF-G into the post-translocation site,

blocking any more GTPase activity and preventing dissociation of EF-G from the post-translocation ribosome, thus arresting the continuation of peptide elongation (Borg *et al.*, 2015). EF-G1B encoded by *fusA2* is more sensitive to the effects of fusidic acid than EF-G1A, and so is most likely to be responsible for the emergence of fusidic acid resistance upon mutation (Palmer *et al.*, 2013).

1.6.3 Regulating protein synthesis

Protein synthesis is one of the most fundamental steps in gene expression. Coordinating the ribosome with mRNA, translation factors and tRNA defines protein abundance and ensures that the protein requirements of the cell are met. Within one cell there is little correlation between mRNA and protein levels, suggesting that protein abundance is predominantly controlled at the translational step (Liu *et al.*, 2016; Rodnina, 2016). Even on a single transcript, rates of protein synthesis vary considerably, with periods of rapid synthesis followed by interspersed pausing. Pauses in elongation may be determined by regulatory signals encoded on the mRNA, but often, it is due to the availability of cellular resources such as aminoacyl-tRNA and translation factors. Prolonged pauses are termed 'ribosomal stalling' and can result from numerous hold ups, but the most common is often peptide-mediated stalling from unsuccessful peptidyl transfer. Ribosome stalling can result in multiple ribosomes queuing along the mRNA transcript which then slows translation across numerous other ribosomes. Stalled ribosomes need to be disassembled and recycled rapidly to prevent downstream effects on the quality and composition of the cellular proteome (Keiler, 2015; Rodnina, 2016).

1.6.4 Ribosome-targeting antibiotics

Because the ribosome plays such a central role in cell survival it is an obvious target for antimicrobial agents. The majority of ribosomal-targeted drugs interfere with the elongation phase of protein synthesis and include aminoglycosides, chloramphenicols, fusidic acid and tetracyclines. These antibiotic binding sites are typically located at positions of mRNA-tRNA interaction which disrupt their association (Wilson, 2014).

Resistance to the major classes of ribosome-targeting antibiotics occurs through the up-regulation of efflux systems to remove the drug from the cell, and through mutations in the genes encoding ribosomal proteins and rRNA, which prevent antibiotic binding (Kotra *et al.*, 2000). The bacterial genome contains duplications of rRNA operons, with *P. aeruginosa* possessing four copies (Bodilis *et al.*, 2012). This means that antibiotic resistance through rRNA mutation is very rare and would require a recurring mutation across all four operons. However, ribosome-associated proteins are usually only found in single copy within the genome, so resistance to antibiotics through mutation to these genes is far more common. Such mutations often cause conformational adjustments in the rRNA which consequently affects antibiotic binding (Wilson, 2014).

One group of ribosome-targeting antibiotics are the aminoglycosides. Aminoglycosides are hydrophilic sugars with an affinity for nucleic acids. Aminoglycosides irreversibly bind to the 16S rRNA within the small subunit of the ribosome and interfere with tRNA selection. It seems that different aminoglycosides, such as gentamicin, kanamycin and paromomycin, all bind to the A-site decoding region in a common manner. Aminoglycosides alter the conformation of the A-site and disrupt interactions between tRNA and mRNA, leading to erratic base pairing and rapid termination of peptide synthesis leading to cell death (Kotra, Haddad and Mobashery, 2000). Resistance to aminoglycosides has been seen to emerge from methylation of the 16S rRNA, up-regulation of antibiotic-modifying enzymes, and the up-regulation of efflux pumps (Livermore, 2002; Doi *et al.*, 2007; Hay *et al.*, 2013).

1.7 Objectives of this study

During the inital stages of this project I observed a mutation in the gene, *fusA1*, which encodes EF-G. This mutation conveyed resistance to gentamicin and a reduction in the expression of a biofilm-associated gene, *cdrA*.

Having identified this interesting mutation, the research aims of this study were to investigate the involvement of EF-G in biofilm formation and develop the understanding of its role in antibiotic resistance. This aim raises the following project objectives:

- To characterise the position of the *fusA1* mutation and determine its effect on the structure of EF-G.
- To measure the effect that the mutated EF-G protein has on biofilm formation, along with assessing the impact it has on bacterial virulence.
- Synthesise data from proteomic and transcriptomic analysis to establish the global effects that the mutation has on a diverse range of cellular processes.

Chapter 2

2 Materials and methods

2.1 Bacterial strains

Bacterial strains used in this study can be found in Table 2.1. Bacterial strains were stored at -80°C in 25% (v/v) glycerol solution. Viable bacteria could be stored on media agar plates at room temperature for up to two weeks.

Table 2.1. List of bacterial strains.

Strain	Genotype	Reference
Pseudomonas aeruginosa		
PAO1	Wild type	B. Iglewski, University of Rochester, USA
PAPcdr	PAO1, Mini-CTX-P*cdrA*::lacZ, Tc^r	This study
FUS443	PAPcdr derivative, containing a cytosine to thymidine substitution in *fusA1* at gene position 1328 (of 2121 bp)	This study
FUS443C	FUS443, expressing *fusA1 in trans* from a pUCP20 expression vector	This study
P*pqsA*::*lux*	PAO1, *pqsA* mutant containing a P*pqsA*::*luxCDABE* gene fusion	Fletcher *et al.*, 2007
Escherichia coli		
DH5α	(F-) *supE44* Δ*lacU169* (φ80*lacZ*Δ*M15*) Δ*argF hsdR17 recA1 endA1 thi-1 relA1*	Gibco, BRL
JM109	*endA1 recA gyrA96 thi hsdR17* (r_k^-, m_k^+) *relA1 sup*E44 Δ(*lac-pro*AB) (F´ *tra*D36, *pro*AB, *laq*I^qZΔM15)	Yanisch-Perron *et* al., 1985
β2163	(F-) RP4-2-Tc::Mu_*dapA*::(*erm-pir*), Km^r Em^r	Demarre *et al.*, 2005
Rosetta	(F-) *ompT hsdS*$_B$(r_B^- m_B^-) *gal dcm* (DE3) pRARE (Cam^R)	Novagen

2.2 Growth conditions

Unless otherwise stated, bacterial cultures were grown in M9 minimal media supplemented with 0.5% (w/v) glucose and incubated at 37°C.

2.2.1 Overnight cultures

A single bacterial colony was used to inoculate 10 mL of growth media in a 25 mL universal tube. The culture was grown at 37°C for approximately 16 h on a rotating wheel. If appropriate, antibiotic selection was maintained throughout incubation.

Unless otherwise stated, experiments were conducted in triplicate using three biological replicates deriving from three independent bacterial colonies.

2.2.2 Planktonic cultures

For planktonic growth, overnight cultures were used to inoculate 50 mL of media in 250 mL conical flasks to a starting optical density (OD_{600}) of 0.05, for growth in LB, or 0.1, for growth in M9 minimal media. Cultures were incubated at 37°C in a shaking water bath at 210 rpm for aeration of the culture. If appropriate, antibiotic selection was maintained throughout growth.

2.2.3 Growth on solid media

Colonies were grown in 10 cm diameter Petri-dishes containing 25mL growth media with 1.5% (w/v) agar and incubated at 37°C overnight.

For growing cells from frozen stocks, frozen cells were defrosted on the surface of the agar at room temperature. A sterile inoculation loop was used to spread the cells across the agar to produce single colonies.

2.2.4 Growth media

Growth media and constituents are listed in Table 2.2. Media, solutions and glassware were sterilised by autoclaving at 121°C for 15 min.

Table 2.2. Growth media and solutions.

Growth media	**Components per litre**
LB broth (Lennox)	10 g peptone 5 g yeast extract 5 g sodium chloride
1X glucose M9 minimal media	200 mL 5X M9 minimal salts (Difco) solution 0.2% (w/v) magnesium sulfate 0.01% (w/v) calcium chloride 0.5% (w/v) glucose
For solid agar plates	Growth media containing 1.5% (w/v) agar
Congo Red solid media	37 g Brain-Heart infusion broth 50 g sucrose 0.8 g Congo Red
Congo Red liquid media	M9 minimal media 0.8 g Congo Red
Solutions	
M9 Minimal Salts, 5X (BD Difco)	33.9 g disodium phosphate 15 g monopotassium phosphate 2.5 g sodium chloride 5 g ammonium chloride
Phosphate buffered saline (PBS)	10 g phosphate buffered saline tablets (Dulbecco A)
Lysis buffer	100 mM Tris-HCl 50 mM sodium chloride 20 mM EDTA 10% (v/v) glycerol 1 mM DTT 1 cOmplete Mini, EDTA-Free protease tablet (Roche) pH 7.5

Table 2.2 continued	
Protein loading dye	50 mM Tris-HCl 2% (w/v) SDS 0.1% (w/v) bromophenol blue 10% (v/v) glycerol 10 mM dithiothreitol
Stacking buffer, 5 X	60 g Tris-HCl 0.5% (w/v) SDS pH 6.8
Resolving buffer, 5 X	151 g Tris-HCl 0.5% (w/v) SDS pH 8.8
SDS-PAGE running buffer	15 g glycine 3 g Tris-HCl 0.1% (w/v) SDS pH 8.3
Protein purification buffer	50 mM sodium phosphate 200 mM sodium chloride 10% (v/v) glycerol 10 mM imidazole pH 8.0
Elution buffer	50 mM sodium phosphate 200 mM sodium chloride 10% (v/v) glycerol 250 mM imidazole pH 8.0
Dialysis buffer	50 mM Tris-HCl 100 mM sodium chloride 5% (v/v) glycerol pH 7.4
TAE buffer	40 mM Tris-HCl 20 mM acetic acid 1 mM EDTA pH 7.6

2.3 Antibiotics

The antibiotics used in this study are listed in Table 2.3. Antibiotics were solubilised in water and stored at 4°C, or in 50% (v/v) ethanol solution and stored at -20°C. All antibiotics were filter-sterilised using 0.2 µm membrane filters (Millipore).

Table 2.3. Antibiotics and media supplements.

Antibiotic	Solvent	Working concentration (µg/mL)	
		P. aeruginosa	*E. coli*
Carbenicillin, Cb	50% (v/v) ethanol	250	50
Fusaric acid	50% (v/v) ethanol	>1300	-
Fusidic acid	50% (v/v) ethanol	1750	-
Gentamicin, Gm	Water	50	10
Kanamycin, Km	Water	1000	25
Rifampicin	Water	100	-
Tetracycline, Tc	50% (v/v) ethanol	50	10
DAPA	Water	-	40
X-gal	Dimethylformamide	30	-
Iron(III)Chloride	Water	0.811	-

2.3.1 Determining minimal inhibitory concentrations

Single colonies were streaked onto M9 minimal media plates, supplemented with glucose and containing increasing concentrations of antibiotic. The concentration at which no cells grew after 24 hours of incubation at 37°C was determined as the minimum inhibitory concentration.

2.4 Measuring growth and harvesting planktonic cells

Planktonic cultures were grown as described in **'2.2.2 Planktonic cultures'.** To measure growth of the culture, the OD_{600} was measured every hour using a spectrophotometer (Jenway 6715). If the optical density exceeded 0.9, bacterial cultures

were diluted in the same growth media to ensure that the readings were within the range of optimal sensitivity.

In M9 minimal media, cells harvested at an OD_{600} of 0.2 – 0.7 represent cells in exponential growth. Cultures harvested at an OD_{600} of 0.7 - 1.2 represent cells in a late exponential phase of growth, and cultures exceeding an optical density of 1.2 are considered to have entered stationary growth.

2.5 Viable cell counts

Bacterial cultures were diluted in increasing dilution factors, from 10^{-3} to 10^{-10}, in fresh growth media. From each dilution, 10 µL was spotted onto a media agar plate and incubated at 37°C overnight. Colonies were counted to determine the number of viable cells per mL. Comparisons were made between viable cell counts on agar plates without antibiotics and those supplemented with antibiotics to assess plasmid retention during growth.

For measuring the retention of antibiotic resistance across bacterial generations, overnight cultures were diluted by 10^{-6}, and 100 µL was plated on agar media, supplemented with and without antibiotics. The remaining culture was sub-cultured and grown for a further 24 h before repeating this process until the bacterial culture had been sub-cultured 3 times.

2.6 Cloning techniques

2.6.1 DNA extraction

Genomic DNA (gDNA) was extracted from bacterial cultures using the GeneJET Genomic DNA Purification Kit. Plasmid DNA was extracted from bacterial cultures using the GeneJET Plasmid Miniprep Kit. The concentration of the extracted DNA was determined on a NanoDrop ND-1000 Spectrophotometer and was stored at -20°C. The plasmids used in this study are shown in Table 2.4.

Table 2.4. Plasmids used in this study.

Plasmid	Description	Source
pUCP20	*Escherichia* to *Pseudomonas* shuttle vector, Cb^r	West *et al.*, 1994
Mini-CTX-P*cdrA*::*lacZ*	Vector for the integration of a single-copy chromosomal P*cdrA*::*lacZ* gene, Tc^r	Welch (unpublished)
pFLP2	Site-specific excision vector with flippase, Cb^r	Becher and Schweizer, 2000
pFLP2-cre	Site-specific excision vector with cre-recombinase, Cb^r	Welch (unpublished)
pTn*Mod*-OGm	Self-cloning mini-transposon for stable integration in the genome, Gm^r	Dennis and Zykstra, 1998
p*fusA1*	pUCP20 for the expression of *fusA1* driven by the *lac* promoter, Cb^r	This study
pP443L	pUCP20 for the expression of *fusA1* containing a cytosine to thymidine substitution at gene position 1328 (of 2121 bp), driven by the *lac* promoter, Cb^r	This study
pSB536	BHL reporter plasmid, *ahyR*::*luxCDABE*, , Cb^r	Swift *et al.*, 1997
pSB1142	OdDHL reporter plasmid, P*lasR*::*luxCDABE*, Tc^r	Winson *et al*., 1998
pET19m::*fusA1*	Vector for inducible expression of N-terminally 10xHis-tagged *fusA1*, Cb^r	This study
pET19m::P443L	Vector for inducible expression of N-terminally 10xHis-tagged *fusA1:P443L*, Cb^r	This study

2.6.2 Polymerase chain reaction (PCR)

PCR was performed using 50 µL of reaction mixture that contained up to 250 ng template DNA, 10 µM of forward and reverse primers, 10 mM dNTPs, Phusion HF buffer, 0 – 10% (v/v) dimethyl sulfoxide (DMSO), and Phusion DNA polymerase. Reaction conditions were determined based on the length of the amplicon and the annealing temperature of the primers. Table 2.5 lists the reaction cycle recommended by the manufacturer for amplification using Phusion polymerase, and Table 2.6 lists the primers used in this study.

Table 2.5. Phusion PCR amplification program.

Phusion DNA polymerase			
Initial denaturation		98°C	1 min
35 cycles	Denaturation	98°C	10 sec
	Annealing	50-72°C	20 sec
	Extension	72°C	20 sec/kb of amplicon
Final extension		72°C	5 min
		4°C	Hold

Table 2.6. Oligonucleotide primers uses in this study.

Primer	Sequence (5' – 3')	Restriction sites
$Pser_{up}$	CGAGTGGTTTAAGGCAACGGTCTTGA	
$Pser_{down}$	AGTTCGGCCTGGTGGAACAACTCG	
fusA1 Forward	ATATATCTGCAGAGGAGGTTAATTGTGGCCCGTA	*Pst*I
fusA1 Reverse	AGCCCGAAGCTTTCAACCTTGTTTTTTAAC	*Hind*III
pUCP20 MCS1	GTTGTAAAACGACGGCCAGT	
pUCP20 MCS2	TTGAGTGAGCTGATACCGCT	
pslA Forward	ATCGAGTACTTCCTGGTCGC	
pslA Reverse	CCCAGGCGAAGAACATGATG	
pcrV Forward	TCAAGGATTTTCTCAGCGGC	
pcrV Reverse	AGGGTGGTCTTCTCGTTGAC	
exsA Forward	GGGCGTATATGTTCTGCTCG	
exsA Reverse	CTCGACTTCACTCAACAGCG	
P443L verification Forward	ATATTTGAATTCGATGACGACAAGGGCATG	
P443L verification Reverse	ATATTTAAGCTTGGACATGGAACGCACGTC	
pET19m::*fusA1* Forward	ATATATCATATGGTGGCCCGTACTAC	*Nde*I
pET19m::*fusA1* Reverse	ACGTTACATATGTCAACCTTGTTTTTT	*Nde*I
Orientation check Forward	AGGGGAATTGTGAGCGGATA	
Orientation check Reverse	TGGTTGACGCCGGTATAGAA	

2.6.3 Colony PCR

For PCR on bacterial colonies, a single colony was diluted in 100 µL of sterile dH_20. In a 50 µL reaction, 2 µL of the diluted cells was added to the PCR mixture in place of the DNA template.

2.6.4 Agarose gel electrophoresis

DNA fragments were separated, based on size, by electrophoresis through agarose gels. Agarose was dissolved in 1x Tris-Acetate-EDTA (TAE) buffer, supplemented with 0.4 µg/mL ethidium bromide, and allowed to set. Nucleotide samples were prepared with 6x DNA Loading dye (Thermo Scientific) and were loaded onto 0.8% (w/v) agarose gels for fragments >2 kb, 1% (w/v) agarose for fragments between 0.5 – 2 kb and 2% (w/v) agarose gels for smaller fragments <0.5 kb. Hyperladder 1 kb (Bioline) was loaded as a sizing reference (200 – 10,000 bp) for DNA fragments and the samples were electrophoresed at 80 V for 1 h. DNA was visualised using a UV transilluminator.

To purify DNA from within agarose gels, bands containing the desired DNA fragments were excised from the gel using a scalpel and the DNA was extracted from the agarose using the GeneJET Gel Extraction Kit. The concentration of the extracted DNA was determined on a NanoDrop ND-1000 Spectrophotometer and samples were stored at -20^{o}C.

2.6.5 Restriction digest and DNA ligation

DNA was digested with restriction enzymes (NEB) according to the manufacturer's instruction. If treated with Shrimp Alkaline Phosphatase (NEB) this was added for 30 min at 37^{o}C following the restriction digest to prevent self-religation of DNA. Samples were checked for successful digestion by gel electrophoresis and were gel-purified.

For the ligation of fragmented DNA into cut plasmid DNA, ligation reactions were prepared according to the manufacturer's instruction for T4 ligase. The reaction mixture

was incubated on ice for 1 h followed by 1 h at room temperature. Ligation mixture was stored at -20°C or used directly for transformation by electroporation.

2.7 Transformation of *P. aeruginosa* by electroporation

Bacterial cultures were sub-cultured for 3 hours in 10 mL fresh media to harvest cells during exponential growth. Cells were sedimented in a centrifuge at 3,200 x *g* for 5 min, at 20°C. The cells were washed 3 times by resuspending the pellet in 10 mL of sterile dH_20 and re-pelleting the sample. The final resuspension was in 100 µL of dH_20 and the sample was incubated for 20 min. Cells were then incubated with 0.2 – 1 µg plasmid DNA, or 2 µL of ligation mixture, for 10 min and transformed by electroporation at 2.5 kV (25 µF, 200 Ω, time constant of 5 ms). Immediately after electroporation, 1 mL of LB was added to the transformed cells and was incubated at 37°C for 1 hour to allow the cells to recover. Cells were then centrifuged at 21,000 x *g* for 5 min, and resuspended in 100 µL of growth media. The transformed cells were plated onto selective agar media and grown at 37°C overnight. Unless otherwise stated, all incubation and centrifugation steps were performed at room temperature.

2.8 Transformation of *E. coli* by electroporation

Bacterial cultures were grown overnight and sub-cultured for 3 hours in 10 mL of fresh media. Cells were centrifuged at 3,200 x *g* for 5 min, 4°C and the pellet washed 3 times in pre-cooled, sterile dH_20. After the final centrifugation, cells were resuspended in 100 µL of cold dH_20 and incubated on ice for 20 min, followed by the addition of 0.2 – 1 µg plasmid DNA and incubation on ice for 10 min. Competent cells were electroporated and plated onto selective agar.

2.9 Construction of the PAPcdr strain

The expression-reporter vector, mini-CTX-P*cdrA*::*lacZ*, contains a gene fusion between the promoter sequence of *cdrAB* and *lacZ*, and stably integrates into a neutral site within the genome as a single copy. Mini-CTX-P*cdrA*::*lacZ* was introduced into PAO1

by electroporation and transformants were selected for on 50 μg/mL tetracycline. pFLP2 was introduced into the transformants through bi-parental conjugation with β2163 (pFLP2), as defined in '**2.12 bi-parental mating'**. Successful conjugants were selected for on carbenicillin. The pFLP2 plasmid encoded a flippase gene which acted on specific Flp-recombinase target (FRT) sites within the mini-CTX construct to excise the tetracycline-resistance cassette. Transformants were streaked onto LB agar supplemented with 5% (w/v) sucrose to remove pFLP2 from the cell, and onto LB agar supplemented with tetracycline to verify successful excision of the tetracycline-resistance cassette. Loss of pFLP2 was confirmed through carbenicillin sensitivity.

$Pser_{up}$ and $Pser_{down}$ primers were used to verify that mini-CTX-P*cdrA*::*lacZ* had been successfully incorporated into the specified neutral site within the genome. Colonies were streaked onto media agar containing X-gal to detect the expression of β-galactosidase from the P*cdrA*::*lacZ* construct, as described in '**2.14.2 β-galactosidase assays**'.

2.10 Construction of p*fusA1* and pP443L expression vectors

The *fusA1* gene was amplified from PAO1 gDNA using primers, '*fusA1* Forward' and '*fusA1* Reverse', and standard PCR conditions for Phusion polymerase. The PCR product was run on an agarose gel and the corresponding band was gel-purified. The amplicon and expression vector, pUCP20, were digested with restriction enzymes, *Pst*I and *Hind*III, and the *fusA1* gene was ligated into the pUCP20 vector downstream of the *lac* promoter. The construct was confirmed by PCR using primers 'pUCP20 MCS1' and 'pUCP20 MCS2'. The same method was used to create an expression vector of the mutated *fusA1*-P443L variant using gDNA extracted from the FUS443 mutant.

2.11 DNA sequencing

DNA sequences were determined through Sanger sequencing conducted by GATC Biotech as per the company's instruction.

2.12 Bi-parental mating

The recipient *P. aeruginosa* strain and donor *E. coli*, β2163, strain were grown individually overnight in LB with the appropriate antibiotic selection and diaminopimelic acid (DAPA) supplementation for β2163.

Bacterial cultures were normalised to an OD_{600} of 1 in LB and centrifuged at 21,000 x *g* for 10 min at room temperature. The bacterial pellets were washed in LB to remove the presence of antibiotics and combined in a 1:1 ratio to a total volume of 1 mL. The cell suspension was pelleted and resuspended in 50 µL of LB which was spotted onto LB agar supplemented with DAPA and incubated at 37°C for 12 - 18h. Cells were scraped from the agar plate and resuspended in 1 mL of PBS. The suspension was diluted by a dilution factor of 2 and 100 µL was plated onto LB agar supplemented with antibiotic selection, and incubated for 24 h at 37°C. DAPA was omitted from the dilution plates to prevent *E. coli* growth,

2.13 Whole genome sequencing

Bacterial strains were sent to MicrobesNG for whole genome sequencing on an Illumina HiSeq 2500 platform. Genomic DNA libraries were prepared using Nextera XT Library Prep Kit (Illumina) following the manufacturer's protocol with the following modifications: two nanograms of DNA were used instead of one, and PCR elongation time was increased to 1 min from 30 seconds. DNA quantification and library preparation were carried out on a Hamilton Microlab STAR automated liquid handling system. Pooled libraries were quantified using the Kapa Biosystems Library Quantification Kit on a Roche light cycler 96 qPCR machine. Libraries were sequenced on the Illumina HiSeq using a 250bp paired end protocol. Reads were adapter trimmed using Trimmomatic 0.30 with a sliding window quality cutoff of Q15. De novo assembly was performed on samples using SPAdes version 3.7, and contigs were annotated using Prokka 1.11.

Genome alignment and analysis of gene disruptions were determined using Mauve Multiple Genome Alignment.

2.14 Phenotypic assays

2.14.1 Biofilm assay

Bacterial cultures were normalised to an OD_{600} of 0.1 in fresh growth media and 100 µL was added per well to a 96-well microtitre plate. Plates were sealed with sterile film (StarLab breathable self-adhesive film) and incubated statically at 37°C or on a shaking platform for 24 hours. Planktonic cells were aspirated from the wells and the remaining biofilm cells that were adhered to the sides of the wells were washed with 120 µL of dH_20 and stained with 100 µL of 0.1% (w/v) crystal violet for 15 min at room temperature. Wells were then washed 3 times with 120 µL dH_20 and dried before re-solubilising the crystal violet in 120 µL of 30% (v/v) acetic acid for 15 min at room temperature. Biofilm mass was quantified by measuring absorbance at 595 nm.

2.14.2 β-galactosidase assays

2.14.2.1 Bacterial colonies

For reporter strains containing a *lacZ* gene fusion, β-galactosidase activity was visualised by streaking or spotting 10 µL of bacterial culture onto media agar supplemented with 30 µg/mL X-gal (5-bromo-4-chloro-3-indolyl β-D-galactopyranoside). β-galactosidase expression and activity was visualised through the production of a blue pigmented product.

2.14.2.2 Planktonic cells

For measuring β-galactosidase activity in planktonic cultures, 100 µL of cell culture was harvested and frozen at -80°C in a 96-well microtitre plate. The plate was defrosted for 30 min at 37°C and 10 µL was transferred to a fresh 96-well microtitre plate. The samples were frozen at -80°C for a second time to further permeabilise the cells, followed by thawing at room temperature. To quantitatively measure the level of β-galactosidase expression, 100 µL of reaction mixture (PBS solution containing 20 mg/mL lysozyme and 250 µg/mL 4-methylumbellifryl-β-galactoside) was added to the cells. The reaction was measured using the Gemini XPS fluorimeter (Molecular

Devices) at an excitation wavelength of 360 nm and emission wavelength of 450 nm, every 30 sec for 30 min at 37°C, with a cut-off wavelength of 435 nm.

2.14.2.3 Colony biofilms

For quantitative measurement of β-galactosidase activity in bacterial colony biofilms, a sterile 0.1 μm membrane filter (Durapore) was placed on the surface of an M9 minimal media agar plate and 10 μL of bacterial culture was spotted onto the filter. The plate was incubated at 37°C for 24 h and the filter was removed and submerged in 1 mL PBS buffer. The solution was vortexed vigorously to displace the bacterial colony from the filter into the solution, from which 100 μL was frozen at -80°C. The cells were defrosted and tested as described in '**2.14.2.2 Planktonic cells**'.

2.14.3 Motility assays

2.14.3.1 Twitching

Agar plates for the detection of twitching motility were prepared using 10 mL of 1.5% (w/v) LB or M9 minimal media agar into 10 cm diameter Petri-dishes. Single colonies were stabbed into the agar and incubated at 37°C for up to 48 h. Twitching was visualised through a halo of dispersion around the point of inoculation.

2.14.3.2 Swimming

Agar plates for the detection of swimming motility was prepared by pouring 25 mL of LB or M9 minimal media containing 0.3% (w/v) Bacto agar into 10 cm diameter Petri-dishes and dried at room temperature for 30 min. Bacterial cultures were normalised to an OD_{600} of 1, and 3 μL of culture was dispensed at the bottom of the plate. Swim plates were incubated for 8 – 18 h.

2.14.3.3 Swarming

For the detection of swarming motility, plates were prepared with 25 mL of LB or M9 minimal media containing 0.75% (w/v) Eiken agar in 10 cm diameter Petri-dishes and dried for 30 min at room temperature. Bacterial cultures were normalised to an OD_{600} of 1, and 5 µL was spotted onto the surface of the agar and left to soak in. Swarm plates were incubated at 37°C for 8 – 18 h.

2.14.4 Exoenzyme assays

2.14.4.1 Caseinase production

Skim milk agar plates were used for the detection of caseinase activity and were prepared with 25 mL of 50 g/L tryptic soy agar containing 2% (w/v) skimmed milk. Bacterial cultures were normalised to an OD_{600} of 1, and 5 µL was spotted onto the agar and left to soak in. Plates were incubated at 37°C overnight after which caseinase activity could be visualised through a proteolytic halo around the bacterial culture.

2.14.4.2 Gelatinase production

Gelatinase activity was measured on 1.6% (w/v) agar plates containing 13 g/L Nutrient broth and 30 g/L gelatin. Bacterial cultures were normalised to an OD_{600} of 1, and 5 µL was spotted onto the agar and left to soak in. Plates were incubated at 37°C overnight, at which point the plates were flooded with saturated ammonium sulfate solution for 15 min to improve visualisation of the proteolytic halo.

2.14.5 Aggregation assay

Auto-aggregation assays were adapted from Sherlock *et al*. (2005). Bacterial cultures were sub-cultured in 10 mL of fresh media and grown at 37°C to an OD_{600} of 0.8. The cultures were left to settle at room temperature without agitation for 3 h. From the top of the culture, 500 µL of the culture, representing the 'non-settled' fraction of the culture, was measured at OD_{600}. The culture was then vortexed vigorously

to disrupt cell aggregates and the OD_{600} was measured. The difference between the optical densities was then used to determine the percentage of aggregated cells within the culture.

2.14.6 Congo red assays

2.14.6.1 Plate assay

Agar plates for the detection of exopolysaccharide production were prepared with 37 g/L Brain Heart Infusion broth supplemented with 50 g/L sucrose, and 0.8 mg/mL Congo Red. Bacterial cultures were normalised to an OD_{600} of 1 and 10 µL was spotted onto the surface of the agar, and incubated at 37°C for 24 h. Congo red binds to polysaccharides and so exopolysaccharide production was visually determined qualitatively through the red pigmentation of the colony.

2.14.6.2 Liquid assay

To quantitatively assess exopolysaccharide production, bacterial cultures were sub-cultured in fresh growth media supplemented with 10 µg/mL Congo red and incubated at 37°C for 24 h on a rotating wheel. The OD_{600} was measured and the cells were pelleted in a centrifuge at 3200 x *g* for 10 min, at room temperature. Congo red bound to polysaccharides was sedimented out of the solution by centrifugation and the optical density of the supernatant at 495 nm was determined. The OD_{495} was normalised against the culture OD_{600}.

2.14.7 Light microscopy

Light microscopy images were obtained using an Olympus BX51 polarising microscope. Cells were grown overnight in the appropriate antibiotics and diluted by a dilution factor of 10^{-1}. From the diluted cell suspension, 5 µL was mounted onto a glass slide and visualised at a total magnification of 1000X.

2.14.8 Quorum sensing bioassay

Overnight cultures were normalised to an OD_{600} of 1. In a 96-well opaque microtitre plate, 30 µL of *P. aeruginosa* culture, or supernatant, was combined with an equal volume of the appropriate biosensor strain. JM109 (pSB1142) was used for OdDHL detection (Winson *et al.*, 1998), JM109 (pSB536) was used for BHL detection (Swift *et al.*, 1997) and PAO1-P*pqsA*::*lux* was used for PQS detection (Fletcher *et al.*, 2007). Plates were incubated at 37°C for 3 h and bioluminescence of the cultures was measured using the Lucy 1 (Anthos Labtec Instruments, Austria) for single point luminometry.

2.14.9 Statistical analysis

Where appropriate, statistical analysis of phenotypic observations were conducted using an unpaired *t*-test based on a two-tailed *p*-value. Significance was denoted on figures by the presence of asterisks, where * represents a *p*-value of <0.05, ** = <0.01 and *** = <0.0001.

2.15 Proteomic analysis

2.15.1 SDS-polyacrylamide-gel electrophoresis

Protein samples were prepared with loading dye and boiled at 95°C for 10 min. Samples were separated on 12% SDS-PAGE gels, prepared as described in Table 2.7. SDS-PAGE was run at 10 V cm^{-1} for 1.5 h. Gels were either stained with Coomassie or used for western blot analysis.

2.15.2 Coomassie staining

Gels were incubated overnight in Coomassie stain (1 g/L Coomassie Brilliant Blue G (Sigma), 50% v/v methanol, 10% v/v acetic acid) and destained for 30 min with Destain I (50% v/v methanol, 7% v/v acetic acid) and twice, for 30 min, with Destain II (10% v/v methanol, 7% v/v acetic acid). Protein sizes were determined by comparing migration against a Precision Plus Protein Standard (BioRad).

Table 2.7. Preparations for a 12% SDS-PAGE gel.

Gel Phase	Components per 10 mL
6% Stacking gel	2 mL 30% Bis-Acrylamide solution (Severn Biotech) 1 mL 5 X Stacking buffer 50 µL 20% (w/v) SDS 100 µL 8% (w/v) APS 5 µL Tetramethylethylenediamine
12% Resolving gel	4 mL 30% Bis-Acrylamide solution (Severn Biotech) 5 mL 5 X Resolving buffer 50 µL 20% (w/v) SDS 100 µL 8% (w/v) APS 5 µL Tetramethylethylenediamine

2.15.3 Western blot

Proteins were transferred from the SDS-PAGE gel onto a polyvinylidene difluoride (PVDF) membrane (high fluorescence) in 7 min using the Trans-Blot Turbo Transfer System (BioRad) with Trans-Blot Mini Transfer Packs.

The membrane was incubated in blocking buffer (5% w/v semi-skimmed milk powder) overnight, and then washed once in wash buffer (PBS and 0.1% v/v Tween 20). The membrane was incubated with a primary antibody, diluted in blocking buffer, for 1 h. The membrane was washed four times in wash buffer with 5 min incubations, before the addition of IRDye 680RD (Li-Cor) secondary antibody diluted in blocking buffer and incubation for 45 min. The membrane was washed as previously stated. All incubation steps involved gentle agitation throughout. The protein bands were detected using an Odyssey CLx imaging system (Li-Cor).

2.15.4 Secretome analysis

Strains were cultured to late exponential phase (OD_{600} of 0.6 – 0.8) in M9 minimal media supplemented with glucose and harvested by pelleting the samples in a centrifuge at 3200 x *g* for 30 min at 4°C. The supernatant was filter-sterilised using 0.2 µm

membrane filters (Millipore) and the protein was precipitated overnight at 4°C by adding 12.5% (w/v) trichloroacetic acid. Samples were centrifuged at 3200 x *g* for 40 min at 4°C. The protein pellets were washed three times in 80% (v/v) acetone and sedimented for a further 15 min at 21,000 x *g* in 2 mL microcentrifuge tubes. The pellets were air dried and resuspended in urea buffer (100 mM Tris-HCl, 6 M urea, 2 M thiourea, pH 8.0). The protein concentration was determined using the DC protein assay (Biorad). Peptides were separated by SDS-PAGE and stained with Coomassie.

2.15.5 Whole-cell protein extraction

Strains were cultured to late exponential phase (OD_{600} of 0.6 – 0.8) in M9 minimal media supplemented with glucose. Cell cultures (45 mL) were harvested at 3200 x *g* in a centrifuge for 30 min at 4°C, washed in PBS and sedimented a second time. Pellets were resuspended in 800 µL of lysis buffer and sonicated (3x 5 sec at 15 amps, MSE microtip). Cells were pelleted at 21,000 x *g* for 30 min at 4°C. The protein concentration of the supernatant was determined using the DC protein assay (Biorad).

2.15.6 Liquid chromatography-tandem mass spectrometry

LC-MS/MS was performed by the Cambridge Centre for Proteomics. Dried peptides were reconstituted in 100mM triethylammonium bicarbonate and labelled using 10-plex TMT (tandem mass tag) reagents according to the manufacturer's (Thermo Scientific) protocol. Tagged peptides were fractionated by reverse-phase chromatographyand were identified and quantified by a high resolution Orbitrap mass spectrometer coupled with Dionex Ultimate 3000 RSLC nano UPLC (Thermo Fischer Scientific). Proteomics data sets were analysed with the empirical Bayes moderated T-test implemented by the limma package (Ritchie *et al.*, 2015). P-values were corrected for multiple hypothesis testing using the Benjamini-Hochberg method (FDR ≤ 0.05). Differential expression was calculated on normalized $\log_2$ ratios (nano LC-MS/MS). The MS/MS fragmentation data was searched against the National Centre for Biotechnology Information (NCBI) database using MASCOT (Matrix Science) search engine.

2.16 Structural analysis

2.16.1 His-tagged EF-G expression

The *fusA1* and mutated *fusA1*-P443L genes were amplified using 'pET19m::*fusA1* Forward' and 'pET19m::*fusA1* Reverse', digested with *Nde*I and ligated into the vector pET19m. As the amplicon was only digested with one restriction enzyme, primers, 'Orientation check Forward' and 'Orientation check Reverse', were used to ensure that the gene was incorporated in the correct orientation downstream of the promoter. The expression vector was introduced into *E. coli* Rosetta cells by electroporation.

Rosetta cells were grown up in 1 L of LB supplemented with carbenicillin, and incubated at 37°C to an OD_{600} of 0.6 - 0.7. Isopropyl-β-D-thiogalactopyranoside (IPTG) was added to the cultures to a final concentration of 1 mM and the culture was incubated at 20°C for 24 hours. Cells were centrifuged at 3430 x *g*, for 20 min at 4°C. The cell pellet was resuspended in 10 mL lysis buffer and lysed by sonication (5x 30 sec at 13 amps), then centrifuged at 14,636 x *g* for 30 min, 4°C, to separate the cellular debris from the protein fraction within the supernatant. The supernatant was filtered through 0.45 μm membrane filters (Millipore).

2.16.2 EF-G protein purification

Cell lysates were loaded onto a Ni-NTA Superflow Cartridge (Qiagen) at 4°C. The column was equilibrated with protein purification buffer (Table 2.2) and the eluate profile of the sample was monitored using a high precision, multi-wavelength UV-Vis monitor (UPC-900) at 230, 250, 280 nm. Samples were eluted with elution buffer (Table 2.2).

The purified protein samples were concentrated using Vivaspin 20 columns (Sartorius) and dialysed by running 1 L of dialysis buffer (Table 2.2) through the Vivaspin columns. The concentration of the purified protein was measured on an Eppendorf Biospectrometer and stored at -80°C in dialysis buffer.

The actual protein concentration was determined using the extinction coefficient for EF-G.

$$protein\ concentration\ (M) = \left(\frac{mg\ ml^{-1}}{extinction\ coefficient}\right) X\ molecular\ weight$$

2.16.3 Structural prediction using tryptophan fluorescence

To analyse the intrinsic protein fluorescence, EF-G protein was diluted in 2 mL dialysis buffer to a final concentration of 0.8 µM. Fluorescence was measured in a quartz cuvette, on a FP-8300 Spectrofluorometer (JASCO) using an excitation wavelength of 295 nm and an emission wavelength of 305 - 400 nm (0.5 nm intervals, 100 nm/min, measurement in triplicate). Fusidic acid was titrated into the protein sample producing increasing final concentrations of 5 µM to 100 µM. The protein was incubated with fusidic acid for 1 min before measuring fluorescence.

One protein sample was tested per condition and the mean fluorescence measurement across three technical replicates was calculated using the Spectra Manager Suite (JASCO) and used to construct a fluorescence spectrum for each protein variant.

2.17 Transcriptomic analysis

2.17.1 RNA extraction

During the isolation of bacterial RNA, work was carried out in a sterile and RNase-free environment using RNase-free tubes and pipette tips.

Strains were cultured in M9 minimal media supplemented with glucose and samples were harvested at late exponential phase (OD_{600} of 0.6 – 0.8) into RNA Later (Ambion). The samples were incubated at 4°C for 15 min and pelleted at 21,000 x *g* for 20 min at 4°C. Total RNA was extracted using the RNeasy Mini Kit (Qiagen) and digested twice with on-the-column DNase I digestion, following manufacturer's guidelines. The concentration and purity of the RNA was measured using a NanoDrop ND-1000 Spectrophotometer. The absence of contaminating proteins and organic compounds was ensured by an $A_{260/280}$ ratio of 1.8 – 2.0 and $A_{260/230}$ nm of 2.0 – 2.2.

2.17.2 Quality checking RNA

To check for RNA degradation and DNA contamination, 2 µg of total RNA was run on a 1% agarose gel. Samples should have 2 clear bands representing the 23S and 16S ribosomal RNA. There should be no smearing below the 16S band which would indicate RNA degradation, and no high molecular weight bands representing gDNA or plasmid DNA contamination.

Using primers '*pslA* Forward' and '*pslA* Reverse' for amplification of the *pslA* gene, 0.5 µg of total RNA was used as the template for PCR, with gDNA as a negative control. In the absence of DNA contamination, no amplicon should be produced.

2.17.3 cDNA synthesis and RT-PCR

For complementary DNA (cDNA) synthesis, 1 µg of RNA was combined with 50 ng oligo(dT)$_{15}$, 300 ng random hexamers, 1 µL dNTP mix and heated at 65^{o}C for 5 min followed by incubation on ice for 2 min. To this, 4 µL of 5x SuperScript III First strand buffer, 1 µL 0.1 DTT and 1 µL SuperScript III Reverse transcriptase (Invitrogen) was added. Samples were incubated at 25^{o}C for 5 min, followed by incubation at 50^{o}C for 60 min. The reaction was inactivated at 70^{o}C for 15 min. cDNA was used as a template for RT-PCR following the program for a standard PCR reaction described in Table 2.5, but using 20 - 25 cycles.

2.17.4 RNA sequencing

Total RNA was sent to GATC Biotech for rRNA depletion and RNA-Sequencing using the Illumina platform (10 million reads per sample, single read, 1 x 50 bp). The RNA-Seq reads were processed using FastaQC and were mapped to the PAO1 genome and analysed using the Tuxedo Suite package. Differentially expressed genes were investigated. The principal component analysis plot and the volcano plots were constructed using R programming language.

Chapter 3

3. Identification of a *fusA1* mutation in *P. aeruginosa*

3.1 Introduction

Biofilms are widely recognised for harbouring antibiotic resistant bacteria that respond inconsistently to treatment and are excruciatingly difficult to eradicate completely (Milla *et al.,* 2014). So far, the molecular mechanisms that underpin the transition from planktonic growth into biofilm formation remain unclear. This is an important problem, as identifying global biofilm regulators may offer therapeutic opportunities for the treatment of chronic infection.

A key protein component of the biofilm matrix is the secreted adhesin, CdrA (cyclic diguanylate-regulated two-partner secretion, partner A). The two-gene, *cdrAB*, operon encodes the secreted adhesin, CdrA, and its transporter, CdrB. CdrA adds strength to the structural scaffold of the matrix by binding neighbouring matrix components together. Expression of the *cdrAB* operon is positively correlated with elevated levels of c-di-GMP, as are a variety of other biofilm-associated genes, such as the polysaccharide biosynthesis operons, *psl* and *pel*. Mutations in *cdrA* result in thin and poorly-structured biofilms, whereas overexpressing *cdrAB* has been found to increase biofilm formation up to six-fold (Borlee *et al.*, 2010). Proteolytic cleavage of CdrA can initiate biofilm dissemination, therefore linking this protein to multiple stages of biofilm development (Cooley *et al.*, 2015). Expression of *cdrA* was found to be up to 15-fold higher in biofilm cells when compared with planktonic cells (Borlee *et al*., 2010), and clinical isolates from CF patients have been found to produce the adhesin in abundance (Wolfgang *et al.*, 2003). These studies highlight its role in biofilm-mediated chronic infection and demonstrate the tight regulation of *cdrA* during biofilm-inducing conditions. Because of this, CdrA is an ideal target for monitoring the expression of biofilm-associated genes.

In this chapter, I used a *lacZ* reporter construct to monitor transcription from the *cdrA* promoter. I then attempted to use random mutagenesis to identify global regulators of biofilm formation in *P. aeruginosa* by measuring changes in *cdrA* expression.

3.2 *CdrA* expression in *P. aeruginosa*

3.2.1 Creation of a *cdrA* transcriptional reporter

To identify regulatory factors that might affect *cdrAB* transcription, a reporter strain was constructed to measure the activity of the *cdrA* promoter. This was achieved by use of a non-replicative mini-CTX-*lacZ* vector, for single-copy integration into the genome. The vector encodes an integrase which directs the recombination of the plasmid at a neutral site within the genome, located at the end of a tRNA^{ser} gene (Figure 3.1), which does not evoke downstream effects on neighbouring genes.

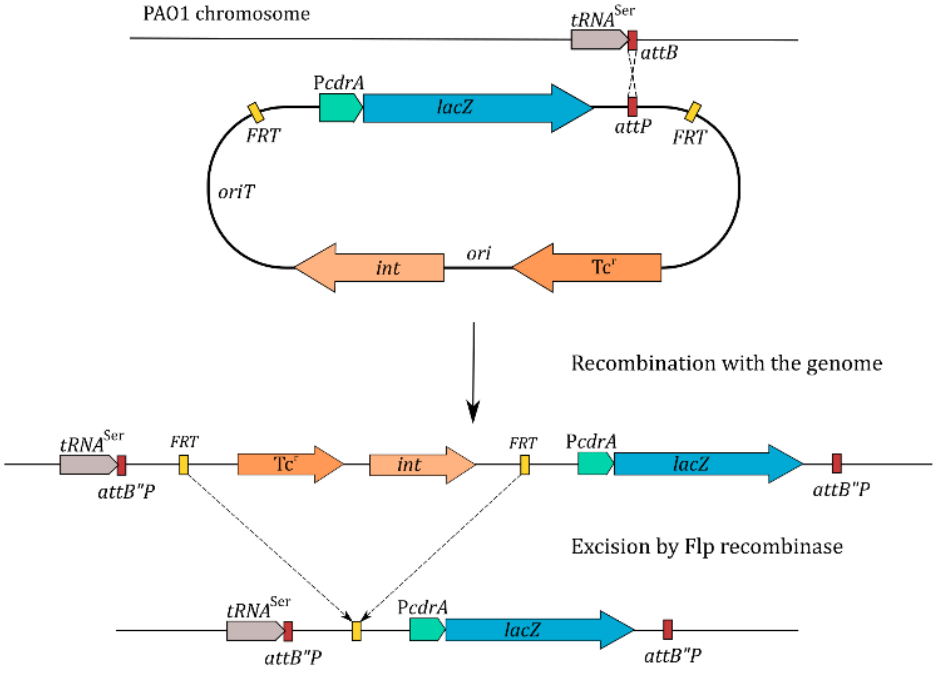

Figure 3.1. Integration of the mini-CTX-*lacZ* fusion vector into a neutral site within the PAO1 genome followed by the excision of the tetracycline resistance cassette and unwanted sequences at Flp recombinase target sites (FRT).

The promoter of the *cdrAB* operon is located directly upstream of the *cdrA* gene. A mini-CTX-*lacZ* construct was used which contained the *cdrA* gene promoter (referred to as P*cdrA*) subcloned into the multiple cloning site (MCS) of the vector, controlling transcription of the downstream *lacZ* gene. The transcriptional activity of P*cdrA* could

then be measured through the production and activity of the *lacZ* encoded protein, β-galactosidase.

The commonly used *P. aeruginosa* reference strain, PAO1, was transformed by electroporation with the mini-CTX-P*cdrA*-*lacZ* vector. Unwanted sequences, including the tetracycline resistance cassette, which were located between Flp recombinase target sites (FRT) were excised by introducing a pFLP2 plasmid encoding Flp recombinase. When verifying the position of the reporter construct by PCR-amplification, I discovered that the frequency at which the mini-CTX vector integrated into the genome at the correct location was low. This may have been due to non-homologous recombination at sites elsewhere in the genome, or the existence of mini-CTX as a non-chromosomal plasmid within the cell. A reporter strain, confirmed to contain the *lacZ* fusion gene downstream of $tRNA^{ser}$, was used in subsequent mutagenesis screens for isolating regulators of biofilm formation and will henceforth be referred to as PAPcdr.

3.2.2 β-galactosidase expression *via* P*cdrA*

The activity of the *cdrA* promoter in the reporter construct is reflected in the production of β-galactosidase, encoded by the *lacZ* gene. Adding the β-galactosidase substrate, X-gal, to growth medium allowed me to measure the level of β-galactosidase produced by the reporter strain under different growth conditions. X-gal is hydrolysed by β -galactosidase to yield galactose and 5-bromo-4-chloro-3-hydroxyindole, the latter of which spontaneously dimerises and oxidises into an insoluble blue product (Burn, 2012). The level of blue pigmentation produced by a colony corresponds to the level of β -galactosidase synthesised and, in the case of the P*cdrA*-*lacZ* fusion, will reflect the activity of P*cdrA*. The activity of P*cdrA* may provide an indication of active biofilm formation and may be reflected in the activity of other biofilm-associated genes. PAO1 containing an empty vector control (a promoter-less mini-CTX-*lacZ* construct integrated at $tRNA^{ser}$ within the genome) did not produce the distinctive blue colouration in the presence of X-gal, verifying that pigmentation of the PAPcdr strain was a result of P*cdrA* activity.

PAPcdr was grown on a variety of carbon sources, supplemented with X-gal, to assess the optimal conditions for activating expression at a basal level. M9 minimal

medium allowed for the greatest level of control when manipulating carbon sources and its pale, translucent consistency was best suited for visualisation of β-galactosidase activity on agar plates. Richer media, such as LB Lennox, Nutrient broth, Brain and Heart infusion broth and Tryptic soy broth were also assessed, but colouration of the media distorted colony pigmentation and so they were not used for these purposes in further investigations.

Where growth on a rich solid medium, such as LB, can take between 18-24 hours, up to 48 hours of incubation was required for growth on minimal medium. This duration also varied with the carbon source and its concentration. The expression of *cdrA* was assessed in response to growth on 24 different carbon sources, each at a fixed concentration of 0.5% (w/v), for up to 48 hours (Table 3.1).

Table 3.1. The effect of different carbon sources (0.5% w/v) on the growth and *lacZ* expression of PAPcdr on M9 minimal media supplemented with X-gal.

Growth defective	Low expression	Low-moderate expression	Moderate-high expression
Arabinose	Alanine	Acetate	Ethanol
Lactose	Arginine	Manitol	Gluconic acid
Mannose	Glycerol	Tryptone	Glucose
Methionine	Sucrose		Glutamic acid
Rhamnose			Mucin
Ribose			Sodium Fumarate
Sorbitol			Sodium Succinate
Xylose			

Some carbon sources, such as lactose and ribose, were not sufficient for growth and the reduced colony size meant that β-galactosidase expression could not be reliably gauged. The biofilm-inducing environment of the CF lung is highly oxygen-limited, however, when cultured under microaerophilic conditions the colonies grew very slowly across all carbon sources making it unsuitable for high throughput screening. A subset of

carbon sources, in which growth was unaffected under aerobic conditions, were found to elicit moderate to high levels of *cdrA* expression, appropriate for analysing changes to expression. However, carbon sources such as sodium fumarate, sodium succinate, gluconic acid and glutamic acid, induced the production of the blue-green secondary metabolite, pyocyanin. Secretion of pyocyanin into the surrounding media masked the colouration of the X-gal catabolite, producing ambiguous results. By a process of elimination, glucose was the best candidate for measuring P*cdrA* activity, as the colonies grew robustly, with no effect on pyocyanin production, and induced sufficient levels of *cdrA* expression for subsequent analysis.

3.3 Identifying regulators of *cdrA*

3.3.1 Plasposon mutagenesis

To identify genes that potentially regulate *cdrA* expression, and may therefore impinge on biofilm formation, a mutant library was created by random transposon mutagenesis using the pTn*Mod*-OGm plasposon (Dennis *et al.*, 1998). This plasposon undergoes a single, stable, and non-specific integration into the PAO1 genome affecting the expression of any disrupted gene. pTn*Mod*-OGm was introduced into PAPcdr via bi-parental conjugation and successful conjugants were isolated using gentamicin selection. Conjugants were screened for abnormal *cdrA* expression on X-gal supplemented glucose plates. Colonies that appeared hyper-blue (caused by an overproduction of β-galactosidase) and those that displayed a paler pigmentation (hypo-production) were further analysed in planktonic culture. Activity in planktonic culture could be monitored by measuring the relative fluorescence of another β- galactosidase substrate, 4-methylumbelliferyl-β-D-galactoside.

One of the isolated transposon mutants (Tn-*PAPcdr*) had a pale appearance on solid media when compared with the progenitor strain (Figure 3.2A). The reduction in P*cdrA* activity was consistent when the strain was grown as a planktonic culture in glucose-supplemented minimal medium. Here, the transcriptional activity of *cdrA* was reduced by up to a third in late exponential phase (Figure 3.2B).

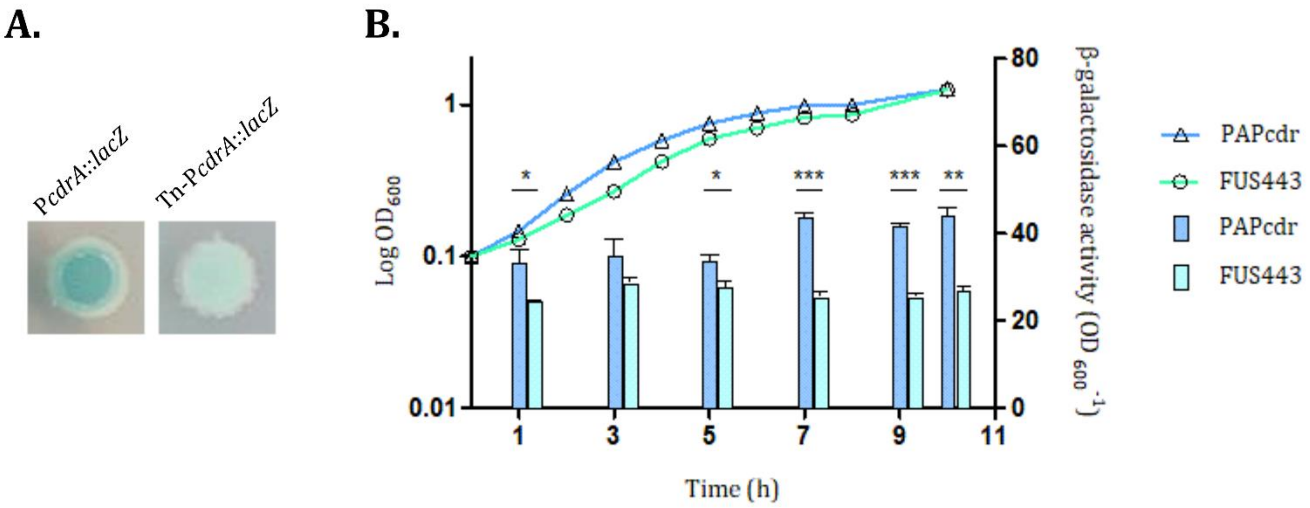

Figure 3.2. β-galactosidase activity in the PAPcdr reporter strain and activity after the introduction of a random transposon insertion (Tn-PAPcdr). β-galactosidase activity was **(A)** visualised by growth on X-gal supplemented solid media and **(B)** measured through the production of a fluorescent product during planktonic growth, relative to optical density. Statistical significance between groups was assessed by an unpaired *t*-test (n=3) (* = p <0.05, ** = p <0.01, *** = p <0.001).

To identify the location of the transposon within the Tn-PAPcdr mutant genome, three approaches were taken. Firstly, a nested-PCR amplification technique was attempted, using primers to read outward from the transposon insert in conjunction with random hexamers. Sequencing the amplicon would identify which gene had been disrupted by the transposon. This method failed to amplify any flanking DNA surrounding the insert. Secondly, I used a replicon-cloning based technique, as described by Dennis and Zylstra (1998), whereby genomic DNA was fragmented and self-ligated to produce circularised mini-chromosomal fractions. These were introduced into *E. coli* and colonies transformed with DNA containing the insert were selected for, using gentamicin. Again, this method was unsuccessful and produced no viable colonies. Finally, a whole genome sequencing approach was used to map the mutant genome and identify the transposon position.

3.3.2 Whole genome sequencing

The genome of the Tn-mutant strain and of the progenitor strain were analysed by whole genome sequencing, which confirmed that the mini-CTX-P*cdrA*::*lacZ* reporter construct had integrated correctly at the specified neutral site. Interestingly, the transposon was absent from the genome of the mutant strain explaining why the previous approaches to identification had failed. This now posed the question of how the isolated mutant acquired gentamicin resistance and exhibited changes in *cdrA* expression if not due to gene disruption by the plasposon insert? To answer this, the mutant genome was analysed for changes that might have given rise to the observed phenotypes. In doing so, numerous single nucleotide polymorphisms (SNP), inversions, deletions and insertions were identified. Closer investigation of these alterations, by PCR amplification and sequencing, revealed that almost all of the apparent mutations were in fact errors occurring from poor quality sequence reads at the end of sequence contigs, a common limitation with whole genome sequencing. From all the identified genome variations only one mutation was confirmed to be real. This was a SNP within the *fusA1* gene, conferring a cytosine to thymidine transition (Figure 3.3). This mutation resulted in a proline to leucine conversion at amino acid 443 of the encoded peptide sequence. This mutant strain is henceforth referred to as FUS443 and the non-mutated progenitor strain, I will continue to call PAPcdr.

```
fusA1       1261 GAGCCGAAGACCAAGGCTGACCAGGAGAAGATGGGTATCGCCCTCGGCAAGCTGGCCCAG
fusA1-P443L 1261 GAGCCGAAGACCAAGGCTGACCAGGAGAAGATGGGTATCGCCCTCGGCAAGCTGGCCCAG

fusA1       1321 GAAGACCCGTCGTTCCGTGTCAAGACCGACGAAGAGTCCGGTCAGACCATCATCTCCGGC
fusA1-P443L 1321 GAAGACCTGTCGTTCCGTGTCAAGACCGACGAAGAGTCCGGTCAGACCATCATCTCCGGC

fusA1       1381 ATGGGCGAGCTGCACCTGGACATCATCGTCGACCGCATGAAGCGCGAGTTCGGCGTCGAG
fusA1-P443L 1381 ATGGGCGAGCTGCACCTGGACATCATCGTCGACCGCATGAAGCGCGAGTTCGGCGTCGAG
```

Figure 3.3. Alignment of the *fusA1* gene from PAO1 with the FUS443 mutated isolate. Alignment shows a cytosine to thymidine transition resulting in a proline to leucine conversion within the amino acid sequence.

3.4 Elongation factor G

3.4.1 Computational structural analysis

The *fusA1* gene encodes elongation factor G (EF-G). As the name suggests, EF-G is vital in the elongation step of translation and coordinates the translocation of mRNA and aminoacyl-tRNA through the ribosome during extension of the peptidyl chain. The crystal structure of EF-G from *P. aeruginosa* has been determined by Nyfeler *et al.* (2012), and was used in this study to identify the position of the P443L mutation within the tertiary structure.

The proline to leucine transition at amino acid 443 was positioned between an alpha helix and beta strand in domain III of EF-G (Figure 3.4). Proline residues are known to provide flexibility to a structure and can induce kinks into the peptide chain, making them a common residue at turn positions within the protein. Introducing a leucine residue at this position is likely to reduce these flexible properties and alter the conformation of the structure. Position 443 also marks an exposed residue, located within a fusidic acid binding pocket.

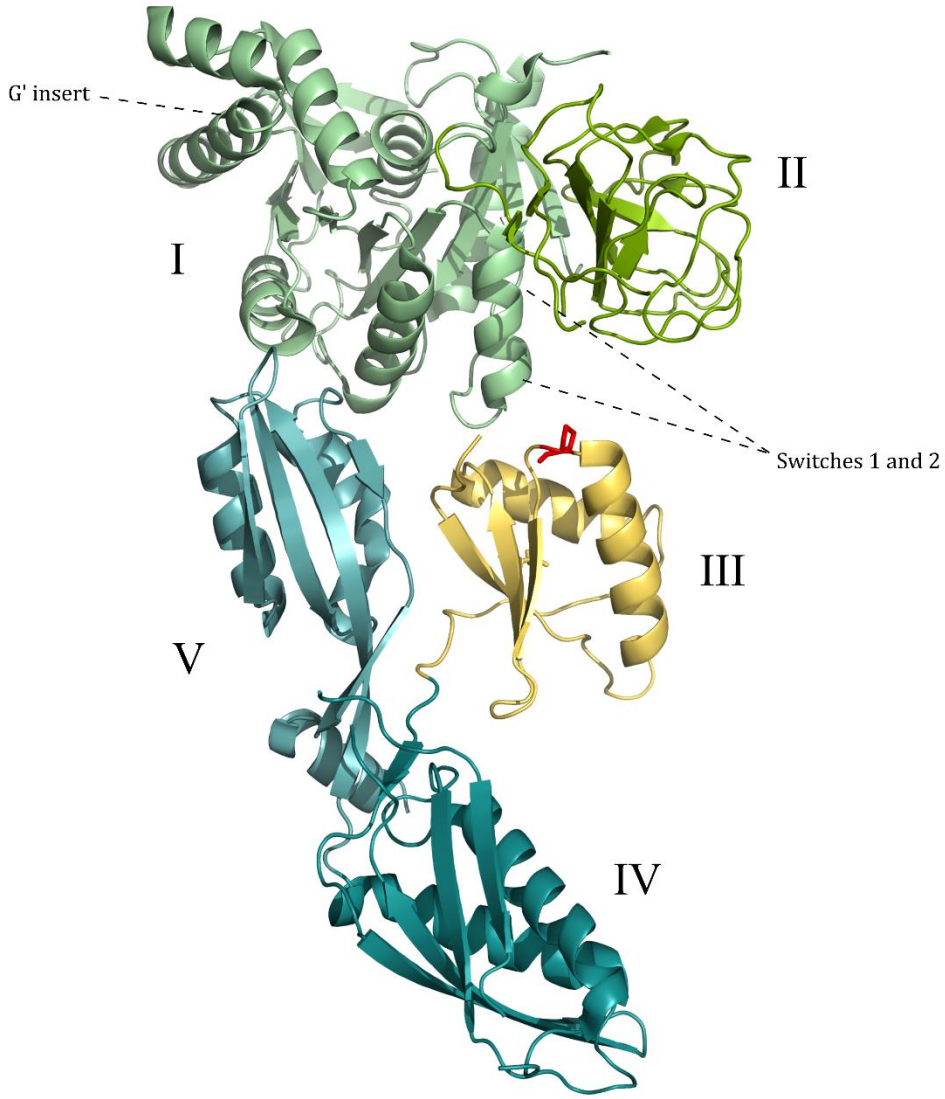

Figure 3.4. Crystal structure of elongation factor G (determined by Nyfeler *et al*., 2012), consisting of five domains. The proline residue highlighted in red shows the position of the 443 proline to leucine transition in the FUS443 mutant.

The GTPase activity of EF-G occurs in domain I, with switch 1 and switch 2 motifs situated opposite proline 443. Switch motifs undergo conformational changes that direct the 'switch' between GTP and GDP and therefore determine the GTPase activity (Vetter, 2014). Due to the close proximity of P443L to these switch domains, it is possible that the dynamics of these switches are disrupted, affecting the ability to recycle GTP. To predict the effect that the mutation might have had on the protein structure, I used a program

called mCSM (Pires *et al.*, 2014), which predicts the impact of a mutation on protein stability and interactions, relying on graph-based signatures. The P443L mutation was predicted to have a destabilising effect on the protein structure (-0.267 kcal/mol) and a destabilising protein-protein affinity change (-0.324 kcal/mol).

I-TASSER was used to generate a 3D structure model of the mutated EF-G protein based on the changes in the amino acid sequence. The predicted structure aligned almost perfectly with the published EF-G structure and the turn between the alpha helix and beta strand was maintained with only minor steric alterations to the neighbouring residues (Figure 3.5).

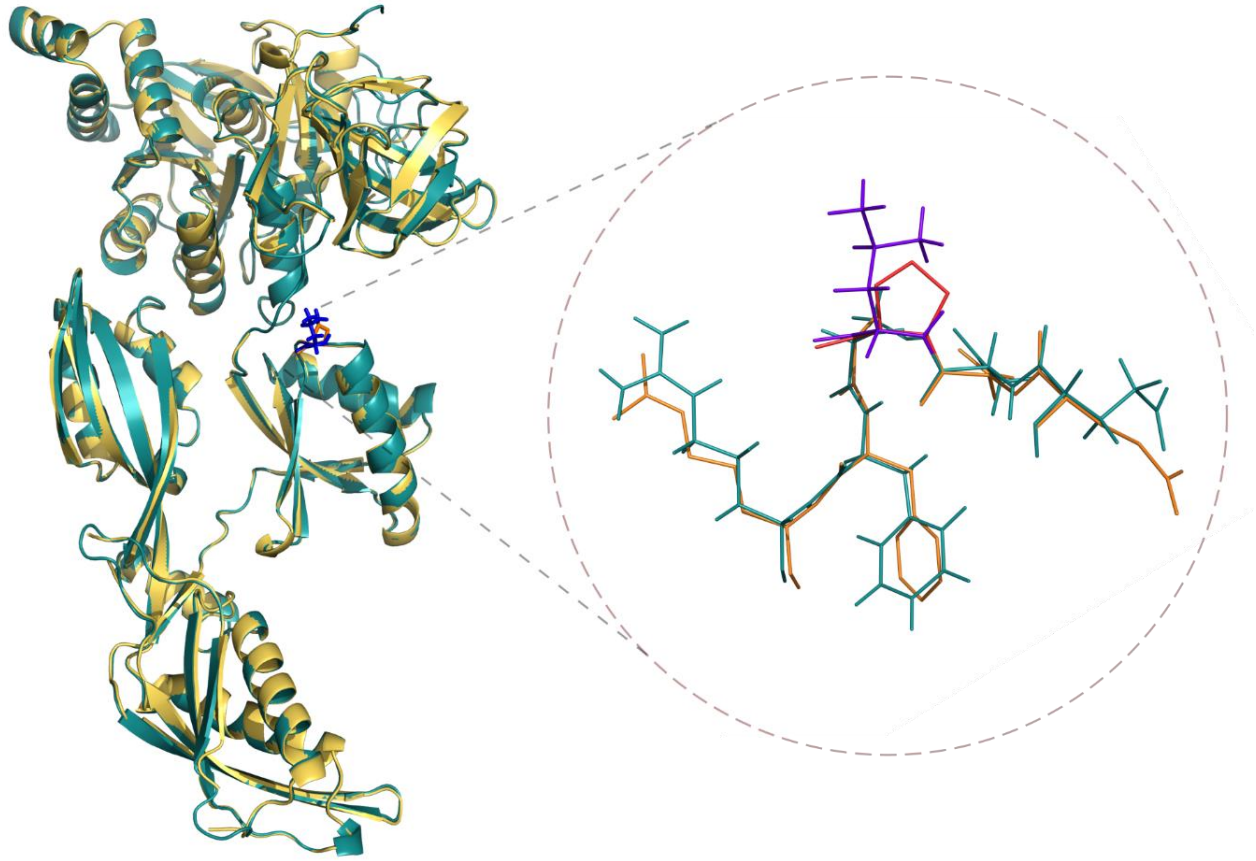

Figure 3.5. Alignment of the mutated EF-G protein structure (teal, with leucine residue 443 in blue) with the published native EF-G protein (yellow, with proline residue 443 in red).

EF-G has two conformations; the un-bound protein adopts a compact structure, but this becomes elongated when bound to the ribosome. The Nyfeler protein crystal structure and I-TASSER-predicted mutant structure are based on the elongated form. It is possible that the mutation may have structural implications on its compact form or during the transition between structural states.

3.4.2 Intrinsic tryptophan fluorescence

Amongst the three fluorescent amino acids (phenylalanine, tyrosine and tryptophan), tryptophan provides the biggest contribution to intrinsic protein fluorescence. Tryptophan is extremely sensitive to its microenvironment and changes to the fluorescent spectra often reflect changes within the protein structure therefore making this a simple, but highly sensitive tool, to measure changes in protein conformation (Ghisaidoobe *et al.*, 2014).

The wild type (WT) and mutated *fusA1* genes from *P. aeruginosa* were expressed in *E. coli* and the WT EF-G and mutant EF-G proteins were purified and verified by SDS-PAGE and Coomassie staining. EF-G has five tryptophan (Trp) residues, Trp-72, Trp-127, Trp-193, Trp-218 and Trp-519. Trp-218 and Trp-519 are exposed on the surface, Trp-193 is partially exposed and Trp-72 and Trp-127 are internalised within the protein. The Trp fluorescence spectra of the WT and mutant protein were measured between 305 nm to 400 nm. The maximum emission (λ_{max}) of the WT EF-G was 333 nm, and was 332.5 nm for the EF-G-P443L protein. However, the fluorescence intensity at λ_{max} was 21.6% lower for EF-G-P443L than the WT protein (Figure 3.6A).

Shifts in λ_{max} are associated with changes in the exposure of tryptophan residues to the surrounding solvent, whilst changes to the intensity of fluorescence can be caused by changes in the microenvironment of the tryptophan. This suggests that the P443L mutation did not cause large structural rearrangements in the protein, but instead, led to smaller adjustments as proposed by the I-TASSER structural prediction.

The P443L mutation in EF-G resides within the fusidic acid binding pocket. To investigate whether the binding of fusidic acid was affected by the mutation, various concentrations of fusidic acid, ranging from 0 μM to 200 μM, were added to 0.8 μM of

EF-G protein. The intrinsic fluorescence intensity was quenched in both the WT EF-G protein and the mutant variant in a dose-dependent manner by fusidic acid (Figure 3.6B). Quenching is a process which reduces the intensity of the fluorescence. This occurs through contact between an excited fluorophore and another molecule which facilitates non-radiative transitions to the ground state. The addition of 200 μM of fusidic acid reduced the fluorescence intensity of the WT protein by 23.8% and the mutated protein by 26.8%.

The efficiency of fusidic acid as a quencher was demonstrated using a Stern-Volmer plot, where the y axis shows the decrease in emission intensity (Figure 3.6C). Initially, quenching occurred rapidly at low concentrations but a less steep gradient was observed at concentrations exceeding 40 μM of fusidic acid titration. This is typical of a non-linear Stern-Volmer plot and is reflective of the subpopulations of trytophans within EF-G which are positioned with varying accessibilities to the quencher. Similar quenching patterns of EF-G and EF-G-P443L suggest that the ability to bind fusidic acid is retained, however, the Trp fluorescence of EF-G-P443L was quenched to a greater degree highlighting variations in their structural composition and their interaction with fusidic acid.

It is highly likely that these minor steric changes could affect the function of EF-G, perhaps by altering protein flexibility or its interaction with the ribosome. This could therefore manifest in changes to gene expression, such as that seen with P*cdrA* activity.

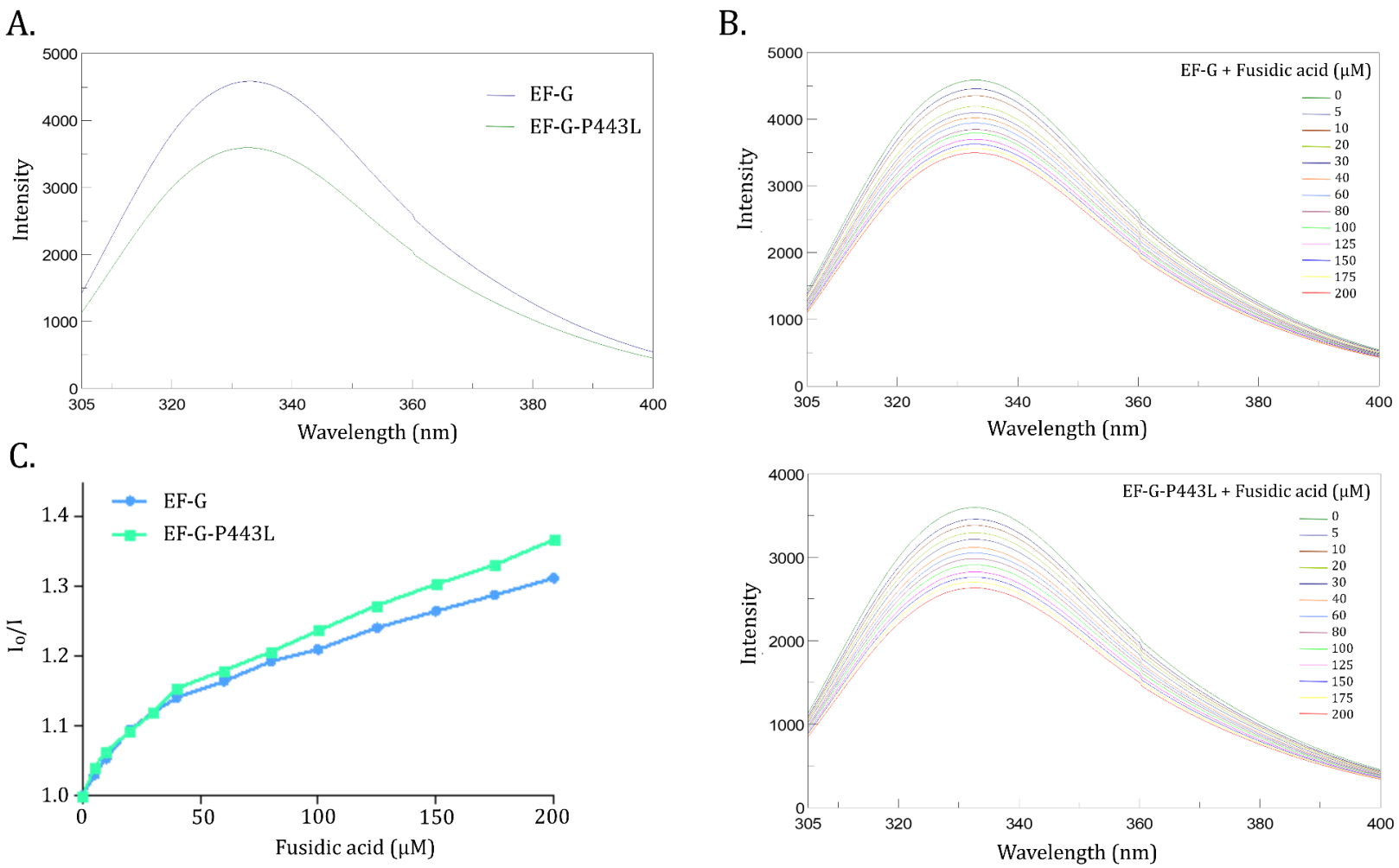

Figure 3.6. Intrinsic tryptophan fluorescence using an excitation wavelength of 295nm and emission as recorded in figure for **(A)** EF-G and EF-G-P443L protein variants, and **(B)** EF-G and EF-G-P443L with increasing concentrations of fusidic acid (0-200 μM) revealing a reduction in fluorescence intensity. **(C)** Stern-Volmer plot for the interaction of EF-G protein variants with increasing concentrations of fusidic acid, highlighting a greater level of fluorescence quenching by fusidic acid on the EF-G-P443L protein variant. Results represent one protein sample measured in triplicate.

3.5 Characterisation of FUS443

3.5.1 Elongation factor G and the biofilm matrix

The FUS443 mutant was assessed for phenotypic changes to the cell, to help identify which signalling networks might be affected by the mutated EF-G.

Initial tests on P*cdrA* activity in planktonic culture revealed that FUS443 had a small growth defect in minimal medium (Figure 3.2). The mutant was grown in LB to see if the growth defect remained when the culture was provided with a richer medium. Unexpectedly, the growth defect of FUS443 was even more prominent in LB, particularly throughout the exponential phase of growth (Figure 3.7). The initial doubling time of PAPcdr over the first two hours of growth was 32.5 min, whereas the doubling time was twice as long in FUS443 at 63.8-69.5 min, maintained over 6 hours of growth.

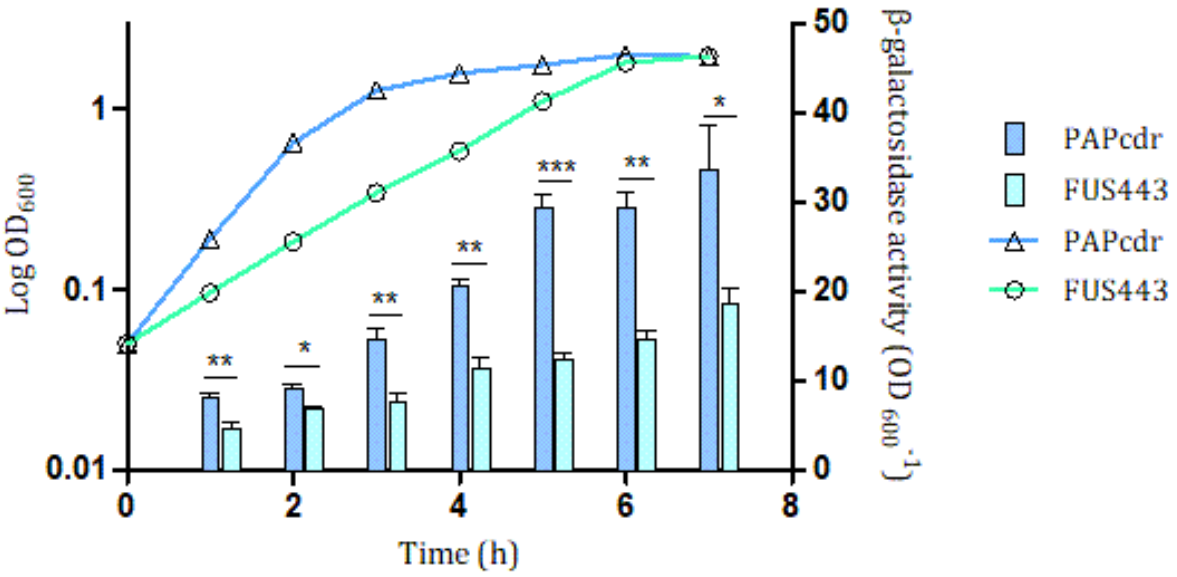

Figure 3.7. Transcriptional activity of the *cdrA* promoter in the mutant FUS443 strain and progenitor strain, PAPcdr, grown in LB and measured through β-galactosidase activity, relative to growth. Statistical significance between groups was assessed by an unpaired *t*-test (n=3, * = p <0.05, ** = p <0.01, *** = p <0.001).

P*cdrA* activity remained at a significantly lower level in the mutant strain during late exponential-stationary phase, at almost half of that observed in the progenitor strain. This suggested that the effect on *cdrA* expression associated with the P443L mutation in EF-G was nutrient-independent and occurred during both growth conditions.

The prominent role CdrA plays in maintaining the biofilm structure meant that it was important to determine whether the reduced *cdrA* expression in FUS443 also impacted on the ability to form robust biofilms. Biofilm formation was measured by growing cultures in microtitre plates. The biofilms formed on the sides of the plastic wells which were stained with crystal violet and quantified by measuring the absorbance at 595 nm. I found that the mutation had no significant effect on the formation of biofilms, both in minimal medium ($t(22)=1.26$, $p=0.219$) and in LB ($t(30)=0.52$, $p=0.610$) (Figure 3.8). This result suggested that either the reduction in *cdrA* expression was not severe enough to negatively impact biofilm formation or that the biofilm was stabilised by compensatory mechanisms, such as the up-regulation of alternative matrix components.

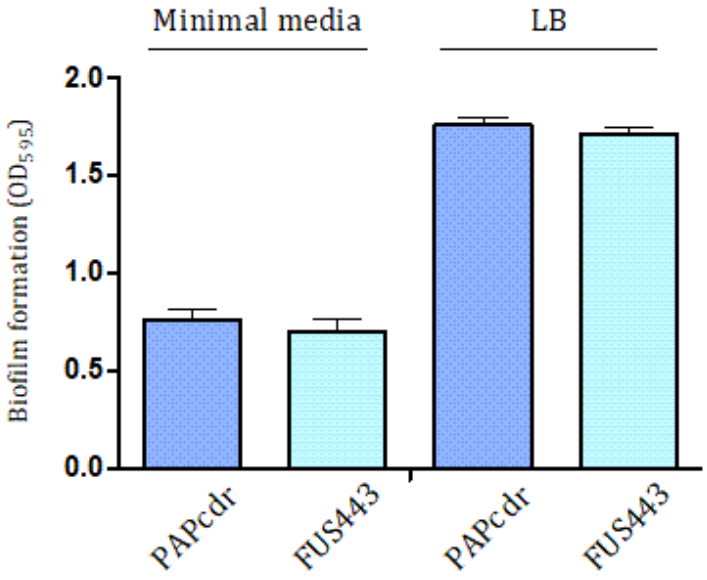

Figure 3.8. Biofilm formation of the FUS443 mutant and progenitor strain PAPcdr in microtitre plates, quantified by staining with crystal violet and measuring absorbance at 595 nm.

To investigate the possibility that other matrix components were maintaining the biofilm in the absence of CdrA, the level of polysaccharide secretion was measured using the polysaccharide-binding dye Congo red. When grown on solid medium supplemented with Congo red, the FUS443 mutant had a dark red pigmentation, whereas the progenitor strain appeared paler. This indicated an increase in the production of exopolysaccharides in FUS443 (Figure 3.9A). In planktonic culture, polysaccharide-bound Congo red can be separated from the supernatant by centrifugation and provides an indication of the level of polysaccharide produced by the cells. The FUS443 culture supernatant had a significantly lower absorbance at 495 nm ($t(10)=5.064$, $p=0.0005$), indicating a decrease in residual free Congo red and therefore an increase in exopolysaccharide production when compared with the progenitor strain (Figure 3.9B). Together these findings provide evidence that the P443L mutation is having pleiotropic and converse effects on numerous biofilm-associated genes, which may explain why biofilm formation is not affected by the reduction in *cdrA* expression.

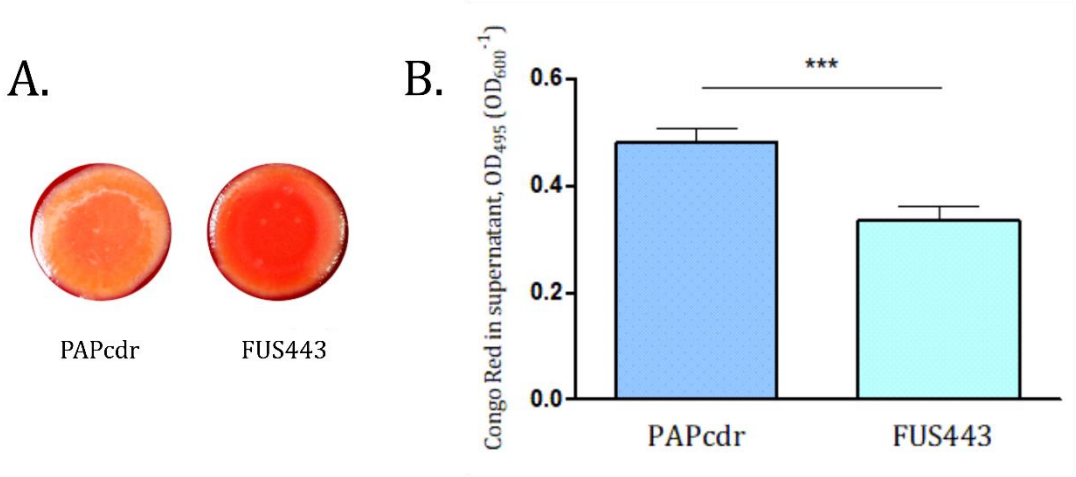

Figure 3.9. Exopolysaccharide production was increased in the FUS443 mutant. **(A)** The redder pigmentation of the FUS443 colony indicated increased binding by the polysaccharide-binding dye, Congo red. **(B)** Reduced levels of Congo red in the supernatant of the mutant strain highlighted an increase in polysaccharide production. Readings were normalised relative to growth (method as described in Ma *et al*. 2006). The data represents the measurements from three biological replicates and two technical replicates. Statistical significance between groups was assessed by an unpaired *t*-test (n=6, *** = p <0.001).

3.5.2 Quorum sensing

Quorum sensing (QS) is a bacterial system used to regulate gene expression in response to population density. Biofilm formation and virulence are amongst the phenotypes that can be regulated by this system. *P. aeruginosa* produces three main QS molecules, PQS, OdDHL and BHL. To investigate whether the mutated EF-G protein affected QS, bioluminescent reporter strains were used to detect the presence of QS molecules secreted into the medium by the *P. aeruginosa* strains. Initial experiments were conducted in LB where the reporter strains for PQS, OdDHL and BHL were co-cultured for three hours with PAPcdr or FUS443, and the QS levels for each were recorded. There was very little difference in the levels of PQS produced by the progenitor and mutant strain, but a significant increase in the production of BHL ($t(10)=20.00$, $p=<0.0001$) and OdDHL ($t(10)=4.35$, $p=0.001$) was observed in the FUS443 culture (Figure 3.10A). To account for differences in growth rate that could have occurred during incubation of the co-culture, cell-free supernatant was incubated with the reporter strains instead. In doing so, the differences between the mutant strain and progenitor were abolished (Figure 3.10B). When the same experiment was conducted with bacterial co-incubation in minimal medium the general abundance of QS molecules was reduced in both strains. Intriguingly, the difference between the OdDHL levels that was observed in the LB culture was no longer apparent, and the difference in BHL secretion was reduced. In fact, an increase in PQS synthesis was observed (Figure 3.10C).

The abundance of QS molecules differed considerably between conditions and so no direct comparison should be made between the different graphs. The level of QS signalling was greatest in the LB culture conditions. The fall in abundance seen in the supernatant condition is likely due to the absence of a cell culture continually synthesising new signalling molecules throughout the co-culture incubation period. The minimal media condition saw the lowest level of QS signalling, which may be due to the lower cell density or repression of QS systems in nutrient-limited conditions. The levels of OdDHL were particularly low in minimal media suggesting that the *las* system, which synthesises OdDHL, is inactivated or repressed under these conditions.

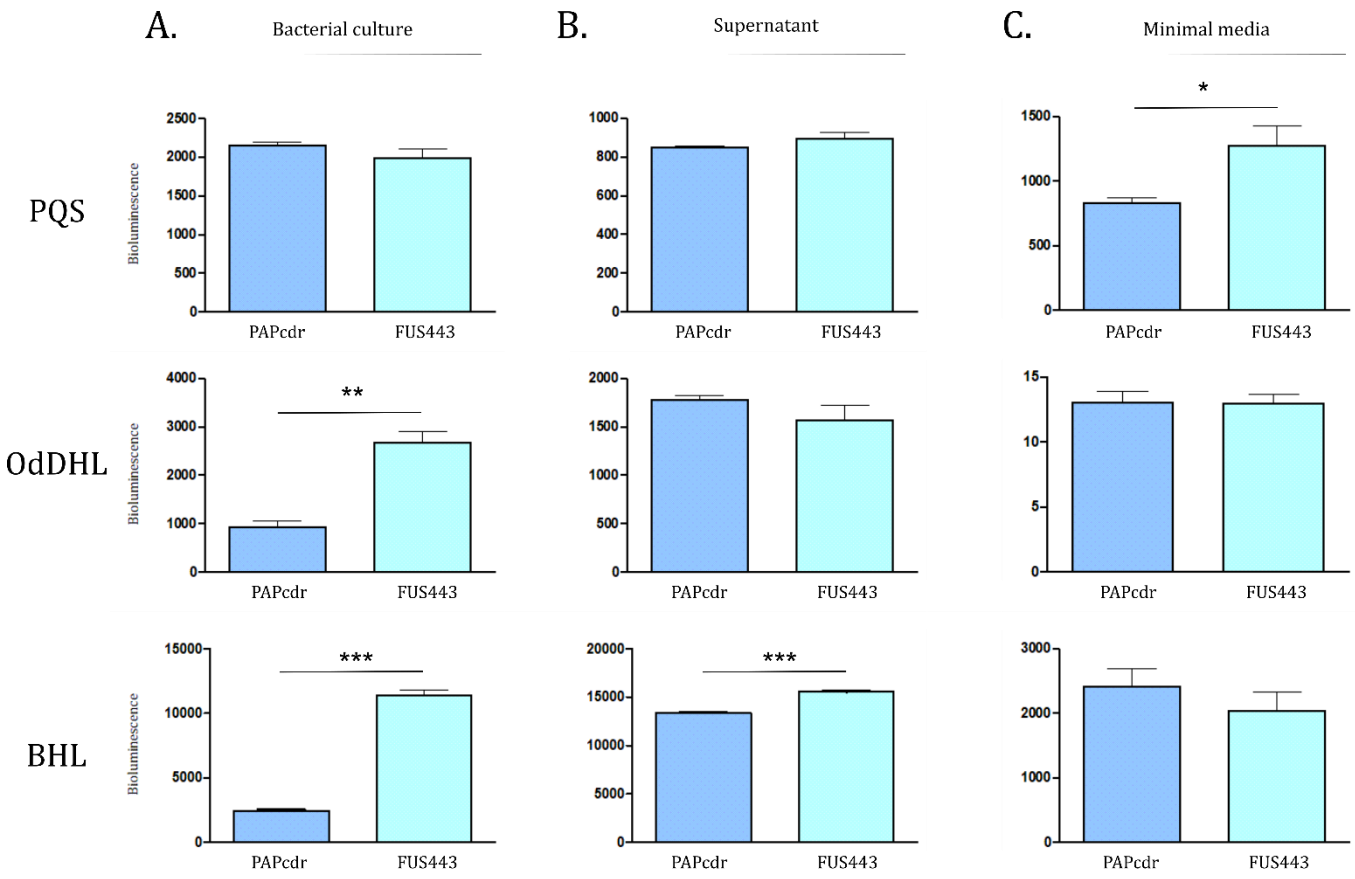

Figure 3.10. Secretion of quorum sensing molecules of PAPcdr and FUS443 during planktonic growth, measured through bioluminescence of reporter strain for PQS, OdDHL and BHL after **(A) i**ncubation of PAPcdr and FUS443 bacterial cultures, grown in LB, with reporter strains, versus **(B)** incubation of the reporter strains with the cell-free supernatant of the *P. aeruginosa* cultures. **(C)** Incubation of PAPcdr and FUS443 bacterial cultures, grown in minimal media, with reporter strains. Statistical significance between groups was assessed by an unpaired *t*-test (n=3) (* = p <0.05, ** = p <0.01, *** = p <0.001).

The PQS reporter is a *P. aeruginosa* strain which is unable to synthesise its own PQS. The reporters for OdDHL and BHL are both *E. coli* strains. As the *P. aeruginosa* PQS-reporter was unaffected by the use of cell culture or supernatant, it was postulated that the *P. aeruginosa* culture was out-competing the *E. coli* OdDHL- and BHL-reporters during incubation. If this was true, the data suggested that the mutant strain was less virulent than the progenitor strain, leading to the increased survival of *E. coli* and therefore a

higher level of bioluminescence than in the progenitor co-culture. This does not, however, explain why this was only observed in the LB growth condition.

To test inter-bacterial virulence, *E. coli* colony counts were taken after three hours of co-culture with the *P. aeruginosa* strains in LB and compared with a culture of *E. coli* grown in the absence of *P. aeruginosa*. At 0 hours the *E. coli* culture contained a high density of $5.6x10^8$ CFU. During the three hours of incubation, this was increased to $6.5x10^8$ CFU in the *E. coli* only condition and co-culture with *P. aeruginosa* reduced the CFU to $2.2x10^8$ and $1.4x10^8$ with PAPcdr and FUS443, respectively (Figure 3.11). Whilst there was evidence of some bacterial competition, an unpaired *t*-test concluded that there was no significant difference in the survival rate of *E. coli* when incubated with the progenitor or mutant strain (p=>0.05). This indicated that the two strains exhibited similar levels of virulence towards other bacterial species and suggested that the increase in QS molecules in the mutant strain was dependent upon a cell-cell interaction between *P. aeruginosa* and *E. coli*, specifically in LB.

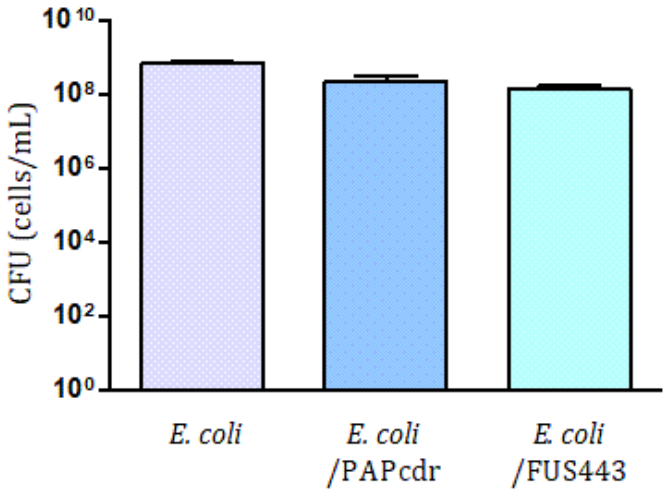

Figure 3.11. Colony counts of an *E. coli* population after three hours of co-culture with *P. aeruginosa* strains in LB show a similar level of interspecies competition when incubated with PAPcdr or FUS443. Values represent the average cell count of three biological replicates.

3.5.3 Stability of the P443L mutation

The growth defect elicited by the P443L mutation suggested that the mutated protein caused the cell to function at a sub-optimal level and was therefore costly to the cell. Costly mutations put pressure on the gene to revert back to its WT form or develop bypass mutations to counteract the cost. Because of this, I was interested to see whether the P443L mutation would be stable in the genome across numerous bacterial generations.

A planktonic culture of the FUS443 mutant was grown overnight in the absence of antibiotics. It was then serially diluted and plated onto antibiotic-free minimal media plates and grown overnight. The same planktonic culture was also sub-cultured into liquid media and grown for a further 24 hours, at which point the procedure was repeated, until a final 72-hour culture was plated. FUS443 was gentamicin resistant and so 40 colonies from each plate were transferred to minimal media plates supplemented with gentamicin, and the emergence of gentamicin sensitive colonies was recorded (Table 3.2).

Table 3.2. The emergence of gentamicin sensitive colonies in the FUS443 strain after growth in the absence of antibiotic selection.

Duration of planktonic growth (hours)	Colonies screened	Gentamicin sensitive colonies
24	40	0
48	40	1
72	40	5

As the cells were passaged, six colonies developed gentamicin sensitivity. The *fusA1* gene from each sensitive colony was PCR-amplified and sequenced. In all six colonies, the P443L mutation had been retained. This data suggested that, even in the absence of antibiotic selection, the P443L mutation provided some benefit to the cell and was worth maintaining. The gentamicin sensitivity was likely to have arisen from

additional mutations in the genome that counteract any negative or energetically expensive effects of the *fusA1* mutation, including unnecessary resistance mechanisms.

3.6 Complementation of the *fusA1* mutation

3.6.1 pUCP20 and cell-aggregation

To verify that the observed phenotypes are indeed a result of the mutation in *fusA1*, a WT copy of the *fusA1* gene was introduced into the mutant strain *via* a complementation vector. The complementation vector was constructed by sub-cloning the WT *fusA1* gene into the MCS of the pUCP20 vector, placing it under the control of a *lac* promoter. The complementation vector (thus referred to as p*fusA1*) was introduced into FUS443 and the progenitor strain, PAPcdr. To control for any effects caused by the presence of the plasmid alone, empty pUCP20 plasmids were also introduced into the two strains to serve as references.

The strains were grown in planktonic culture to assess whether the p*fusA1* plasmid reduced the growth defect observed in the mutant strain. Cultures were grown in the presence of carbenicillin to maintain the replication of the plasmid, however, it became evident that the FUS443 strain containing the empty vector formed prominent aggregates (Figure 3.12). An unpaired *t*-test concluded that the difference in aggregation between FUS443(pUCP20) and PAPcdr(pUCP20) was not considered to be statistically significant at p=<0.05, nevertheless, aggregation meant that I was unable to record an accurate measurement of the optical density. With the addition of p*fusA1*, the formation of cellular aggregates was reduced to a level comparable with the control strains, that did not contain a pUCP20 vector (and were grown in antibiotic-free media).

The addition of antibiotic selection likely exacerbated the pre-existing growth defect in the mutant strain. Aggregation may have resulted from cell lysis or an altered cell surface which promoted cell-to-cell contacts. Polysaccharides are known to mediate cell contacts during the formation of microcolonies in the CF lung. FUS443 was recognised as an overproducer of exopolysaccharides earlier within this chapter and so antibiotic stress may induce the production of molecules that add to or reinforce these cell-cell contacts.

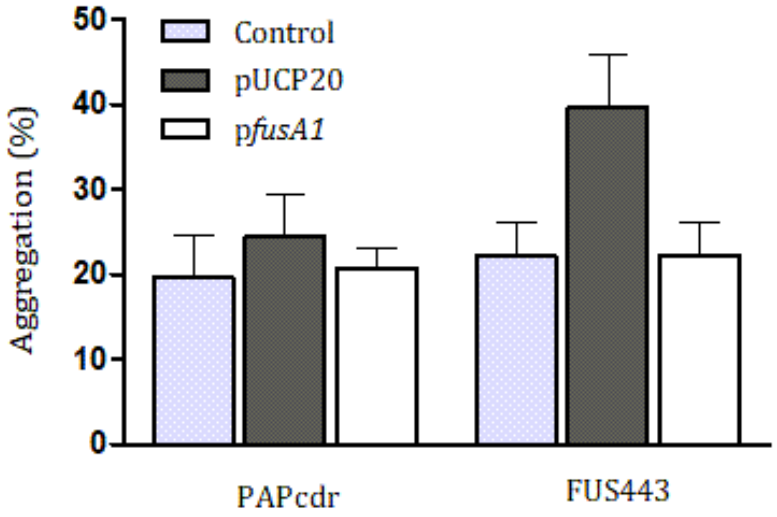

Figure 3.12. Percentage of aggregated cells within a culture of the progenitor, PAPcdr, and mutant, FUS443, strains in response to replication of an empty pUCP20 vector or pUCP20 vector expressing *fusA1* (p*fusA1*). Percentage aggregation is calculated by the optical density of settled cultures and the optical density after resuspension of aggregates. The respective strains without pUCP20 or antibiotic selection were used as controls.

3.6.2 Retention of the complementation vector

Aggregation meant that planktonic cultures had to be grown in the absence of antibiotic selection so that accurate measurements of growth rate could be determined. In the absence of antibiotic pressure there was a risk that the plasmid would be discarded from the cell, and so to test this, colony counts were taken from antibiotic-free cultures that had been grown for 6.5 hours (to early-stationary phase growth) in minimal media. There was almost complete retention of the p*fusA1* complementation plasmid in the mutant strain (Figure 3.13A). As expected, the greatest level of plasmid loss occurred in the mutant strain replicating the empty vector, which was considered to be statistically significant by an unpaired *t*-test ($t(4)=3.904$, $p=0.018$). However, the mutant strain often experienced lags in growth when transferred between different types of media composition or between liquid and solid media. Therefore, it is likely that the colony counts were low because the bacteria struggled to grow during the transition from an

antibiotic-free, liquid culture to growth on an antibiotic-supplemented, solid medium. Therefore, plasmid retention within the planktonic culture was likely to be greater than recorded.

When grown in the absence of antibiotic selection the cells did not form aggregates allowing for reliable measurement of optical density. The growth defect of FUS443 that occurred in both LB and minimal media conditions was recovered with the expression of the p*fusA1* vector. The rate of growth in the mutant strain was then comparable with the progenitor strains (Figure 3.13B) and provided evidence that the growth defects and cell aggregation was a result of the mutation in EF-G.

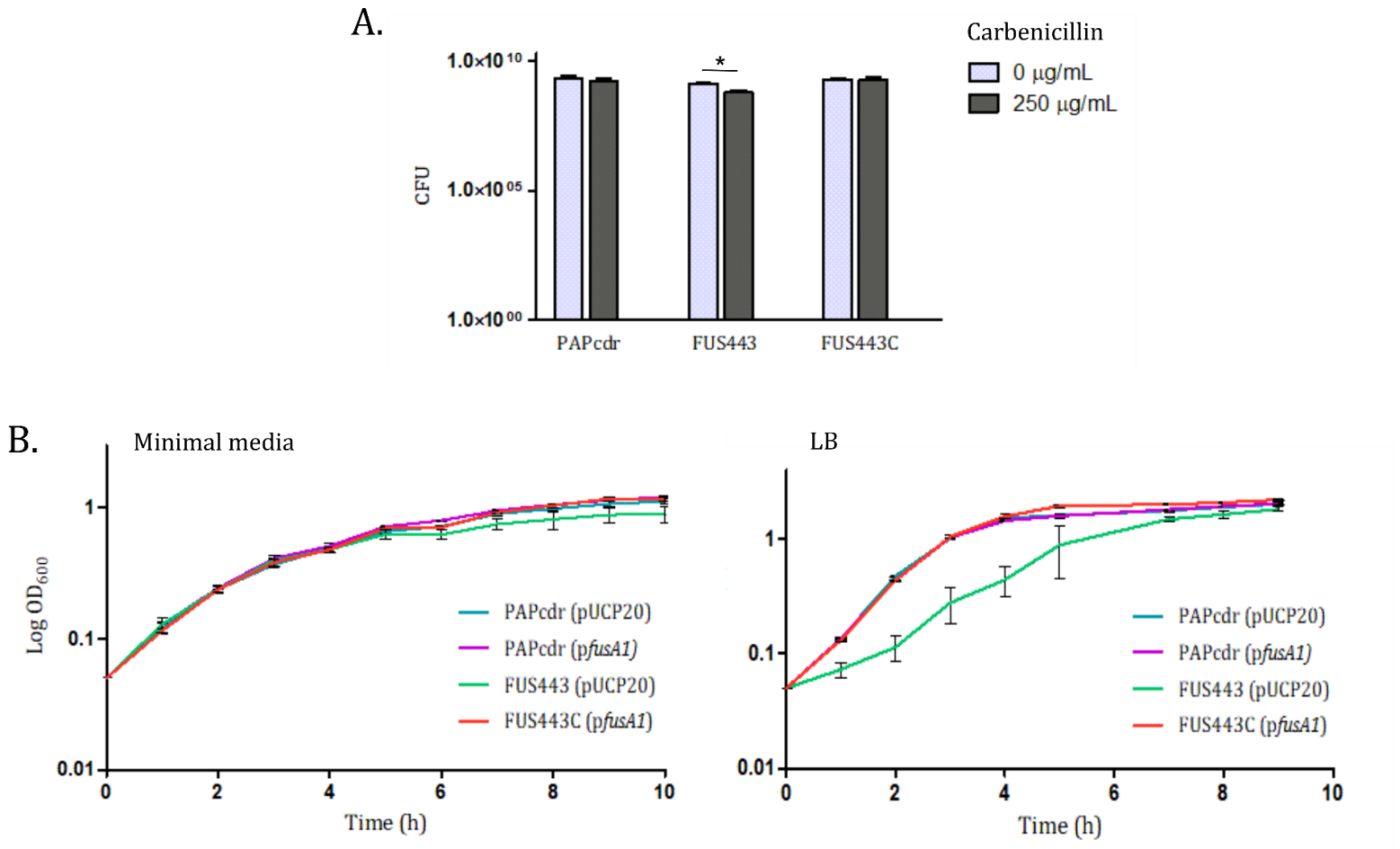

Figure 3.13. (A) The number of cells that retained the pUCP20 vector (Cb^r) after planktonic growth in antibiotic-free minimal media for 6.5 hours. Colony counts were calculated on plates containing (+/-) 250 µg/mL carbenicillin. **(B)** Growth of PAPcdr and FUS443 in minimal media and LB with the expression of either the empty vector (pUCP20) or complementation vector (p*fusA1*). Statistical significance between groups was assessed by an unpaired *t*-test (n=3, * = p <0.05).

3.6.3 pUCP20 disrupts *cdrA* expression

β-galactosidase assays were repeated to investigate whether the lower level of *cdrA* expression observed in the FUS443 mutant was complemented by the addition of a functional *fusA1* gene. Cells were either grown as a planktonic culture (Figure 3.14A) or as a colony biofilm on solid media (Figure 3.14B). Assessment of colony biofilms is similar to the measurement of P*cdrA* activity in planktonic culture, except that the cells are extracted from a colony grown on solid media. The control strains for PAPcdr and FUS443 were not transformed with pUCP20.

During both planktonic and colony biofilm growth, P*cdrA* activity was lower in the FUS443 mutant control strain than the progenitor controls, analogous with previous β-galactosidase experiments. Introducing the empty pUCP20 vector caused changes in β-galactosidase activity in both strains and in both planktonic and colony biofilm growth conditions. Introducing the complementation vector also produced some unexpected and inconsistent results that were not comparable to the control strain. This suggested that the regulatory system for *cdrA* expression is highly sensitive to changes in the cell and that the replication of a plasmid, alone, is enough to disrupt its normal expression. Despite a rise in P*cdrA* activity in the FUS443C strain, the inconsistency of the empty vector strains meant that I was unable to attribute this change solely to the P443L mutation.

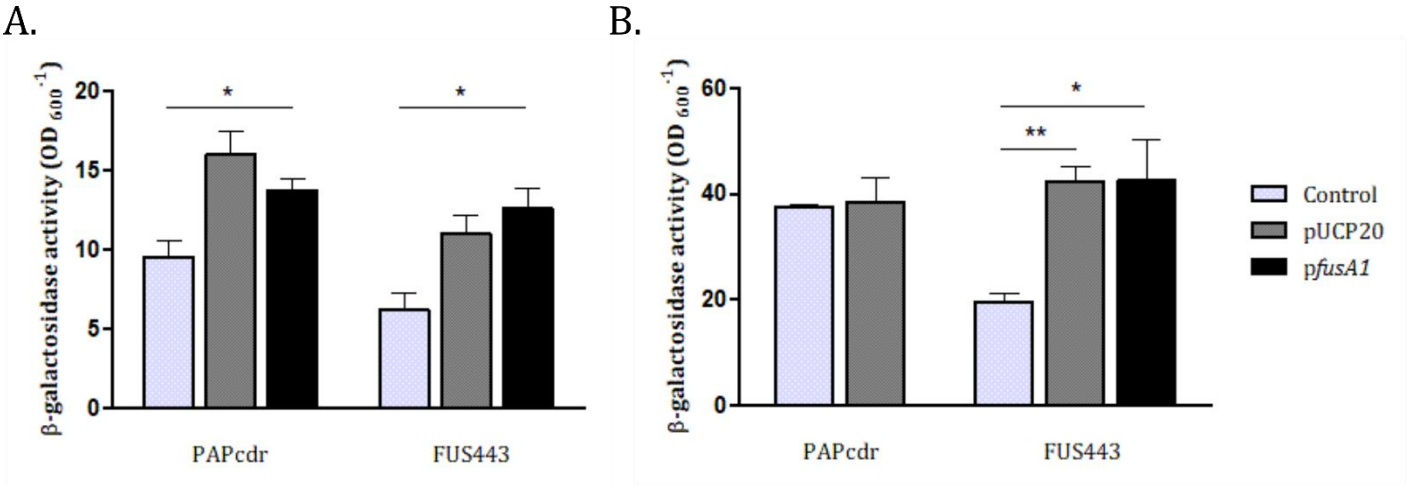

Figure 3.14. The effect of the pUCP20 vector and p*fusA1* complementation vector on the transcriptional activity of the *cdrA* promoter, measured by β-galactosidase activity in minimal media **(A)** during planktonic growth or **(B)** in a colony biofilm, in comparison with control strains containing no plasmids. Statistical significance between groups was assessed by an unpaired *t*-test (* = p <0.05, ** = p <0.01).

3.7 Phenotypic analysis of FUS443 complementation

3.7.1 Microscopy

On solid media, single colonies of the FUS443 strain had a slight wrinkled phenotype that is often associated with the production of exopolysaccharides, such as the pellicle forming polysaccharide, Pel (Friedman and Kolter 2004.a). Cells were grown as a planktonic culture and were observed under a light microscope to investigate changes in cell morphology. FUS443 did not appear different to the progenitor strain, however, the introduction of the pUCP20 vector resulted in an elongated cell-phenotype that was complemented by the expression of a WT *fusA1* gene (Figure 3.15). As seen in the aggregation assays, it is likely that the added stress of maintaining the vector, in combination with the reduced fitness of the mutant strain, caused the cells to become unhealthy and to develop problems with cell division. The inability for the FUS443 cells to divide properly may also contribute to the reduced growth rate that was observed in planktonic culture. This elongated phenotype is not a direct result of the P443L mutation

but is a further example of the reduced fitness of the mutant strain and how additional pressures, such as antibiotic selection or plasmid replication, alter cellular functions and reduce cell viability.

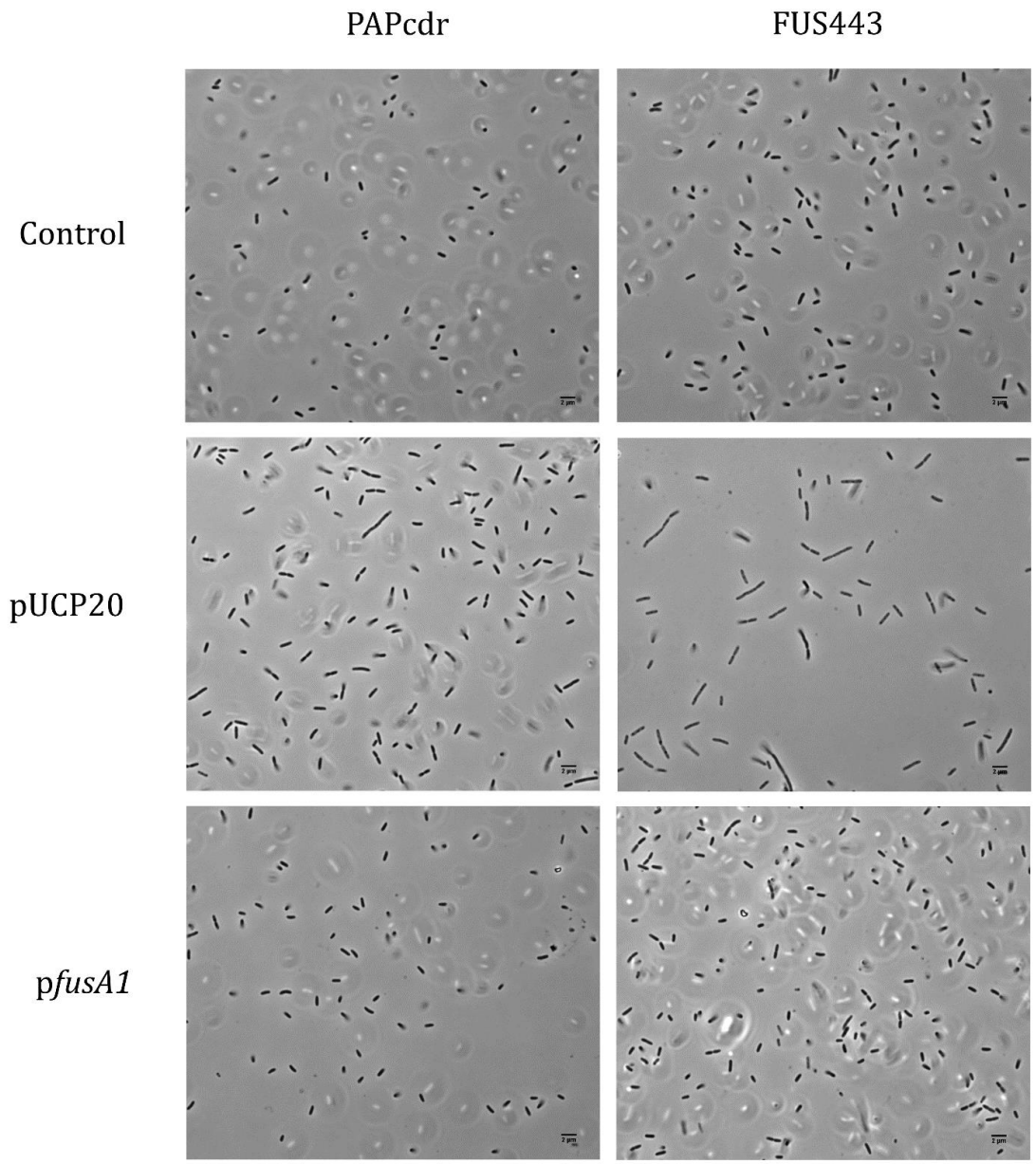

Figure 3.15. Light microscopy at 1000X magnification of the FUS443 mutant and progenitor strain, highlighting the formation of elongated cells after introducing the pUCP20 empty vector into FUS443. Cell length was recovered by expressing a WT *fusA1* gene *in trans via* p*fusA1* (scale bar = 2 µM). Images are representative of the cell morphology observed across three biological replicates from each strain.

3.7.2 Protease secretion

The secretion of proteases is extremely important in bacterial survival and the invasion of host tissues. To screen for protease production, bacteria were grown on two types of media containing enzyme substrates; milk protein and gelatin. The proteolytic activity of the bacteria was observed by a hydrolytic zone of clearing as the protein in the media was degraded. The PAPcdr and FUS443 strains were spotted onto caseinase and gelatinase assay plates, along with the respective strains containing an empty vector or the p*fusA1* complementation vector. The mutated *fusA1* gene from FUS443 was also sub-cloned into pUCP20 (henceforth referred to as pP443L) and introduced into the progenitor and FUS443 strains to investigate how expression of the mutant EF-G affects the cell (Figure 3.16).

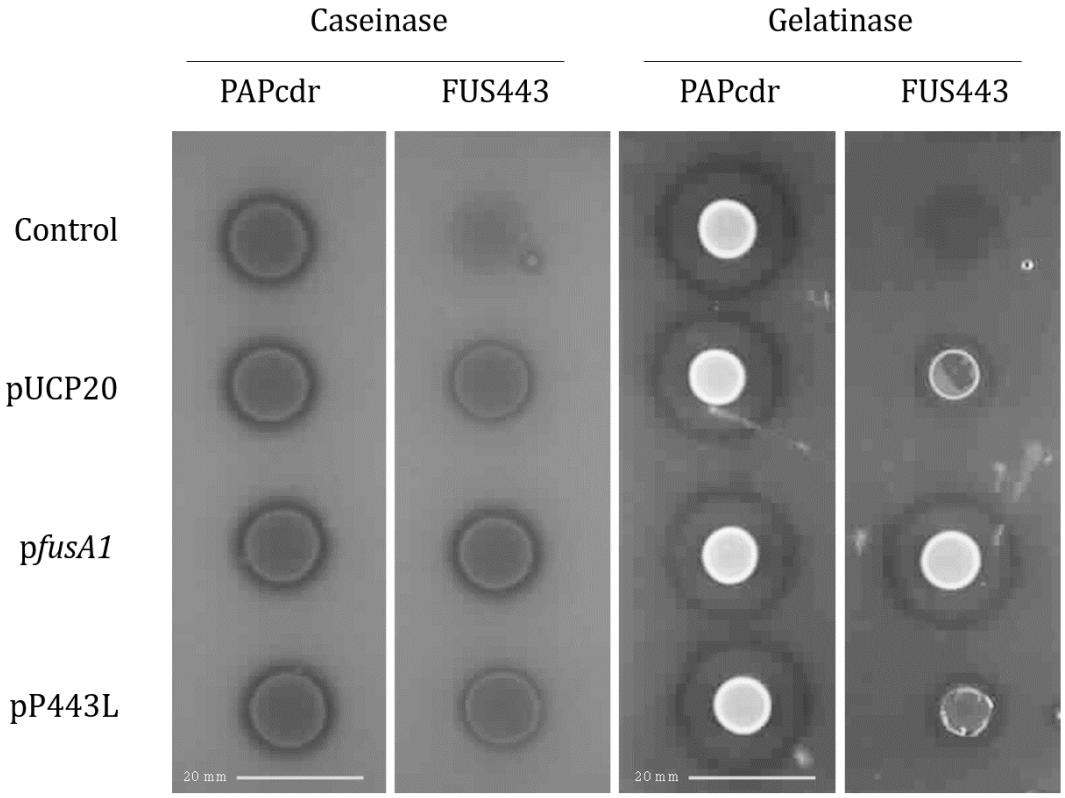

Figure 3.16. The secretion of exoenzymes, caseinase and gelatinase, by PAPcdr and FUS443. Secretion was visualised on plates supplemented with skim milk or gelatin by a hydrolytic zone of clearing around the colony and revealed that FUS443 exhibited reduced exoenzyme secretion which was recovered by introducing the p*fusA1* complementation vector.

Neither the expression of the WT *fusA1* gene nor the mutant gene affected the secretion of caseinases or gelatinases in the PAPcdr progenitor strain. This suggested that the endogenous WT version of EF-G had a dominant effect over the P443L variant, when expressed *in trans*. The FUS443 mutant could not grow on either of the protease plates indicating that protease secretion was too low for the bacteria to obtain nutrients from the media to support growth. Interestingly, the introduction of the pUCP20 empty vector induced a small increase in protease secretion but growth was still minimal. A similar finding was observed with the over-expression of the mutated gene *via* pP443L, however, expression of p*fusA1*, complemented the reduced production of both proteases, reaching levels comparable to the WT on both assay plates.

3.7.3 Motility

P. aeruginosa uses three main forms of motility; swimming, swarming and twitching. These different forms of motility are important in infection and play distinct roles in the formation of biofilms (Kazmierczak *et al.*, 2015). To assess whether the P443L mutation impacts motility, the strains were spotted onto swim, swarm and twitch agar. Motility was visualised by colony expansion around the initial point of inoculation as the bacteria navigate outwards.

The assay plates showed that the P443L mutation reduced motility both in type IV-mediated twitching and in flagellar-mediated swimming (Figure 3.17). This was complemented by p*fusA1*, suggesting that the P443L mutation was indeed causing the motility defect. Introducing the pP443L plasmid into the progenitor strain resulted in a subtle reduction in swimming motility. One explanation for this could be that the mutated protein is competing with the WT EF-G, preventing it from activating swimming motility at the normal level.

Swarming is also flagellum dependent but requires the additional production of two biosurfactants; rhamnolipids and 3-hydroxyalkanoic acids (Ha *et al.*, 2014). The FUS443 mutant appeared to have increased swarming motility, however, as with some of the previous phenotypes, this was abolished with the introduction of the pUCP20 plasmid.

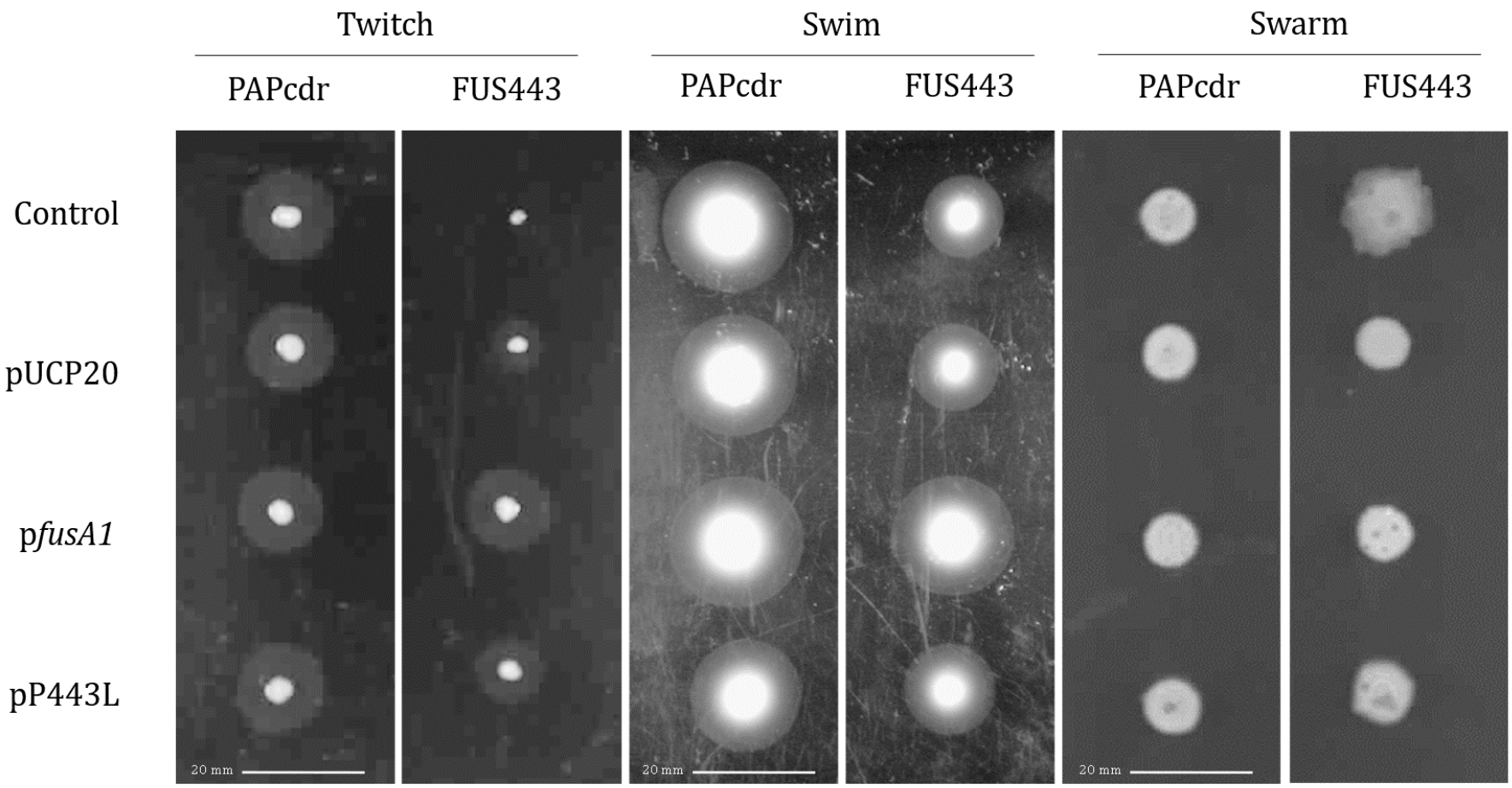

Figure 3.17. Twitching, swimming and swarming motility of the PAPcdr and FUS443 strains on glucose M9 minimal media containing varying concentrations of agar (1.5%, 0.3% and 0.75% (w/v) for twitching, swimming and swarming assay plates respectively). Motility was assessed in strains containing an empty vector plasmid, pUCP20 expressing a wild type *fusA1* gene (p*fusA1*) and pUCP20 expressing the mutated *fusA1* gene variant (pP443L). Images are representative of the motility observed across three biological replicates of each strain.

3.7.4 Exopolysaccharide production

Having previously established that exopolysaccharide synthesis was increased in the FUS443 mutant, the Congo red assay was repeated to include the strains containing the p*fusA1* and pP443L plasmids. On Congo red supplemented agar, the up-regulation of polysaccharide synthesis observed in FUS443 appeared to be complemented by the p*fusA1* plasmid. The FUS443 -pP443L strain produced an even deeper red pigmentation, indicating a further increase in exopolysaccharide production (Figure 3.18A.). These findings were supported by the planktonic Congo red assay in which the FUS443 control strain (containing no vector) and FUS443 containing an empty vector removed over twice as much Congo red from the supernatant than the progenitor strains (Figure 3.18B). This suggested that polysaccharide production was doubled in the mutant strain. p*fusA1* partially complemented this phenotype in the mutant strain but still produced more polysaccharide than the PAPcdr strains. From this, we can conclude that the P443L mutation is, at least in part, responsible for a change in exopolysaccharide production.

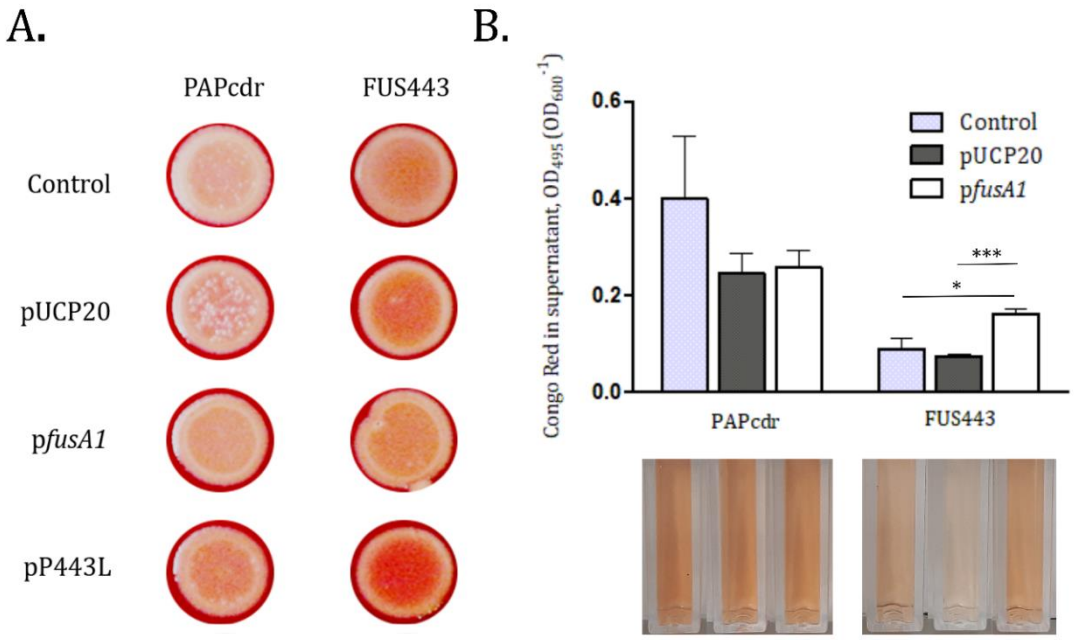

Figure 3.18. Congo red assay for the production of exopolysaccharides on **(A)** solid media or **(B)** in planktonic culture where cell-bound Congo red was sedimented and measurement of the remaining dye in the supernatant was taken. Statistical significance between groups was assessed by an unpaired *t*-test (n=3) (* = p <0.05, ** = p <0.01).

3.8 Antibiotic resistance

P. aeruginosa has high intrinsic resistance to a wide variety of antibiotics. The MIC of gentamicin for *P. aeruginosa* was 20 μg/mL and standard laboratory selection uses concentrations as high as 50 μg/mL. The FUS443 strain was initially selected from the plasposon screening due to its resistance to gentamicin at this concentration. Further investigation into the gentamicin resistant properties of this strain, by plating onto increasing concentrations of gentamicin, revealed that resistance was increased by 7.5-fold (Table 3.3) and was fully complemented with the introduction of a functional *fusA1* gene. As an aminoglycoside, gentamicin binds to the A-site of the ribosome, also occupied by EF-G, where it interferes with translation. It is possible that an altered conformation in the EF-G mutant protein disrupts the binding of aminoglycosides within this site and therefore prevents their cytotoxic effect. To investigate this, resistance to another aminoglycoside, kanamycin, was tested. *P. aeruginosa* has a high intrinsic level of kanamycin resistance, requiring concentrations as high as 1.5 mg/mL, however, this was further increased to over 2 mg/mL in the FUS443 strain. Again, this was fully complemented, suggesting that the SNP alone caused the enhanced antibiotic resistance.

Tetracycline and chloramphenicol are also ribosome-targeting antibiotics, binding to the small and large ribosomal subunits, respectively. The FUS443 mutant did not possess any resistance to these antibiotics, nor did it confer resistance to the ribosome-independent antimicrobial, rifampicin. This suggests that antibiotic resistance occurred in a binding-site specific manner through changes within the ribosome A-site.

Structural investigation using the intrinsic fluorescence of EF-G indicated that fusidic acid binding was maintained in the FUS443 mutant. *In vivo*, the mutation had no effect on sensitivity to fusidic acid (Table 3.3) confirming that the antibiotic could still bind the mutated EF-G protein. This also verifies that the mutation is unlikely to have caused large structural alterations within the fusidic acid binding pocket.

Conversely, during the screening for antibiotic resistance, I noticed the emergence of *fusaric acid* sensitivity in the mutant strain. Whilst *P. aeruginosa* has high intrinsic resistance to fusaric acid, the mutant strain exhibited 1.6-fold increased sensitivity. Little is known about the mode of action of fusaric acid, but current research has not indicated any interaction with the ribosome. Fusaric acid sensitivity is likely to be due to

downstream effects induced by the P443L mutation, and not due to a direct interaction between the protein and antibiotic.

All of the changes in antibiotic sensitivity or resistance mentioned here were completely complemented by the p*fusA1* plasmid and the MIC of antibiotics for strains containing the p443L plasmid were consistent with the original mutant and mutant empty-vector control. None of the plasmid variations had an effect on the MIC of the progenitor strain.

Table 3.3. Minimum inhibitory concentrations (MIC) of antibiotics for the FUS443 mutant and its progenitor strain.

Antibiotic	Mode of Action	PAPcdr MIC (μg/mL)	FUS443 MIC (μg/mL)
Gentamicin	Binds 30S ribosome and disrupts reading of tRNA	20	150
Kanamycin	Binds 30S ribosome and disrupts reading of tRNA	1500	>2000
Tetracycline	Binds 30S ribosome and inhibits incorporation of tRNA	20	20
Chloramphenicol	Binds 50S ribosome and inhibits peptide bond formation	250	250
Rifampicin	Inhibits RNA polymerase	100	100
Fusidic acid	Inhibits EF-G	1750	1750
Fusaric acid	Inhibits norepinephrine synthesis	>1300	800

3.9 Discussion

In the work described in this chapter I set out to identify global regulators of biofilm formation in *P. aeruginosa*, in the hope of highlighting potential targets that could be used to develop effective treatment for chronic infection. One mutant was found to contain a SNP in the EF-G-encoding gene, *fusA1*. This mutation impacted on a variety of biofilm- and virulence-associated phenotypes and whilst not predicted to drastically affect protein structure, the mutation clearly altered the protein function, placing the cell under a considerable amount of stress. This stress manifested in poor growth, aggregation, changes in cell morphology and alterations to cell signalling networks, such as QS. Whilst characterisation of the mutant provided a lot of evidence for suboptimal cell function, the benefits provided by the mutation, such as antibiotic resistance, meant that the mutation was maintained following passaging. The findings presented here highlight, for the first time, a role for EF-G in the regulation of biofilm- and virulence-associated phenotypes which may be relevant in CF chronic infections.

3.9.1 Structure and function of elongation factor G

The mutated *fusA1* gene contained a non-synonymous single base substitution resulting in a proline to leucine conversion. Proline residues have a distinct cyclical structure which is important for protein folding and introducing turns and kinks. They are often found at the end of alpha helices or in turns, and in most cases on the protein surface (Gray *et al.*, 2008; Bach *et al.*, 2013), which is consistent with the position of the P443 residue in EF-G. Leucine, however, is not cyclical but possesses a branched hydrocarbon chain and, unlike proline, it is generally buried within the protein due to its hydrophobicity (Barnes *et al.*, 2003). Computational predictions of the EF-G mutated protein did not indicate any significant changes to the EF-G protein structure, which was partially supported by analysing the intrinsic tryptophan fluorescence of the protein.

Changes in fluorescence intensity often indicate structural alterations in the protein which adjust the microenvironment around the tryptophan residue. The wavelength of maximum emission can also shift, such as a 'blue-shift' as the tryptophan residue moves to a more nonpolar environment within the protein, or a 'red-shift' as the residue becomes more exposed to the surrounding solvent (Ghisaidoobe *et al.*, 2014). The

P443L mutation caused only a very slight blue-shift in maximum emission which suggested that there was very minimal movement in the position of tryptophan residues which would affect their exposure to the solvent. There was however a large change in intensity, which is due to a change in quantum yield. The fluorescence quantum yield is the ratio of photons absorbed versus photons emitted through fluorescence, and informs regarding the probability that the excited state is being deactivated by fluorescence or by other non-radiative mechanisms (Fery-Forgues *et al.*, 1999). In simpler terms, the fluorescence of the tryptophan residues is altered in response to changes in local residues or nearby molecules. A decrease in quantum yield has been associated with electron transfer by quenching, for example, *via* neighbouring amino acid sidechains (Ghisaidoobe *et al.*, 2014). Fluorescence was quenched by the addition of fusidic acid to varying degrees in EF-G and the mutated form, consistent with the hypothesis that EF-G-P443L is structurally different from the WT form.

With this, it appeared that the P443L mutation was not causing dramatic alterations to the structure, as the exposure of the multiple trytophans to the solvent was unchanged, but the change in quantum yield suggested minor structural changes throughout the protein. Interestingly, four of the five tryptophan residues were positioned within domain I, and the fifth was located in domain IV. Both of these domains play important roles in GTP hydrolysis and mRNA binding. It is conceivable that the minor adjustments within these domains maintained some level of function, which would likely have been abolished through larger structural alterations.

EF-G adopts a series of large conformational changes throughout ribosome translocation. The function of EF-G relies heavily on protein flexibility, and so small changes can have large implications on protein function. The most dynamic movement occurs in domain IV, which dictates rotation of the other domains, most notably domains III and V. GTP and GDP exchange within domain I also mediate large conformational changes which bring the switch 1 region within bonding distance of domain III (Li *et al.*, 2011). As the majority of tryptophan residues resided in domain I, changes in fluorescence indicated that structural changes to this domain were likely to have occurred and may have disrupted such processes as guanosine phosphate exchange.

EF-G binds the ribosome in its GTP-bound state. GTP hydrolysis occurs rapidly upon binding and coincides with rotation of the 30S ribosome subunit during tRNA

translocation. Counter-rotation of the ribosome is presumed to dissociate the deacylated-tRNA from the E-site as well as releasing the (now GDP-bound) EF-G. Translocation can proceed without GTP hydrolysis, but occurs at a far slower rate, and the dissociation of EF-G from the ribosome is severely inhibited (Holtkamp *et al.*, 2014). It is therefore possible that the growth defects observed in the FUS443 mutant were the result of poor guanine nucleotide exchange causing slow progression of protein synthesis.

3.9.2 Variations in the phenotypic profile of FUS443

The *fusA1*-P443L mutation exerted pleiotropic effects on several seemingly unrelated phenotypes. These could be complemented in almost all cases by the re-introduction of a functional *fusA1* gene. The reduced growth rate of FUS443 during planktonic growth was an indicator that the mutant EF-G protein did not function as efficiently as the WT protein. Unexpectedly, the growth defect in rich media was abated under minimal media conditions. It is possible that the nutrient-limited environment triggered a stress response in the *P. aeruginosa* strains, which in fact could benefit its growth. Bacteria are well equipped to deal with environmental and internal stressors, and in almost all cases adaption requires a change in protein synthesis. Stress response systems typically shut down unnecessary pathways, or pathways which exacerbate the stress, so that the cell can direct more energy into growth and survival (Gottesman, 2017). One such stress response is the nutrient-induced stringent response, mediated by the alarmone (p)ppGpp, which is triggered upon disruption to protein synthesis. The stringent response effects gene expression to promote survival during cell starvation and encourage persistence through environmental stress conditions (Beljantseva *et al.*, 2017). A stress response such as this may have directly affected EF-G or down-regulated some of the pathways affected by the mutated protein, therefore reducing its deleterious effects on the cell. In nutrient-rich conditions, these pathways remain active allowing for their reduced efficiency to become apparent. Alternatively, the cell may have activated mechanisms to compensate for the mutational defects, which are energetically-expensive and so reduce the amount of energy directed towards growth.

Several virulence-factors were down-regulated in the FUS443 mutant. Reduced exoenzyme production meant that the mutant was unable to degrade the protein-based

media and so could not draw out these nutrients for growth. This would be particularly limiting for *P. aeruginosa* within the environment and would reduce the bacteria's highly adaptable nature. In addition to this, swimming and twitching motility was severely reduced, meaning that the mutant strain was unable to explore its environment as efficiently as the progenitor strain. In contrast to the down-regulation of virulence factors, exopolysaccharide production was increased by the P443L mutation, which would be expected to promote biofilm formation. However, this was not the case, as biofilm formation was unaffected in the mutant strain. The up-regulation of exopolysaccharides may have been triggered as a compensatory mechanism to counteract the reduction in CdrA synthesis and maintains biofilm formation at a consistent level.

These phenotypic studies also revealed that the WT EF-G had a dominant presence over any dysfunctional copies of the protein. In the cell, the WT and mutant proteins should have been competing for ribosome binding and so complete complementation was not expected. But in almost all cases the complemented strains could not be distinguished from the progenitor controls. It is likely that this was a result of the multi-copy plasmid producing greater abundance of the WT EF-G than the chromosomally encoded mutant form. Overexpressing the mutated *fusA1* gene *in trans* saw a reduction in motility of the PAPcdr, progenitor strain. This provided evidence for the competition between the two EF-G forms and highlighted the sensitivity of motility regulation to changes in protein synthesis.

Another distinctive phenotype which related to the *fusA1* mutation was the dramatic up-regulation of BHL and OdDHL signalling molecules. These changes in QS signalling, in the FUS443 mutant, were dependent on the presence of the *P. aeruginosa* culture during incubation with the *E. coli* reporter strain. Any *in vivo* environment plays host to a wide variety of microbial flora, which communicate, cooperate and compete with one another to survive. *P. aeruginosa* competes with other bacterial species directly *via* the type VI secretion systems, producing toxins, siderophores and secondary metabolites (Beaume *et al.*, 2015). I therefore considered that reduced virulence in FUS443 was responsible for increased detection of QS signal *via* reduced killing of the *E. coli* reporter strains. However, this theory is unlikely as similar levels of *E. coli* were recovered after incubation with either the progenitor or mutant strain.

In *P. aeruginosa*, QS regulates a diverse range of phenotypes, including virulence, biofilm formation and antibiotic production. QS is important for the secretion of exoenzymes and secreted toxins which help *P. aeruginosa* to dominate the microbial community within its environment. Strains of bacteria usually possess unique QS networks, which differ by stimuli and response, making QS as a therapeutic target difficult to work with (Laverty *et al.*, 2014). The apparent up-regulation of QS signalling molecules in the mutant strain is inconsistent with the observed down-regulation of virulence phenotypes such as motility and protease production. It is possible that the spike in FUS443 QS signalling only occurs when in the presence of other microbial species (*E. coli* in this instance) to stimulate the production of the otherwise down-regulated virulence factors. The purpose of this may be to increase inter-bacterial competition, but appears to occur in a media-dependent manner.

3.9.3 Antibiotic resistance

The FUS443 mutant developed resistance to two aminoglycosides, kanamycin and gentamicin, with nearly a 3-fold increase in the gentamicin MIC. Aminoglycosides are a class of ribosome-targeting antibiotics which bind tightly to the A-site of the 30S subunit. Binding of aminoglycosides disrupts the correct selection of tRNA within this decoding site and blocks translocation of the tRNA into the P-site (Tsai *et al.*, 2013). Typically, bacteria acquire aminoglycoside resistance through the expression of aminoglycoside acetyltransferases and phosphotransferases, or ribosomal mutation. Various studies have identified low-cost mutations in *E. coli* EF-G in response to sub-lethal concentrations of kanamycin (Mogre *et al.*, 2014). These mutations spread rapidly through the population and were often located at the tip of domain IV which interacts with mRNA transcripts and the 30S subunit. Whilst the P443L mutation isolated in this study is located within domain III, it is possible that it has caused subsequent conformational changes which affect its interaction with the ribosomal A-site and disrupt aminoglycoside binding.

Fusidic acid inhibits protein synthesis by binding to EF-G after GTP-hydrolysis, trapping it in the post-translation site and preventing further elongation. The fusidic acid binding pocket is situated between domains II and III, close to the switch regions which

control GTP hydrolysis. The P443L transition resides deep within the fusidic acid binding site, adjacent to residues that have been found to interact directly with the bound fusidic acid compound. Residue 443 of EF-G has been marked as a mutational site giving rise to fusidic acid resistance in *Thermus thermophilus, Salmonella enterica* serovar Typhimurium and *Staphylococcus aureus* (Palmer *et al.*, 2013). However, the FUS443 *P. aeruginosa* mutant maintained fusidic acid sensitivity and binding of fusidic acid to EF-G did not appear to be affected by the mutation. This supports the structural predictions that the mutation had not significantly altered the structure of the fusidic acid binding pocket.

In a study on *S. aureus*, an overwhelming number of fusidic acid resistant mutations were mapped to domain III. Hydroxyl radical probing and structural data showed that domain III was positioned in close proximity to protein S12 of the 30S ribosome (Norström *et al.*, 2007). Whilst the FUS443 mutation in this study was unaffected in fusidic acid binding, the positioning of this mutation may still be key to changes in protein interactions with the ribosome and protein function.

Interestingly, the FUS443 mutation also gave rise to antibiotic sensitivity. The progenitor strain displayed a high level of intrinsic antibiotic resistance to the myotoxin, fusaric acid, produced by *Fusarium heterosporum*. The mechanism of action for this antimicrobial agent is not well understood but resistance has been reported in *P. fluorescens*, a plant pathogen, that can colonise roots infected with fusarium (Quecine *et al.*, 2015). Fusaric acid is reported to chelate cations, inhibit dopamine hydrolase, and has many similarities to the QS molecule, *N*-hexanoyl-L-homoserine lactone, which may act directly or indirectly to influence gene expression in *P. aeruginosa* (Tung *et al.*, 2017). At this stage it is unclear how the *fusA1* P443L mutation gives rise to fusaric acid sensitivity.

3.10 Conclusion

P. aeruginosa has posed a serious challenge to the medical community for decades due to the high frequency at which it acquires resistance to a wide variety of antibiotics (Lister *et al.*, 2009). The unexpected and spontaneous emergence of a gentamicin resistant mutant, presented in this chapter, is a brazen reminder of this issue. My findings have shown how a SNP in EF-G, unlikely to have polar effects on downstream genes, has brought about resistance to multiple aminoglycosides, impacted upon several biofilm-associated phenotypes, such as *cdrA* expression and the secretion of matrix exopolysaccharides. The SNP also affected virulence factors, including motility and protease production, and has caused potential changes to the cell communication network. The successful complementation of almost all of these characteristics strongly indicate the influence of the mutated EF-G protein on these systems and highlights how disruption to EF-G function can disturb the maintenance of a planktonic or biofilm lifestyle in *P. aeruginosa*.

Chapter 4

4. Proteomic analysis of FUS443

4.1 Introduction

The previous chapter saw the identification of a SNP in the EF-G encoding gene, *fusA1*. This mutation resulted in distinctive changes to cell morphology, affecting the expression of *cdrA* at a transcriptional level and altering the secretion of various proteins and polysaccharides. To investigate the global effects that the *fusA1* mutation has on the cell, proteomic profiling of the FUS443 mutant was carried out and analysed for alterations to the secretome and the whole-cell proteome. Any proteomic data that has not been specifically defined within the tables presented in this chapter has been included within '**7. Appendix**'.

4.2 Secretome

P. aeruginosa secretes an abundance of proteins from the cell, such as proteases and exotoxins, many of which contribute to bacterial virulence. Previous findings highlighted a change in exoenzyme production in the FUS443 mutant and so the secretome was analysed to see if changes to the abundance of secreted proteins were large enough to be visualised by SDS-PAGE.

The *Pseudomonas* Genome Database predicts that only 94 proteins are found extracellularly or are secreted from the cell (Winsor *et al.*, 2016). Growth in minimal media restricts protein secretion further to retain resources in nutrient limited conditions. Previous studies have found that growth in M9 minimal media generates a completely different secretome profile compared with cells grown in LB, with one study identifying only 52 extracellular proteins from supernatants of PAO1 when grown to stationary phase in M9 minimal media (Scott *et al.*, 2013).

The FUS443 mutant (containing the empty pUCP20 vector), its progenitor, PAPcdr (pUCP20), and the complemented mutant, FUS443C (p*fusA1*) were grown in M9 minimal media, supplemented with glucose, to late exponential phase, at which point the

abundance of secreted proteins was expected to be at its greatest. Proteins within the supernatant were extracted and run on a 1D-SDS PAGE gel (Figure 4.1).

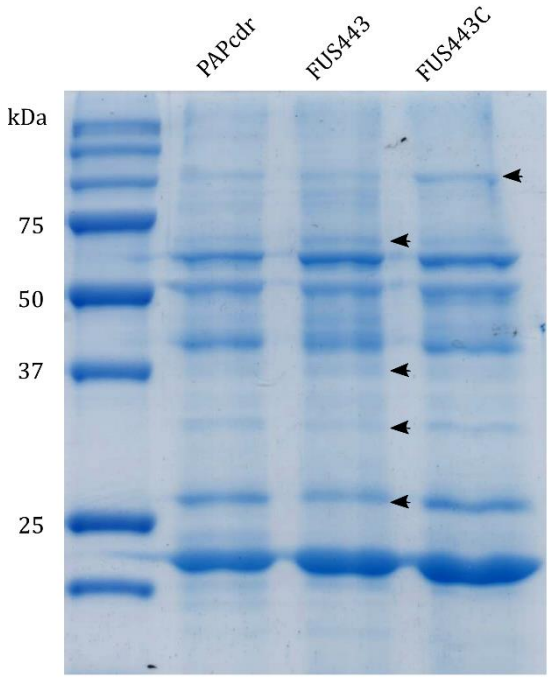

Figure 4.1. Secreted proteins of the progenitor strain (PAPcdr), FUS443 mutant and the complemented strain (FUS443C), cultured in minimal media with glucose, were separated by SDS-polyacrylamide gel electrophoresis. Arrows point to protein bands that appear more or less intense than those of the progenitor and complemented strain. This figure is representative of the cell secretome observed across two biological replicates.

There were minor changes in the abundance of secreted proteins across the different strains, indicated by the arrows on Figure 4.1. There appeared to be an increase in the quantity of higher molecular mass proteins at around 80 kDa in size, and also in a distinct band at approximately 70 kDa. The majority of secreted proteins in *P. aeruginosa* have a molecular weight of between 30 and 50 kDa and so the band at 37 kDa, which appeared more prominent in the mutant strain, and the band at approximately 32 kDa, which appeared to be reduced in FUS443, could therefore have represented a number of proteins.

The protein bands discussed here were only altered in the FUS443 mutant, with the progenitor and complemented strains having comparable protein levels. This suggested that the P443L mutation in EF-G was indeed affecting protein secretion or the synthesis of secreted proteins. There was one band at ~50 kDa in the complemented strain that is absent in the mutant and progenitor strains, suggesting that over-expression of the *fusA1* gene may also have had additional downstream effects that go beyond complementation of the P443L mutation.

4.3 Proteomic profile of FUS443

4.3.1 Sample preparation

With changes having been observed in the secretome of FUS443, I wanted to investigate the effect of the *fusA1* mutation on the global proteomic profile of the strain, and investigate any potential proteomic involvement in changes to cell physiology. Therefore, the whole-cell proteome of the progenitor, FUS443 mutant and complemented strain was analysed. Planktonic cultures were grown in M9 minimal media and were harvested at late exponential phase. The cell-associated protein was extracted and the concentrations were determined using the DC Protein Assay kit.

Samples were first visualised on a 1D-SDS PAGE gel (Figure 4.2), where the vast majority of bands remained constant across all strains and across all biological replicates. A few subtle differences could be seen in some of the proteins below 25 kDa from the FUS443 cultures, but there were no clear banding patterns. The over-expression of EF-G (77.8 kDa) from the p*fusA1* vector could be seen in the four replicates of the complemented strain (black arrow). pUCP20 has a high copy number in *E. coli*, achieved through the pMB1 origin of replication, whilst the encoded pRO1600 origin for replication in *P. aeruginosa* maintains this plasmid at a low copy number. Even with low level replication of p*fusA1*, the gel clearly indicated the extent to which EF-G was being overexpressed in the complemented strain compared with the other strains. It was also interesting to see that there was no obvious change in the abundance of EF-G in the FUS443 mutant, despite the high probability of reduced protein function. This suggested that the mutated protein was not impinging on its own regulation or stability in a significant way.

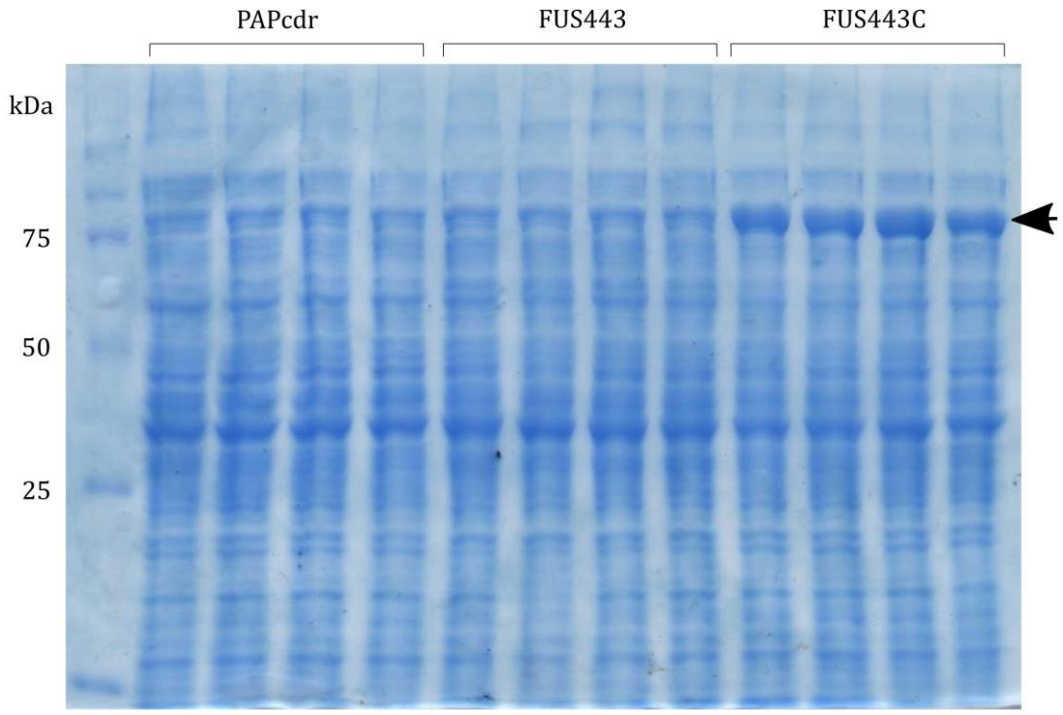

Figure 4.2. The total protein extracted from four biological replicates of the progenitor strain (PAPcdr), FUS443, and the complemented strain (FUS443C) cultured in minimal media with glucose were separated by SDS-polyacrylamide gel electrophoresis and stained with Coomassie blue. Arrow points to the over-expression of elongation factor G.

To ensure that the changes in band intensity were not due to inaccurate measurement of the protein concentration or inconsistent loading onto the SDS-PAGE gel across the lanes, a duplicate gel was transferred by western blot onto a PVDF membrane and blotted with antibodies against the housekeeping protein, isocitrate dehydrogenase (ICD) (Figure 4.3). ICD, with a molecular weight of 45.6 kDa, was consistent across the blot. The background signal in the later lanes was likely to have been caused during separation through the gel and not due to errors in sample concentration. Confident that the protein concentrations were accurately measured, the samples were processed for further proteomic analysis.

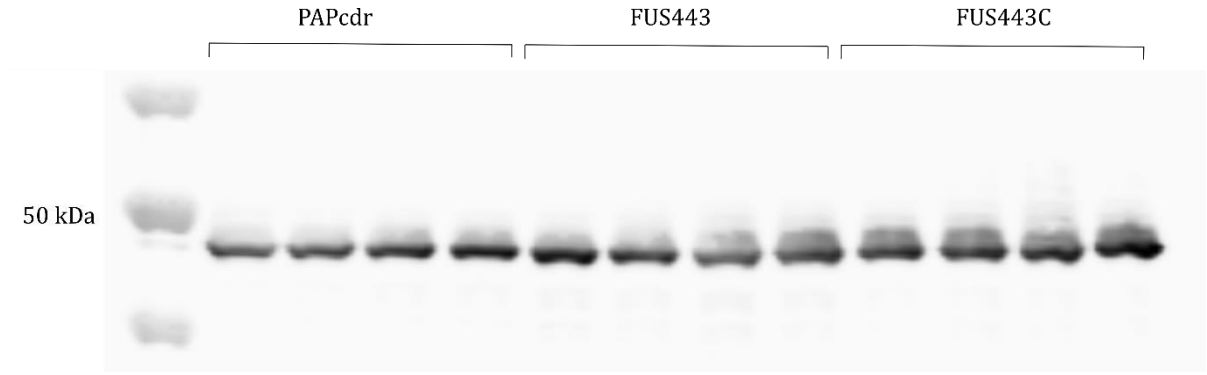

Figure 4.3. Western blot analysis of the total protein extract from the progenitor strain (PAPcdr), FUS443 mutant and the complemented strain (FUS443C), using antibodies against ICD.

4.3.2 Whole-cell proteomics

4.3.2.1 TMT and LC/MS-MS

Whole-cell protein extracts were sent for proteomic analysis using tandem mass tag (TMT) labelling and protein identification with liquid chromatography/tandem mass spectrometry (LC/MS-MS) at the Cambridge Centre of Proteomics. The dataset obtained from these samples contained 3506 proteins, from a total of 5570 predicted ORFs in the *P. aeruginosa* genome. This provided a good representation of the proteome, based on previously reported proteomic studies in PAO1 (Hare *et* al. 2012b, Park *et al*. 2014 and Guilbaud *et al*. 2017), and many of the absent proteins would not have been expressed in these growth conditions or would have been too low in abundance for detection.

Protein quantitation values were $\log_2$ transformed to facilitate the comparison between conditions. Many proteins were affected by the mutation in *fusA1*. Of the proteins that had been up-regulated in response to the mutation, 177 had a $\log_2$ fold change (FC) of > 1, and 41 proteins had a $\log_2$ FC > 2. In contrast, 204 proteins had been down-regulated by a $\log_2$ FC of < -1 and 31 proteins had a $\log_2$ FC < -2 (Figure 4.4). For this study, modulations that were considered statistically significant had a $\log_2$ fold change of > 1 or < -1 and FDR (False Discovery Rate) adjusted P-value of ≤ 0.01.

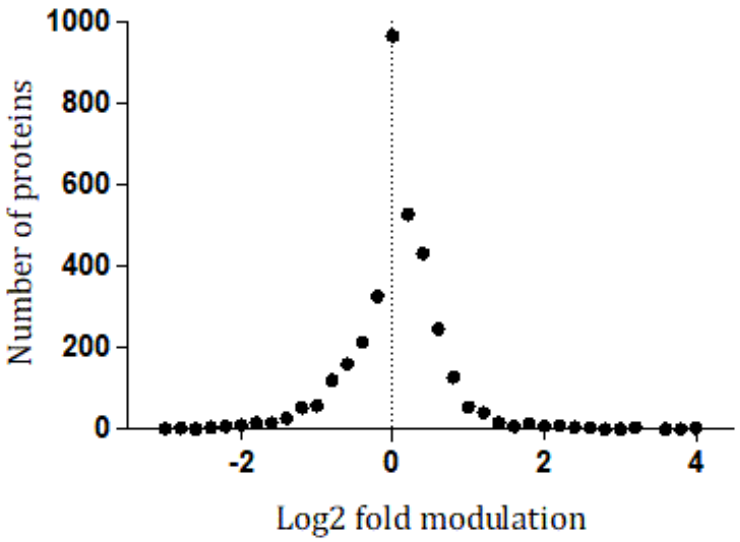

Figure 4.4. Modulation of protein abundance in the FUS443 mutant compared with the protein abundance of the progenitor strain.

4.3.2.2 Box plots

Box-and-whisker plots (box plots) provide a convenient way to compare protein expression distribution in different LC/MS runs and assess the impact of normalising data. The upper and lower lines of the box represent the 25th and 75th percentiles of the distribution and the middle line of the box represents the median value. The whiskered lines, that extend below and above the box, indicate the most extreme values that are not considered as outliers. Points that exist beyond the whiskers represent outlying values that are more than 1.5 times the interquartile range, from the first and third quartile.

Figure 4.5A represents the raw distribution of protein abundance for each biological replicate from each condition. Global biases, which affect all peptides, are indicated by shifts up or down in the box plots and can be removed by normalisation of the data. The distributions of protein abundance are similar across all samples and any minor differences were corrected by normalisation of the data to each channel median (Figure 4.5B).

A.

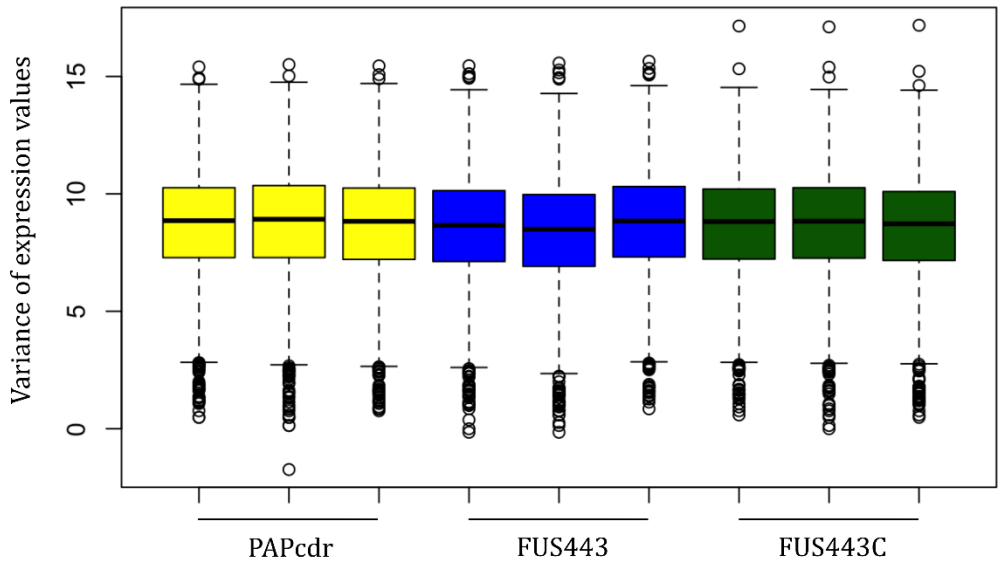

B.

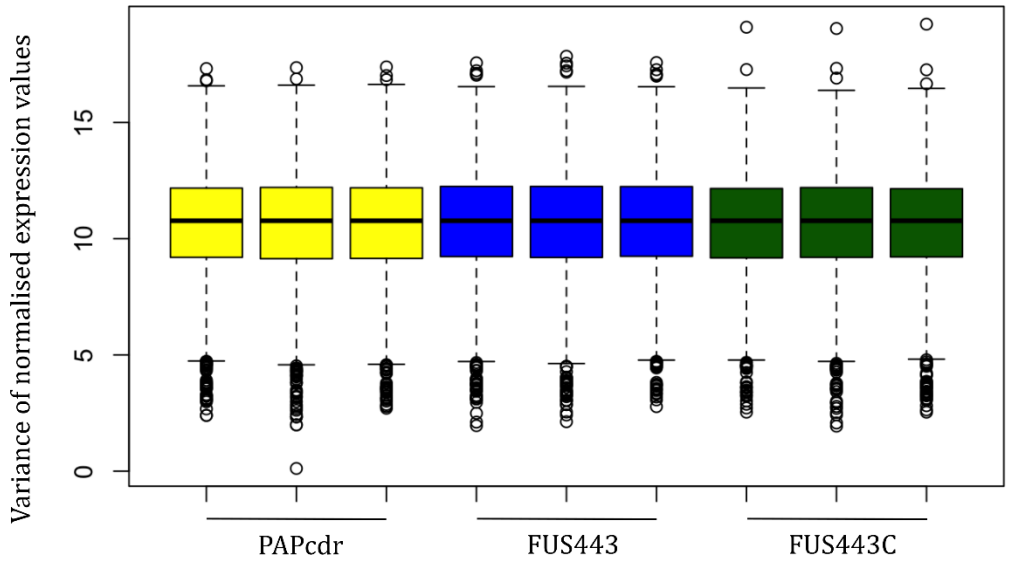

Figure 4.5. Box plots of the $\log_2$ protein abundance distribution for nine LC-MS runs, composed of three replicates from each strain (PAPcdr, FUS443, FUS443C). **(A)** Raw data and **(B)** data normalised to the median.

4.3.2.3 Principal components analysis

Principal components analysis (PCA) was employed to assess the similarities in gene expression amongst the three sample types. The PCA scores plot showed two clusters of data points, one containing the mutant samples and the other containing the progenitor and complemented samples (Figure 4.6). This indicated that the proteomic profile of the FUS443 mutant was distinct from the other two groups whereas the proteomic profiles of the progenitor and complemented strains appeared to be similar. This was a good indication that many of the changes occurring in the FUS443 mutant were a result of the *fusA1* mutation.

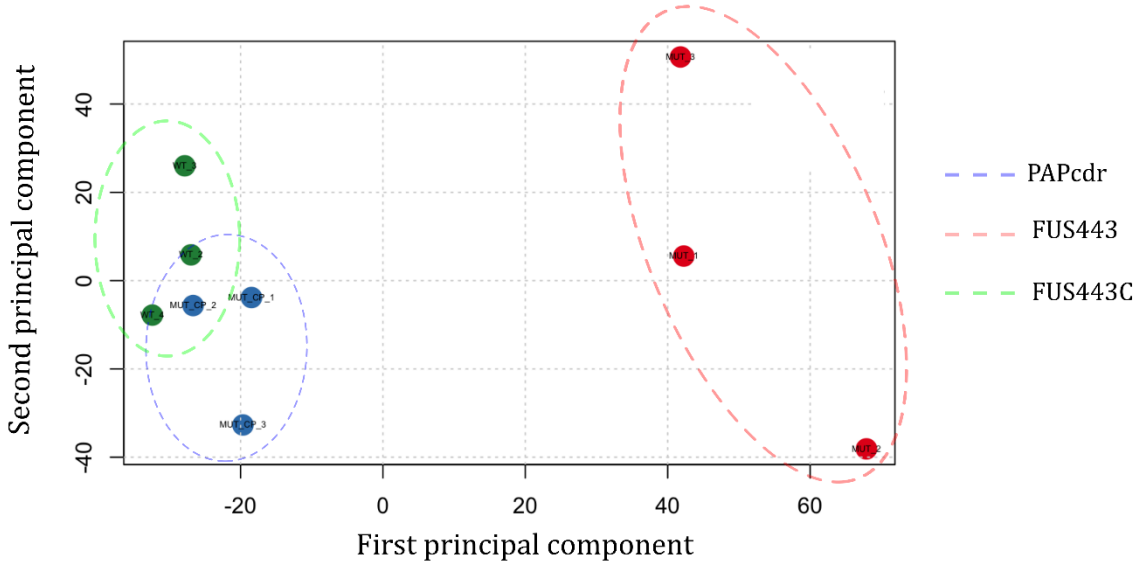

Figure 4.6. Principal component analysis of proteomic data from PAPcdr, FUS443 and FUS443C. Each point on the graph represents one biological replicate.

4.3.2.4 Volcano plots

Volcano plots are a way of illustrating the fold change (of $\log_2$ transformed protein abundance data) with the P-value (-$\log_{10}$ transformed) for all the quantified proteins. This allows for quick visualisation of global changes in the proteome and identifies proteins that have been highly modulated and are statistically significant in the mutant strain

compared with the progenitor. Data points that appear high on the Y axis have low P-values and are more significant.

The volcano plot compared the combined replicates of the progenitor strain and the combined replicates of the FUS443 mutant strain (Figure 4.7A). Of all the proteins found to be up-regulated in the mutant, 129 were statistically significant, and 166 proteins were significantly down-regulated. In comparison, the volcano plot depicting changes between the complemented FUS443C strain and the progenitor revealed that the protein abundance of these two strains were very similar (Figure 4.7B). In fact, only two proteins, EF-G and PscL, were significantly up-regulated in the complemented strain and no proteins were significantly down-regulated. This supported the PCA scores and together provided a clear indication that the proteomic changes induced by the P443L mutation in FUS443 could be recovered by complementation with a functional copy of the *fusA1* gene.

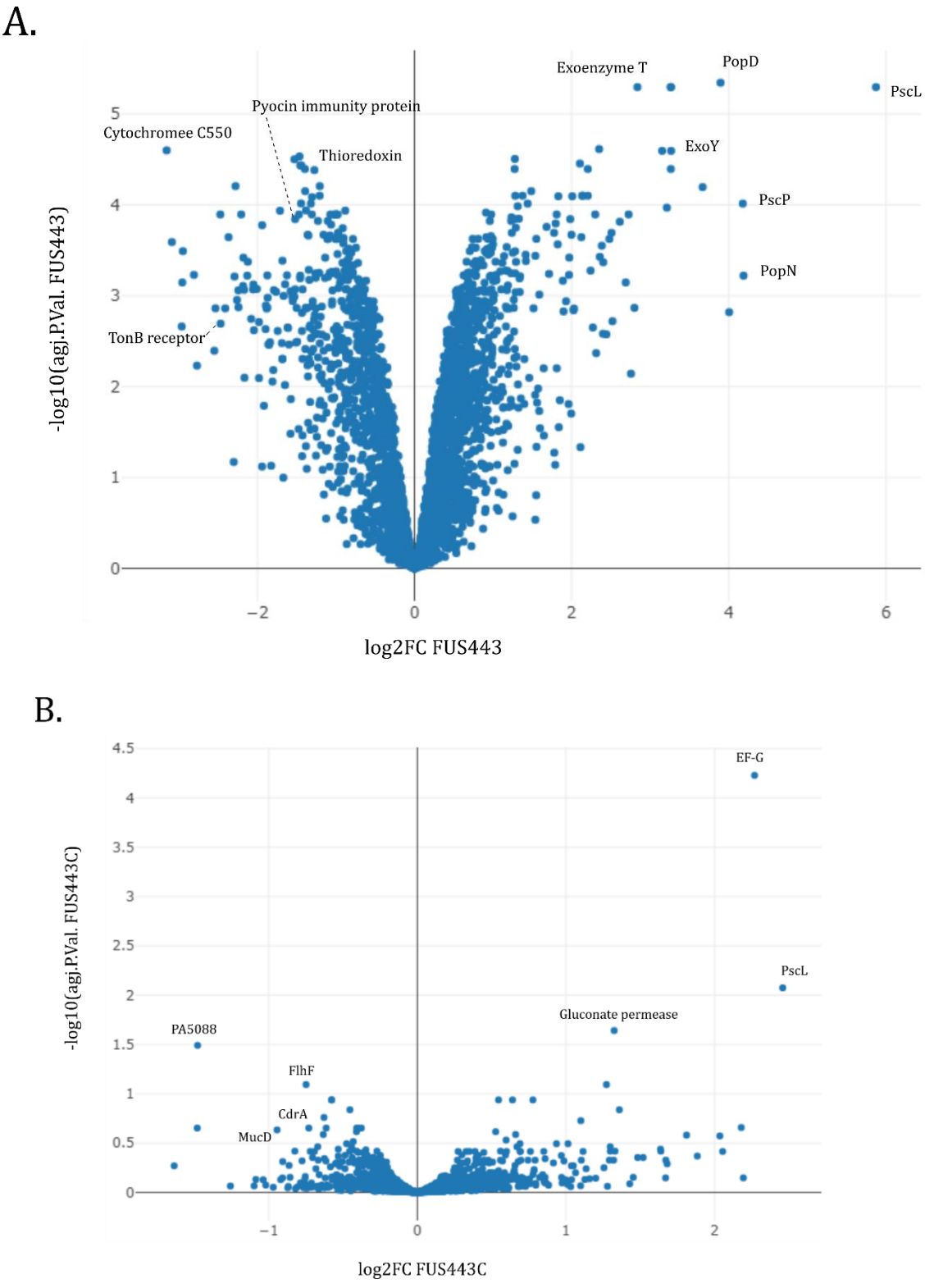

Figure 4.7. Volcano plot representing the $\log_2$ fold change (FC) of protein abundance against statistical significance for **(A)** the FUS443 mutant, and **(B)** the complemented FUS443C strain in relation to the PAPcdr progenitor strain. Several points have been annotated with the corresponding protein.

4.3.3 Modulated proteins in FUS443

4.3.3.1 Proteins of an increased abundance

The top 20 proteins with the greatest increased abundance in FUS443 are listed in Table 4.1. The log_2 FC of the complemented mutant strain, FUS443C, was used to indicate if the modulation could be attributed to the P443L mutation.

Table 4.1. List of up-regulated proteins associated with the *fusA1*-P443L mutation. Proteins associated with the T3SS are featured in the shaded boxes. A P-value of 0.000 represents < 0.0005.

				FUS443		FUS443C	
	Protein	**Locus tag**	**Protein function**	**log_2 FC**	**P-value**	**log_2 FC**	**P-value**
1	PscL	PA1725	Type III secretion export protein	5.873	0.000	2.458	0.008
2	PopN	PA1698	Type III secretion outer membrane protein	4.187	0.001	0.172	0.973
3	PscP	PA1695	Type III secretion translocation protein	4.178	0.000	-0.179	0.953
4		PA3661	Hypothetical protein	4.004	0.002	-0.452	0.923
5	PopD	PA1709	Type III secretion outer membrane protein	3.895	0.000	-0.113	0.903
6		PA1325	Hypothetical protein	3.667	0.000	-0.086	0.973
7	ExoY	PA2191	Adenylate cyclase	3.266	0.000	-0.193	0.881
8	SpcS	PA3842	ExoS chaperone	3.263	0.000	-0.156	0.866
9	PcrH	PA1707	Regulatory protein	3.262	0.000	-0.352	0.777
10	ExoS	PA3841	Exoenzyme S	3.261	0.000	0.157	0.861
11	PcrG	PA1705	Type III secretion regulator	3.211	0.000	-0.502	0.729
12	PopB	PA1708	Type III translocator protein	3.151	0.000	-0.055	0.973
13	ExoT	PA0044	Exoenzyme T	2.836	0.000	0.138	0.861
14	AprX	PA1245	Metalloproteinase	2.798	0.001	0.452	0.88
15	AprA	PA1249	Alkaline metalloproteinase	2.755	0.007	0.679	0.869
16	PelA	PA3064	Exopolysaccharide biosynthesis	2.725	0.000	-0.166	0.923
17		PA0630	Hypothetical protein	2.688	0.001	-0.070	0.982
18		PA0620	R-type pyocin, related to P2 phage	2.613	0.000	0.275	0.861
19	SsuD	PA3444	Hypothetical protein	2.519	0.002	1.811	0.262
20	PscF	PA1719	Type III export protein	2.507	0.000	-0.304	0.855

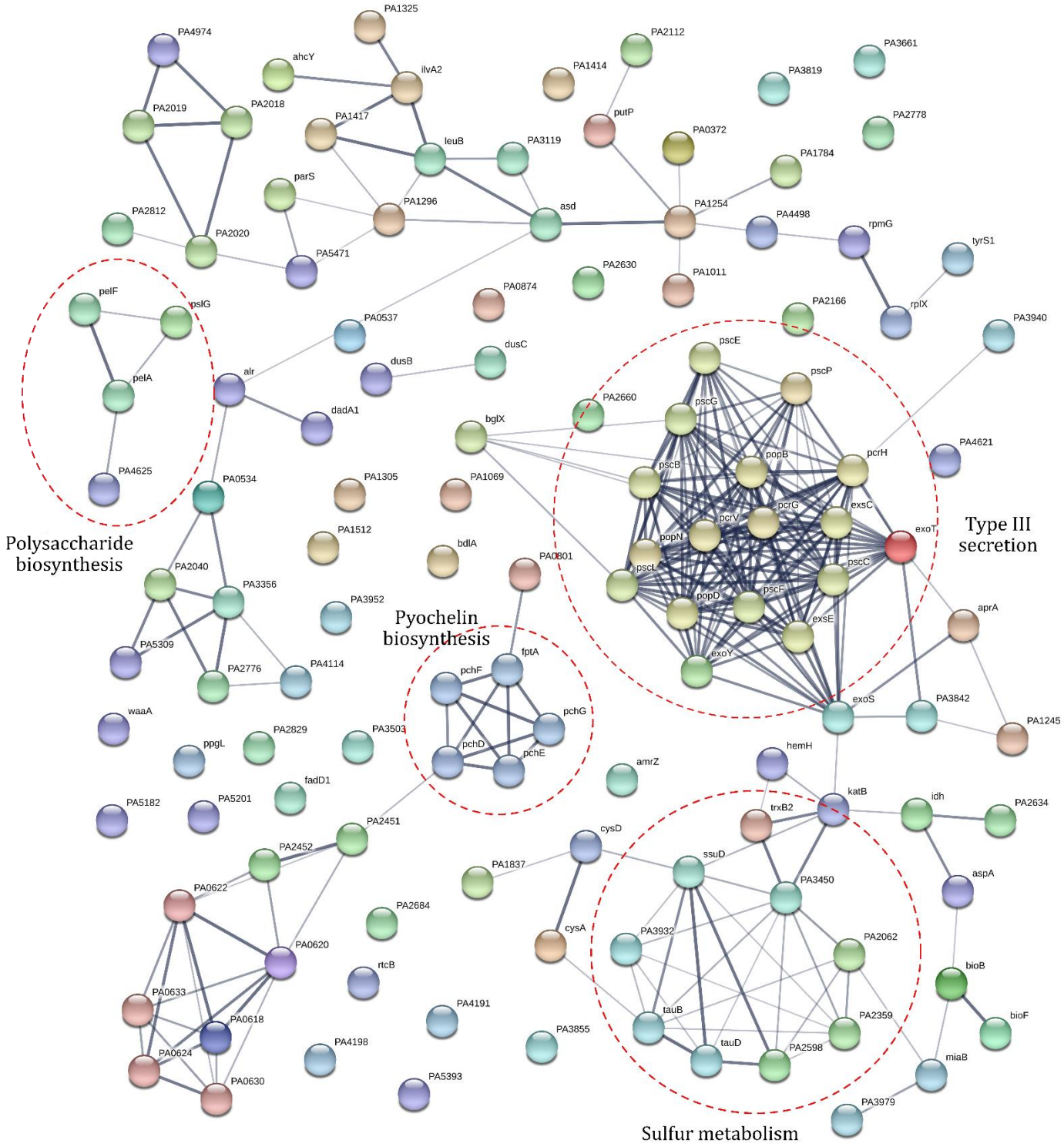

Figure 4.8. Network of interacting proteins. STRING was used to identify groups of interacting proteins that had been significantly up-regulated in the FUS443 mutant strain. Thick lines between nodes represent a high confidence level for that interaction.

Of the top 20 proteins with an increased abundance in the mutant strain, 12 proteins were linked to T3S (shaded rows in Table 4.1). All but one of the T3SS proteins that were significantly up-regulated in the mutant were complemented in the FUS443C strain. This demonstrates that the expression of a functional *fusA1* gene *in trans* reverses the changes in protein abundance associated with the mutated EF-G protein. The protein with the greatest fold change was PscL, a component of the T3SS found adjacent to the inner membrane. PscL underwent a significant $\log_2$ FC of 5.9 in the FUS443 strain, and the $\log_2$ FC in the complemented strain was also significant at 2.5. However, this corresponds to a FC of 58.6 in the mutant strain *versus* a 5.5 FC in the complemented strain, emphasising a distinct recovery in the abundance of this protein with the expression of *fusA1*. Another highly-modulated T3SS protein was PscP, a translocation protein of 38.5 kDa in weight. It is therefore a potential candidate for the 37 kDa band that was observed at an increased intensity in the FUS443 secretome (Figure 4.1). If this band does indeed represent PscP, together the proteomic data and secretome analysis support the notion that FUS443 exhibits increased levels of T3SS synthesis and secretion activity.

STRING is a database of known and predicted protein-protein interactions. These interactions can be direct physical interactions or indirect, functional associations. The 128 proteins that were found to be significantly up-regulated in the FUS443 mutant were analysed in STRING to identify clusters of associated proteins. A large number of the proteins could be organised into several distinct clusters representing different biological processes (Figure 4.8). As indicated in the top 20 modulated proteins, a dense cluster of interacting proteins contained those of the T3SS, such as PcrV, ExsE and ExoT. Another cluster was comprised of proteins associated with sulfur metabolism, such as the sulfate transporter, CysA, sulfate adenyltransferase, CysD and SsuD, involved in desulfonation of aliphatic sulfonates. TauB and TauD were also linked to this cluster as they are involved in metabolising taurine as a sulfur source, along with BioB, a biotin synthase which inserts a sulfur atom into dethiobiotin. A cluster of exopolysaccharide biosynthesis proteins, PelA, PelF and PslG, were up-regulated in the mutant, corroborating the phenotypic results in chapter three. A selection of pyochelin biosynthesis proteins were significantly up-regulated, as were a number of proteins encoded by the bacteriophage-like R2-type pyocin gene cluster; PA0618, PA0620, PA0622. R-type pyocins cause membrane depolarisation and inhibit active transport in closely related species to reduce

bacterial competition (Llamas *et al.*, 2007). Numerous ribosomal and metabolic proteins were also present in the list of affected proteins. With this, it appeared that the mutation in EF-G was affecting numerous biological networks which will be assessed in detail within this chapter.

Alongside the T3SS proteins, two metalloproteinases, AprX and AprA, were amongst the most highly modulated proteins in FUS443. These proteases are secreted through a T1SS and, whilst not operonic, the encoding genes are clustered together on the chromosome alongside *aprDEF* which encode the corresponding ABC transporter. However, it appears that only AprA and AprX were significantly up-regulated in the mutant strain (Table 4.2). AprI is a protease inhibitor which provides protection for self-made proteins prior to protease secretion and was found at a significantly lower abundance in the mutant strain. AprI binds AprA to from a strong inhibitor complex with a stoichiometry of 1:1, blocking the AprA catalytic site (Bardoel *et al.*, 2012). As AprA is a virulence factor typically involved in altering the bacterial cell surface to evade the host immune system (Bardoel *et al.*, 2012), the increase in AprA abundance may have enhanced the proteolytic activity of the mutant strain, causing increased degradation of the central complement protein C3, IFN-gamma and flagellin. However, the lower abundance of AprI would increase the level of AprA activity prior to secretion and may have led to the degradation of proteins within the cell, disrupting various cellular processes and impacting cell fitness.

Table 4.2. Abundance modulation of the proteins located within the *apr* gene cluster, organised by gene order. Shaded boxes represent proteins that have been significantly modulated.

Protein	FUS443		FUS443C	
	log_2 FC	**P-value**	**log_2 FC**	**P-value**
AprX	2.798	0.001	0.452	0.88
AprD	-0.099	0.646	0.284	0.743
AprE	-0.33	0.341	0.514	0.738
AprF	0.27	0.126	0.065	0.962
AprA	2.755	0.007	0.679	0.869
AprI	-1.026	0.001	-0.077	0.94

In *P. fluorescens*, QS, temperature and iron availability have all been shown to influence the production of AprX (Burger *et al.*, 2001). Both *aprX* and *aprA* promoter sequences contain binding sites for iron response regulators, Fur and PvdS (Ithín Maunsell *et al.*, 2017). My data shows that the abundance of Fur and PvdS was unchanged from that of the progenitor strain but as both are post translationally regulated their activity cannot be determined through this screen.

4.3.3.2 Proteins of a decreased abundance

As with analysing proteins of increased abundance, the significance of the down-regulated proteins was defined as a $\log_2$ FC < -1 and an FDR (False Discovery Rate) adjusted P-value of ≤ 0.01. Table 4.3 lists the top 20 proteins in FUS443 that have the greatest reduction in protein abundance. The $\log_2$ FC of proteins from the complemented strain are also included to highlight the recovery of the progenitor phenotype.

Table 4.3. List of down-regulated proteins associated with the *fusA1* mutation in FUS443.

				FUS443		FUS443C	
	Protein	**Locus tag**	**Protein function**	**log_2 FC**	**P-value**	**log_2 FC**	**P-value**
1	ExaB	PA1983	Ethanol oxidation	-3.154	0.000	-0.097	0.950
2		PA5086	Predicted T6SS lipase immunity protein	-3.088	0.000	-1.481	0.222
3		PA2565	Hypothetical protein	-2.962	0.002	-0.718	0.828
4		PA3865	Probable amino acid binding protein	-2.955	0.001	-0.248	0.938
5		PA3785	Hypothetical protein	-2.947	0.000	-0.288	0.899
6		PA5481	Hypothetical protein	-2.807	0.001	-0.194	0.950
7		PA0270	Hypothetical protein	-2.768	0.006	-0.601	0.888
8		PA3576	Hypothetical protein	-2.548	0.004	-0.428	0.903
9		PA2134	Hypothetical protein	-2.533	0.001	-0.474	0.858
10		PA2807	Hypothetical protein	-2.471	0.000	-0.667	0.470
11		PA5505	Probable TonB-dependent receptor	-2.467	0.002	-0.109	0.973
12		PA4697	Hypothetical protein	-2.409	0.001	-0.180	0.962
13		PA5359	Hypothetical protein	-2.366	0.000	-0.514	0.689
14		PA4063	Hypothetical protein	-2.300	0.067	-1.098	0.858
15		PA3318	Hypothetical protein	-2.291	0.001	-0.660	0.660
16		PA2781	Hypothetical protein	-2.278	0.000	-0.066	0.969
17	ModA	PA1863	Molybdate-binding protein	-2.259	0.001	-0.194	0.944
18	FliY	PA0314	Flagellar rotor protein	-2.241	0.001	-0.160	0.956
19		PA5330	Hypothetical protein	-2.240	0.001	-0.201	0.944
20		PA5088	Predicted T6SS lipase immunity protein	-2.205	0.000	-1.478	0.032

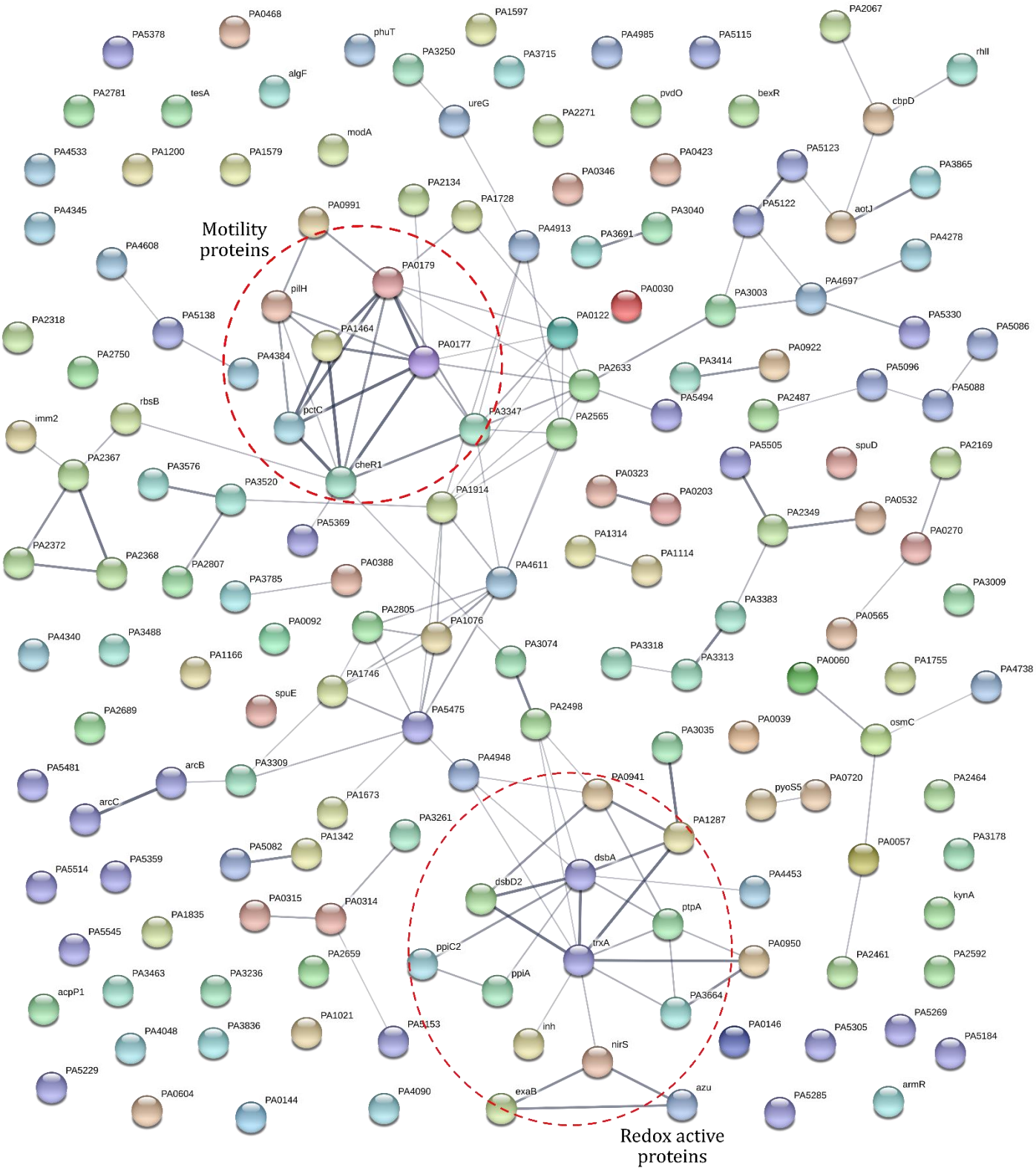

Figure 4.9. Network of interacting proteins. STRING was used to identify groups of interacting proteins that had been significantly down-regulated in the FUS443 mutant strain. Thick lines between nodes represents a high confidence level for that interaction.

The majority of the top 20 down-regulated proteins in FUS443 were uncharacterised (Table 4.3). The protein with the greatest FC was ExaB, a cytochrome C_{550}. Cytochrome C_{550} is an electron acceptor involved in the breakdown of ethanol to aldehyde (Schobert *et al.*, 1999). From the STRING map in Figure 4.9, ExaB was amongst a small cluster of proteins including nitrite reductase, NirS, and azurin, Azu. Azurin transfers electrons from another c-type cytochrome, cytochrome C_{551}, to cytochrome oxidase. Cytochrome C_{551} is the electron donor of nitrite reductase and plays a role in dissimilative denitrification (Cutruzzolà *et al.*, 2002). PA3785, a predicted copper chaperone of the PCuAC family was also amongst the top 20 proteins. This protein chaperones copper to cytochrome oxidase, which contains a binuclear Cu-Cu centre (Serventi *et al.*, 2012). These findings indicated that the mutated EF-G was influencing bacterial respiration.

There were fewer predicted interactions between the down-regulated proteins, compared with the distinctive clustering of the up-regulated proteins. This is likely to be due to the high number of uncharacterised proteins and therefore uncharacterised interactions. Still, several distinct clusters were determined, such as the aforementioned cluster of cytochrome C and respiratory proteins, and a larger set of proteins localised to the periplasm with roles in disulphide bond formation, including DsbA, DsbD2 and TrxA. This group of proteins are all involved in protein folding and are closely linked to the electron transfer chain and cell respiration.

Reduced abundance was identified for ModA, a binding protein for the metal, molybdenum, which is often used as a cofactor, for example, in the reduction of nitrate to nitrite. ModA functions alongside ModB and ModC to transport the metal into the cell. Several other highly down-regulated proteins were linked to the T6SS. PA5086 and PA5088 are predicted to encode T6SS lipase immunity proteins, which protect the cell from lipase inflicted self-harm, or protect against toxic effectors from the same species (Dong *et al.*, 2013). PA5088 is operonic with a T6S phospholipase D effector and with VgrG5, which were not detected in this screen. VgrG proteins are secreted by the T6SS to form complexes that perforate host cell membranes, and its genomic position besides PA5088 makes it likely that its expression was also reduced. The down-regulation of T6SS-assocated proteins observed here is consistent with its inverse regulation with T3SS proteins.

Another cluster of proteins was related to cell motility and chemotaxis, including CheR1, PA0177, PctC, PA1464, and the twitching motility protein, PilH. The flagellar motor protein, FliY, and an uncharacterised protein, PA2781, were also down-regulated in FUS443. PA2781 is operonic with PA2780 (*bswR*), a bacterial swarming regulator (undetected in the proteomic analysis), and PA2781 is predicted to interact with FlgB, a structural component of the bacterial flagellum. This strongly suggests that PA2781 is involved in flagellar mediated motility.

4.4 Motility

Bacteria respond to changes in environmental chemicals through cell surface chemoreceptors. The complex chemosensory system of *P. aeruginosa* comprises of over 20 chemotaxis genes, arranged across five gene clusters. Flagellar motility is organised through *che* genes (clusters I, II and V), whereas T4P synthesis is controlled by the *pil-chp* gene cluster (IV) (Schmidt *et al.*, 2011). Table 4.4 lists how the expression of these clusters were represented at a proteomic level. Cluster III encodes seven Wsp proteins which have been linked to *pel* and *psl* expression (Schmidt *et al.*, 2011), but the Wsp proteins were not modulated in the mutant strain and so are not shown in Table 4.4.

Table 4.4. List of proteins encoded by the *P. aeruginosa* chemosensory system and their log_2 fold change in the FUS443 and complemented mutant. Shaded boxes represent proteins that have been significantly modulated.

Protein		Cluster	FUS443		FUS443C	
			log_2 FC	P-value	log_2 FC	P-value
CheY	Two component response regulator	I	-0.708	0.001	-0.104	0.897
CheZ	Chemotaxis protein	I	-0.373	0.017	-0.058	0.950
CheA	Probable two-component sensor	I	-0.365	0.029	-0.281	0.630
CheB	Methylesterase	I	-0.560	0.002	-0.126	0.841
MotD	Flagellar motor protein	I	-0.569	0.002	-0.340	0.973
Orf1	Probable plasmid portioning protein	I	-0.332	0.103	-0.034	0.980
Orf2	Hypothetical protein	I	-0.159	0.143	-0.077	0.897
CheW	Purine-binding chemotaxis protein	I	-1.103	0.000	-0.359	0.450
CttP	Chemotactic transducer for trichloroethylene	II	0.098	0.740	-0.199	0.899
CheY2	Probable two component response regulator	II	-1.260	0.001	0.052	0.973
CheA2	Probable two component sensor	II	0.074	0.776	0.227	0.858
CheW2	Probable purine-binding chemotaxis protein	II	-1.313	0.003	-0.034	0.987
Aer2	Aerotaxis transducer	II	-0.294	0.118	0.105	0.915
CheR2	Probable methyltransferase	II	0.001	0.996	-0.138	0.933
CheD	Hypothetical protein	II	-0.054	0.887	-0.035	0.988
CheB2	Probable methylesterase	II	-0.474	0.289	-0.057	0.985
PilG	CheY-like response regulator	IV	-0.972	0.000	-0.041	0.966
PilH	CheY-like response regulator	IV	-1.274	0.000	-0.150	0.743
PilI	Chemoreceptor adapter protein	IV	-0.251	0.360	-0.001	1.000
PilJ	Chemoreceptor	IV	0.446	0.091	0.573	0.480
PilK	Methyltransferase	IV	0.316	0.035	-0.135	0.855
ChpA	Histidine kinase	IV	0.140	0.558	0.123	0.932
ChpB	Methylesterase	IV	-0.170	0.134	0.006	0.993
CheV	Probable chemotaxis protein	V	-0.242	0.232	-0.021	0.987
CheR	Methyltransferase	V	-1.205	0.000	-0.180	0.696

The abundance of five of chemotaxis proteins (CheW, CheR, CheY2, CheW2 and PilH) was significantly lower in the FUS443 mutant and was complemented by the p*fusA1* plasmid. CheW conveys signals from cell surface chemoreceptors to the cytoplasmic histidine kinase, CheA. CheA relays this signal into the cell by activating CheY which controls the rotational switch on flagellar motors. CheR, a methyltransferase works antagonistically with the methylesterase, CheB, to reset the chemoreceptor after ligand binding by altering its methylation status (Ferrández *et al.*, 2002). However, the homologs encoded in cluster II are predicted to form functionally distinct signalling complexes to that of cluster I, for example, there is no support to suggest that CheY2 interacts with the flagellar motor (Ferrandez *et al.*, 2002). The majority of flagellar-associated proteins had been down-regulated in the mutant strain and, where PilG, PilH and PilI were all down-regulated, several of the other twitch-related proteins were marginally up-regulated.

Phenotypic analysis of the mutant strain saw a decrease in swimming and twitching motility. Here, I have presented proteomic evidence that a large number of chemotaxis and motility proteins are reduced in abundance, many of which were complemented by the expression of p*fusA1*. The distribution of up-regulated proteins amongst different motility operons suggests that this change in abundance is occurring at a post-transcriptional level and so the mutated EF-G protein may be affecting mRNA stability or protein degradation systems.

4.5 Type III secretion and ribosomal stress

4.5.1 Type III secretion

In *P. aeruginosa*, over 30 genes are involved in the regulation and biosynthesis of the T3SS (H. Yang *et al.*, 2007). Due to the prevalence of T3SS-associated proteins amongst those most highly-modulated in FUS443, the proteomic abundance for the whole T3SS operon was investigated (Table 4.5).

Table 4.5 List of proteins encoded by the *P. aeruginosa* T3SS and their log_2 fold change in the FUS443 and complemented mutant. Shaded boxes represent proteins that have been significantly modulated.

Protein	FUS443		FUS443C	
	log_2 FC	**P-value**	**log_2 FC**	**P-value**
Basal body				
PscD	0.382	0.291	0.199	0.926
PscJ	0.758	0.002	0.027	0.980
PscC	2.133	0.000	-0.076	0.962
PscL	5.873	0.000	2.458	0.008
Translocon				
PopB	3.151	0.000	-0.055	0.973
PopD	3.895	0.000	-0.113	0.903
PcrV	2.143	0.000	-0.305	0.738
Needle				
PscF	2.507	0.000	-0.304	0.855
PscP	4.178	0.000	-0.179	0.953
Export apparatus				
PopN	4.187	0.001	0.172	0.973
PscB	2.349	0.000	-0.017	0.987
Regulatory network				
ExsC	2.358	0.000	-0.019	0.993
ExsE	2.401	0.000	-0.162	0.945
ExsA	0.894	0.000	0.068	0.925
ExsD	0.846	0.000	-0.036	0.973
Chaperones				
SpcS	3.263	0.000	-0.156	0.866
PcrH	3.262	0.000	-0.352	0.777
PcrG	3.211	0.000	-0.502	0.729
PscE	1.982	0.000	-0.300	0.769
PscG	2.205	0.000	-0.189	0.861
Secreted toxins				
ExoS	3.261	0.000	0.157	0.861
ExoT	2.836	0.000	0.138	0.861
ExoY	3.266	0.000	-0.193	0.881

The majority of T3SS genes are clustered together in the *P. aeruginosa* genome, encoded across five operons. At least six other genes are distributed elsewhere in the chromosome, including the secreted exotoxins and their chaperones. All of the T3SS proteins identified in the proteomic screen were found to be up-regulated in the mutant strain, suggesting that the mutation to EF-G is disrupting the global regulation of all T3SS genes.

The master regulator of the T3SS is ExsA, which binds to the promoter of T3SS operons and activates transcription. In FUS443, the abundance of ExsA was increased by a FC of 1.9 (86% more abundant than in the progenitor strain) and was completely complemented by the introduction of a functional *fusA1* gene. ExsA regulates the T3SS through a 'catch-and-release' network with ExsCDE, all of which are positively regulated by ExsA (Brutinel *et al.*, 2010). Whilst the change in ExsA abundance was not considered significant under the parameters of this study, this relatively small change may be enough to tip the balance and activate T3S expression. The abundance of another T3SS transcriptional regulator, PsrA, was unaffected in this study.

4.5.2 Ribosomal stalling

Over 60 ribosomal proteins were up-regulated in the mutant strain, of which the top 15 are represented in Table 4.6.

Table 4.6. List of ribosomal and ribosome-associated proteins encoded by *P. aeruginosa* and their log_2 fold change in the FUS443 and complemented mutant strains. Shaded boxes represent proteins that have been significantly modulated in the mutant strain.

Protein		FUS443		FUS443C	
		log_2 FC	**P-value**	**log_2 FC**	**P-value**
RplX	50S ribosomal protein L24	1.712	0.001	0.380	0.743
RpmG	50S ribosomal protein L33	1.643	0.006	0.165	0.964
RpmE	50S ribosomal protein L31	1.248	0.268	1.098	0.855
RpsT	30S ribosomal protein S20	0.892	0.001	0.182	0.830
YcfB	Probable DNA methylase	0.891	0.001	0.155	0.847
DeaD	probable ATP-dependent RNA helicase	0.878	0.002	0.250	0.794
RplB	50S ribosomal protein L2	0.872	0.006	0.324	0.764
RplA	50S ribosomal protein L1	0.863	0.008	0.382	0.729
RplU	50S ribosomal protein L21	0.854	0.004	0.331	0.729
RplT	50S ribosomal protein L20	0.845	0.008	0.276	0.828
SmpB	RNA binding protein	0.839	0.001	0.236	0.703
RplC	50S ribosomal protein L3	0.825	0.007	0.311	0.775
RplI	50S ribosomal protein L9	0.813	0.001	0.220	0.742
RpsM	30S ribosomal protein S13	0.786	0.010	0.300	0.802
FusA1	Elongation factor G (1A)	0.495	0.006	2.269	0.000
FusA2	Elongation factor G (1B)	0.624	0.009	-0.025	0.985

The abundance of ribosomal complexes is adjusted to meet the demand for protein synthesis in the cell (Aseev, Koledinskaya and Boni, 2016). If the EF-G protein reduces the efficiency of translation, as speculated, the cell may upregulate the synthesis and assembly of ribosomal proteins to compensate for this defect and to maintain a sufficient level of protein synthesis for cell survival.

Amongst the ribosome-associated proteins was the RNA binding protein, SmpB. In *E. coli*, SmpB binds the RNA molecule, *ssrA,* which functions as both tRNA and mRNA. It binds to the A-site of stalled ribosomes where it acts as a surrogate mRNA transcript and directs the translation of a short peptide tag which targets the stalled peptide for proteolysis, preventing the accumulation of stalled ribosomes (Karzai *et al.*, 1999). Whilst *ssrA* cannot be detected under proteomic analysis, SmpB is essential in stabilising the

association between *ssrA* and the ribosome, and so the increased abundance of SmpB may indicate an increase in *ssrA.* This suggests that the mutated EF-G is causing the ribosome to stall. Unlike with previous modulations which have typically shown complete complementation by p*fusA1*, the abundance of ribosomal proteins was only partially recovered. The endogenous, mutated form of EF-G was still expressed in the complemented strain and so EF-G-P443L and the WT EF-G, expressed *via* p*fusA1*, would be competing for ribosomal binding, leading to incomplete complementation.

4.5.3 Induction of *exsA* expression *via* ribosomal stress

Amongst the up-regulated ribosomal proteins was the DEAD-box protein, DeaD. DeaD is an RNA helicase that is important in processing RNA prior to translation. Interestingly, DeaD has been found to stimulate ExsA translation and therefore promotes the expression of the T3SS (Intile *et al.*, 2015). The abundance of DeaD in the mutant strain was increased by a FC of 1.8 (an 84% increase from that of the progenitor), similar to the increase in ExsA abundance. Therefore, it is possible that the global up-regulation of ribosomal proteins, induced by the mutant EF-G protein, may be causing an up-regulation of T3SS genes *via* DeaD.

Alternatively, amongst the highly down-regulated proteins was the copper-binding protein, PA2807. This is encoded directly downstream of *ptrA*, also involved in copper tolerance, but unfortunately not detected in this screen. PtrA has been identified as a direct inhibitor of ExsA and its over-expression completely inhibits secretion *via* the T3SS (Ha *et al.*, 2004). If *ptrA* was also down-regulated with PA2807 in response to copper levels, this may have added to the increased ExsA abundance.

4.5.4 *FusA* homologs

Two EF-G homologs exist in *P. aeruginosa.* The *fusA1*-encoded EF-G1A was found at a greater abundance than the *fusA2*-encoded EF-G1B, in the mutant and progenitor strains. The mutant strain expressed both homologs at a higher abundance than in the progenitor, but not to a significant level. This up-regulation may have been induced through a common mechanism with the other ribosome-associated proteins. The *fusA1*

and *fusA2* sequences are highly conserved among *P. aeruginosa* species, and previous transcriptomic studies have shown that *fusA2* is expressed around 30-fold less than *fusA1* (Bielecki *et al.*, 2012). The ratio between the two encoded proteins was not as skewed in this study but was consistent with *fusA1* being the dominantly expressed homolog.

One study found that EF-G1B was more susceptible to the action of fusidic acid than EF-G1A (Palmer *et al.*, 2013). The two homologs share 84% amino acid sequence identity. None of the amino acid variations are positioned within the fusidic acid binding pocket and so sensitivity to the antibiotic is likely to be due to global conformational differences that effect binding. The majority of amino acid variations are positioned in domain I, the site of GTP binding and hydrolysis, as well as numerous changes to domain IV. As these domains are key to the function of EF-G, this supports the idea that EF-G1A and EF-G1B play distinct roles in the cell.

The proteomic data also quantified the abundance of EF-G in FUS443C at 4.8-fold greater than that observed level in the progenitor strain and the potential effects of this over-expression should be taken into consideration. The over-expression of *fusA1* in the complemented strain did not lead to a change in abundance of the EF-G1B protein, showing that there was limited feedback between these two homologs. This suggests that the increase in EF-G1B in the mutant strain did not result from any interaction with the mutated EF-G1A and was induced through an independent mechanism, such as that of the other ribosomal proteins.

4.6 Up-regulation of siderophore biosynthesis in FUS443

4.6.1 Pyochelin-associated proteins

Also amongst the proteins most affected by the P443L mutation was a variety of pyochelin-biosynthesis proteins that had been up-regulated (Table 4.7). Pyochelin is an iron-scavenging siderophore that is secreted into the environment to acquire iron for bacterial growth. Iron-bound pyochelin is detected by receptors on the cell surface membrane and is internalised where the iron can then be utilised by the cell. *P. aeruginosa* synthesises two siderophores; pyochelin and pyoverdine, the abundance of pyoverdine-associated proteins was unchanged in FUS443 whereas the expression of a

wide variety of pyochelin-associated proteins was increased. Interestingly, the abundance of regulatory proteins for pyochelin synthesis, such as PchR and Fur, was unchanged in the mutant strain, but the regulators may have been functioning at an altered level of activation. Expression of the p*fusA1* complementation plasmid only partially restored protein abundance levels to that of the progenitor strain, making it difficult to attribute this phenotype solely to the P443L mutation.

Also amongst the down-regulated proteins was the hypothetical protein, PA2134, and FeoA. PA2134 shares homology with the iron storage protein, ferritin, and FeoA, encoded on the *feoABC* operon, is involved in ferrous iron acquisition. FeoA is a cytosolic protein thought to activate the iron permease FeoB, perhaps serving as GTPase activating protein, to promote iron transport into the cell (Seyedmohammad *et al.*, 2016). The down-regulation of these proteins demonstrates how the P443L mutation is influencing multiple iron-uptake systems in different ways.

Table 4.7. List of pyochelin-associated proteins encoded by *P. aeruginosa* and their log_2 fold change in the FUS443 and complemented mutant. Shaded boxes represent proteins that have been significantly modulated in the mutant strain.

Protein		FUS443		FUS443C	
		log_2 FC	**P-value**	**log_2 FC**	**P-value**
PchE	Dihydroaeruginoic acid synthetase	2.441	0.003	1.321	0.470
PchG	Pyochelin biosynthetic protein	2.312	0.004	1.483	0.442
PchD	Pyochelin biosynthesis protein	1.888	0.001	0.657	0.532
PchH	Probable ATP-binding component of ABC transporter	1.836	0.028	1.884	0.428
PchF	Pyochelin synthetase	1.810	0.006	1.050	0.536
PchI	Probable ATP-binding component of ABC transporter	1.552	0.046	1.672	0.470
PchA	Salicylate biosynthesis isochorismate synthase	1.398	0.016	0.562	0.808
FptA	Fe(III)-pyochelin outer membrane receptor precursor	1.106	0.006	0.851	0.384
PchR	Transcriptional regulator	-0.025	0.905	-0.120	0.908

4.6.2 Siderophore secretion

With the up-regulation of pyochelin synthesis proteins, I expected FUS443 to secrete higher levels of siderophores than the progenitor strain. To test this, a Siderotech assay kit was used to detect the release of siderophores into the culture supernatant. If siderophores are detected within the cell-free supernatant the solution turns red in colour, as seen with the progenitor and the complemented strains. In a very unexpected result, the mutant strain did not secrete detectable levels of siderophores into the medium (Figure 4.10). This kit is not specific for pyochelin secretion which suggests that pyoverdine was also not being secreted from the mutant cells.

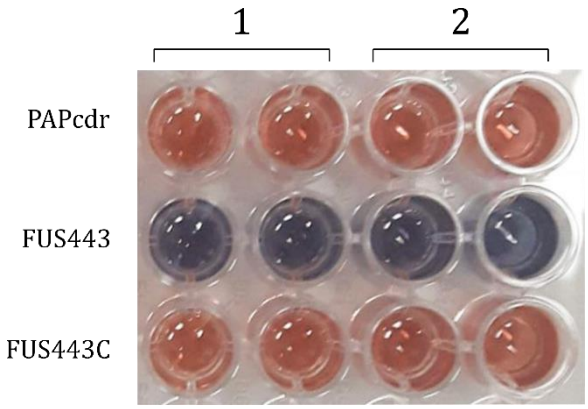

Figure 4.10. Siderotech assay was used for the detection of siderophores in the culture supernatants of the progenitor strain (PAPcdr), the FUS443 mutant and the complemented mutant strain (FUS443C). The supernatant from two biological replicates (1 and 2) were tested twice for each strain. Solution turns from blue to red upon the detection of siderophores in the culture supernatant.

The lack of siderophore secretion suggests that either the siderophore-biosynthesis pathways in the mutant strain were disrupted, or the secretory systems. Unlike for the secretion of pyoverdine, very little is known about the secretion of pyochelin from the cell. The protein, TonB, is vital for iron uptake and is required by all of the siderophore transport systems (Cuív *et al.*, 2007). Amongst the top down-regulated proteins was PA5505, predicted to be a TonB-dependent receptor related to iron acquisition, possibly as a siderophore shuttle between the plasma membranes. A

reduction in the abundance of PA5505 highlights it as a potential bottleneck in siderophore secretion.

An inability to acquire iron *via* siderophore secretion would mean that the cells would not grow well under iron limited conditions. To investigate this, the mutant strain, the progenitor and the complemented strain were grown on minimal media plates containing increasing concentrations (0.1 to 100 mM) of the iron chelator, ethylenedinitrilo tetra-acetic acid (EDTA) (Figure 4.11). Overall, little difference in growth was observed across the strains and all strains struggled to grow on media containing over 10 mM EDTA. This suggests that the mutant strain, despite disruption to siderophore secretion, is equally capable of surviving under iron limited conditions to the progenitor strain.

Figure 4.11. Growth on minimal media supplemented with increasing concentrations of the metal chelator, EDTA. The formation of strains, labelled on the first plate, is consistent across all assay plates.

4.7 Antibiotic resistance

In chapter three, antibiotic resistance assays suggested that the mutated EF-G protein plays a direct role in resistance to aminoglycosides by disrupting binding at the ribosomal A-site. Now, with the proteomic analysis, it was revealed that the mutant strain exhibited an increased abundance of efflux pumps, which were complemented with the p*fusA1* plasmid (Table 4.8). This proposed that the mutated EF-G protein is promoting antibiotic resistance indirectly, *via* the up-regulation of efflux systems to expel antibiotics from the cell.

Table 4.8. List of protein efflux systems encoded by *P. aeruginosa* which were found to be up-regulated in the FUS443. Log_2 FC for the mutant and complemented mutant are shown. Shaded boxes represent proteins that have been significantly modulated in the mutant strain.

Protein name		FUS443		FUS443C	
		log_2 FC	**P-value**	**log_2 FC**	**P-value**
ArmZ	MexZ anti-repressor	2.106	0.000	0.022	0.985
MexY	Multidrug efflux transporter	1.929	0.001	0.170	0.942
MexX	Multidrug efflux membrane fusion protein	1.830	0.000	0.110	0.915
OpmH	Probable outer membrane protein precursor	1.282	0.001	-0.134	0.903
MexZ	Transcriptional regulator	1.183	0.001	0.055	0.973
OprM	Efflux outer membrane protein	-0.359	0.137	-0.150	0.907

Of the main efflux systems encoded by *P. aeruginosa* (MexAB-OprM, MexCD-OprJ, MexEF-OprN and MexXY-OprM), only the MexXY system was seen to be significantly up-regulated in the FUS443 mutant. This was reflected in the increased abundance of its regulators MexZ and ArmZ. However, the outer membrane protein for the MexXY system, OprM, was the only component not to be up-regulated and actually exhibited a slight decrease in protein abundance. The successful complementation with p*fusA1* strongly suggested that the P443L mutation was causing changes in the abundance of this efflux system which may contribute to the increased aminoglycoside resistance observed in the mutant strain.

4.8 Discussion

4.8.1 Type III secretion

The T3SS is a major virulence determinant and is one of the approaches used by bacteria to induce the cell death of eukaryotic host cells during infection. The needle complex of the T3SS penetrates the plasma membranes of adjac3333ent host cells and 'injects' exotoxins into the host cell cytoplasm. These exotoxins disrupt cytoskeletal components to induce cell rounding and cell death. T3SS biogenesis and regulatory proteins are encoded across five clustered operons, consisting of 36 genes (Figure 1.4), with genes encoding the effector proteins and chaperones spread out throughout the genome (Hauser, 2009). Almost all of the T3SS proteins detected in the FUS443 proteomic analysis were of a markedly higher abundance than in the progenitor and complemented strain. Typically, T3S is maintained at low basal levels until activated by environmental stimuli such as a low calcium concentration or host cell contact, which promote transcription of the system *via* the master regulator ExsA (H. Yang *et al.*, 2007). Conditions across all replicates and strains in this study were kept constant, meaning that the T3SS should not have been activated by either of these stimuli. Therefore, the P443L mutation must have been inducing T3S *via* a different mechanism.

The proteomic analysis of the mutant strain confirmed an increase in ExsA abundance, whose activity is controlled by the ExsECD interaction cascade. Under non-inducing conditions, two protein partnerships are formed; ExsD/A and ExsC/E. Activation of the T3SS results in secretion of ExsE through the injectosome, causing a series of partner-switching actions, where the newly relinquished ExsC binds to ExsD. ExsA is released and is free to activate the expression of T3SS genes, including its own promoter, creating a surge in the assembly of T3S complexes on the cell membrane (Intile *et al.*, 2015). All of the proteins within this regulatory cascade were more abundant in the FUS443 strain but to varying degrees. ExsC underwent a far greater increase in abundance than ExsD, which would have increased the level of ExsD sequestration by ExsC. In doing so, more ExsA would be relinquished, and would be free to initiate the up-regulation of T3SS genes.

A known T3SS regulatory system, the Gac/Rsm pathway, was not affected on a proteomic level by the presence of the P443L mutation. Similarly, two other regulatory

systems, Vfr and cAMP signalling, were unchanged. One protein, DeaD, was found in higher abundance in FUS443 and has been found to directly regulate translation of the *exsA* transcript. DeaD is a DEAD-box RNA helicase, which assists in the translation of proteins by relaxing mRNA secondary structures and encouraging ribosome binding. Previous studies have identified DeaD as a positive post-transcriptional regulator of *exsA* through this mechanism (Intile *et al.*, 2015). Control of the ExsECDA cascade is finely balanced and small changes can disrupt this equilibrium to create larger changes to T3S activity. With this, the small increase in the abundance of DeaD may raise ExsA levels enough to induce a positive feedback cascade on the expression of T3SS genes.

In *E. coli* there are 5 DEAD-box RNA helicases, including DeaD, that facilitate the assembly of the 50S ribosomal subunit (Vakulskas *et al.*, 2014). Synthesis of ribosomal proteins is adjusted so that the synthesis of cellular components can be maintained at an optimal level for growth. As protein biosynthesis is the largest consumer of energy in the cell, excess translation causes negative feedback on rRNA and tRNA genes (Nomura, 1999). Suboptimal translation should therefore cause the inverse, seeing a rise in the number of ribosomal proteins to maintain growth. The reduced functional efficiency predicted for the mutated EF-G would put a strain on the ribosome to meet the protein synthesis requirements for optimal cell growth. This increased pressure may have led to the increase in ribosome-associated protein abundance in FUS443, including DeaD, and in doing so, promoted the expression of *exsA* and T3S.

Alternatively, T3S induction might have occurred *via* PtrA, a transcriptional repressor that is known to negatively regulate ExsA. PtrA was absent from the proteomic profile of FUS443, however the neighbouring gene PA2807 was found at a reduced abundance. Both PA2807 and PtrA are involved in copper tolerance and so are likely to be co-expressed. It is postulated that PtrA negatively regulates ExsA, whilst up regulating copper resistance genes, to shut off energetically expensive systems such as the T3SS during unfavourable growth conditions (Ha *et al.*, 2004). If the reduced levels of PA2807 reflect a reduction in PtrA abundance, then this would elevate *exsA* repression and promote T3S. The role of EF-G in PA2807 and PtrA expression is unclear, but it is possible that the mutation affects the way in which the mutant cell senses copper, leading to dysregulation of copper response systems.

4.8.2 Antibiotic resistance

Phenotypic analysis of FUS443 identified that the strain was resistant to at least two aminoglycosides; kanamycin and gentamicin. As both EF-G and aminoglycosides target the A-site of the ribosome, it was logical to presume that a change in EF-G conformation had led to steric hindrance, preventing the action of the antibiotics on the ribosome. The proteomic data presented an alternative explanation by highlighting the up-regulation of an efflux system that is specific for aminoglycoside export.

Expression of the MexXY efflux system is the predominant mechanism of aminoglycoside resistance in CF lung isolates and is induced upon exposure to antibiotics (Hay *et al.*, 2013). But even in the absence of antibiotic selection, the MexXY efflux system was drastically up-regulated in the FUS443 mutant. ArmZ is the main activator of the MexXY efflux system which functions by inhibiting the *mexXY* repressor, MexZ. *MexZ* is the most commonly mutated gene in CF isolates and is predominantly mutated in aminoglycoside-resistant strains (Morita *et al.*, 2012; Hay *et al.*, 2013). During activation of the MexXY system, ArmZ is expressed in response to disrupted translation caused by the presence of antibiotics. During translocation the 30S ribosome rotates relative to the 50S subunit, at which point the tRNA is moved into the next ribosomal position. Gentamicin has been shown to lengthen the non-rotated state and lock the tRNA into a conformation that stabilises its position within the A-site. This causes the ribosome to stall and peptide synthesis is aborted to allow the ribosome to be 'reset' (Tsai *et al.*, 2013). Upstream of the *armZ* coding sequence lies a leader peptide that forms secondary structures to prevent transcription of the downstream *armZ* gene. If the ribosome does not translate the mRNA efficiently and stalls on the leader peptide, indicative of aminoglycoside action, the leader peptide cannot form the inhibitor secondary structure and promotes high-level constitutive expression of *armZ.* As a result, the *mexXY* operon is transcribed in response to the antibiotic action taking place on the ribosome (Morita *et al.*, 2009).

In chapter three, the intrinsic tryptophan fluorescent analysis indicated that there were likely to be changes in the structural conformation of domain I, which contained four tryptophan residues and is the site of GTP binding and hydrolysis. Being unable to hydrolyse GTP would lock EF-G in the ribosome and reduce the rate of its dissociation. If the mutation is indeed affecting EF-G in this way, translation would be halted, mimicking

the translational stalling caused by aminoglycosides. The presence of ribosomal stalling in the mutant strain was supported by the up-regulation of SmpB, which works with the RNA, *ssrA*, to prevent the accumulation of stalled ribosomes by targeting the problem peptide for degradation (Karzai *et al.*, 1999). Therefore, even in the absence of antibiotics, ribosomal stalling would cause *armZ* to be fully transcribed and would induce the expression of the MexXY system. The mutant strain would then be prepared for the export of aminoglycosides resulting in increased resistance.

4.8.3 Iron chelation and fusaric acid

Iron is essential for almost all biological processes but due to the formation of insoluble ferric hydroxides its bioavailability is quite limited. To counter this, bacteria secrete siderophores which chelate the insoluble iron from the environment and deliver it back into the cell where it is made available for use (Brandel *et al.*, 2012). *P. aeruginosa* synthesises two major siderophores to cover its need for Fe^{3+}; pyoverdine and pyochelin. Pyoverdine is considered to be more essential for growth than pyochelin, which is produced at a lower abundance (Brandel *et al.*, 2012). Despite this, many of the pyochelin biosynthesis and receptor proteins are up-regulated in the FUS443 mutant strain, whereas the abundance of pyoverdine biosynthesis proteins was unaffected. Pyochelin biosynthesis genes are encoded on two divergent operons, *pchDCBA* and *pchEFGHI*, with the regulatory gene, *pchR*, located between the two. Pyochelin binds iron with a stoichiometry of 2:1 ($PCH:Fe^{3+}$), and is transported back into the cell through the outer membrane transporter, FtpA, and the inner membrane transporter, FptX. Once in the cytosol the iron-bound pyochelin binds to PchR to induce further expression of pyochelin biosynthesis genes (Figure 1.7). If iron accumulates in the cell, the iron binds to Fur, which inhibits the expression of iron-uptake genes, including *pch* genes, by binding the promoter sequences and blocking transcription (Cunrath *et al.*, 2015).

The *fusA1* mutation heavily induced the expression of pyochelin biosynthesis proteins, including the uptake receptor, FtpA. But it was interesting to see that there was limited secretion of siderophores into the surrounding media. As all of the detected pyochelin biosynthesis proteins were up-regulated it appears that the issue with iron acquisition was occurring through an inability to successfully synthesise the siderophore

or unsuccessful transport out of the cell. Whilst studies have shown that pyoverdine is exported from the cell by the outer membrane efflux system, PvdRT-OpmQ, little is known about the export of pyochelin (Hannauer *et al.*, 2010). Mutation to exporters can result in the accumulation of siderophores within the cell (Miethke *et al.*, 2007) and so it is possible that the mutated EF-G protein is affecting the synthesis or activation of siderophore secretion systems, creating an internal iron-starved environment and perpetuating the synthesis of pyochelin biosynthesis proteins.

Phenotypic characterisation revealed that FUS443 had developed sensitivity to fusaric acid. In *P. protegens*, the presence of fusaric acid causes an up-regulation of genes involved in iron acquisition, including those for siderophore synthesis. Mutants in siderophore production were far less tolerant to fusaric acid, and as a consequence of these observations fusaric acid was identified as an iron chelator (Ruiz *et al.*, 2015). As iron acquisition appeared to be disrupted in FUS443 the cell was likely to already be in an iron-limited state and so the presence of fusaric acid further reduced iron availability meaning that FUS443 was unable to obtain enough iron for cell survival. Therefore, fusaric acid may have exerted a toxic effect on the FUS443 mutant, indirectly, through iron sequestration and not by direct antimicrobial action. However, the FUS443 mutant did not show impaired growth in the presence of another metal chelator, EDTA. This supports the notion that fusaric acid toxicity resulted from a direct interaction with the cell, however, a limited understanding as to the mechanism of action by which this antibiotic functions makes it unclear how this would have occurred. It is possible that the combination of siderophore disruption, iron-chelation by fusaric acid and a direct effect on the cell led to increased fusaric acid sensitivity.

4.8.4 Motility

In chapter three I found that the *fusA1* mutation caused a reduction in swimming and twitching motility. The proteomic data in this chapter supported this finding, as numerous motility-associated proteins had been modulated. This confirmed that the effect on motility was a result of direct changes to motility systems and not due to the reduced growth rate.

Unlike the single set of *che* genes in *E. coli*, *P. aeruginosa* encodes four chemotaxis signal transduction systems; the Pil-Chp system for twitching motility, the Che and Che2 systems for flagella motility and the Wsp system for Cup fimbria expression and Pel/Psl biosynthesis. The assembly and function of T4P, which mediates twitching motility, requires over 40 genes and its regulation involves numerous signal transduction systems, including the two-component system, PilR/S and AlgR/FimS, the global carbon metabolism regulator Crc, the virulence factor regulator Vfr and the chemosensory system PilGHIJK-ChpABC (Bertrand *et al.*, 2010). Proteomic data revealed that the PilR, PilS, AlgR, Vfr and Crc regulators were relatively unaffected by the mutation, and FimS was not identified in the screen. Regardless, the Pil chemosensory system saw large decreases in the abundance of PilG and PilH. PilG is involved in pili extension whilst PilH is required for retraction, and previous studies have found that mutation to PilH causes aberrant twitching (Bertrand, West and Engel, 2010). With the reduced abundance of these two proteins the FUS443 mutant may be unable to coordinate directional twitching motility leading to a reduced bacterial spread across twitch agar.

P. aeruginosa has a single polar flagellum which, like T4P, is coordinated by over 40 genes, making these two systems extremely energetically expensive. Flagellar motility is regulated by a hierarchical regulatory network, of which the master regulator is FleQ (Dasgupta *et al.*, 2003). FleQ was not affected in the FUS443 mutant, but may have had an altered activation status differentially impacting flagellar genes. Several of the Che proteins involved in flagellar motility were found at a reduced abundance in the mutant strain, in particular were CheW and CheR. CheW is a coupling protein that associates with the chemoreceptors on the cell surface and assists in signal transduction between the receptor and the sensor kinase, CheA. CheA activates CheY which interacts with the rotational switch of FliM and disrupts the flagellar motor. The reduced abundance of these proteins will therefore affect flagellar rotation and propulsion through a semi-solid media.

The other significantly down-regulated protein, CheR, is a methyltransferase. Methyltransferases are important in 'resetting' the chemoreceptors after ligand binding to allow for continual sensing of the environment. The antagonistic action between CheR and the methylesterase, CheB, provides a kinetically fast feedback system for rapid adaption to the bacterial surroundings (Ferrández *et al.*, 2002; Sampedro *et al.*, 2014). Disruption to the abundance or activation of either of these proteins will reduce the

responsiveness of *P. aeruginosa* to the environment. Because of this, FUS443 may therefore be less efficient at moving up a nutrient gradient and would produce a smaller zone of swimming, as observed in the swimming assay.

The cluster II protein, CheW2, was also significantly down-regulated in the mutant strain. Unlike cluster I genes, the cluster II genes are not essential for chemotaxis. In some cases, cluster II proteins can complement cluster I mutants, but previous studies have found that this is not the case for CheW2 and CheW (Ferrandez *et al.*, 2002). This suggests that the cluster II proteins have distinct roles from that of cluster I and so demonstrates that the mutated EF-G protein is modulating the protein abundance of specific pathways involved in motility, covering both T4P movement and flagellar motility.

In addition to the effect on chemotaxis proteins, the mutant also expressed MotD at a reduced abundance. *P. aeruginosa* encodes two homologous sets of Mot proteins, MotA/B and MotC/D which generate the torque that drives the rotation of the flagellum. The MotC/D complex is used for propulsion in liquid, whilst MotA/B are more efficient at movement through high-viscosity medium. The elimination of either MotC or MotD reduces swimming speed and radial expansion in semi-solid agar (Doyle *et al.*, 2004), and so it is possible that the reduction in MotD may be contributing to the reduced motility on the swim assay plates. MotA/B are regulated as part of the flagellar biogenesis hierarchy, involving RpoN, FleQ and FleR, however, MotC/D appear to be regulated independently of this system (Doyle *et al.*, 2004), and so it appears that the P443L mutation is impacting cell motility outside of the central regulatory networks.

4.8.5 Disulfide bond formation

Another prominent cluster of down-regulated proteins included numerous redox proteins, such as DsbA, DsbD2 and TrxA. Dsb proteins are from the thioredoxin superfamily and contain a disulphide bond in their catalytic site, making Dsb proteins strong oxidants. Various secreted proteins are transported in an unfolded state into the periplasm. In *E. coli*, the folding of these proteins operates in two stages; oxidation by DsbA and DsbB, and isomerisation/reduction by DsbC and DsbD (Figure 4.12) (Grabowska *et al.*, 2011). After synthesis, DsbA introduces disulfide bonds on consecutive cysteines as they emerge through the cytoplasmic membrane and DsbC, a disulfide

isomerase, corrects the disulfide pairings for correct protein folding (Cho *et al.*, 2013). The electron source for the reducing stage comes from the cytoplasmic protein thioredoxin (TrxA) which transfers electrons to DsbD, and are shuttled through to DsbC (Chung *et al.*, 2000; Cho *et al.*, 2013). During this pathway, electrons are shuttled to quinone molecules located within the cytoplasmic membrane, where they are transferred into the respiratory chain for the reduction of molecular oxygen (Arts *et al.*, 2013).

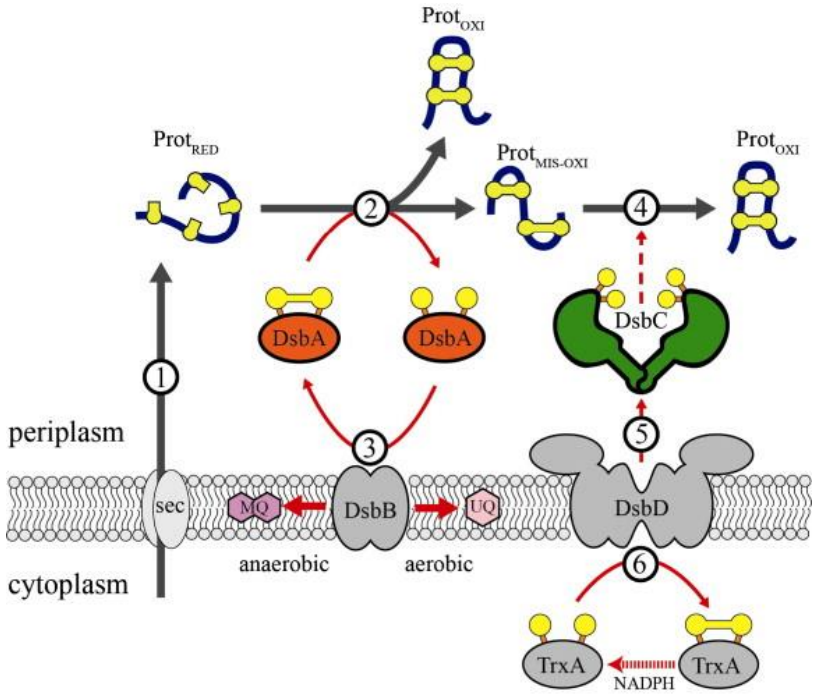

Figure 4.12. *E. coli* disulphide bond formation in the periplasm (figure taken from Berkmen, 2012).

Whilst the reduction pathway remains similar in *P. aeruginosa*, the *P. aeruginosa* genome encodes multiple sets of Dsb proteins which are predicted to serve distinct roles. Many proteins are dependent on the Dsb reduction pathway, including cytochrome C (Cho and Collet, 2013), LasB, PilA, chitin binding protein (CbpD), immunomodulating metalloprotease and PrpL protease (Arts *et al.*, 2013). With the down-regulation of Dsb proteins, it is likely that proteins dependent on disulphide bond formation will be less abundant as misfolding and protease degradation will be more prevalent, and may be the cause for the reduced abundance of cytochrome C_{550} and CbpD in FUS443. Alongside Dsb proteins was the down-regulation of two peptidyl-prolyl *cis-trans* isomerase proteins,

PpiA and PpiC2. Also located in the periplasm, these enzymes catalyse protein isomerisation, a process which is often responsible for regulating protein activity or function (Imperi *et al.*, 2009). Together, these findings showed that aberrant protein folding is highly likely in the mutated strain and will have implications on protein activity and function.

DsbA and DsbB are implicated in numerous cellular processes, including respiration and motility, with Dsb mutants being defective in both swimming and twitching motility. This then affects virulence and early biofilm formation through problems with pili and flagellum assembly (Arts *et al.*, 2013). Therefore, the decrease in DsbA, DsbD2 and TrxA expression in the FUS443 mutant may be another additive to the reduction in cell motility.

Induction of Dsb proteins has been linked to oxidative stress (as seen through its STRING map-association with glutathione peroxidase, PA1287) and to iron limitation, in a Fur-dependent manner. It is predicted that iron regulatory proteins are subjects of the Dsb reducing pathway and require the system for appropriate protein folding (Grabowska *et al.*, 2011). It is clear that iron uptake has been dysregulated in FUS443, and so this may have impacted upon the Dsb pathway, or conversely, the disruption to the Dsb pathway may be a cause for the poor secretion of siderophores into the environment.

4.9 Conclusion

This chapter has shown how a single residue mutation in EF-G causes dynamic cell-wide changes at a proteomic level. The mutation has affected distinct biological processes, such as motility by affecting the cell's ability to respond appropriately to chemotactic agents in its surroundings, thus preventing directional flagellum and T4P movement. The mutated EF-G disrupted iron acquisition on a global scale, causing the increased biosynthesis of pyochelin whilst preventing its secretion from the cell. The dysregulation of iron uptake may have had downstream effects on antibiotic sensitivity and respiration which would then influence cell growth and viability.

One of the main characteristics of the FUS443 strain was the substantial up-regulation of the T3SS. It appears as though the up-regulation of T3S was induced by an

increase in the abundance of the master regulator, ExsA. The increase in T3S is likely to enhance host invasion and promote pathogenicity, making this strain an interesting model for monitoring bacterial virulence. Fortunately for sufferers of CF, this mutation appears to have deleterious effects on the cell which stunt fitness, most likely arising from disruption to respiration and the central metabolism.

At this stage it is unclear how the mutation in EF-G is having a prominent effect on the distinct clusters of proteins discussed in this chapter. However, it is possible that the mutation is affecting the translation of transcription factors or post-translational regulators, whose action is dependent on protein abundance.

Chapter 5

5.Transcriptomic analysis of FUS443

5.1 Introduction

The proteome is the final product of gene expression whilst the initial point of expression is represented by the transcriptome. RNA makes up approximately 6% of a bacterial cell's total weight, the majority of which is ribosomal RNA and only 1-4% of total RNA encompasses the coding mRNA (Brown, 2002). A complex series of mechanisms are in place to maintain the transcriptome, from transcriptional regulators and sigma factors influencing gene expression, to post-transcriptional regulation *via* RNA processing, stabilisation or degradation. Together these mechanisms alter the number of transcripts that are used as templates for protein synthesis. The proteome is then regulated *via* protein turnover, secretion and protein modification, and so in many cases the proteome is not an exact reflection of the transcriptome.

Chapter four describes changes in the proteome of FUS443 resulting from the P443L mutation in EF-G. To gain an understanding of how the mutation affects the cell on a global scale, this chapter investigates the transcriptomic profile of FUS443. Any transcriptional data not specifically defined within the tables has been included within '**7. Appendix**'.

5.2 RNA extraction for transcriptomic analysis

5.2.1 Sample preparation

The role which EF-G plays during translation meant that the changes in protein abundance discussed in chapter four could have occurred directly by disrupting protein synthesis. To investigate whether the mutant variant was also having effects on gene expression, the transcriptomic profile of the mutant was analysed. The conditions within which the cultures were grown were kept consistent with those used in the proteomic study to allow for a comparison to be made between the two data sets.

Planktonic cultures of the progenitor (PAPcdr), mutant (FUS443) and complemented (FUS443C) strains were grown, in triplicate, in M9 minimal media and were harvested at late exponential phase into RNA Later (Ambion) to preserve the RNA transcripts. Total RNA was extracted using the RNeasy Mini Kit (Qiagen) and a Nanodrop spectrophotometer was used to determine the concentration and purity of the RNA. The extracted RNA samples had the ideal $A_{260/280}$ purity of 1.8 – 2.0 and $A_{260/230}$ purity of 2.0 – 2.2.

RNA is highly susceptible to degradation and so the total RNA was separated by gel electrophoresis to ensure that the RNA was intact. Two clear bands, representing the 16S and 23S rRNA, were observed for each sample with no smearing below the 16S band (Figure 5.1), indicating that minimal damage had occurred during sample preparation. Unfortunately, due to the column-based process of extraction, the majority of small RNAs were not recovered. Atypically, a faint, higher molecular weight band of approximately 4 - 4.5 k nucleotides was also identified above the 23S rRNA. A similar banding pattern was also recovered by Heera *et al.* (2015) using a phenol-free extraction kit where this band was predicted to represent the whole 70S ribosomal unit.

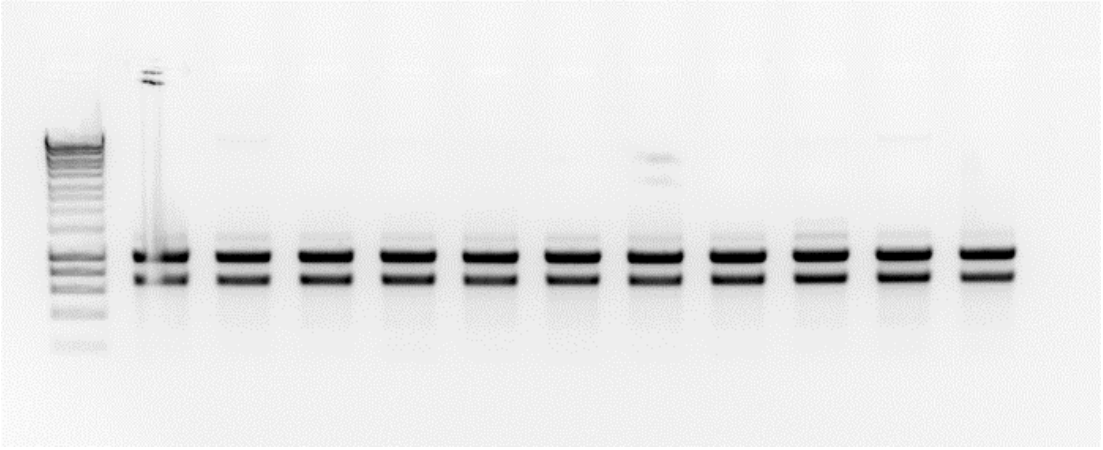

Figure 5.1. Total RNA extracted from *P. aeruginosa* strains grown in planktonic culture and harvested during the late exponential phase of growth.

DNA contamination can be detrimental to accurate RNA-sequencing and so on-the-column DNase I treatment was conducted during the extraction procedure. RNA

samples were used as template sequences for a standard PCR, none of which produced an amplification product, verifying that DNA was not present in these samples.

5.2.2 cDNA synthesis and RT-PCR

cDNA was synthesised from the total RNA using reverse transcriptase. The cDNA samples were subject to RT-PCR, amplifying the exopolysaccharide biosynthetic gene, *pslA*, and two T3SS genes, *exsA* and *pcrV*.

Figure 5.2A shows that the expression of *pslA* was not obviously affected by the P443L mutation. Consistent with the proteomic data, the FUS443 mutant had a distinct up-regulation of T3SS genes, but changes in the expression of *exsA* were subtle and could only be visualised when the number of amplification cycles was reduced. The injectosome tip-encoding gene, *pcrV*, appeared to be expressed at a distinctly greater level compared with the progenitor and complemented strain. Western blot analysis against PcrV verified that the increase in *pcrV* mRNA was reflected in the increased abundance of the PcrV protein (Figure 5.2B).

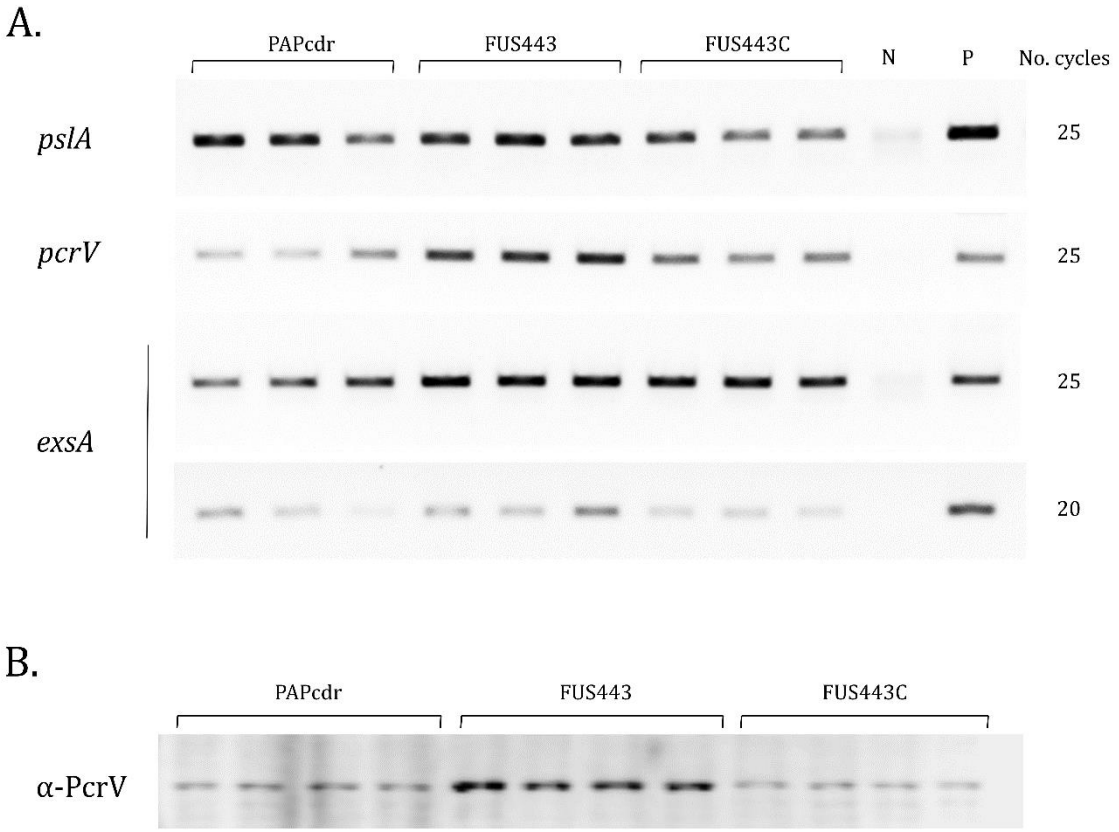

Figure 5.2. (**A**) RT-PCR on cDNA, synthesised from the total RNA of the FUS443 mutant strain, progenitor and complemented strain. *ExsA* was amplified twice, with a reduced number of cycles in the lower frame. (**B**) Western blot analysis using α-PcrV antibodies on whole cell protein samples of the aforementioned strains.

5.3 Transcriptomic analysis

5.3.1 RNA-Sequencing

The total RNA from each triplicate sample of a strain was sent for single read RNA-Seq using Illumina sequencing, at GATC Biotech. The dataset obtained from these samples consisted of 5628 recognised gene transcripts, out of a total 5678 predicted ORFs in the *P. aeruginosa* genome. This provided a very good representation of genome wide transcription. It is possible that a number of the genes that were unidentified or underrepresented in this screen belong to the families of small RNAs that would have

been lost during the extraction process. RNA quantitation values were $\log_2$ transformed and, for this study, a $\log_2$ FC in gene expression was considered to be statistically significant when > 1 or < -1 and with a P-value of ≤ 0.01. On the whole more genes were found to be down-regulated in FUS443, however, of all the modulated genes only 374 were considered to be significantly down-regulated whereas 657 were significantly up-regulated (Figure 5.3).

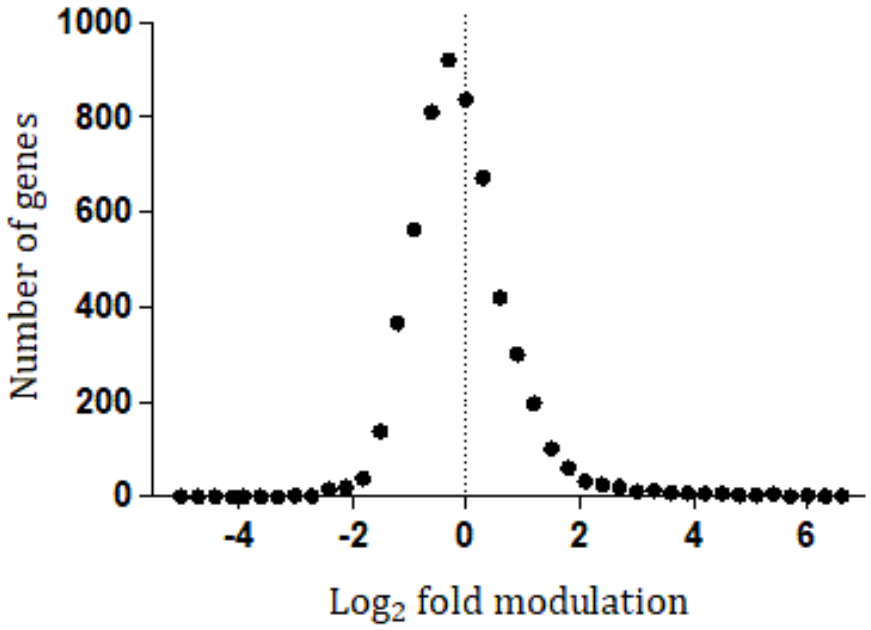

Figure 5.3. Modulation of gene expression in FUS443 compared with the gene expression in the progenitor strain, PAPcdr.

5.3.2 Principal components analysis

As with the proteomic data, PCA was employed to assess any similarities in gene expression amongst the three strains. The PCA plot showed three main clusters of data points, each corresponding to the three strains analysed (Figure 5.4). The plot indicated that the transcriptomic profile of the FUS443 mutant was distinct from the transcriptomic profile of the progenitor and complemented strains. The progenitor and complemented strains also showed some variability indicating that differences also exist between their transcriptomic profiles.

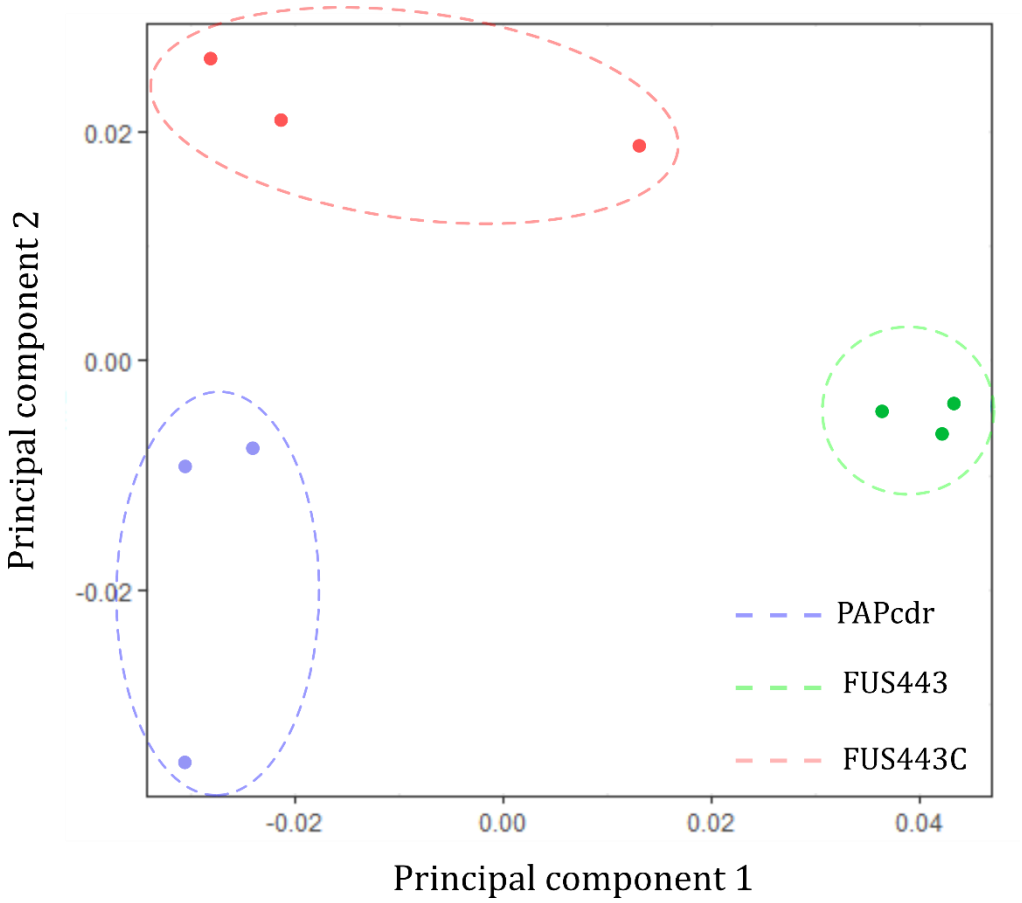

Figure 5.4. Principal components analysis of transcriptome data from *P. aeruginosa* strains, FUS443, PAPcdr, FUS443C. Each point on the graph represents one biological replicate.

5.3.3 Volcano and FPKM scatter plots

Volcano plots were produced to illustrate the fold change (log_2 transformed) against the P-value ($-log_{10}$ transformed) for all the quantified transcripts. This allowed for comparative analysis of the FUS443 mutant transcriptome or the complemented strain transcriptome against the PAPcdr progenitor. Data points that appear high on the Y axis have low P-values and are more highly significant.

The volcano plot, comparing the combined replicates of the progenitor strain and the combined replicates of the FUS443 mutant strain, shows that a large number of transcripts had been modulated in the mutant (Figure 5.5A). Far fewer transcripts were significantly modulated when comparing the progenitor strain with the complemented

strain (Figure 5.5B), indicating that the mutated EF-G induced a large number of significant changes in the cell at a transcriptomic level that were recovered by the expression of WT *fusA1* from p*fusA1*.

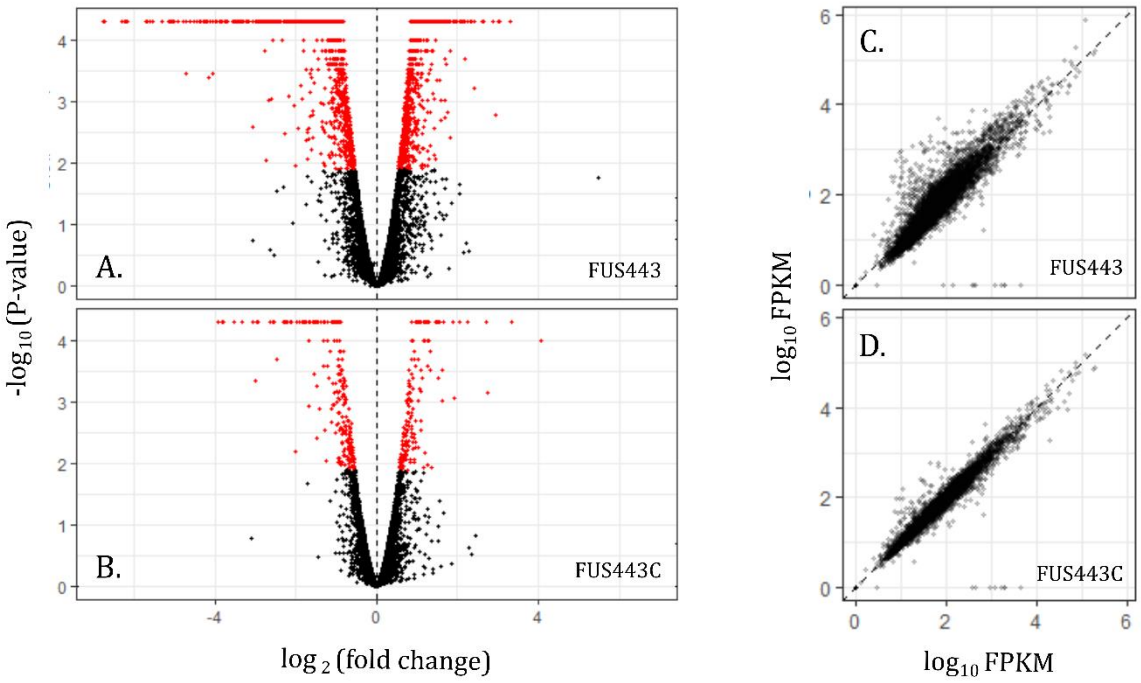

Figure 5.5. Volcano plot representing the $\log_2$ fold change (FC) of RNA transcript abundance against statistical significance for **(A)** the FUS443 mutant, and **(B)** the complemented FUS443C strain in relation to the PAPcdr progenitor strain. Significantly modified transcripts are highlighted in red. A FPKM (fragments per kilobase, per million) scatter plot comparing the $\log_{10}$ ratios of FPKM expression values for the progenitor strain with **(C)** the FUS443 mutant, and **(D)** the complemented FUS443C strain.

A FPKM (fragments per kilobase, per million) scatterplot is a common tool used in RNA-Seq analysis to quantify expression and visualise the level of variation between the transcriptomic profiles of two samples. Gene transcripts that have a similar level of abundance across the analysed conditions align closely to the midline. A FPKM scatter plot was constructed to assess the similarities between the transcriptomic profile of the progenitor strain with that of the mutant strain (Figure 5.5C) and the complemented strain (Figure 5.5D). The complemented strain aligned more closely to the midline than

the non-complemented mutant strain highlighting that a large number of gene transcripts were modulated in the mutant strain, which could be recovered with the expression of *fusA1* from the p*fusA1* vector.

5.4. Genes with significantly increased expression

Due to the large number of genes affected by the *fusA1* mutation, I focused on the transcripts that were complemented by the introduction of p*fusA1*, unless otherwise stated. Table 5.1 contains a list of the top 20 genes which exhibited the greatest positive change in expression. The $\log_2$ FC and P-values of the complemented mutant strain were included to indicate the degree to which the fold modulation could be attributed to the EF-G-P443L mutant protein.

Table 5.1. List of up-regulated gene transcripts associated with the *fusA1* mutation. Shaded boxes feature genes associated with the T3SS and a P-value of 0.000 represents < 0.0005.

	Gene	Locus tag	Function	FUS443		FUS443C	
				log_2 FC	P-value	log_2 FC	P-value
1	*ilvA2*	PA1326	Threonine dehydratase	6.746	0.000	0.451	0.067
2		PA1325	Hypothetical protein	6.180	0.000	0.166	0.754
3	*popN*	PA1698	Type III secretion outer membrane protein	5.536	0.000	0.253	0.470
4	*pscN*	PA1697	Type III secretion basal body protein	5.101	0.000	0.078	0.903
5	*pcr1*	PA1699	Type III secretion secreted protein	5.026	0.000	-0.072	0.898
6	*pcr3*	PA1701	Type III secretion secreted protein	4.723	0.000	-0.139	0.811
7	*pscO*	PA1696	Type III secretion translocation protein	4.718	0.000	0.061	0.964
8	*spcS*	PA3842	ExoS chaperone	4.461	0.000	0.370	0.106
9	*pcrV*	PA1706	Type III secretion needle tip protein	4.411	0.000	-0.429	0.053
10		PA4192	ABC binding protein	4.213	0.000	0.822	0.283
11	*pcrH*	PA1707	PopB/PopD chaperone	4.173	0.000	-0.816	0.276
12	*pcr2*	PA1700	Type III secretion secreted protein	4.057	0.000	-0.330	0.529
13	*exoY*	PA2191	Adenylate cyclase	4.057	0.000	-0.207	0.344
14	*popB*	PA1708	Type III translocator protein	4.051	0.000	-0.875	0.004
15	*pscP*	PA1695	Type III secretion translocation protein	3.961	0.000	-0.292	0.575
16	*exoS*	PA3841	Exoenzyme S	3.879	0.000	-0.479	0.070
17	*exoT*	PA0044	Exoenzyme T	3.863	0.000	-0.440	0.073
18		PA2202	Probable permease	3.856	0.000	0.675	0.005
19	*popD*	PA1709	Type III translocator protein	3.827	0.000	-0.885	0.001
20	*cysD*	PA4443	ATP sulfurylase subunit	3.754	0.000	-0.035	0.918

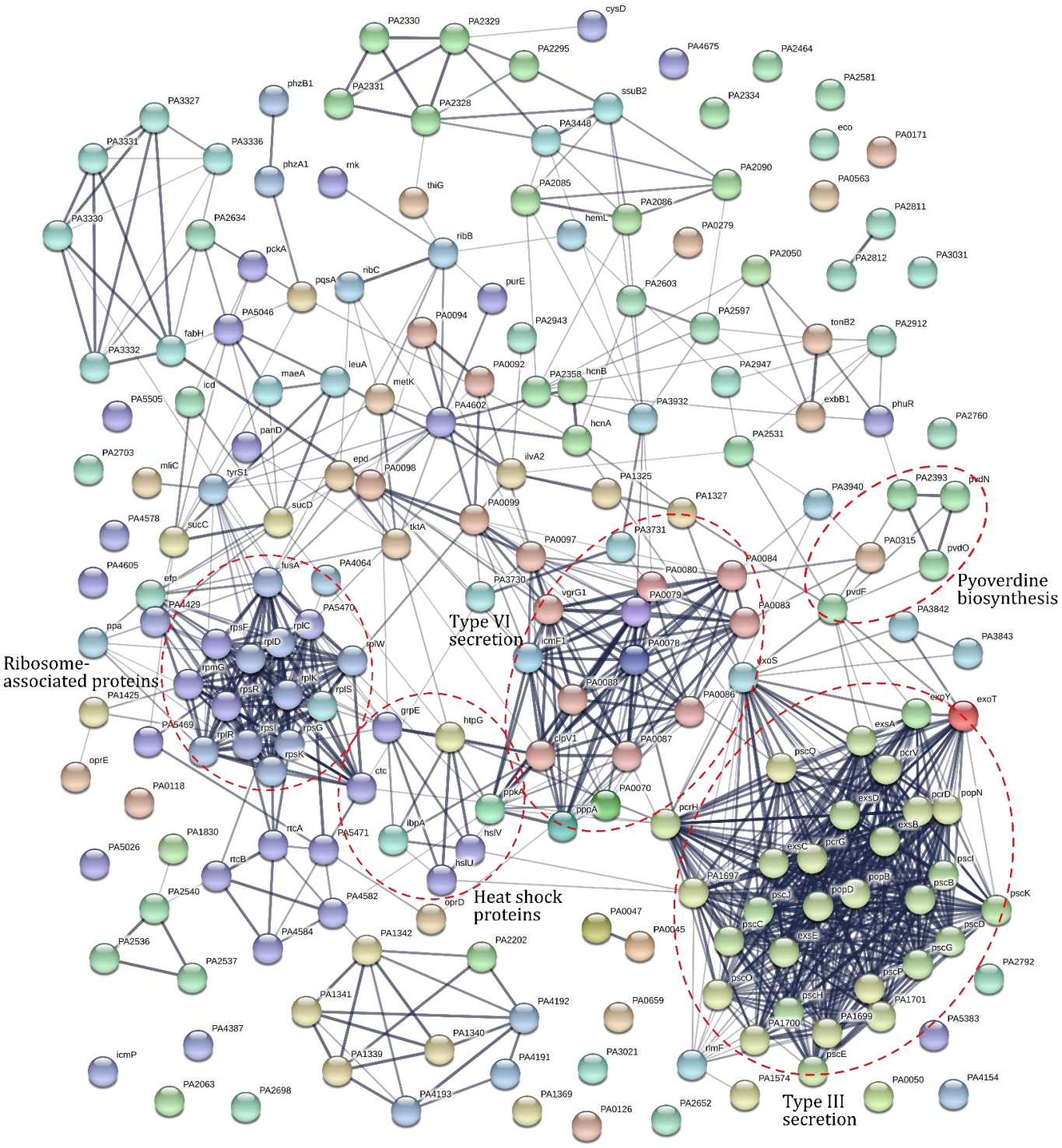

Figure 5.6. Network of interacting proteins. STRING was used to identify groups of potentially interacting proteins encoded by the top 200 genes that had been significantly up-regulated in the FUS443 mutant strain. Thick lines between nodes represents a high confidence level for that interaction.

As observed in the proteomic profile, the majority of up-regulated genes encoded components of the T3SS, showing an increase in gene expression as high 46-fold. This verifies that the T3SS is up-regulated at a transcriptional level as well as at a translational level in FUS443, and was complemented with the introduction of a functional *fusA1* gene *in trans*. T3SS genes also make up the largest cluster on the STRING protein interaction map (Figure 5.6). Due to the large number of significantly affected genes, only the top 200 modulated genes were used to predict interactions between the encoded proteins. There were several other distinct clusters predicted by STRING, including a group of ribosome-associated proteins and a cluster of T6SS-associated proteins, which will be discussed in detail later within this chapter.

5.4.1 Amino acid biosynthesis

The genes with the greatest modulation in FUS443 were *PA1325* and *PA1326*. *PA1326* (*ilvA2*) encodes a threonine dehydratase, involved in glycine, serine and threonine metabolism, and is second in a two-gene operon with *PA1325. PA1325* encodes a hypothetical protein but is likely to have a similar involvement in metabolism. Amongst this region of the genome there were a number of genes that were linked to amino acid metabolism and were found to be up-regulated. For example, shortly downstream, *ggt* (*PA1338*) encodes a gamma-glutamyltranspeptidase, involved in glutathione catabolism, and a selection of genes encoding ABC transport systems for glutamate and aspartate transportation (*aatJ*, *aatM*, *aatP* and *aatQ*, (*PA1339-PA1342*)) (Kahlon, 2016). Up-regulated elsewhere in the genome was *metK*, encoding a methionine adenosyltransferase for methionine biosynthesis, *glyA3*, encoding a serine hydroxymethyltransferase for glycine biosynthesis, and *oprD*, a porin for the transport of basic amino acids. Finally, two genes encoding glutamine ABC transporters, *PA4192* and *PA4193*, were also up-regulated.

Another up-regulated gene was *PA3965*, which encodes an AsnC-type transcriptional regulator and, whilst largely uncharacterised, it is one of two Lrp homologs encoded in the genome. In *P. aeruginosa*, Lrp regulates genes for amino acid biosynthesis and catabolism (Diraviam Sriramulu, 2009). It is possible that the *PA3965*

encoded regulator plays a similar role in amino acid metabolism and may be influencing the expression of amino acid transport systems.

5.4.2 Heat shock proteins

Amongst the STRING network were five heat shock protein (HSP) encoded genes; *htpG*, *hslV*, *hslU*, *ibpA* and *grpE* (Table 5.2). Several other HSP genes were significantly up-regulated in the transcriptomic data, including *groEL* which underwent a FC of 2.4. HSPs are typically expressed in response to high temperatures, but can be induced by alternative stress conditions including chemical and oxidative stressors. *RpoH* encodes the major sigma factor involved in the heat shock response and was up-regulated by a FC of 2.0 in FUS443, suggesting its involvement in the altered expression of HSPs in the mutant strain. Interestingly, genes encoding the DnaK-DnaJ-GrpE chaperone group, which control the turnover of RpoH, were also significantly up-regulated.

Table 5.2. Modulation in the expression of genes involved in the heat shock response.

		FUS443		FUS443C	
Gene	**Function**	**log_2 FC**	**P-value**	**log_2 FC**	**P-value**
htpG	Hsp90	2.827	0.000	-0.487	0.098
hslV	ATP-dependent protease	2.442	0.000	-0.803	0.000
hslU	ATP-dependent protease	2.231	0.000	-0.732	0.005
grpE	Nucleotide exchange factor	2.019	0.000	-0.942	0.000
ibpA	Hsp20	1.987	0.000	-1.318	0.000
dnaK	Hsp70	1.618	0.000	-1.020	0.005
rpoA	RNA polymerase	1.576	0.000	0.449	0.191
groES	Chaperonin	1.554	0.000	-0.359	0.104
dnaJ	Chaperonin	1.491	0.000	-0.784	0.004
clpB	Chaperonin	1.460	0.000	-0.942	0.003
PA1068	Hsp90	1.443	0.000	0.169	0.481
rpoD	Sigma factor	1.125	0.001	0.173	0.578
rpoH	Sigma factor	1.031	0.002	0.040	0.890

Due to the potential post-transcriptional regulation of RpoH by DnaKJ-GrpE, I referred to the proteomic profile of the FUS443 mutant. RpoH and HSPs were not significantly modulated during proteomic analysis, indicating that this response occurred

specifically in the culture prepared for transcriptomic analysis. From this I determined that HSPs were not constitutively expressed as a result of the *fusA1* mutation, but were modulated in response to biological stressors occurring within the mutant strain at the time of harvest for RNA extraction.

In *P. aeruginosa* activation of the heat shock response induces the expression of the sigma factor, RpoD, and the RNA polymerase subunit, RpoA. Both of the encoding genes for these proteins were significantly up-regulated in FUS443, suggesting that the heat shock response was activated. RpoD is the primary sigma factor in the transcriptional regulation of housekeeping genes (Miura *et al.*, 2015), and so RpoD up-regulation may have contributed to a wide variety of changes across the mutant transcriptome.

5.5 Genes with significantly decreased expression

A large number of genes were down-regulated in FUS443 and I have focused on the genes whose expression was complemented when introducing p*fusA1*. Table 5.3 contains a list of the top 20 most down-regulated genes in FUS443. The $\log_2$ FC and P-values of the complemented strain were included to indicate the degree to which changes in gene expression could be attributed to the *fusA1* mutation.

Table 5.3. List of down-regulated genes associated with the EF-G P443L mutation.

	Gene	Locus tag	Function	FUS443		FUS443C	
				$\log_2$ FC	P-value	$\log_2$ FC	P-value
1		PA5475	Hypothetical	-2.875	0.000	-0.439	0.107
2	*arcD*	PA5170	Arginine/orthithine antiporter	-2.625	0.000	-0.393	0.223
3		PA1414	Hypothetical protein	-2.427	0.000	-0.377	0.167
4	$tRNA_{Met}$	PA4746.1	tRNA-Met	-2.417	0.000	-0.399	0.269
5		PA2274	Hypothetical protein	-2.345	0.000	0.224	0.339
6		PA5027	Hypothetical protein	-2.300	0.000	-0.741	0.005
7		PA4523	Hypothetical protein	-2.235	0.000	-0.385	0.275
8		PA4352	Hypothetical protein	-2.188	0.000	0.127	0.560
9	*olsA*	PA4351	Membrane lipid biosynthesis protein	-2.166	0.000	-0.388	0.276
10		PA0200	Hypothetical protein	-2.134	0.000	-0.491	0.031
11		PA1673	Metal binding	-2.120	0.000	0.178	0.466
12		PA3431	Hypothetical protein	-2.071	0.000	0.362	0.401
13		PA3430	Probable adolase	-2.045	0.000	1.092	0.000
14	*feoB*	PA4358	Iron transport protein	-1.972	0.000	-0.440	0.052
15	*mexH*	PA4206	Resistance nodulation cell division multidrug efflux transporter	-1.946	0.000	-0.282	0.304
16	*rsmY*	PA0527.1	Non-coding RNA	-1.925	0.000	0.148	0.501
17	*mexG*	PA4205	Hypothetical protein	-1.922	0.000	0.150	0.585
18	*glpF*	PA3581	Glycerol uptake facilitator protein	-1.901	0.000	0.488	0.030
19		PA0718	Hypothetical protein of bacteriophage Pf1	-1.882	0.000	-0.980	0.000
20		PA4364	Hypothetical protein	-1.882	0.000	-0.039	0.875

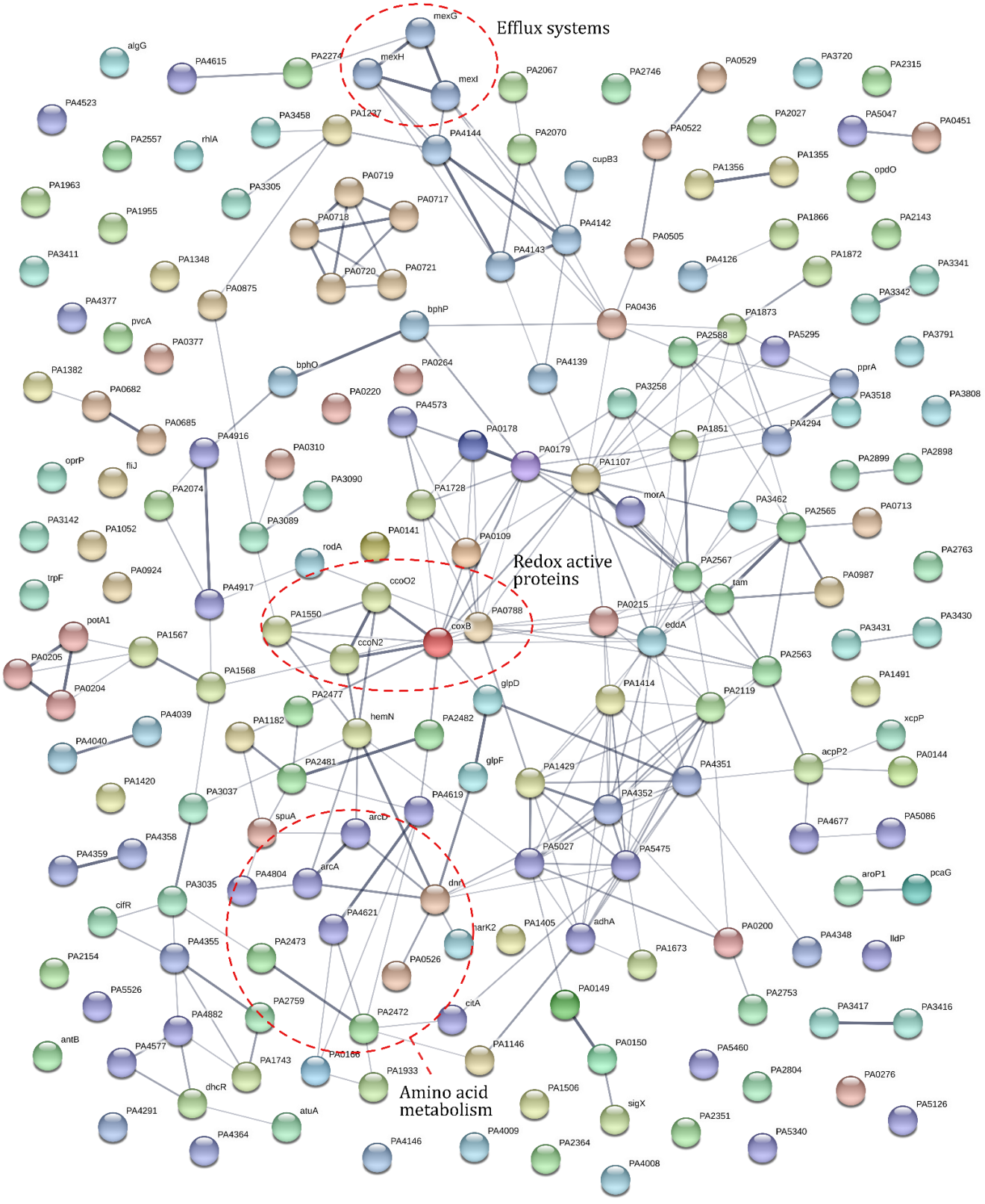

Figure 5.7. Network of interacting proteins. STRING was used to identify groups of potentially interacting proteins encoded by the top 200 genes that had been significantly down-regulated in the FUS443 mutant strain. Thick lines between nodes represents a high confidence level for that interaction.

A large number of the down-regulated genes were uncharacterised. The second most down-regulated gene was *arcD* which encodes an arginine/ortnithine antiporter and is a part of the *arcDABC* operon which is responsible for arginine fermentation. The sensor kinase, NarX, and its response regulator, NarL, repress the expression of *arcDABC* during anaerobic growth (Benkert *et al.*, 2008). The transcriptomic data of FUS443 showed a significant down-regulation of both *narL* and *narX*, highlighting that NarX-NarL-controlled denitrification pathways were inactive and *arc* repression was occurring *via* an alternative mechanism.

Other amino acid-associated genes that were down-regulated included *PA0220,* an amino acid APC family transporter gene, *PA3035*, encoding glutathione S-transferase, the *opdO* pyroglutamate porin gene and *aroP1* encoding an aromatic amino acid transporter. It is possible that a surplus of their respective amino acids negatively fed back on these systems to reduce amino acid uptake and metabolism to prevent energy loss from these systems.

Other top down-regulated genes included efflux systems and iron transport systems, which will be discussed in more detail within this chapter. The small noncoding RNA, *rsmY*, of the Gac/Rsm pathway was also down-regulated. Almost all of the other Gac/Rsm pathway components (*ladS*, *retS*, *gacA*, *gacS*, *rsmZ*) had not been modulated in the mutant strain, apart from the transcriptional regulator *rsmA*, which was decreased by a FC of 3.7. However, the complemented strain exhibited a 10.2-fold decrease in *rsmA* expression and so this modulation may be linked to the over-expression of *fusA1* and not specifically due to the mutated EF-G protein. This highlights the involvement of EF-G in the regulation of the Gac/Rsm pathway, and its effect on this pathway may be the cause of changes to expression of the T3SS. However, this does not explain why the up-regulation of the T3SS was complemented in FUS443C by expression a WT *fusA1* gene *in trans*.

5.5.1 Antibiotic resistance mechanisms

In chapter four, the proteomic analysis revealed an increased abundance of the MexXY efflux transporter proteins in FUS443. Consistent with this, *mexXY* gene expression was also up-regulated at a transcriptional level (Table 5.4), but with no effect

on expression of the *mexXY* transcriptional repressor, *mexZ*. This indicated that the *mexXY* system is constitutively up-regulated in response to the *fusA1* mutation and is the most promising explanation for the observed aminoglycoside resistance.

The transcriptomic data also identified the down-regulation of another resistance nodulation division efflux pump in FUS443, *mexGHI-opmD* (Table 5.4). This efflux system provides resistance to ethidium bromide, vanadium, norfloxacin and acriflavine, but has no known association with gentamicin resistance (Sekiya *et al.*, 2003; Sakhtah *et al.*, 2016). However, MexI, MexG and OpmD were not detected in the proteomic analysis and MexH abundance was not modulated in the mutant compared with the progenitor.

Table 5.4. Gene expression of the Mex efflux systems in *P. aeruginosa*.

		FUS443		FUS443C	
Gene	**Function**	**log_2 FC**	**P-value**	**log_2 FC**	**P-value**
mexI	Multidrug resistance efflux transporter	-1.215	0.000	-0.387	0.244
mexG	Multidrug resistance efflux transporter	-1.922	0.000	0.150	0.585
mexH	Multidrug resistance efflux transporter	-1.946	0.000	-0.282	0.304
opmD	Outer membrane porin	-0.429	0.296	-0.418	0.398
mexX	Multidrug resistance efflux transporter	1.365	0.000	-0.161	0.468
mexY	Multidrug resistance efflux transporter	0.981	0.000	-0.345	0.156

The mutant also exhibited a down-regulation of *pprA* expression by 2.4-fold. PprA and PprB are predicted to be part of a two component regulatory system for membrane permeability. *PprAB* expression leads to higher membrane permeability and increased sensitivity to antibiotics, including aminoglycosides (Wang *et al.*, 2003). The *fusA1* mutation did not alter *pprB* expression, but decreased the expression of *pprA*. This may have been enough to prevent activation of the two component system and reduce cell permeability, adding to the increased antibiotic resistance observed in the FUS443 strain.

PprAB reduce cell permeability by altering membrane transportation systems. PprAB may have affected the outer membrane porin, OprP, which is associated with carbapenem influx and was down-regulated by 2.3-fold at a transcriptional level. The

sigma factor SigX is thought to reduce *mexXY-oprM* expression *via* PprAB (Gicquel *et al.*, 2013) and exhibited a 2.4-fold reduction in gene expression in FUS443. The reduced expression of both *sigX* and *pprA* may explain the increased *mexXY* expression, observed in the proteomic and transcriptomic data.

5.6 Secretion systems

5.6.1 The type III secretion system

Building on the proteomic data, the transcriptomic profile of FUS443 also demonstrated an increase in T3SS expression at a transcriptional level (Table 5.5). More T3SS genes were identified than in the proteomic screen, all of which were up-regulated and the majority were completely complemented by the introduction of p*fusA1*.

After proteomic analysis, western blot analysis and RT-PCR, it was not surprising to see an up-regulation of *exsA* gene expression in FUS443. ExsA is most likely to be the main cause for the global up-regulation of the T3SS, however, the transcriptional regulator PsrA is thought to be required for full activation of the *exsCEBA* operon (Shen *et al.*, 2006). Quite unexpectedly, the *psrA* gene exhibited a 2.1-fold reduction in expression. These findings suggest that PsrA is, in fact, not a major requirement for T3S and low levels of *psrA* transcription do not prevent the expression of the *exsCEBA* operon.

The transcriptomic data also recorded the up-regulation of four small hypothetical T3SS proteins namely, *pcr1*, *pcr2*, *pcr3* and *pcr4*. These genes reside in second to fifth position within the *popN* T3SS operon, although the function of the *pcr1234* gene products is not well understood in *P. aeruginosa*.

Table 5.5. List of genes encoding the T3SS and their log_2 fold change in expression in the FUS443 mutant and complemented strain.

Gene	FUS443		FUS443C	
	log_2 FC	**P-value**	**log_2 FC**	**P-value**
Basal body				
pscC	2.196	0.000	0.019	0.944
pscD	1.928	0.000	0.525	0.065
pscH	2.358	0.000	0.361	0.545
pscI	2.579	0.000	0.693	0.275
pscJ	2.383	0.000	0.730	0.738
pscK	2.119	0.000	0.454	0.231
pscL	1.157	0.000	0.364	0.208
pscO	4.718	0.000	0.062	0.964
pscQ	2.772	0.000	-0.230	0.557
pscN	5.101	0.000	0.078	0.903
pcrD	2.078	0.000	-0.004	0.988
Translocon				
popB	4.051	0.000	-0.875	0.004
popD	3.827	0.000	-0.885	0.001
pcrV	4.411	0.000	-0.429	0.053
Needle				
pscF	3.466	0.000	1.275	0.000
pscP	3.961	0.500	-0.292	0.575
Export apparatus				
popN	5.536	0.000	0.253	0.470
pscB	2.642	0.000	0.326	0.524
Regulatory network				
exsC	1.689	0.000	-0.714	0.005
exsE	1.976	0.000	-0.275	0.272
exsA	1.697	0.000	0.388	0.201
exsD	2.236	0.000	-0.062	0.814
Chaperones				
spcS	4.608	0.000	0.370	0.106
pcrH	4.173	0.000	-0.816	0.276
pcrG	3.730	0.000	-0.643	0.016
pscE	2.395	0.000	0.183	0.789
pscG	2.987	0.000	0.848	0.128
Secreted toxins				
exoS	3.879	0.000	-0.479	0.070
exoT	3.863	0.000	-0.440	0.073
exoY	4.057	0.000	-0.207	0.344
Hypothetical T3SS proteins				
pcr1	5.026	0.000	-0.073	0.898
pcr2	4.057	0.004	-0.330	0.529
pcr3	4.723	0.000	-0.139	0.811
pcr4	3.068	0.180	-0.330	0.679

5.6.2 The type II secretion system

Unlike the T3SS genes, several T2SS genes were significantly down-regulated. This included three pseudopilin encoding genes, *hxcT*, *hxcW* and *hxcX*, as well as the secretin, *hxcQ* (Table 5.6). Pseudopilin form the pseudopilus through which the T2SS secretory proteins are expelled from the cell. This phenotype was complemented completely with the introduction of p*fusA1,* confirming the influence of the *fusA1* mutation on this system.

The *hxc* cluster is named after homology to *xcp* genes, which are the main T2SS cluster. The *xcp* encoded cluster secrete elastases, lipases, phospholipases and exotoxin A, whereas the *hxp* cluster is specific for alkaline phosphatases, such as LapA, and secretins such as the lipoprotein, HxcQ (Ball *et al.*, 2002). The main T2SS cluster (*xcp*) was unaffected by the P443L mutation, with the exception of *xcpP* (2.3-fold decrease). Another gene, *xqhB*, is predicted to encode a probable T2SS protein and was significantly down-regulated in FUS443. This gene is located independently from the other two clusters showing how the mutant EF-G was causing the specific down-regulation of select T2SS genes.

Table 5.6. List of genes encoding the T2SS and their $\log_2$ fold change in expression in the FUS443 and complemented mutant. Shaded boxes represent modulations that are statistically significant.

		FUS443		FUS443C	
Gene	**Function**	**$\log_2$ FC**	**P-value**	**$\log_2$ FC**	**P-value**
hxcW	Pseudopilin	-1.129	0.000	0.021	0.934
hxcU	Pseudopilin	-0.895	0.095	-0.425	0.446
hxcP	Inner membrane protein	-0.742	0.004	-0.327	0.194
hxcV	Pseudopilin	-0.883	0.008	0.112	0.692
hxcT	Pseudopilin	-1.046	0.001	0.007	0.983
hxcX	Pseudopilin	-1.264	0.000	0.036	0.893
hxcZ	Inner membrane protein	-1.320	0.158	-0.169	0.838
hxcQ	Secretin	-1.285	0.000	-0.175	0.611
hxcR	ATPase	-1.231	0.030	-0.261	0.645
lapA	Alkaline phosphatase A	-0.961	0.000	-0.220	0.303
lapB	Alkaline phosphatase B	-1.142	0.000	-0.034	0.885
xcpP	Secretion protein	-1.214	0.000	-0.037	0.895
xqhB	Probable T2SS protein	-1.318	0.000	0.134	0.605

I was unable to confirm that the down-regulation of *hxc* genes corresponded to a reduction in protein abundance, as none of the Hxc proteins were detected in the intracellular proteomic data. Again, XcpP was the only protein of the detected Xcp proteins that was reduced in protein abundance, indicating the presence of specific regulatory efforts against *xcpP* expression.

5.6.3 The type VI secretion system

As with the T3SS, the T6SS was up-regulated in FUS443. The T6SS is reminiscent of major bacteriophage tail proteins, and is composed of Hcp and VgrG proteins which assemble to form a puncturing device (Chen *et al.*, 2015). TssB and TssC form a contractile sheath structure which extends to puncture the target cell and drive the delivery of effector proteins. This retraction and extension is powered by the ATPase, ClpV, and the secretion complex is anchored to the membrane by an envelope-spanning complex, composed of TssL, TssM and TssJ (Figure 5.8). The T6SS transports numerous different effector proteins including amidases, lipases, nucleases and chaperone proteins (Alteri *et al.*, 2016). The transcriptomic data revealed that the majority of T6SS were up-regulated, some as high as 11-fold, including the aforementioned *vgrG1*, *hcp1*, *clpV1*, *tssB1*, *tssC1*, *tssL1*, *tssJ1* and *tssM1* (Table 5.7).

The T6SS exports at least three toxins, including Tse1, Tse2 and Tse3. Tse1 and Tse3 target and degrade peptidoglycan whilst Tse2 acts within the cytoplasm. *P. aeruginosa* also encodes three immunity proteins, Tsi1, Tsi2 and Tsi3, which inhibit the activity of the Tse proteins to prevent self-intoxication (Chen *et al.*, 2015). The majority of exotoxin-encoding genes were up-regulated in FUS443, further confirming that all of the main components required for T6S were over-expressed.

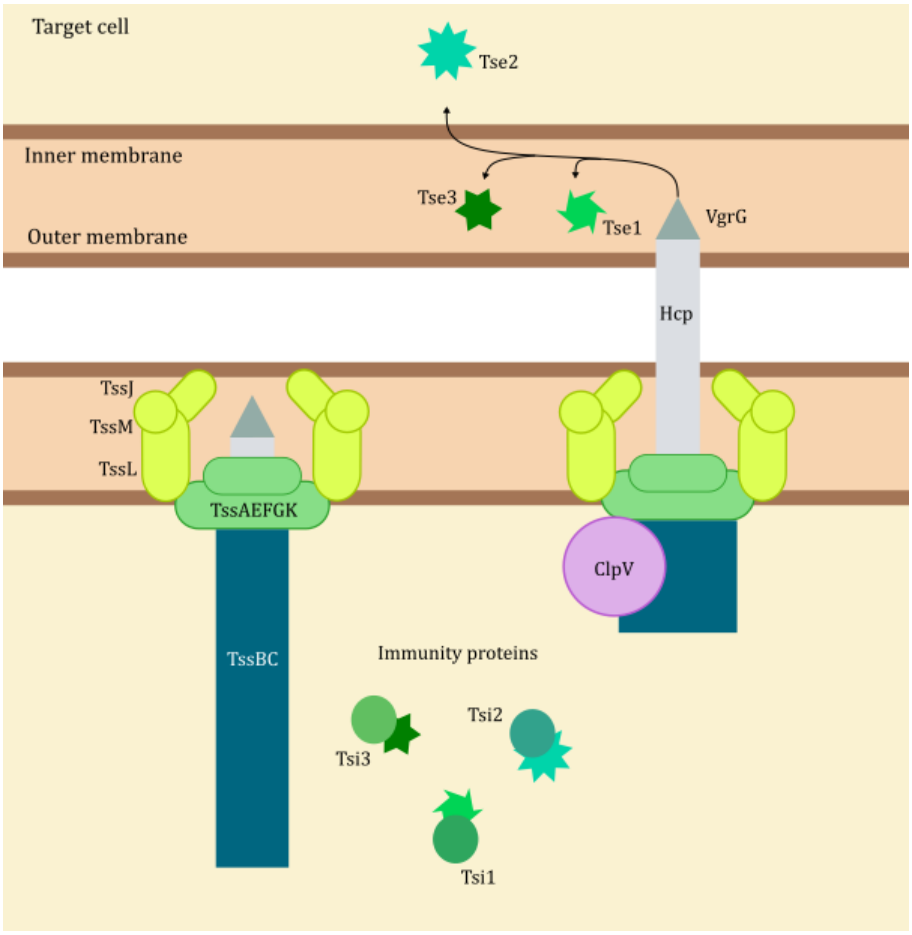

Figure 5.8. The type VI secretion system of *P. aeruginosa*.

P. aeruginosa encodes three T6SS clusters, termed HSI for Hcp secretion island. The genes discussed here represent the main T6SS cluster, HSI-I. A number of the HSI-II genes were also significantly up-regulated in FUS443, such as *hsiB2, hsiC2, orfX* and *fha2*, along with a general up-regulation of the remaining HSI-II genes. HSI-III was mostly unaffected by the *fusA1* mutation and so shows that the mutated EF-G is affecting subclasses of T6SS expression in different ways.

Table 5.7. A list of T6SS encoding genes that have been modulated in FUS443. Shaded boxes represent genes whose expression was significantly modulated.

		FUS443		FUS443C	
Gene	**Function**	**log_2 FC**	**P-value**	**log_2 FC**	**P-value**
hcp1	Secretion tip	3.717	0.000	1.554	0.000
tagQ1	Regulatory protein	3.473	0.000	0.514	0.040
tssA1	T6SS basal body	3.195	0.000	-0.246	0.441
tssB1	T6SS basal body	3.195	0.000	0.964	0.002
tssC1	T6SS basal body	3.005	0.000	0.959	0.008
tssE1	T6SS basal body	2.748	0.009	0.879	0.010
tssF1	T6SS basal body	2.667	0.000	0.703	0.002
pppA	Phosphatase	2.597	0.000	0.668	0.007
tagF1	Regulatory protein	2.468	0.028	0.295	0.770
tssL1	T6SS basal body	2.434	0.000	-0.083	0.709
tagJ1	T6SS basal body	2.430	0.000	0.073	0.770
vgrG1	Secretion tip	2.229	0.000	0.882	0.003
tssM1/icmF1	T6SS basal body	2.213	0.000	0.102	0.739
clpV1	ATPase	2.137	0.000	0.702	0.104
tssK1	T6SS basal body	2.056	0.000	0.341	0.274
ppkA	Ser/thr protein kinase	2.041	0.001	0.184	0.795
tssJ1	T6SS basal body	2.032	0.000	0.799	0.014
tagT1	Regulatory protein	1.274	0.648	0.215	0.902
tagS1	Regulatory protein	1.121	0.679	0.158	0.864
Tse3	Effector protein	1.091	0.000	0.324	0.276
Tse2	Effector protein	1.046	0.000	0.340	0.117
fha1	Fork head associated protein	0.437	0.083	-0.095	0.691

A threonine phosphorylation pathway has been found to activate T6S *via* the forkhead-associated protein, Fha, which assists the recruitment of ClpV1. The kinase, PpkA, activates Fha through phosphorylation, a process that is facilitated by TagQ, TagR, TagS and TagT (Hood *et al.*, 2010; Alteri *et al.*, 2016). The transcriptomic data revealed only modest up-regulation of *fha1*, whereas *ppkA*, *tagQ1*, *tagS1* and *tagT1* are up-regulated significantly. Even without the significant modulation of *fha* expression, its post-translational activation may be the main mechanism behind the up-regulated T6SS in FUS443. Typically, high levels of T6S occur due to a reduction in PppA, a phosphatase that deactivates Fha. However, my results showed that *pppA* was significantly up-regulated in FUS443 which is in discordance with the up-regulated T6SS. *PppA* resides

within the *tagQRSTF-ppkA-pppA* operon and so is up-regulated with the rest of the T6SS genes, highlighting the importance of post-translational regulation in this system.

With the increase in T6S it was possible that the mutant strain would be better equipped for inter-species competition. When co-cultured with *E. coli* for 5 hours, and plated onto *E. coli*-selective agar, there was no significant difference between the *E. coli* cell count for the mutant and progenitor co-culture conditions (unpaired *t*-test, $t(4)=0.998$, $p=0.375$) (Figure 5.9). This suggested that the mutant EF-G protein did not improve the ability of *P. aeruginosa* to out-compete other bacterial species.

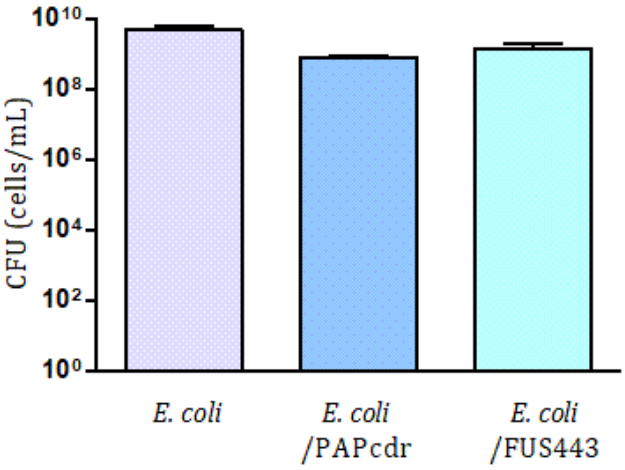

Figure 5.9. *E. coli* total colony counts after a 5 hour co-culture with *P. aeruginosa* strains, FUS443 or PAPcdr, in glucose M9 minimal media. Values represent three biological replicates for each condition and a culture of *E. coli* grown in the absence of *P. aeruginosa* was used as a control.

5.7 Iron homeostasis

5.7.1 Siderophore biosynthesis

Proteomic data had highlighted the up-regulation of iron-uptake and -regulatory proteins in FUS443, although the strain appeared to be defective in the secretion of siderophores from the cell. A large number of iron response genes were also over expressed at a transcriptional level in the mutant strain, suggesting that a global transcriptional regulator of iron uptake had been affected by the mutated EF-G protein.

The proteomic analysis revealed an increase in the abundance of pyochelin-biosynthesis proteins, whereas pyoverdine-biosynthesis proteins remained relatively unaffected by the *fusA1* mutation. However, in the transcriptomic data, pyoverdine biosynthesis genes, including *pvdA, pvdF*, *pvdN* and *pvdP*, were up-regulated (Table 5.8). Of the pyochelin biosynthesis genes that were detected in the transcriptome analysis, *pchA*, *pchB, pchC* and *pchD* were up-regulated, however none of these changes were considered statistically significant due to a high P-value. Therefore, the effect on iron uptake systems was variable across the two profiled conditions.

Table 5.8. List of genes associated with iron acquisition that have been modulated in FUS443. Shaded boxes represent genes whose expression has been significantly modulated.

		FUS443		FUS443C	
Gene	**Function**	**log_2 FC**	**P-value**	**log_2 FC**	**P-value**
exbB1	Ton-B dependent transport	2.808	0.000	0.357	0.112
tonB2	TonB2 protein	2.465	0.000	0.475	0.051
pvdN	Pyoverdine biosynthesis protein	2.033	0.000	0.799	0.014
PA5505	TonB-dependent receptor	1.945	0.000	0.618	0.026
pvdF	Pyoverdine biosynthesis protein	1.726	0.000	0.498	0.177
chtA	TonB-dependent receptor	1.693	0.000	0.421	0.077
pvdP	Pyoverdine biosynthesis protein	1.416	0.000	0.452	0.175
exbD1	Ton-B dependent transport	1.389	0.000	0.454	0.046
PA3268	TonB-dependent receptor	1.349	0.000	0.445	0.051
pvdA	Pyoverdine biosynthesis protein	1.310	0.010	0.112	0.827
PA1271	TonB-dependent receptor	1.297	0.000	0.234	0.295
PA1365	Siderophore receptor	1.243	0.000	0.424	0.089
pchD	Pyochelin biosynthesis protein	1.199	0.247	0.039	0.966
pchC	Pyochelin biosynthesis protein	1.050	0.655	-0.019	0.970
pchB	Pyochelin biosynthesis protein	0.882	0.641	-0.046	0.979
pchA	Pyochelin biosynthesis protein	0.599	0.505	-0.309	0.731
feoA	Ferrous iron transporter A	-1.498	0.000	0.364	0.107
feoB	Ferrous iron transporter B	-1.972	0.000	-0.533	0.063

5.7.2 Iron transporter systems

In addition to siderophore biosynthesis genes, numerous iron transport systems were expressed at higher levels in the FUS443 mutant, including *PA1365*, which encodes

a probable siderophore receptor, and numerous TonB-dependent transporters (*PA5505*, *PA4675*, *PA3268* and *PA1271*). Whilst the general trend appeared to promote iron acquisition, two genes, *feoA* and *feoB*, which encode ferrous-iron transport proteins A and B, were significantly down-regulated. The changes in expression of all these genes was largely complemented by p*fusA1*. The down-regulation of *feoA* was consistent with the reduced abundance of FeoA protein (1.6-fold decrease) in the FUS443 proteomic profile, whereas FeoB protein abundance was not detected.

The protein, TonB, is essential for siderophore-mediated iron acquisition (Takase *et al.*, 2000). The TonB protein is anchored to the cytoplasmic membrane *via* ExbB and ExbD, which were transcriptionally up-regulated in FUS443. The uptake of iron-bound siderophores through the outer membrane proteins, FpvA (for pyoverdine uptake) and FptA (for pyochelin uptake), both require the presence of TonB (Figure 1.7) (Takase *et al.*, 2000). *P. aeruginosa* encodes two TonB proteins; *tonB1* is monocistronic and *tonB2* is located within an operon with *exbBC* genes. TonB1 has a dominant and well defined role in iron uptake, whereas the role of TonB2 in iron acquisition has not been defined. It does, however, contain a Fur box within its promoter, identifying this gene as an iron response gene (Cornelis *et al.*, 2009). *TonB2* was up-regulated in the FUS443 mutant by 5.5-fold, along with *exbB1* and *exbD1*, highlighting an effect on the whole operon. In *Vibrio* strains, the TonB-ExbB-ExbD complex creates a proton motive force that drives the transport of iron compounds into the periplasm (Zhao *et al.*, 2000; Chakraborty, 2013). Changes in the expression of this system would therefore affect all TonB-dependent receptors and affect the ability to translocate iron into the cell. With this, the up-regulation of these three genes, and their successful complementation by p*fusA1*, shows how the mutated EF-G protein is affecting not only iron scavenging mechanisms, but also iron transportation across the membrane.

5.7.3 Regulatory systems of iron uptake

Very few sigma factors that respond to iron starvation are highly characterised in *P. aeruginosa*. FpvI, FiuI and FoxI are sigma factors which regulate the uptake of iron *via* pyoverdine, ferrichrome and ferrioxamine B, respectively. Their transcriptional expression was decreased in the FUS443 mutant but not by a statistically significant level.

The most highly affected system was the Fiu ferrichrome uptake system where FUS443 exhibited a significant down-regulation in *fiuA* and *fiuR* expression. The ferrichrome receptor FiuA transduces its signal through FiuR to activate the sigma factor FiuI (Llamas *et al.*, 2006). All of the *fiu* transcripts were down-regulated indicating that there is an abundance of intracellular ferrous iron in FUS443, repressing this system. Expression of the Fox system was also slightly reduced and functions in a similar manner to the Fiu transduction pathway, with the receptor, FoxA, transducing a signal through FoxR to activate the sigma factor FoxI. The *fox* operon also encodes an uncharacterised gene *PA2469* which is a probable transcriptional regulator. *PA2469* was under-expressed in FUS443 at 2.2-fold lower than the progenitor strain. It is uncertain how PA2469 interacts with the Fox proteins but it's expression is consistent with the reduced transcription of the Fox iron-response system (Bastiaansen *et al.*, 2015).

Another sigma factor, PvdS, controls pyoverdine biosynthesis, exotoxin A and PrpL endoprotease production (Llamas *et al.*, 2007). *PvdS* was not considered to be significantly modulated in FUS443 although it's expression was increased 1.9-fold, and was partially complemented with the expression of a WT *fusA1* gene *via* p*fusA1*. However, the downstream effects of this modulation were not evident in *toxA* expression, encoding exotoxin A, or *prpL* expression.

Fur was not significantly affected at a transcriptional or proteomic level however this is not to say that the post-translational activity of Fur was not affected in FUS443. Fur is a transcriptional repressor when iron-bound and releases promoter sequences to allow for transcription under iron-limited conditions. Several factors indicate that Fur is functioning in its iron-unbound state in FUS443, such as the global up-regulation of a wide variety of iron-uptake genes. Another indicator of de-repression by Fur was *via* the PhuR regulatory system for heme uptake. PhuR may be considered quite primitive as it is regulated by Fur alone, and is not dependent on any sigma factors as far as our current understanding goes (Cornelis *et al.*, 2009). The transcriptional data revealed that *phuR*, was up-regulated 3.9-fold, providing a strong indication that the intracellular environment of FUS443 is iron-limited. However, several Fur-induced genes do not follow this pattern of expression. For example, Fur controls the transcription of two small RNAs, *prrF1* and *prrF2* involved in the regulation of iron-associated proteins (Cornelis *et al.*, 2009). *PrrF1* expression was not affected in the mutant strain and *prrF2* was not detected in the analysis.

It is difficult to determine the activity of the key iron response regulators due to the amalgamation of numerous regulatory pathways on target genes, and the opposing expression profiles of different iron uptake systems makes it difficult to uncover how EF-G impinges upon the iron response system. However, there does appear to be a particular emphasis on the up-regulation of siderophore based ferric-iron-acquisition.

5.7.4 Iron and type III secretion

Several studies have linked iron availability to the activation of the T3SS. To investigate if the dysregulation of the iron-response system was causing the up-regulation of the T3SS, strains were grown in media supplemented with Fe^{3+} and were analysed by western blot to identify changes in the expression of the T3SS protein, PcrV.

The addition of 100 μM of Fe(III) chloride to minimal media improved the growth rate of both the progenitor strain and the mutant strain. No change in growth rate was observed for the complemented FUS443C strain (Figure 5.10A). Proteins were extracted from each culture and were separated by SDS-PAGE, then transferred to PVDF membrane for blotting against PcrV. As previously demonstrated, PcrV was up-regulated in the mutant strain in the absence of iron supplementation, as observed through a visual increase in the protein band intensity for PcrV (Figure 5.10B). The addition of iron in the growth media did not affect the expression of PcrV in the progenitor strain or in the complemented strain, however the intensity of the PcrV band was stronger in the mutant strain indicating that iron had further promoted the expression of PcrV.

This showed that the up-regulation of the T3SS was not due to iron limitation, but could perhaps be due to the converse, whereby the mutant is importing more iron into the cell than required. The excess iron appears to be promoting the expression of the T3SS.

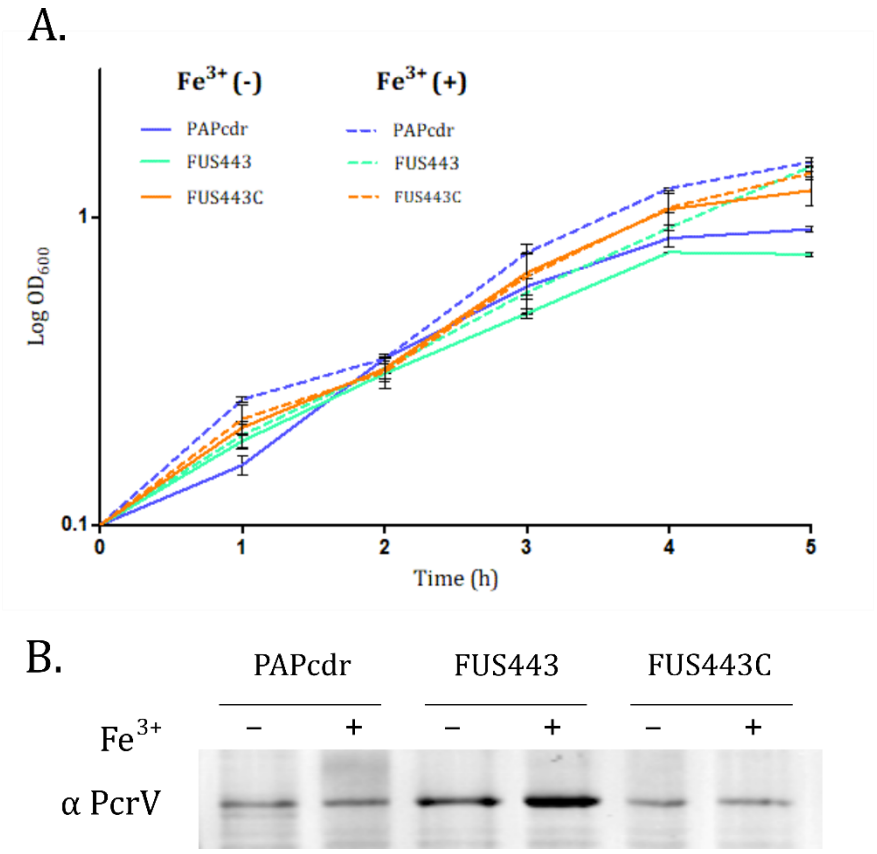

Figure 5.10. The effect of iron supplementation on **(A)** growth in M9 minimal media with glucose and **(B)** on the expression of the type III secretion system protein, PcrV.

5.8 EF-G and translation

5.8.1 Ribosomal proteins

As highlighted from the STRING protein-interaction map, a large cluster of the up-regulated genes in FUS443 consisted of ribosome-associated genes, which was consistent with the proteomic profile of FUS443. In total, 62 genes encoding ribosomal or ribosomal-associated proteins were upregulated, 20 of which encoded 30S ribosomal proteins, 26 for 50S ribosomal proteins, three peptide chain release factors, elongation factor Tu and initiation factor 2. The top 15 most highly modulated ribosomal genes are represented in Table 5.9.

Table 5.9. List of ribosomal and ribosomal-associated proteins encoded by *P. aeruginosa* and their log_2 fold change in the FUS443 and complemented mutant strains.

		FUS443		FUS443C	
Gene	**Function**	**log_2 FC**	**P-value**	**log_2 FC**	**P-value**
PA5470	Peptide chain release factor	3.346	0.000	0.329	0.541
rpsR	30S ribosomal protein S18	2.022	0.000	0.850	0.003
efp	Elongation factor P	2.011	0.000	0.757	0.004
rplW	50S ribosomal protein L23	2.006	0.011	0.840	0.222
rpsI	30S ribosomal protein S9	1.940	0.000	0.606	0.022
rplD	50S ribosomal protein L4	1.923	0.000	0.563	0.140
rpmG	50S ribosomal protein L33	1.801	0.000	0.789	0.010
rpsG	30S ribosomal protein S7	1.767	0.000	0.307	0.284
rpsF	30S ribosomal protein S6	1.749	0.000	0.649	0.022
rplC	50S ribosomal protein L3	1.720	0.000	0.554	0.067
rplK	50S ribosomal protein L11	1.713	0.003	0.357	0.515
rpsK	30S ribosomal protein S11	1.703	0.000	0.753	0.013
rplR	50S ribosomal protein L18	1.681	0.000	0.692	0.014
rplY	50S ribosomal protein L25	1.663	0.000	0.297	0.270
fusA1	Elongation factor G	1.657	0.000	-	-
fusA2	Elongation factor G	0.298	0.321	-0.316	0.273

In addition to ribosomal genes, the transcriptomic data highlighted several genes involved in RNA processing. Two such genes were, *rtcA* and *rtcB*, which were up-regulated in FUS443. *RtcA* encodes an RNA 3'-terminal phosphate cyclase whose expression was increased by 5.2-fold in FUS443. *RtcB* encodes a probable RNA ligase and was up-regulated 9.3-fold. RNA ligases join RNA molecules that have been cleaved by RNases and are important in the processing of tRNA and defence against phage attack. RNA ligases have also been shown to cap 3' DNA which would protect DNA from exonuclease attack (Maughan *et al.*, 2015). Because of this, the *rtcBA* operon is often induced by cellular stress to prevent damage caused by the RNA toxins that are released by the cell to regulate growth rate and facilitate the cells stress response (Zhabokritsky *et al.*, 2011; Maughan *et al.*, 2015). The *rtcBA* operon is regulated by RtcR, however the *rtcR* gene does not appear to be drastically altered by the *fusA1* mutation and so its action may be regulated post-transcriptionally.

Six tRNA synthetase genes were also up-regulated for the charging of tyrosyl-tRNA (*PA4138*), tryptophanyl-tRNA (*PA4440*), glutamyl-tRNA (*PA3134*), alanyl-tRNA

(*PA0903*), phenylalanyl-tRNA (*PA2740*) and prolyl-tRNA (*PA0956*). This may be due to an increased demand for protein synthesis in FUS443. Conversely to this, many of the detected tRNA encoding genes had been down-regulated. Those most affected included two $tRNA^{Thr}$ genes and a $tRNA^{Met}$ gene that were down-regulated by between 3- and 8-fold. Whilst tRNA levels could not be detected in the proteomic screen, the up-regulation of tRNA-synthetase genes was also evident at a protein level in FUS443.

Unlike in the proteomic data which did not reveal any significant increase in the expression of *fusA1* or *fusA2* in the mutant strain, *fusA1* transcriptional expression was increased whilst *fusA2* remained relatively unaffected. This further verifies the notion that these two genes and gene products are regulated distinctly from one another.

5.8.2 DeaD

The consistent up-regulation of ribosomal proteins and T3SS proteins across the proteomic and transcriptomic profile of FUS443 strongly suggests that these systems are constitutively activated in response to the mutated EF-G protein. In chapter four the RNA helicase DeaD was suggested as a potential regulatory link between these two systems. The transcriptomic data revealed that *deaD* transcription was unaffected by the mutation in *fusA1*. It is possible that post-translational regulation of DeaD led to an increased abundance at a proteomic level which would, in turn, promote ExsA expression. But as *deaD* expression does not reflect the transcriptomic profile of other ribosomal proteins it appears unlikely that the expression of the T3SS is linked to the up-regulation of ribosomal proteins, at least *via* DeaD.

5.9 Morphology

5.9.1 Motility

Phenotypic analysis and proteomic profiling revealed a decrease in the motility of FUS443 and in the abundance of motility apparatus. In part, this was reflected in the transcriptomic profile of FUS443 through the down-regulation of several flagellar-related genes. This included the flagellar biosynthesis gene, *flhB*, and flagellar biosynthesis

chaperone, *fliJ* (Table 5.10). Yet, a larger number of motility genes were up-regulated as a result of the *fusA1* mutation, including five genes encoding chemotaxis transducers, multiple flagellar encoding genes and several genes encoding T4P.

Table 5.10. List of genes associated with cell motility that were modulated in FUS443.

		FUS443		FUS443C	
Gene	**Function**	**log_2 FC**	**P-value**	**log_2 FC**	**P-value**
PA2652	Chemotaxis transducer	1.683	0.000	0.058	0.819
pctB	Chemotaxis transducer	1.475	0.000	-0.210	0.618
pilA	Type 4 fimbrial protein	1.375	0.000	0.291	0.401
chpE	Chemotaxis transducer	1.370	0.000	0.172	0.471
flgC	Flagellar basal body rod protein	1.342	0.000	0.190	0.384
cupE4	Pili assembly chaperone	1.266	0.000	-0.129	0.575
PA5072	Chemotaxis transducer	1.263	0.000	0.550	0.022
flgB	Flagellar basal body rod protein	1.133	0.000	0.067	0.765
flgD	Flagellar basal body rod modification protein	1.116	0.000	0.147	0.539
flgG	Flagellar basal body rod protein	1.045	0.000	-0.064	0.803
PA2654	Chemotaxis transducer	1.012	0.000	0.328	0.223
PA1608	Chemotaxis transducer	1.011	0.000	0.509	0.043
ctpL	Chemotaxis transducer	-1.036	0.000	0.089	0.685
flhB	Flagellar biosynthesis protein	-1.137	0.000	-0.204	0.351
morA	Motility regulator	-1.163	0.000	-0.260	0.335
cheY2	Probable two component response regulator	-1.277	0.000	0.231	0.460
cheA2	Probable two component sensor	-1.427	0.000	-0.073	-0.133
fliJ	Flagellar biosynthesis chaperone	-1.533	0.000	-0.062	0.794

The inconsistencies observed between the expression of motility genes and their corresponding protein abundance indicates the presence of strong post-transcriptional regulation controlling the turnover of mRNA or proteins, or that the motility genes are not constitutively effected by the *fusA1* mutation. In the latter case, the differences in the proteomic and transcriptomic profiles may have arisen as a consequence of environmental influences or biological stressors acting at the point of cell harvest. It is expected that these profiles would differ from the plate assays in chapter three, as motility gene expression will vary on solid/semi-solid media versus the liquid culture used in the proteomic and transcriptomic analysis.

Amongst the down-regulated genes were the two-component chemotaxis response genes, *cheY2*, and *cheA2*, which were addressed in the proteomic profile. The Che system is essential for flagellar motility and the Che2 system is also implicated in flagellar-based chemotaxis but not with the same prominence (Güvener *et al.*, 2006). If chemotaxis is dysregulated the cells will be incapable of directional movement, regardless of the up-regulation of flagellar genes, therefore would not move far from the point of inoculation.

Several transcriptional regulators were modulated in the FUS443 mutant which may play a role in the opposing changes associated with motility. One such regulatory gene was *PA3341* which was expressed 2.4-fold lower than in the progenitor strain. *PA3341* encodes a probable transcriptional regulator that could potentially play a regulatory role in motility due to its genomic position upstream of a flagellar biosynthesis cluster and *hsb* genes (*PA3343-PA3353*). The *hsb* gene cluster is known to regulate biofilm formation, twitching, swimming, swarming and chemotaxis by intersecting the Gac/Rsm pathway (Valentini *et al.*, 2016). This cluster of genes was down-regulated in FUS443, including the response regulator *hsbR*. HsbR promotes flagellar motility by activating HsbA, which subsequently binds to the anti-sigma factor FlgM. Sequestration of FlgM relinquishes the corresponding sigma factor, FliA, which then induces the expression of flagellar biosynthesis and assembly genes (Figure 5.11) (Bhuwan *et al.*, 2012; Valentini *et al.*, 2016). Because of this, the down-regulation of *hsbR* would have a negative effect on cell motility. Interestingly, HsbA also activates the diguanylate cyclase HsbD which has been found to increase *rsmY* levels though an unknown mechanism (Francis *et al.*, 2017). This may therefore link into the down-regulation of *rsmY* transcripts that was observed in FUS443.

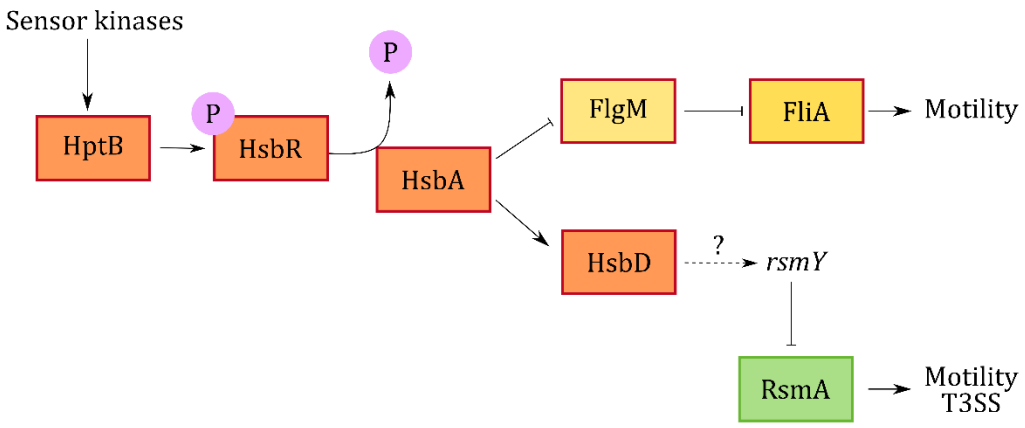

Figure 5.11. Regulation of motility in *P. aeruginosa via* the histidine phosphotransfer protein (HptB) and Hsb proteins in response to activation by sensor kinases, PA1611, SagS and ErcS'.

The transcriptional expression of FliA, along with another well characterised sigma factor that regulates chemotaxis and motility, RpoN, were unaffected in this screen. Due to the high level of post-translational regulation involved in bacterial motility and the inconsistency of expression across motility genes in this study, the precise mechanism behind the involvement of EF-G on motility remains unclear. However, the mutated EF-G variant did appear to have impacted upon numerous subgroups of motility genes but these were not affected constitutively.

5.9.2 Cell division

Analysis of cell morphology by light microscopy revealed that the FUS443 strain had an elongated cell morphology which appeared to be associated with the replication of the pUCP20 plasmid. The transcriptomic analysis revealed how this phenotype was reflected in changes to the expression of genes involved in the maintenance of cell shape. Disturbance to cell morphology appeared to have resulted from the up-regulation of numerous genes that inhibit the cell division process; *minD* encodes a cell division inhibitor and was up-regulated 2.5-fold, whilst *zapE* was increased by 2.8-fold and encodes a protein that reduces the stability of the cell division protein, FtsZ. Other up-regulated genes included *spoOJ* (2.0-fold), encoding a chromosome partitioning protein,

and *mreB* (2.9-fold), encoding a rod-shape determining protein. Conversely, *rodA* was down-regulated (2.3-fold), which encodes another rod shape-determining protein. All of these genes were complemented, at least in part, by the p*fusA1* plasmid showing that the *fusA1* mutation indirectly affected cell shape. The reduced fitness of the FUS443 mutant is likely to be exacerbated by the added pressure of replicating the pUCP20 plasmid, leading to the disruption of basic cellular processes such as cell division.

5.10 Redox pathways

A variety of redox-active proteins, typically located within the periplasm, were transcriptionally modulated in response to the *fusA1* mutation. This included the down-regulation of numerous cytochrome C encoding genes; *PA2482*, *PA1856*, *cooN2* and *cooO2*, whilst the cytochrome B encoding gene, *PA4430*, and cytochrome P450 encoding *PA3331* gene, exhibited increased expression (Table 5.11). Several other genes encoding redox-active proteins such as thioredoxin, glutaredoxin and numerous oxidoreductases were up-regulated in the mutant strain. The cluster I phenazine biosynthesis genes were also up-regulated, with *phzA1* and *phzC1* expression increased by 3.5- and 7.1-fold respectively. Phenazines are virulence factors produced by *P. aeruginosa* to damage competing bacteria or host cells as a consequence of their redox-active properties.

Table 5.11. List of genes involved in oxidation/reduction pathways within the periplasm of *P. aeruginosa* and their log_2 fold change in expression in FUS443 and the complemented strain.

		FUS443		FUS443C	
Gene	**Function**	**log_2 FC**	**P-value**	**log_2 FC**	**P-value**
PA3331	Cytochrome P450	2.763	0.000	0.745	0.168
PA4061	Thioredoxin	1.616	0.000	-0.268	0.283
PA4430	Cytochrome B	1.567	0.001	0.243	0.614
grx	Glutaredoxin	1.382	0.000	0.402	0.080
ahpF	Alkyl hydroperoxide reductase	1.375	0.000	0.087	0.713
PA3795	Oxidoreductase	1.160	0.000	0.162	0.536
PA0840	Oxidoreductase	1.096	0.000	0.314	0.150
PA1856	Cbb3-type cytochrome C	-1.076	0.000	-0.164	0.478
PA2477	Thiol:disulfide interchange protein	-1.179	0.011	-0.328	0.451
coxB	Cytochrome C oxidase subunit II	-1.249	0.000	-0.208	0.520
fprB	Oxidoreductase	-1.299	0.000	-0.317	0.251
PA4621	Oxidoreductase	-1.343	0.000	0.057	0.843
PA2482	Cytochrome C	-1.402	0.000	-0.148	0.694
ccoN2	Cbb3-type cytochrome C subunit I	-1.590	0.000	0.109	0.685
ccoO2	Cbb3-type cytochrome C subunit II	-1.590	0.000	0.267	0.242

PA3398 encodes the transcriptional regulator FinR, and was up-regulated 2.2-fold in FUS443. FinR senses oxidative stress and has been found to induce the expression of its neighbouring gene, *fprA*, upon exposure to superoxides. *FprA* encodes a ferredoxin NADP-reductase which participates in iron acquisition, iron-sulfur cluster biogenesis and oxidative defence (Boonma *et al.*, 2017). In FUS443, *fprA* expression was increased by 2.5-fold. If FinR was responsible for the up-regulation of *fprA*, this defines a link between the oxidative stress response and iron uptake in FUS443. In addition to this, SoxR is a transcriptional regulator involved in mediating the oxidative stress response with its activity regulated post-translationally *via* the oxidation state of its iron-sulfur cluster (Sheplock *et al.*, 2013). Transcriptomic data saw the expression of *soxR* reduced by 2.1-fold. SoxR negatively regulates FinR and so the reduction in its transcriptional expression may have caused the up-regulation of *finR* and other redox-active proteins in FUS443.

5.11 Sulfur metabolism

A large number of genes that were affected by the *fusA1* mutation were involved in sulfur metabolism and uptake. Sulfate esters are the most abundant sulfur source in aerobic soils and bacteria produce enzymes to hydrolyse these compounds to release usable sulfur. Many bacteria can grow on alkylsulfates, such as sodium dodecyl sulfate (SDS), which requires arylsulfatase. Arylsulfatase genes (*astABC*) and the regulator of this operon, *astR*, were up-regulated in *fusA1*^{P433L} (Table 5.12), which suggests that the mutant is not obtaining enough sulfur from its environment or that sulfur stores are diminishing faster in FUS443 than in the progenitor and complemented strain.

The *ssu* gene cluster was highly up-regulated in FUS443, with some genes being expressed as high as 108-fold higher than in the progenitor strain. This cluster is required for growth on aliphatic sulfonates, excluding the compound, taurine. The uptake and release of sulfite from taurine is dependent on the *tauABCD* operon, which was also highly up-regulated as a result of the *fusA1* mutation. These genes were only partially complemented by the expression of the WT *fusA1* gene. The high level of modulation that also occurred in FUS443C made it difficult to decipher the degree to which expression was complemented. By converting the $\log_2$ FC to FC helps to emphasise the recovery of the WT expression profile, for example, the 108-fold increase of *ssuD* expression in FUS443 is reduced to 11.6-fold in FUS443C. This makes it clearer that the *fusA1* mutation is most likely to be the leading cause of these modulations and incomplete complementation was likely to be due to the presence of the remaining mutated *fusA1* variant in the genome of FUS443C.

Another protein that is central to the regulation of sulfur metabolism is CysB, which is the primary transcriptional regulator of the *cys* genes for cysteine biosynthesis. The *cys* genes are not clustered together but are distributed throughout the genome. In FUS443, *cysB* is up-regulated along with all of the *cys* genes, indicating that the CysB protein is highly active in the mutant strain. CysB is not only involved in the regulation of cysteine biosynthesis but also positively regulates taurine metabolism (through the *tau* genes), sulfate metabolism (through *ssu* regulation), and sulfate-ester transport (*via astRBC*). This shows how the *fusA1* mutation caused the global up-regulation of sulfur metabolism genes *via cysB*, and was also supported by the proteomic data which saw both taurine and sulfate metabolising proteins at an increased abundance.

Table 5.12. List of genes involved in sulfur metabolism and their log_2 fold change in expression in FUS443 and the complemented strain.

		FUS443		FUS443C	
Gene	**Function**	**log_2 FC**	**P-value**	**log_2 FC**	**P-value**
ssuB	ATP-binding component of ABC transporter	4.518	0.000	1.495	0.004
ssuC	Permease of ABC transporter	6.198	0.000	2.463	0.000
ssuD	Hypothetical protein	6.766	0.000	3.540	0.000
ssuE	Hypothetical protein	5.544	0.000	3.060	0.000
ssuF	Molybdopterin-binding protein	3.419	0.000	2.654	0.000
tauA	Taurine binding protein	5.042	0.000	3.342	0.000
tauB	ATP-binding component of ABC transporter	5.322	0.000	3.023	0.000
tauC	Permease of ABC transporter	4.118	0.000	1.675	0.001
tauD	Taurine dioxygenase	3.989	0.000	1.293	0.000
astR	Binding protein component of ABC transporter	1.096	0.000	0.487	0.025
astA	Arylsulfatase	0.706	0.001	-0.076	0.724
astB	ATP-binding component of ABC transporter	0.756	0.025	-0.109	0.720
astC	Permease of ABC transporter	0.900	0.008	-0.021	0.951
cysB	Transcriptional regulator	0.962	0.001	0.434	0.113
cysA	Sulfate transport protein	5.141	0.000	1.590	0.000
cysD	ATP sulfurylase	3.754	0.000	2.141	0.000
cysH	3'-phoshoadenosine-5'-phoshoulfate reductase	1.471	0.000	0.888	0.000
cysI	Sulfite reductase	3.741	0.000	1.515	0.000
cysK	Cysteine synthase	1.311	0.000	0.116	0.642
cysN	ATP sulfurylase	3.913	0.000	1.802	0.000
cysP	Sulfate-binding protein of ABC transporter	3.561	0.000	1.814	0.000
cysT	Sulfate transport protein	5.620	0.000	2.290	0.000
cysW	Sulfate transport protein	4.917	0.000	1.173	0.000

5.12 Discussion

5.12.1 Motility

The expression of a large number of genes was modulated in the FUS443 mutant, affecting distinct clusters of cellular processes that played diverse roles across the cell.

Motility and chemotaxis are systems that have been consistently disrupted throughout FUS443 phenotypic analysis, proteomic analysis and transcriptomic analysis, although not always to the same extent. Several of the proteins that were up-regulated in the proteomic screen were down-regulated at a transcriptional level, but the cluster II flagellar-chemotaxis genes remained consistently down-regulated across both profiles.

Well-known regulators and sigma factors of chemotaxis, such as FlgM, RpoN and FliA, were unaffected at a transcriptional level in the mutant strain, but this is not to say that their post-translational activity had not been altered. There was however, a reduction in *hsbR*, which encodes a response regulator related to flagellar motility. HsbR is involved in the post-translational activation of the HptB pathway, implicated in biofilm formation, twitching, swimming, swarming and chemotaxis. This pathway culminates in the sequestration of the anti-sigma factor FlgM and induces flagellar gene expression through the release of the sigma factor, FliA (Valentini *et al.*, 2016). The down-regulation of *hsbR* might therefore have caused the changes in gene expression of some of the motility genes and proteins.

The differences in protein and transcript abundance suggest that the motility-regulatory network is heavily dependent upon post-transcriptional activation or inhibition. This makes it difficult to determine the molecular mechanisms that were responsible for the changes in motility by just using the transcriptomic and proteomic methods undertaken in this study. It is also likely that any modulations induced as a result of the mutated EF-G protein were minor and expression was vulnerable to other regulatory inputs from the cell and its surroundings. One exception to this was the cluster II chemotaxis genes and proteins which were consistently down-regulated. In this case, the mutated EF-G is likely to affect the activity of a regulator that specifically targets the *che2* genes with minimal input from alternative pathways.

5.12.2 Amino acid biosynthesis

Central metabolism and amino acid biosynthesis were among the major processes affected by the *fusA1* mutation. The most over-expressed genes in FUS443 were *ilvA2* and its operonic gene partner, *PA1325*. These genes are important in central metabolism by controlling the complex synthesis of aspartate-derived amino acids (Rosenberg *et al.*, 2016). The Ilv pathways can be induced by a shortage of aminoacylated-tRNAs, an abundance of substrates or through catabolite repression (Tarleton *et al.*, 1991). A number of tRNA synthetase genes were also up-regulated in FUS443, and so together, this suggests that there was an increased demand for aminoacyl-tRNAs and protein synthesis in the mutant strain. With these findings echoed at proteomic level, this indicates that the *fusA1* mutation is constitutively affecting amino acid metabolism and tRNA-charging.

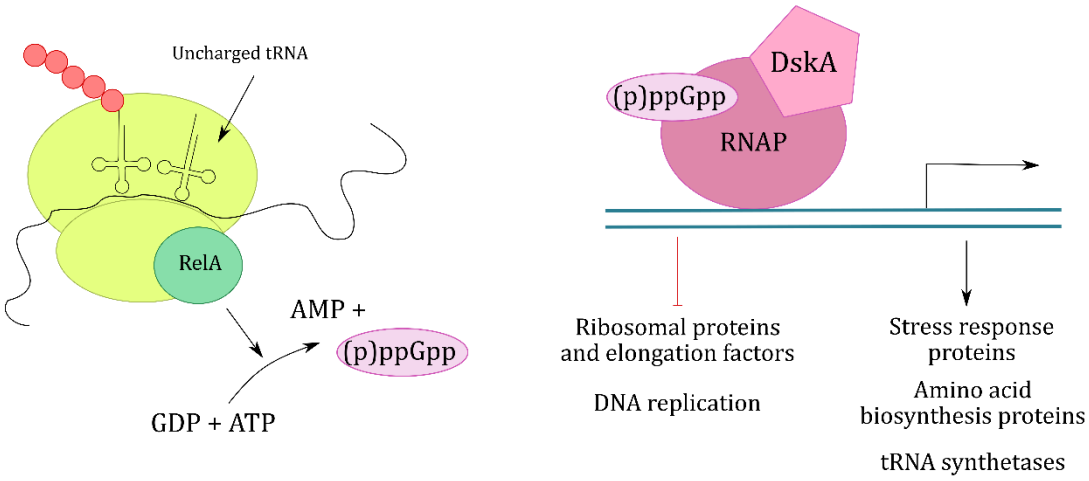

Figure 5.12. The (p)ppGpp-mediated stringent response in *P. aeruginosa*.

Having uncharged tRNA molecules positioned within the ribosome is a sign of amino acid depletion and is the major cause of ribosomal stalling. In chapter four I highlighted the increased abundance of SmpB in FUS443, which is a protein involved in the recovery of stalled ribosomes. This finding supported the notion that ribosomal stalling was occurring in the mutant strain, and now the transcriptomic data has provided evidence that this was potentially caused by the accumulation of uncharged tRNAs. RelA is a ribosome-associated protein which senses the presence of uncharged tRNA molecules on the ribosome and triggers the stringent response. To do this, RelA synthesises the alarmone, (p)ppGpp, which binds to RNA polymerase and coordinates the up-regulation of amino acid biosynthesis genes. During the stringent response rRNA and tRNA synthesis is inhibited and metabolism is down-regulated to reduce energy wastage (Figure 5.12) (Raina *et al.*, 2014). The transcriptomic data identified the up-regulation of *dskA*, which encodes a transcriptional regulator. DskA functions as a general accessory factor of (p)ppGpp and assists in the repression of rRNA genes and promotes amino acid biosynthesis and transport (Paul *et al.*, 2004; Blaby-Haas *et al.*, 2011). The up-regulation of tRNA synthetase genes, several amino acid biosynthesis operons and *dskA* support the idea that the stringent response was activated in the mutant strain. Initiation of the stringent response may benefit the cell by limiting the activity of EF-G on the ribosome. EF-G, along with EF-Tu and IF-2, are targets of the stringent response and are inhibited by (p)ppGpp (Kanjee *et al.*, 2012; Corrigan *et al.*, 2016; Beljantseva *et al.*, 2017) and so by

initiating the stringent response the cell could reduce the deleterious effects that the mutated protein is having on the cell.

Nevertheless, this was not consistent with the up-regulation of a large number of ribosomal-associated proteins that were significantly modulated in FUS443, as these should be repressed by (p)ppGpp and DskA (Vogt *et al.*, 2011). As the down-regulation of ribosomal proteins is one of the major objectives of the stringent response its activation appears improbable in FUS443. In addition to this, *fusA* mutations in *S. enterica* have been linked to a decrease in ppGpp levels as it was proposed that EF-G interferes with RelA-mediated synthesis of ppGpp on the ribosome (Macvanin *et al.*, 2000, 2004). Therefore, I postulate that the up-regulation of tRNA synthetases, amino acid metabolism genes and ribosomal proteins is due to a common regulatory mechanism that coordinates the rate and demand of protein synthesis.

5.12.3 Ribosomal protein expression

The up-regulation of ribosomal proteins in FUS443 was another observation that was consistent across both the proteomic and transcriptomic profile, showing that these changes are direct effects of the *fusA1* mutation. In chapter four I discussed the possibility that the up-regulation of ribosomal proteins was a direct result of inadequate EF-G functioning and was induced to counteract poor translational efficiency. Whilst this may still be true, the transcriptomic profile of the mutant provided further insight and an alternative explanation for these findings.

The main regulatory system for ribosomal gene expression occurs *via* direct negative feedback from excess ribosomal proteins which bind to and prevent translation of their own mRNA (Nomura *et al.*, 1984; Aseev *et al.*, 2016). With the up-regulation of ribosomal proteins in FUS443, this suggests that ribosomal proteins are not in excess, and are successfully being incorporated into ribosomal complexes and used for protein synthesis. It is possible that FUS443 has an increased demand for protein synthesis, reducing negative feedback by ribosomal proteins, and draining the intracellular pools of amino acids, triggering the up-regulation of amino acid metabolic genes.

An increase in the demand for protein synthesis in FUS443 may be down to cell morphology. Protein synthesis has a well-defined correlation with cell size, and over-

expression can lead to the production of large, slow growing cells (Basan *et al.*, 2015). FUS443 had an elongated cell morphology likely due to the dysregulation of various cell division-associated genes. This added mass would demand a greater level of protein synthesis to maintain cellular functions and growth, explaining why there was an increase in ribosomal protein synthesis. This elongated cell morphology was also found in *fusA* mutants of *S. enterica* which exhibited a decreased growth rate. In these mutants the defective EF-G was believed to disrupt the size threshold at which the cell begins dividing (Macvanin *et al.*, 2000). It should be noted, however, that the elongated phenotype in FUS443 was only apparent through a combination of the *fusA1* mutation and replication of the pUCP20 vector, and was not observed in the original vector-free mutant. With this, it is also possible that the up-regulation of ribosomal proteins did not occur in the absence of the pUCP20 vector.

5.12.4 Antibiotic resistance

The MexXY system was consistently up-regulated at a transcriptional level as well as at a proteomic level indicating its permanent up-regulation in response to the mutation in *fusA1*. Unlike in the proteomic profiling, the transcriptional expression of *mexZ* was not affected in FUS443 despite being divergently transcribed from the *mexXY* operon. MexZ is a transcriptional repressor of the MexXY system and several MexXY over-producing strains have been described which contain mutations in the *mexZ* gene (Suresh *et al.*, 2018). Whole genome sequencing of FUS443 verified the absence of any mutations in *mexZ* and so if MexZ was the cause of *mexXY* up-regulation this would be due to post-transcriptional regulation of the protein affecting it's activity.

Alongside *mexXY* modulation, the transcriptomic data also uncovered the down-regulation of *mexGHI-opmD*. Whilst the MexGHI-OpmD efflux system does not affect gentamicin susceptibility, mutants in this system have been found to be defective in the production of elastases, rhamnolipids and pyocyanin. These are all AHL-regulated exoproducts and so it has been postulated that the MexGHI system plays into QS systems by removing precursors of PQS (Aendekerk *et al.*, 2005; Sakhtah *et al.*, 2016). This efflux system has also been linked to the exportation of OdDHL, produced by the *las* QS system, affecting cell-cell communication (Southey-Pillig *et al.*, 2005). QS is a key regulator of

virulence and so its disruption *via* MexGHI may also contribute to the observed changes in QS signalling, motility, secretion and virulence in the FUS443 mutant.

Membrane permeability was potentially affected by the *fusA1* mutation through down-regulation of the *ppr* genes, which represent the *Pseudomonas* permeability regulators (Giraud *et al.*, 2011). Membrane impermeability can occur from changes to porins and lipopolysaccharide structures, and in combination with secondary resistance mechanisms, such as efflux systems and modifying enzymes, these adjustments can dramatically enhance the cells resistance to a variety of antibiotics (Wang *et al.*, 2003). *PprAB* is under the control of SigX, which was also down-regulated at a transcriptional level. The sigma factor SigX is a putative pleiotropic regulator and its mutation has been linked to transcriptional changes in chaperones and HSPs, antibiotic resistance genes, and genes involved in metabolism and motility, all of which have been affected in the mutant strain. PprB has also been found to downregulate the *mexXY* operon (Gicquel *et al.*, 2013), therefore, both decreased membrane permeability and increased *mexXY* expression may have resulted from *sigX* down-regulation or inactivity.

It is still formally possible that the structural changes to EF-G are having a direct impact on the binding of aminoglycosides to the ribosome. However, there is now accumulating evidence to suggest that the activation of efflux systems and membrane impermeability are the main cause of aminoglycoside resistance in FUS443.

5.12.5 Iron homeostasis

5.12.5.1 Siderophores and iron uptake

In addition to the up-regulation of pyochelin biosynthesis proteins in the proteomic profile, pyoverdine biosynthesis and uptake genes were up-regulated at a transcriptomic level. The ferric uptake regulator, Fur, is the master regulator of the iron starvation response and was unaffected in both the proteomic and transcriptomic data. However, its effect on some downstream targets, such as PhuR, suggests that Fur is in a de-repressing, iron-free state. Therefore, Fur may have caused the up-regulation of pyoverdine and pyochelin biosynthesis genes and proteins.

PvdS is another sigma factor that has been identified as a positive regulator of iron-response genes, including the *pvd* operon. The expression of *pvdS* was up-regulated in FUS443 and, whilst under the control of Fur at a transcriptional level, PvdS is also controlled at a post-translational level by the anti-sigma factor FpvR (associated with the cell surface FpvA pyoverdine receptor) in the absence of ferric-bound pyoverdine (Figure 5.13) (Imperi *et al.*, 2010; Edgar *et al.*, 2014). PvdS acts exclusively as a positive regulator, binding to IS (iron starvation) boxes within the promoters of iron-uptake and metabolism genes (Ochsner *et al.*, 2002). Therefore, the combination of Fur de-repression and PvdS activity may have led to the increased activation of *pvd* genes and iron-uptake systems in FUS443.

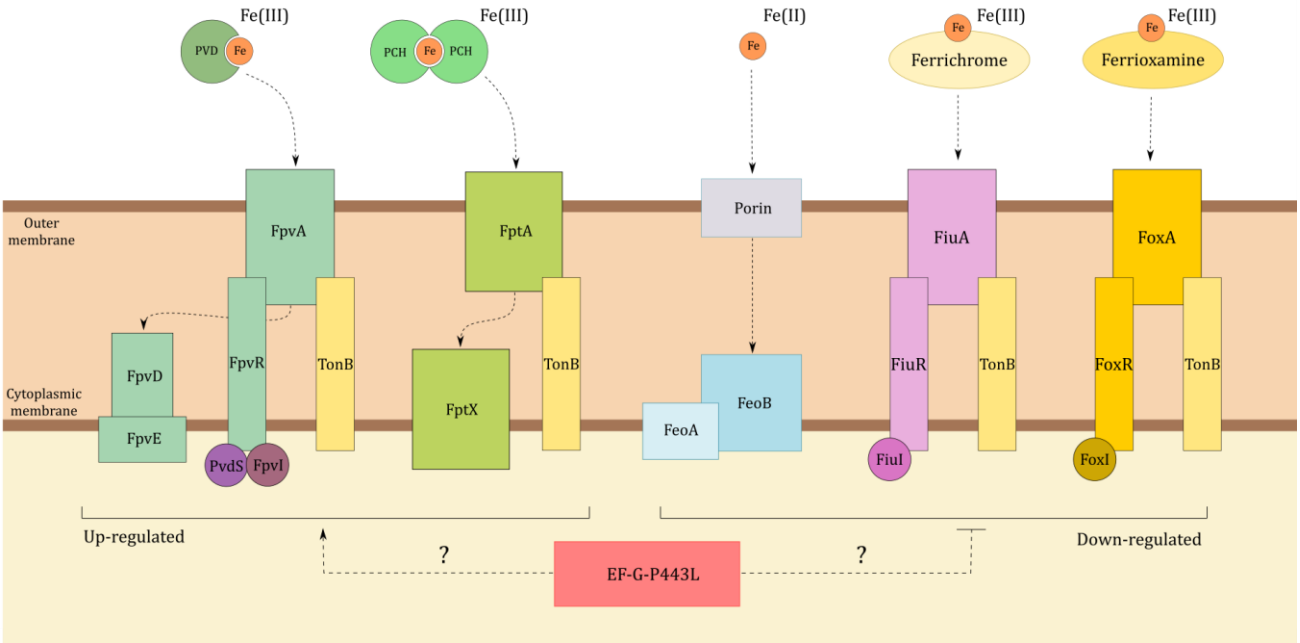

Figure 5.13. Iron uptake systems in *P.* aeruginosa that were affected by a mutation in the *fusA1* gene.

Siderophores are required for the chelation of insoluble Fe^{3+} from the environment and are taken into the cell *via* TonB-dependent transportation systems. Ferrous iron (Fe^{2+}), however, is soluble and is imported directly through Fe^{2+} Feo transporters (Figure 5.13). *FeoAB* is under the control of Fur, but FeoA can also modulate

the activity of FeoB in response to intracellular Fe^{2+} levels to prevent Fe^{2+} accumulation toxicity (Kim *et al.*, 2012; Cornelis *et al.*, 2013). *Feo* genes are typically expressed at a constitutive level (Lau *et al.*, 2016), but the expression of *feoAB* was down-regulated in FUS443. With the previous findings predicting the de-repressive activity of Fur, this data suggests that the mutant EF-G protein was causing *feoAB* suppression independently of Fur, through an unknown mechanism.

The *fiu* system for ferrichrome uptake and the *fox* system for ferrioxamine uptake were also down-regulated in FUS443. Therefore, the EF-G mutation appears to only promote the expression of a subgroup of iron-uptake systems that involve pyoverdine and pyochelin-based iron acquisition and suppresses the uptake of ferrous iron, ferrichrome and ferrioxamine. The opposing regulation of different iron uptake systems highlights the dense network of regulatory pathways in place to maintain iron homeostasis and contradicts a strong involvement by Fur which would see a global up-regulation of all systems.

5.12.5.2 Iron and sulfur co-regulation

Sulfur metabolism and iron homeostasis are coordinated systems. One possibility for this association is the need to maintain iron-sulfur ([Fe-S]) cluster biogenesis. [Fe-S] clusters are co-factors for a wide variety of proteins and can act as catalysts or redox sensors for electron transfer, gene regulation, environmental sensing and substrate activation (Imperi *et al.*, 2010; Roche *et al.*, 2013). There are three systems for [Fe-S] biosynthesis in bacteria, only one of which, the Isc (iron-sulfur cluster) system, is found in *P. aeruginosa*. IscR is a global regulator for [Fe-S] biogenesis by binding to, and detecting the levels of intracellular [Fe-S] (Romsang *et al.*, 2016). Expression of *iscR*, was not significantly modulated in FUS443, but as with many transcriptional regulators, its activity is managed post-translationally, and so cannot be reliably assessed by the work presented here.

Sulfate or cysteine limitation induces the expression of a variety of sulfate metabolising proteins. The *ssuBCDEF* gene cluster is required for growth on aliphatic sulfonates, except for taurine which requires the *tau* operon. The *tauABCD* operon encodes a transporter system and α-ketoglutarate dependent dioxygenase, involved in

the release of sulfite from taurine (van der Ploeg *et al.*, 1997; van Der Ploeg *et al.*, 1999). The *tauABCD* and *ssuBCDEF* operons were both amongst the most highly up-regulated genes in FUS443, indicating that the cells were in a sulfur-starved state.

CysB is central in the regulation of sulfur metabolism and is closely associated with promoting cysteine biosynthesis *via* the *cys* regulon. CysB also positively regulates the *tau* and *ssu* operons (Hummerjohann *et al.*, 2000; Imperi *et al.*, 2010) and controls the sulfate-ester transportation system, encoded by *astRBC*, that was up-regulated in the mutant (Hummerjohann *et al.*, 2000). This data showed that the mutation in *fusA1* caused a global up-regulation of sulfur uptake and metabolism, most likely *via* the key regulator CysB. CysB then provided a link between iron and sulfur homeostasis as it has been found to directly, and positively, regulate PvdS (Imperi *et al.*, 2010).

Interestingly, the *tonB2-exbB1-exbD1* operon is strongly up-regulated in response to sulfur starvation, along with several putative TonB-dependent receptors, and was significantly up-regulated in FUS443. TonB1 is characterised as a key player in the iron-response system whilst the role of TonB2 in iron uptake appears to be far more redundant (Cornelis *et al.*, 2009). However, the involvement of *tonB2* in sulfur metabolism is consistent with its position within a "sulfur island" containing a number of genes involved in sulfate-ester metabolism (Tralau *et al.*, 2007), and may play a role in the importation of sulfur into the cell. This may explain the rise in *tonB2-exbB1-exbD1* expression whereas *tonB1* was relatively unaffected in FUS443. Co-regulating iron and sulfur homeostasis ensures that intracellular pools of each element are available for the biogenesis of [Fe-S] clusters, and is also a way of preventing the toxicity of accumulating sulfur and the wastage of free iron (Imperi *et al.*, 2010).

5.12.6 Heat shock proteins and the oxidative stress response

Across eukaryotic and prokaryotic species, the heat shock response is characterised by the rapid expression of HSPs to prevent damage induced by thermal stress. HSPs can also be induced by numerous non-thermal stressors such as antimicrobial agents, ethanol exposure, reactive oxygen species (ROS), glucose starvation and hyperosmolality (Allan *et al.*, 1988; Wheeler *et al.*, 2007). The FUS443 mutant exhibited an increase in the expression of HSPs at non-inducing temperatures, suggesting

that induction was triggered *via* an alternative stimulus. RpoH is one of the major sigma factors involved in the initiation of the heat shock response and upregulates the expression of numerous HSPs and molecular chaperones, including DnaK, DnaJ, GrpE, GroEL and GroES (Potvin *et al.*, 2008). RpoH translation is itself thermo-regulated through secondary structures positioned within the *rpoH* mRNA. These structures restrict access by the ribosome under non-stress conditions but are disrupted during elevated temperatures, enhancing translation and increasing the abundance of the sigma factor in the cell. Transcription from RpoH-dependent promoters is then increased, which in turn controls the expression of *rpoH* (Morita *et al.*, 1999; Gunesekere *et al.*, 2006). The transcriptomic profiling of the FUS443 mutant revealed that the mutant strain was over-expressing *rpoH*, which explains the over-expression of HSPs. HSPs allow cells to adapt to stress conditions by influencing a variety of protein processing mechanisms, including protein folding, stabilisation, protein-complex assembly, transportation and protein degradation (Grudniak *et al.*, 2018). Having affected the expression of *rpoH*, the mutated EF-G protein would subsequently affect a diverse range of cellular processes.

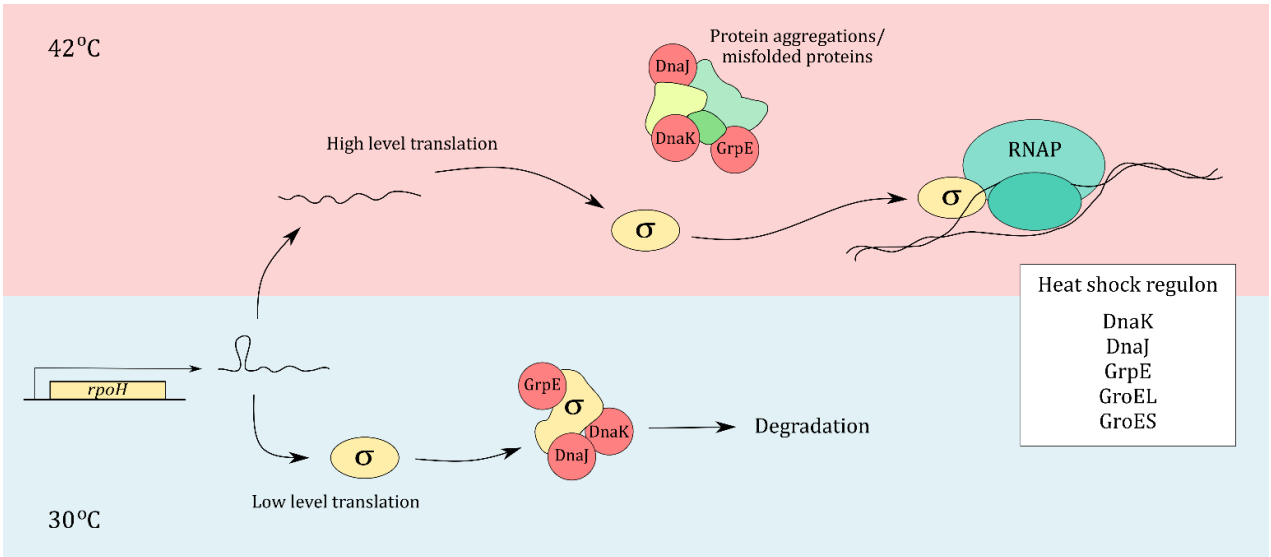

Figure 5.14. Regulation of the heat shock response by RpoH.

Among the heat-shock response genes, expression of the *dnaKJ-grpE* chaperone system was up-regulated. The DnaK-DnaJ-GrpE complex targets proteins for refolding, degradation and disaggregation. Together they repress the heat shock response by targeting RpoH for degradation (Figure 5.14). However, when the cell experiences stress conditions DnaKJ-GrpE is recruited to the accumulating body of aggregated proteins, meaning that RpoH protein levels rise and initiate the heat shock response (de Bruijn, 2016; Anglès *et al.*, 2017). This explains how the up-regulation of both *dnaKJ-grpE* and heat shock response genes can co-exist in the FUS443 mutant, and adds to the growing evidence that the mutant strain has a stressed intracellular environment as a result of the *fusA1* mutation.

There is a strong link between the cellular redox state and the induction of the stress response (Wheeler and Wong, 2007). Numerous redox-active proteins were up-regulated in FUS443 suggesting that oxidative stress may have initiated the heat shock response. Part of the host immune response is the release of ROS in an attempt to kill invading bacterial species. The bacteria themselves also generate ROS as by-products of respiration and for these two reasons it is highly important that the cells can protect themselves from oxidative damage. *P. aeruginosa* implement numerous methods to reduce oxidative damage, such as the production of antioxidants, including catalases, superdioxide dismutases and thiol peroxidases (Boonma *et al.*, 2017). The increased transcriptional expression of redox-active proteins in FUS443 indicates that there is pressure to maintain a redox balance in the cell or a requirement for electron acceptors during the process of energy generation.

5.12.7 Crosstalk between iron, sulfur and oxidative stress

The periplasm is a highly reducing environment within which FUS443 up-regulated a variety of redox active molecules. Maintaining a buffered redox state is vital to the function of a wide variety of biological molecules in the cell. *P. aeruginosa* uses the Entner-Doudoroff pathway and TCA cycle for glucose metabolism, which is coupled with the reduction of nicotinamide adenine dinucleotide (NAD^+) to NADH. Reduced NADH is utilised in the respiratory chain by transferring electrons to oxygen or nitrogen. The NAD^+/NADH ratio can provide an indication of the redox state of the cell and can be used

to buffer the oxidising activities of molecules like phenazines, which are produced, among other reasons, for their toxic oxidising properties against competing bacteria and host cells (Price-Whelan *et al.*, 2007; Cezairliyan *et al.*, 2013). Phenazine biosynthesis genes were up-regulated in FUS443 and so this would increase the pressure on redox systems to buffer their damaging effects on the cell.

SoxR gene expression was down-regulated as a result of the *fusA1* mutation. SoxR is a transcriptional regulator that senses a range of redox-cycling compounds, such as hydrogen peroxide, superoxide and nitric oxide. SoxR is constitutively expressed and is activated upon oxidation of its [2Fe-2S] cluster which causes it to de-repress promoter sequences, activating their transcription (Sheplock *et al.*, 2013). Therefore, the down-regulation of *soxR* in FUS443 may account for the increased expression of a variety of oxidoreductases and alkyl hydroperoxide reductases. Interestingly, SoxR has also been reported to positively regulate the *mexGHI-opmD* operon, and therefore its down-regulation may have contributed to the down-regulation of *mexGHI-opmD* in FUS443. So far this is the first redox-responsive Mex system to be identified but its role in the oxidative stress response is unclear (Du *et al.*, 2015).

Another transcriptional regulator that was affected by the *fusA1* mutation was FinR, whose expression was transcriptionally up-regulated. FinR is under the negative control of SoxR through which its expression is promoted during superoxide stress (Yeom *et al.*, 2010). Its up-regulation may therefore be due to the reduced expression of *soxR* or the presence of ROS. FinR regulates its neighbouring gene, *fprA*, and its own expression through their joint bi-directional promoter. FprA encodes a ferredoxin $NADP^+$ reductase which catalyses the transfer of electrons between NADPH and ferredoxin, which is a small iron-sulfur protein that mediates electron transfer reactions for numerous metabolic reactions. Because of this, FprA plays an important role in maintaining $NADP^+$/NADPH pools in the cell (Elsen *et al.*, 2010; Boonma *et al.*, 2017) and mutants in either *finR* or *fprA* have increased sensitivity to oxidative stress (Lewis *et al.*, 2013). This suggests that the FUS443 mutant would be more resistant to highly oxidative environments, such as in the CF lung.

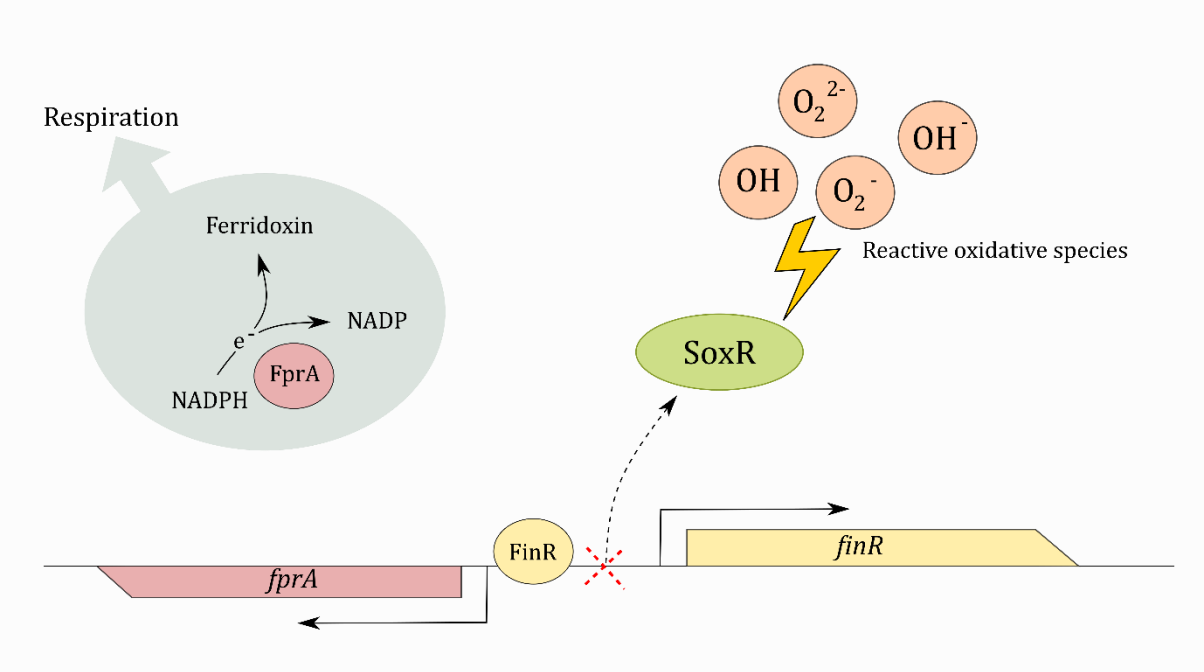

Figure 5.15. Oxidative stress-induced expression of the transcriptional regulator, FinR, and its implications on the respiratory chain and maintaining the redox-state of the cell by modulating NADP/NADPH pools.

FprA is also involved in cysteine biosynthesis and is induced upon sulfur-limitation. It is postulated that FprA is associated with sulfur assimilation *via* an interaction with the sulfite reductase, CysI. Ferredoxin-dependent sulfite reductases have been identified in other proteobacteria and so it is also possible that FprA transfers electrons directly to CysI. The crosstalk between sulfur metabolism and FprA is unclear, and the role of FinR in this activation has not been determined. But it is possible that oxidised sulfur species such as sulfoxides and sulfonates could be a trigger for *fprA* induction (Lewis *et al.*, 2013).

In addition to induction by oxidative stress and sulfur-limitation, *fprA* expression is also induced under iron-limited conditions (Yeom *et al.*, 2010). [Fe-S] clusters are particularly sensitive to oxidative damage and dysregulation of [Fe-S] biogenesis during oxidative stress would have a detrimental impact on the central metabolism (Goldová *et al.*, 2011; Boonma *et al.*, 2017). The redox system also relies on iron homeostasis as the majority of enzymes involved in preventing the accumulation of radicals, such as peroxidases, catalases and some superoxide dismutases, contain iron (Messenger *et al.*,

1983). Because of these links, the iron, sulfur and oxidative stress systems must be closely balanced through tight regulatory connections between the systems (Figure 5.16). It is possible that the mutated EF-G protein only affected the activity of one of the key regulators, Fur, PvdS, CysB, or SoxR, to have radiating effects across the cell.

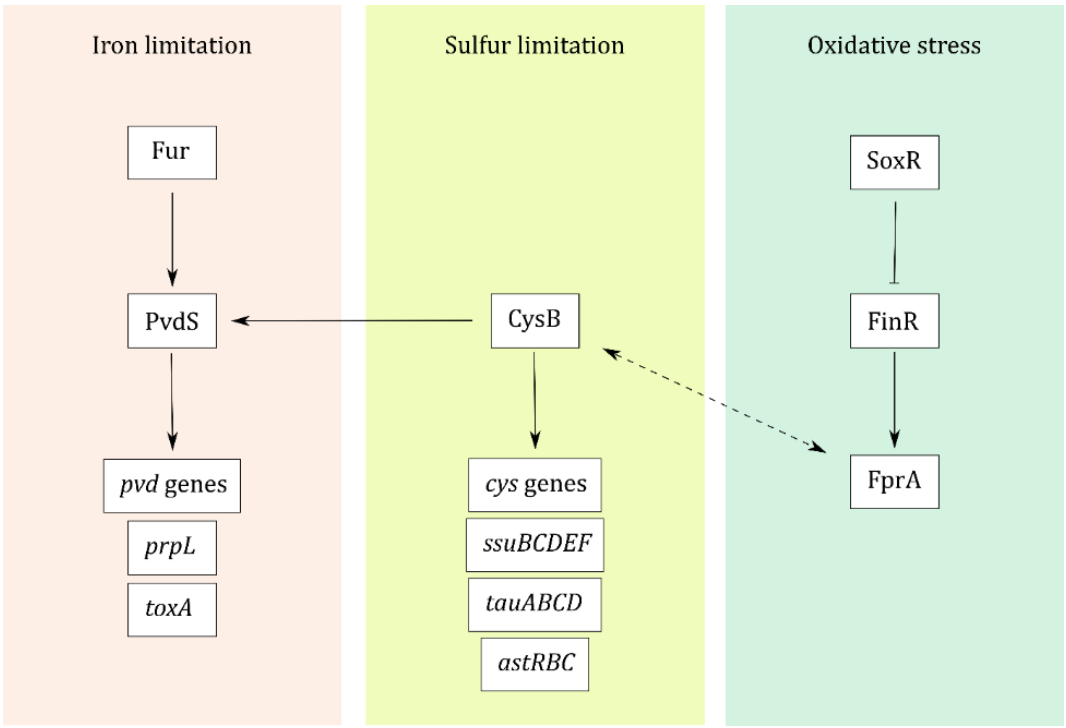

Figure 5.16. The interconnecting networks of iron homeostasis, sulfur metabolism and oxidative stress that were affected in by mutation to EF-G.

5.12.8 Secretion systems

5.12.8.1 The type III secretion system

Seven secretion systems have been identified in *P. aeruginosa*, each with distinct roles in protein translocation (Mougous *et al.*, 2006; Pukatzki *et al.*, 2006). At least three of these secretion systems had been affected by mutation to *fusA1*. The most affected, at both a transcription and proteomic level, was the T3SS.

All of the T3SS genes detected in the transcriptomic screen were up-regulated, including the master regulator ExsA. The up-regulation of four genes, *pcr1*, *pcr2*, *pcr3*, and

pcr4, was also identified at a transcriptomic level. These genes are largely undefined but their products have been found to form interacting partners that affect the functionality of the T3SS. In some *Yersinia* and *Shigella* strains, these proteins come together to form plug or cap-like structures on the secretion tip of the injectosome to regulate translocation. Pcr1 was also found to bind PopN creating a T3SS repressor complex, with mutation to *popN* or *pcr1* causing constitutive T3SS activation (H. Yang *et al.*, 2007). The up-regulation of these genes alongside the other T3SS proteins suggests a negative feedback mechanism to post-translationally control the activity of the T3SS. From this study it is unclear if expression of the *pcr1234* genes is having a negative effect on secretion.

The Gac/Rsm pathway is a global regulatory network that had been found to control the transcription of T3SS genes. The transcriptomic profile of FUS443 revealed the down-regulation of two Gac/Rsm pathway constituents; *rsmY* and *rsmA*. Small RNAs, *rsmY* and *rsmZ*, sequester RsmA to prevent its promotive or repressive effects on mRNA targets (Moscoso *et al.*, 2014). RsmA typically promotes the expression of the T3SS and so the down-regulation of *rsmA* suggests that T3SS expression in FUS443 is a result of activation by a Gac/Rsm-independent mechanism. However, this pathway cannot be completely disregarded as the simultaneous downregulation of *rsmY* transcripts may increase the abundance of "free" RsmA, even during low level *rsmA* transcription.

The expression of another transcriptional regulator, PsrA, was down-regulated in the FUS443 mutant strain. There are contradictory studies relating to repression or induction of T3S by PsrA (Shen *et al.*, 2006; Gooderham *et al.*, 2008). Kang *et al.* (2009) proposed that PsrA possesses a dual regulatory role, dependent upon the presence of long chain fatty acids (LCFAs). It was noted that LCFA-bound-PsrA caused de-repression of *fadAB*, which encodes a complex for fatty acid degradation. These genes were up-regulated in FUS443, supporting the notion that PsrA activity was lower in the mutant. Kang *et al.* then found that regulation of *exsCEBA* functioned in a similar LCFA-dependent manner, with de-repression in the presence of LCFAs. The abundance of LCFA in FUS443 is unclear, but this model suggests that the down-regulation of PsrA may have contributed to the up-regulation of ExsA in the mutant strain.

The host environment is purposely limited in iron to prevent bacterial invasion. Because of this, bacteria not only adopt a number of processes to overcome iron

limitation but iron abundance becomes an environmental signal for the presence of competing bacteria or host cells, which in turn induces the expression of virulence factors. (Bronstein *et al.*, 2008; Chakraborty *et al.*, 2011; Kurushima *et al.*, 2012). The link between iron availability and T3S has been thoroughly documented in several bacterial species, including *Bordetella*, *Salmonella*, *Shigella*, *Edwardsiella*, *Vibrio* and *Yersinia* species (Wilderman *et al.*, 2004; Bronstein *et al.*, 2008; Gode-Potratz *et al.*, 2010; Chakraborty *et al.*, 2011; Kurushima *et al.*, 2012; H. K. Miller *et al.*, 2014). In these cases, Fur is considered to act as a simple repressor of T3SS genes in the presence of iron. To investigate if the up-regulation of T3S in FUS443 was due to iron limitation, cultures were grown under iron-rich conditions. Unexpectedly, this led to an increase in T3S in the mutant whilst the progenitor and complemented strain were unaffected.

There is limited research on the relationship between Fur and T3S in *P. aeruginosa*, however, in the plant pathogen *P. syringae*, the addition of iron was found to suppress siderophore biosynthesis and induce genes involved in T3S and other proteins that use iron as a co-factor (Bronstein *et al.*, 2008). Whilst this observation was not reflected perfectly in FUS443, my findings do support the inducive properties of iron. From these investigations it appeared that the induction of T3S by iron, in FUS443 under standard conditions, may be linked to the up-regulation of pyochelin and pyoverdine-iron acquisition systems, leading to an increase in intracellular iron. This phenotype is then exaggerated under iron-rich conditions causing a further increase in T3SS expression as the mutant strain appears to be unable to maintain iron homeostasis. The precise mechanism by which iron acts on T3S is currently unclear, but is likely to act independently of Fur which is repressive during iron-repletion.

From these findings, I was able to determine that the mutation in *fusA1* affected the expression of the T3SS *via* the altered expression of the master regulator ExsA, which may have been influenced by PsrA. The cause of this up-regulation was linked to the dysregulation of iron acquisition systems that occurred in the cell as a result of the mutation in *fusA1*.

5.12.8.2 The type II secretion system

The T2SS is very structurally similar to T4P and is comprised of an outer membrane complex, inner membrane complex, ATPase and pseudopilus. The pseudopilus is composed of numerous pilin-like proteins known as pseudopilins, which polymerise to form a piston-like structure through which secreted proteins are pushed from the cell (Durand *et al.*, 2003). Out of all the secretion systems, the T3SS and T2SS are the major secretors of toxins, with the T2SS secreting exotoxin A, LasA and LasB, type IV protease, and phospholipase H (Jyot *et al.*, 2011). *P. aeruginosa* encodes two main T2SSs; the Xcp system and the Hxc system. In FUS443, only the expression of the *hxc* cluster was affected by the mutation in *fusA1*. The *hxc* gene cluster consist of genes *hxcP-Z* which represent homologs to all of the *xcp* genes and produce characteristically similar proteins. Despite their similarity the two homologous sets do not have overlapping functions and will not substitute one another in the case of mutation. This helps to explain why only one of the T2SS clusters was affected by the *fusA1* mutation (Ball *et al.*, 2002). The *hxc* gene cluster is involved in the secretion of alkaline phosphatases and expression is induced upon phosphate limitation (Jyot *et al.*, 2011).

The *fusA1* mutation induced the down-regulation of the *hxc* T2SS. This suggests that the mutant strain may be more efficient at acquiring phosphate from its surroundings or, as with iron homeostasis, the phosphate response system has become dysregulated. Inorganic phosphate in the environment is sensed by the two component system PhoB/PhoR which promotes the expression of a large set of genes involved in phosphate acquisition, including the Pst phosphate-uptake system (Blus-Kadosh *et al.*, 2013; Faure *et al.*, 2013). Neither *phoAR* nor *pstBACS* were affected on a transcriptional or proteomic level indicating that the downregulation of the *hxc* cluster is independent of phosphate availability.

5.12.8.3 The type VI secretion system

The T6SS is the most recently identified secretion system. *P. aeruginosa* encodes three potential T6SSs, *via* three Hcp Secretion Islands (HSI-I, HSI-II, HIS-III) (Casabona *et al.*, 2014). T6S is used to kill competing bacterial cells and can be used to discriminate

between same-species and non-pseudomonas bacteria. It is used as defence against same-species cells and has been implicated in a phenomenon known as 'T6SS duelling' involving the back and forth retaliation of attacks between neighbouring *P. aeruginosa* cells. Because of the direct contact between adjacent cells, the T6SS is often used in dense biofilms and during surface growth, when the cells are less motile. It has also been implicated in the formation of biofilm structures and the HSI-I cluster is in fact co-regulated with several biofilm-associated genes including as *psl* and *pel*, for exopolysaccharide synthesis, *via* the Gac/Rsm pathway (Hood *et al.*, 2010). However, during planktonic growth the system is expressed at a low level (Alteri and Mobley, 2016) which meant that the up-regulation of the HSI-I cluster in FUS443 in planktonic culture was highly unusual. This could, however, be linked to the observed increase in exopolysaccharide production. The up-regulation of this system was also not reflected in any enhanced killing of *E. coli* during co-culture, putting the activity of the T6SS under question.

Several mechanisms are in place to regulate the T6SS, some of which respond to environmental conditions such as iron limitation, temperature and osmotic stress. Transcriptional regulation has been recognised through the activating properties of RpoN, and negative control by Fur and RetS (Mougous *et al.*, 2006; Hachani *et al.*, 2011; Alteri *et al.*, 2016), none of which were modulated in FUS443. A second level of regulation occurs post-translationally *via* a threonine phosphorylation cascade orchestrated by the kinase PpkA. PpkA phosphorylates Fha1, to activate the Fha1-ClpV1 complex which induces the export of effector proteins through the T6SS (Figure 5.17) (Casabona *et al.*, 2014; Chen *et al.*, 2015). Both PpkA and the phosphatase PppA were up-regulated as a result of the *fusA1* mutation and are likely to be involved in the activity of the T6SS at a post-translational level.

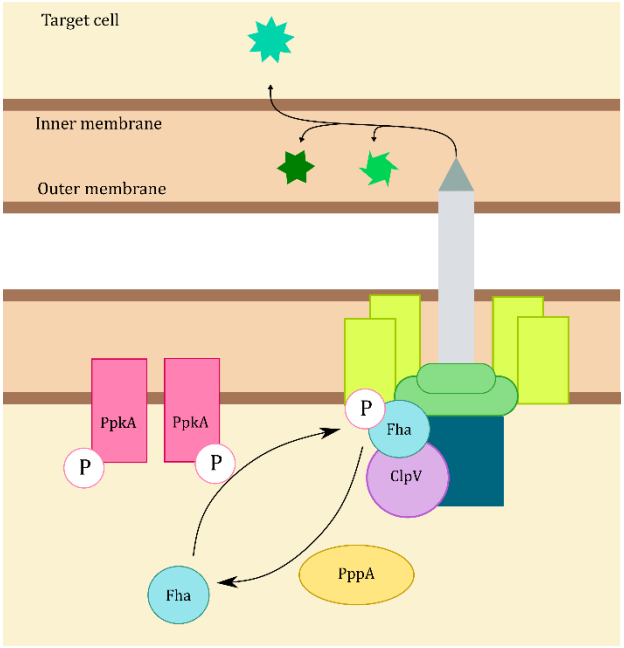

Figure 5.17. Regulation of the T6SS by PpkA and PppA threonine phosphorylation cascade.

The T3SS and T6SS are typically mutually exclusive phenotypes due to antagonistic regulation by the Gac/Rsm pathway (Line Lucchetti-Miganeh *et al.*, 2014). RsmA positively regulates the T3SS but negatively regulates *ppkA*, leading to a down-regulation of the T6SS (Chen *et al.*, 2015). Each secretion system has a distinct role from the other; T3S is linked to pathogenicity in planktonic cultures and typically targets eukaryotic cells, whereas the T6SS promotes interspecies bacterial competition (as well as targeting eukaryotic cells), and has a more prominent role in persistence and biofilm-associated antibiotic resistance (Zhang *et al.*, 2011; Green *et al.*, 2016). This study identified the complete dysregulation of the T3SS/T6SS resulting in activation of the two systems simultaneously in the FUS443 mutant strain. One study investigating clinical isolates of *P. aeruginosa* identified a similar phenomenon, whereby the level of T6SS proteins and transcripts did not correlate with *rsmY/Z* levels, resulting in the expression of T6SS during planktonic growth but not during biofilm formation (Line Lucchetti-Miganeh *et al.*, 2014). In addition to this, the T3SS and T6SS of *Burkholderia pseudomallei* was found to be co-expressed *via* the T6SS positive regulator, BsaN, located within a T3SS gene cluster (Chen *et al.*, 2011). *P. aeruginosa* has no clear homologue to BsaN, however,

all of these findings point toward the presence of a Gac/Rsm independent regulatory system for either the T3SS or T6SS causing their simultaneous up-regulation.

5.12.9 Conclusion

This chapter developed upon the phenotypic and proteomic findings to provide a more in depth understanding of how the *fusA1* mutation in FUS443 affected particular biological processes. In most cases, the transcriptomic data reflected the main findings of the proteomic analysis, confirming that the T3SS and iron homeostasis were severely impacted by the mutated EF-G protein. Central metabolism was also affected by the mutation, as well as sulfur metabolism and the oxidative stress response, which are likely to be linked with the disruption to iron homeostasis *via* interconnecting networks. Dysregulation of iron acquisition is also likely to be a causal factor for the increased activity of the T3SS, through a currently undefined mechanism.

The molecular mechanisms behind several characteristics of FUS443 still remain unclear, such as the cause of motility or chemotaxis perturbation, the up-regulation of exopolysaccharide production, and the simultaneous expression of the T6SS and T3SS. The most likely explanation for these occurrences is that the mutated EF-G protein is affecting the expression or activity of regulatory factors that specifically target these systems.

Chapter 6

6. Final Conclusions

Acquisition of *P. aeruginosa* by the CF lung occurs, on average, at one-year-old and if left untreated chronic infections can lead to the development of bronchiectasis and respiratory failure (Silva Filho *et al.*, 2013). Biofilm formation is closely associated with chronic infection and often coincides with increased antibiotic resistance, immune evasion and persistence within the host environment, making biofilm formation in *P. aeruginosa* the subject of intense study. Being able to eradicate early stage colonisation would prevent the progression into chronicity and improve the prognosis of the patient. Planktonic cells, which are associated with the initial acute infection, also come with their own detrimental characteristics, as the virulent nature of planktonic cells means that the host is damaged at a considerable rate. Despite this, planktonic growth proves to be a susceptible window in which infection can be successfully treated with antimicrobials. Understanding the biological processes underpinning planktonic growth is key to improving the effectiveness of treatment before infection progresses into a chronic phase.

During this study, a SNP was identified in the EF-G encoding gene, *fusA1*. This mutation occurred spontaneously most likely as a result of the antibiotic selection pressure in place during the transposon mutagenesis screening of *P. aeruginosa* strains. Having identified that the SNP in *fusA1* was having pleiotropic effects on the cell, the first objective of this study was to identify how this mutation affected the structure of EF-G. I found that the resulting non-synonymous mutation caused minor conformational changes in EF-G which is likely to have affected the way in which the protein interacted with the ribosome or associating proteins, therefore disrupting the efficiency at which it coordinated translational elongation. The mutation did not, however, affect the adjacent fusidic acid binding pocket in a way that prohibited fusidic acid binding.

As this project started as an investigation into the regulation of biofilm formation, my second objective was to identify if the mutated EF-G protein had any implications in the formation of biofilms or in the inverse expression of virulence factors. The involvement of EF-G in biofilm formation had not been documented before in

P. aeruginosa, but initial screenings showed FUS443 to exhibit decreased expression of the key biofilm matrix component, CdrA. Further analysis showed that the mutated EF-G also affected the biosynthesis of exopolysaccharides, although the overall level of biofilm formation remained unchanged. Although the FUS443 mutant was less relevant in biofilm formation, the phenotypic analysis began to unveil the large effect that the mutated EF-G protein had on virulence. This included an effect on cell motility, QS and the secretion of exoenzymes. It also became evident that the mutated EF-G protein was inducing various changes to antibiotic sensitivity. The *fusA1* mutation caused the emergence aminoglycoside resistance to kanamycin and gentamicin, and also introduced sensitivity to fusaric acid. Many of the characteristics that were altered by the mutated EF-G protein are controlled independently of one another and so it was of great interest to have identified a SNP in one gene which had such widespread effects across the cell.

I was able to analyse both the transcriptomic and the proteomic profile of the FUS443 mutant strain to produce a global representation of the cellular changes that had occurred as a result of the *fusA1* mutation. This was the third objective of this study, and I was able to support many of the findings that had been observed in the phenotypic analysis, as well as identify numerous other characteristics that had previously gone undetected. For example, the collective data sets provided evidence that antibiotic resistance had emerged through the up-regulation of the *mexXY* efflux system, and the increased production of exopolysaccharides was a result of the increased expression of *pel* and *psl* biosynthesis genes and proteins.

By far, one of the most notable characteristics of FUS443 that emerged from the transcriptomic and proteomic data was the up-regulation of the virulence determinant, the T3SS. This up-regulation included the T3SS master regulator, ExsA, whose positive feedback is likely to have provided the initial induction of this system. Other systems that were affected at a global level included proteins involved in iron homeostasis, sulfur metabolism and the oxidative stress response, all of which are likely to have been induced by a common regulator. In a similar way, cell morphology, altered growth rate and changes in the expression of ribosomal proteins are likely to have derived from a common mechanism influenced by the mutated EF-G protein.

The precise molecular mechanism by which the mutated EF-G protein affected gene expression and protein abundance was less clear, as it appeared that the activity of

a diverse range of regulatory factors were modulated by the mutation. It is most likely that the mutation in EF-G affected gene expression indirectly due to its altered protein structure which led to a change in the efficiency of protein synthesis. The majority of proteins in the cell can withstand small adjustments in abundance without having large downstream effects on their cellular role. However, proteins that play regulatory roles, such as transcription factors, sigma factors and post-translational regulators, can be highly sensitive to such changes, causing large downstream effects on the expression of target genes or the activity of target proteins.

The role of EF-G in translation has long been established across a diverse variety of bacterial species. This study revealed a novel involvement for EF-G in numerous biological processes, including T3S, iron and sulfur homeostasis, cell motility, cell division, the oxidative and heat stress responses, cell communication and central metabolism. These systems were all sensitive to the minor functional alteration that had occurred in the mutated EF-G protein and, whilst the impact on these systems was most likely to be indirect, the study highlights the dynamic downstream effects that can be brought about by just a single SNP in *fusA1*.

FusA1 is located within the core genome (approximately 82% of the total genome) (Ozer *et al.*, 2014), within which the average rate of nucleotide substitution is low due to the importance of core genes in cell survival (Morales *et al.*, 2004). Changes in the function or expression of these core genes can have damaging implications to cell viability, making mutations such as the one identified in this study relatively rare. Core genes include members of the *pvd* operon, for pyoverdine biogenesis, as well as those encoding the T3SS secreted proteins, *exoT*, *exoY*, *exoU* and *exoS* (Valot *et al.*, 2015). The FUS443 mutant provides a perfect example as to the broad changes that can occur when the expression of these core genes is altered.

The up-regulation of the T3SS in FUS443 is of particular relevance to CF infection models, as T3S plays a prominent role in colonisation and acute infection of the respiratory tract. Individuals with CF produce antibodies against the T3S effector proteins as an infection progresses and so the T3SS in *P. aeruginosa* is suppressed during chronic infection to evade the host immune system and promote colony persistence. Consistent with this, isolates from the CF airways also develop mutations in genes that

are essential for T3S, such as *cyaB*, *vfr*, and *exsA,* to prevent activation of the host immune response (Hauser, 2009; Kruczek *et al.*, 2016).

As the FUS443 mutant continually expressed T3S it could provide a useful tool for understanding how T3S is activated, aside from the two known inducers; calcium and host contact. Identifying how to promote the continual expression of T3S during infection may encourage the host immune system to target *P. aeruginosa* and enhance bacterial killing. Promoting T3S could also prolong the 'susceptible' acute infection stage and, in combination with antimicrobial therapies, would improve *P. aeruginosa* eradication and reduce the survival of persister cells within the lung. Alternatively, numerous pharmacological inhibitors are being identified which impair T3S to reduce the severity of the infection, elevate symptoms and lower the level of damage caused during acute infection (Anantharajah *et al.*, 2016). The exaggerated T3SS expression in FUS443 could therefore provide a beneficial model for current research that is looking to target the regulatory network behind T3S, the T3SS itself, the effector proteins or the assessment of molecules that counteract their toxic effects.

Whilst virulence factors are generally not essential for survival, using known virulence determinants as therapeutic targets may decrease pathogenicity and assist in slowing disease progression. In modern-day medicine, iron chelators are being used to treat numerous disorders, including neurodegenerative diseases and β-thalassemia, and more and more research is going into investigating the potential antimicrobial effects of iron chelation (Thompson *et al.*, 2012). It is clear that the disruption to iron homeostasis in FUS443 reduced cell fitness and potentially caused the emergence of sensitivity to fusaric acid. Further investigation is required to identify how the mutated EF-G protein could be used to disrupt cellular iron balance, but this may provide a potential mechanism to reduce cell survival or induce antimicrobial sensitivity. As iron is also an essential cofactor in eukaryotic cells, toxicity of metal chelators used in antimicrobial therapy would need to be assessed.

The emergence of antibiotic resistance in FUS443 would also benefit its survival within a host environment. Aminoglycosides have been in use since the 1940s (Gad *et al.*, 2011) and have been implemented in the management of acute exacerbations in CF patients. *FusA1* is not typically considered an antibiotic resistance gene but more and more studies are identifying its importance in resistance to aminoglycosides. Mutation to

the *fus* genes have been identified in CF aminoglycoside-resistant isolates, with the implication that the mutated EF-G directly disrupts antibiotic-ribosomal binding (Greipel *et al.*, 2016; López-Causapé *et al.*, 2017). The documented mutations in *fusA1* are commonly located in the mRNA-interacting domain (domain IV), or in the GTP hydrolysis domain, (domain I), none of which map near the P443L transition identified in this study. With this I have been able to provide evidence of another region within the protein that is sensitive to viable structural alterations and elicits an antibiotic resistance-inducing phenotype upon mutation. Going beyond the published works on EF-G mutations, the use of transcriptomic analysis and proteomic analysis provided a greater insight into the mechanism behind this resistance and suggested that resistance occurred through the modulation of the aminoglycoside efflux system, MexXY. Adaptive mutations in *mexXYZ* genes have also been identified in CF isolates and demonstrate how the use of aminoglycosides in antimicrobial therapy is placing high evolutionary pressure on this system, directly or indirectly, as seen in this study *via fusA1* (López-Causapé *et al.*, 2017; Prickett *et al.*, 2017).

The mechanism through which the EF-G mutant protein influenced the cell could not be determined comprehensively from this study. The main reason behind this was the dependency of transcription factors and regulatory proteins on post-translational regulation. It is possible that the mutated EF-G only affects a relatively small number of transcriptional factors whose modulation causes a dynamic upset across the cell. Focusing in on specific regulators and altering their expression could help to underpin their involvement and impact, downstream of the mutated EF-G.

FusA1 shares a sequence identity of around 40% with eukaryotic mitochondrial EF-G, and around 24% with cytosolic EF-2 (Bielecki *et al.*, 2012). This makes *P. aeruginosa* EF-G an unfavourable target for antibacterial therapeutics as any effect on host EF-G homologs could have damaging effects on the patient's own cells. But, by identifying which regulatory proteins are mediating the changes in FUS443, these could be used to target specific biological processes to reduce the viability of *P. aeruginosa* cells within the host. Increased focus into these areas could therefore help in the development of new combinational therapies to manage acute infections and improve pulmonary function in CF patients.

7. Appendix

		Transcriptomic data				Proteomic data			
		FUS443		FUS443C		FUS443		FUS443C	
Gene name	**Locus**	log_2 FC	P-value	log_2 FC	P-value	log_2 FC	P-value	log_2 FC	P-value
The type II secretion system									
hxcW	PA0677	-1.129	0.000	0.021	0.934				
hxcU	PA0678	-0.895	0.095	-0.425	0.446				
hxcP	PA0679	-0.742	0.004	-0.327	0.194				
hxcV	PA0680	-0.883	0.008	0.112	0.692				
hxcT	PA0681	-1.046	0.001	0.007	0.983				
hxcX	PA0682	-1.264	0.000	0.036	0.893				
hxcY	PA0683	-0.345	0.585	-0.198	0.797				
hxcZ	PA0684	-1.320	0.158	-0.169	0.838				
hxcQ	PA0685	-1.285	0.000	-0.175	0.611				
hxcR	PA0686	-1.231	0.030	-0.261	0.645				
lapA	PA0688	-0.961	0.000	-0.220	0.303				
lapB	PA0689	-1.142	0.000	-0.034	0.885				
toxA	PA1148	0.347	0.135	0.450	0.121	0.688	0.147	-0.232	0.938
xqhB	PA1382	-1.318	0.000	0.134	0.605				
xcpZ	PA3095	-0.547	0.010	-0.255	0.232				
xcpY	PA3096	-0.537	0.215	-0.510	0.229				
xcpX	PA3097	-0.634	0.298	-0.404	0.518				
xcpW	PA3098	-0.437	0.449	-0.175	0.757				
xcpV	PA3099	-0.037	0.968	-0.217	0.801				
xcpU	PA3100	0.396	0.547	-0.128	0.868				
xcpT	PA3101	0.348	0.133	-0.090	0.703				
xcpS	PA3102	-0.158	0.777	-0.209	0.712	0.109	0.701	0.377	0.743
xcpR	PA3103	-0.210	0.488	-0.288	0.351	0.473	0.156	0.197	0.915
xcpP	PA3104	-1.214	0.000	-0.037	0.895	-1.211	0.016	0.044	0.987
xcpQ	PA3105	-0.084	0.740	0.108	0.673	0.562	0.032	0.044	0.976
lasB	PA3724	0.664	0.066	-0.602	0.072	0.297	0.751	0.027	0.995
The type III secretion system									
exoT	PA0044	3.863	0.000	-0.440	0.073	2.836	0.000	0.138	0.861
vfr	PA0652	0.521	0.058	0.376	0.173	-0.101	0.556	0.192	0.819
pscP	PA1695	3.961	0.000	-0.292	0.575	4.178	0.000	-0.179	0.953
pscO	PA1696	4.718	0.000	0.061	0.964				
pscN	PA1697	5.101	0.000	0.078	0.903				
popN	PA1698	5.536	0.000	0.253	0.470	4.187	0.001	0.172	0.973
pcr1	PA1699	5.026	0.000	-0.072	0.898				
pcr2	PA1700	4.057	0.000	-0.330	0.529				
pcr3	PA1701	4.723	0.000	-0.139	0.811				
pcrG	PA1705	3.729	0.000	-0.643	0.015	3.211	0.000	-0.502	0.729
pcrV	PA1706	4.411	0.000	-0.429	0.053	2.143	0.000	-0.305	0.738
pcrH	PA1707	4.173	0.000	-0.816	0.276	3.262	0.000	-0.352	0.777
popB	PA1708	4.051	0.000	-0.875	0.004	3.151	0.000	-0.055	0.973
popD	PA1709	3.827	0.000	-0.885	0.001	3.895	0.000	-0.113	0.903
exsC	PA1710	1.689	0.000	-0.714	0.005	2.358	0.000	-0.019	0.993
exsE	PA1711	1.976	0.000	-0.275	0.272	2.401	0.000	-0.162	0.945
exsB	PA1712	1.913	0.000	-0.536	0.022				
exsA	PA1713	1.697	0.000	0.388	0.201	0.894	0.000	0.068	0.925
exsD	PA1714	2.236	0.000	-0.062	0.814	0.846	0.000	-0.036	0.973
pscB	PA1715	2.642	0.000	0.326	0.524	2.349	0.000	-0.017	0.987
pscC	PA1716	2.196	0.000	0.019	0.944	2.133	0.000	-0.076	0.962
pscD	PA1717	1.928	0.000	0.525	0.065	0.382	0.291	0.199	0.926
pscE	PA1718	2.395	0.000	0.183	0.789	1.982	0.000	-0.300	0.769
pscF	PA1719	3.466	0.000	1.275	0.000	2.507	0.000	-0.304	0.855
pscG	PA1720	2.987	0.000	0.848	0.128	2.205	0.000	-0.189	0.861
pscH	PA1721	2.358	0.000	0.361	0.545				
pscI	PA1722	2.579	0.000	0.693	0.275				

pscJ	PA1723	2.383	0.000	0.730	0.074	0.758	0.002	0.027	0.980
pscL	PA1724	2.119	0.000	0.454	0.231				
PscL	PA1725	1.157	0.000	0.364	0.207	5.873	0.000	2.458	0.008
exoY	PA2191	4.057	0.000	-0.207	0.344	3.266	0.000	-0.193	0.881
ptrA	PA2808	0.557	0.038	-0.245	0.390				
psrA	PA3006	-1.060	0.000	0.153	0.556	-0.111	0.530	-0.025	0.984
exoS	PA3841	3.879	0.000	-0.479	0.070	3.261	0.000	0.157	0.861
spcS	PA3842	4.461	0.000	0.370	0.106	3.263	0.000	-0.156	0.866
The type VI secretion system									
tagQ1	PA0070	3.473	0.000	0.514	0.040	0.167	0.556	-0.240	0.868
tagS1	PA0072	1.121	0.679	0.158	0.864				
tagT1	PA0073	1.274	0.648	0.215	0.902	0.497	0.145	0.072	0.973
ppkA	PA0074	2.041	0.001	0.184	0.795	0.412	0.091	0.079	0.966
pppA	PA0075	2.597	0.000	0.668	0.007	0.101	0.661	-0.264	0.802
tagF1	PA0076	2.468	0.028	0.295	0.770	0.427	0.010	-0.159	0.802
tssM1	PA0077	2.213	0.000	0.102	0.739	0.359	0.319	0.002	1.000
tssL1	PA0078	2.434	0.000	-0.083	0.709	0.929	0.018	0.095	0.973
tssK1	PA0079	2.056	0.000	0.341	0.274	0.637	0.031	-0.039	0.983
tssJ1	PA0080	2.032	0.000	0.799	0.014	0.387	0.286	-0.435	0.802
fha1	PA0081	0.437	0.083	-0.095	0.691	0.980	0.001	-0.070	0.956
tssa1	PA0082	3.195	0.000	-0.246	0.441	0.488	0.248	0.003	1.000
tssB1	PA0083	3.195	0.000	0.964	0.002	0.207	0.260	-0.326	0.660
tssC1	PA0084	3.005	0.000	0.959	0.008	0.224	0.176	-0.283	0.676
hcp1	PA0085	3.717	0.000	1.554	0.000	0.587	0.014	-0.287	0.742
tagJ1	PA0086	2.430	0.000	0.073	0.770	0.350	0.084	-0.288	0.729
tsse1	PA0087	2.748	0.009	0.879	0.010	0.270	0.296	-0.252	0.855
tssf1	PA0088	2.667	0.000	0.703	0.002	0.495	0.245	-0.222	0.932
clpV1	PA0090	2.137	0.000	0.702	0.104	0.244	0.435	-0.121	0.962
vgrG1	PA0091	2.229	0.000	0.882	0.003	-0.163	0.595	-0.180	0.915
hcpA	PA1512	1.124	0.002	0.785	0.031	1.007	0.008	0.215	0.897
hsiA2	PA1656	-0.448	0.046	0.081	0.736				
hsiB2	PA1657	1.273	0.000	0.858	0.005	-0.901	0.292	0.523	0.915
hsiC2	PA1658	1.334	0.000	0.789	0.008	-0.430	0.577	0.797	0.842
hsiF2	PA1659	0.923	0.000	0.467	0.093				
hsiG2	PA1660	0.303	0.271	0.179	0.536				
hsiH2	PA1661	0.301	0.447	0.074	0.864				
clpV2	PA1662	0.308	0.189	0.053	0.831	-0.646	0.354	0.722	0.848
sfa2	PA1663	0.557	0.009	-0.153	0.512	-0.227	0.656	0.495	0.855
orfX	PA1664	1.203	0.007	-0.655	0.202				
fha2	PA1665	1.308	0.000	0.311	0.209				
lip2	PA1666	0.819	0.155	0.014	0.986	-0.873	0.011	0.449	0.703
hsiJ2	PA1667	0.363	0.153	0.032	0.898	-0.030	0.951	0.675	0.711
dotU2	PA1668	0.840	0.000	0.195	0.421				
icmF2	PA1669	0.773	0.044	0.223	0.630				
stp1	PA1670	0.340	0.688	0.272	0.741	-1.324	0.030	0.050	0.990
stk1	PA1671	-0.796	0.136	0.103	0.836				
hsiB3	PA2365	1.355	0.000	0.638	0.030	-0.252	0.481	-0.199	0.923
hsiC3	PA2366	0.587	0.032	0.343	0.317	-0.467	0.100	-0.249	0.860
hcp3	PA2367	0.974	0.000	0.470	0.135	-1.355	0.008	-0.620	0.712
hsiF3	PA2368	0.169	0.838	-0.202	0.830	-1.939	0.000	-0.329	0.742
hsiG3	PA2369	0.210	0.536	-0.233	0.560	-0.920	0.008	-0.163	0.915
hsiH3	PA2370	-0.500	0.349	-0.618	0.316				
clpV3	PA2371	-0.517	0.043	-0.433	0.148	-0.916	0.017	-0.222	0.903
	PA2372	-0.081	0.740	0.115	0.700	-1.304	0.000	-0.576	0.115
vgrG3	PA2373	-0.091	0.706	-0.093	0.704	0.061	0.667	0.088	0.907
tseF	PA2374	-0.936	0.000	-0.299	0.162				
tse2	PA2702	1.046	0.000	0.340	0.117	0.758	0.122	-0.403	0.870
tse3	PA3484	1.091	0.000	0.324	0.276	-2.548	0.004	-0.428	0.903
vgrG5	PA5090	0.355	0.299	-0.071	0.847				
Ribosomal and translation associated proteins									
tRNA-Met	PA0574.1	-0.402	0.260	0.302	0.368				

alaS	PA0903	1.494	0.000	0.498	0.065				
relA	PA0934	0.583	0.046	-0.011	0.970	0.357	0.194	0.086	0.971
proS	PA0956	1.032	0.001	0.157	0.560				
ycfB	PA1678	0.560	0.012	0.000	0.998	0.891	0.001	0.155	0.847
fusA2	PA2071	0.298	0.321	-0.316	0.273	0.624	0.009	-0.025	0.985
pheS	PA2740	1.389	0.000	0.344	0.184	0.706	0.014	0.166	0.901
rplT	PA2741	-0.285	0.511	-0.365	0.416	0.845	0.008	0.276	0.828
deaD	PA2840	2.011	0.000	0.757	0.004	0.878	0.002	0.250	0.794
efp	PA2851	2.011	0.000	0.757	0.004	0.224	0.167	0.045	0.973
gltX	PA3134	1.537	0.000	0.449	0.078	0.574	0.036	0.228	0.858
recQ	PA3344	0.162	0.534	0.014	0.958	0.466	0.059	0.368	0.703
tyrS	PA4138	2.977	0.000	0.004	0.987	2.240	0.001	0.426	0.802
rpsK	PA4240	1.703	0.000	0.753	0.013	0.489	0.004	0.015	0.985
rpsM	PA4241	1.108	0.000	0.584	0.058	0.786	0.010	0.300	0.802
rplR	PA4247	1.681	0.000	0.692	0.014	0.716	0.004	0.269	0.727
rplX	PA4252	1.247	0.000	0.627	0.044	1.712	0.001	0.380	0.743
rplB	PA4260	1.607	0.000	0.456	0.171	0.872	0.006	0.324	0.764
rplW	PA4261	2.006	0.011	0.840	0.222	0.454	0.007	0.145	0.828
rplD	PA4262	1.923	0.000	0.563	0.140	0.832	0.013	0.338	0.802
rplC	PA4263	1.720	0.000	0.554	0.067	0.825	0.007	0.311	0.775
fusA1	PA4266	1.657	0.000	0.000	1.000	0.495	0.006	2.269	0.000
rpsG	PA4267	1.767	0.000	0.307	0.284	0.736	0.012	0.263	0.828
rplA	PA4273	1.601	0.001	0.359	0.413	0.863	0.008	0.382	0.729
rplK	PA4274	1.713	0.003	0.357	0.515	0.579	0.009	0.172	0.855
	PA4277.1	-3.017	0.000	-1.306	0.000				
	PA4430	1.567	0.001	0.894	0.049				
rpsI	PA4432	1.940	0.000	0.952	0.000	0.392	0.082	0.080	0.962
trpS	PA4439	1.616	0.000	0.520	0.029	0.78	0.000	-0.014	0.985
rpsT	PA4563	1.970	0.000	1.023	0.000	0.892	0.001	0.182	0.830
rplU	PA4568	0.671	0.013	0.205	0.433	0.854	0.004	0.331	0.729
rtcB	PA4583	3.214	0.000	-0.246	0.441	1.263	0.001	-0.340	0.743
rtcA	PA4585	2.372	0.000	-0.265	0.496	0.993	0.013	-0.347	0.841
rplY	PA4671	1.663	0.000	0.297	0.270	0.703	0.001	0.080	0.897
dksA	PA4723	1.406	0.000	0.924	0.000	0.211	0.244	0.134	0.895
	PA4746.1	-2.417	0.000	-0.399	0.269				
smpB	PA4768	-0.161	0.464	0.205	0.360	0.839	0.001	0.236	0.703
rplI	PA4932	1.571	0.000	0.472	0.114	0.813	0.001	0.220	0.742
rpsR	PA4934	2.022	0.000	0.850	0.003	0.560	0.002	0.037	0.969
rpsF	PA4935	1.749	0.000	0.649	0.022	0.578	0.001	0.049	0.950
rpmE	PA5049	1.072	0.000	0.684	0.008	1.248	0.268	1.098	0.855
tRNA-Thr	PA5160.1	-1.731	0.069	-0.446	0.492				
rpmG	PA5315	1.801	0.000	0.789	0.010	1.643	0.006	0.165	0.964
	PA5470	3.346	0.000	0.329	0.541	0.502	0.006	0.139	0.855
Biofilm associated genes									
rsmY	PA0527.1	-1.925	0.000	0.148	0.501				
rsmA	PA0905	1.339	0.000	-0.006	0.985	0.201	0.271	0.078	0.950
gacS	PA0928	-0.321	0.193	-0.268	0.284	-0.177	0.640	0.163	0.950
pslG	PA2237	-0.342	0.618	-0.361	0.597	1.317	0.009	-0.906	0.486
gacA	PA2586	-0.104	0.694	0.194	0.463	-0.460	0.003	-0.065	0.914
pelF	PA3059	-0.321	0.404	0.301	0.450	1.439	0.000	-0.304	0.537
pelA	PA3064	-0.387	0.206	0.120	0.707	2.725	0.000	-0.166	0.923
hptB	PA3345	-0.660	0.004	0.302	0.171	-0.688	0.007	-0.185	0.858
rsmz	PA3621.1	-0.359	0.112	0.588	0.015				
ladS	PA3974	-0.441	0.072	-0.045	0.858				
retS	PA4856	-0.078	0.766	-0.410	0.123	-0.018	0.880	-0.006	0.994
Motility and Chemotaxis									
cheB2	PA0173	-0.167	0.467	-0.320	0.168	-0.474	0.289	-0.057	0.985
cheD	PA0174	-0.136	0.580	-0.517	0.037	-0.054	0.887	-0.035	0.988
cheR2	PA0175	0.166	0.443	-0.858	0.000	0.001	0.996	-0.138	0.933
aer2	PA0176	-0.653	0.015	-0.512	0.056	-0.294	0.118	0.105	0.915
cheW2	PA0177	-0.733	0.287	0.012	0.988	-1.313	0.003	-0.034	0.987

cheA2	PA0178	-1.427	0.000	-0.073	-0.133	0.074	0.776	0.227	0.858
cheY2	PA0179	-1.227	0.000	0.231	0.460	-1.260	0.001	0.052	0.973
fliY	PA0314	0.611	0.008	0.043	0.846	-2.241	0.001	-0.160	0.956
pilG	PA0408	-0.112	0.662	0.193	0.454	-0.972	0.000	-0.041	0.966
pilH	PA0409	0.275	0.232	0.280	0.227	-1.274	0.000	-0.150	0.743
pilI	PA0410	0.128	0.558	-0.053	0.811	-0.251	0.360	-0.001	1.000
pilJ	PA0411	0.841	0.002	0.163	0.565	0.446	0.091	0.573	0.480
pilK	PA0412	0.214	0.353	-0.173	0.490	0.316	0.035	-0.135	0.855
chpA	PA0413	-0.041	0.904	-0.369	0.345	0.140	0.558	0.123	0.932
chpB	PA0414	0.099	0.467	-0.431	0.755	-0.170	0.134	0.006	0.993
chpC	PA0415	0.581	0.793	0.028	0.975	0.000		0.000	
chpD	PA0416	0.650	0.004	0.553	0.015	0.000		0.000	
chpE	PA0417	1.370	0.000	0.172	0.471	0.000		0.000	
flgB	PA1077	1.133	0.000	0.067	0.765	0.000		0.000	
flgC	PA1078	1.342	0.000	0.190	0.384	0.000		0.000	
flgD	PA1079	1.116	0.000	0.147	0.539	0.002	0.994	-0.182	0.882
flgE	PA1080	0.411	0.164	-0.418	0.141	0.650	0.022	-0.487	0.574
flgF	PA1081	0.827	0.000	-0.143	0.521	0.000		0.000	
flgG	PA1082	1.045	0.000	-0.064	0.803	1.226	0.014	-0.574	0.743
flgH	PA1083	0.933	0.000	-0.094	0.700	0.427	0.294	0.035	0.991
flgI	PA1084	0.754	0.002	-0.245	0.297	-0.022	0.952	-0.062	0.973
flgJ	PA1085	0.648	0.014	-0.349	0.157	0.000		0.000	
flgK	PA1086	0.530	0.069	-0.599	0.029	0.774	0.001	-0.106	0.897
flgL	PA1087	0.630	0.025	-0.397	0.136	0.752	0.001	0.058	0.956
fleq	PA1097	0.479	0.104	-0.261	0.364	-0.076	0.511	0.037	0.970
fleS	PA1098	0.556	0.028	-0.045	0.852	0.000		0.000	
fleR	PA1099	0.979	0.000	-0.343	0.178	0.562	0.002	0.046	0.962
fliE	PA1100	0.595	0.006	0.214	0.337	0.000		0.000	
fliF	PA1101	0.340	0.168	-0.159	0.512	-0.196	0.146	0.043	0.969
fliG	PA1102	0.243	0.338	-0.291	0.246	0.268	0.051	0.033	0.973
	PA1103	-0.663	0.045	-0.397	0.270	0.108	0.424	-0.065	0.940
fliI	PA1104	-0.921	0.020	-0.155	0.689	0.056	0.676	-0.040	0.973
fliJ	PA1105	-1.533	0.000	-0.062	0.794	-0.372	0.030	-0.085	0.923
fliM	PA1443	-0.056	0.831	-0.438	0.097	0.223	0.143	-0.121	0.881
flhB	PA1449	-1.137	0.000	-0.204	0.351	0.000		0.000	
cheY	PA1456	0.415	0.090	0.157	0.511	-0.708	0.001	-0.104	0.897
cheZ	PA1457	-0.127	0.628	-0.262	0.319	-0.373	0.017	-0.058	0.950
cheA	PA1458	0.179	0.574	-0.137	0.667	-0.365	0.029	-0.281	0.630
cheB	PA1459	-0.051	0.845	-0.268	0.309	-0.560	0.002	-0.126	0.841
motC	PA1460	-0.258	0.257	-0.222	0.329	0.000		0.000	
motD	PA1461	-0.755	0.001	-0.333	0.152	-0.569	0.002	-0.340	0.973
orf1	PA1462	0.222	0.364	-0.283	0.246	-0.332	0.103	-0.034	0.980
orf2	PA1463	0.236	0.372	-0.294	0.258	-0.159	0.143	-0.077	0.897
cheW	PA1464	0.093	0.735	-0.233	0.391	-1.103	0.000	-0.359	0.450
	PA1608	1.011	0.000	0.509	0.043	0.000		0.000	
	PA2652	1.683	0.000	0.058	0.819	0.254	0.391	0.295	0.855
	PA2654	1.012	0.000	0.328	0.223	0.060	0.853	0.366	0.802
bswR	PA2780	-1.086	0.011	-0.305	0.485	0.000		0.000	
	PA3341	-1.292	0.000	-0.340	0.215	0.005	0.975	0.167	0.848
hsbD	PA3343	-0.944	0.000	0.006	0.979	0.000		0.000	
hsbR	PA3346	-1.044	0.000	-0.206	0.436	-0.256	0.124	-0.094	0.915
hsbA	PA3347	-0.287	0.255	0.041	0.877	-1.157	0.000	-0.207	0.742
cheR1	PA3348	-0.526	0.075	-0.016	0.956	-1.205	0.000	-0.180	0.696
	PA3349	-0.109	0.727	-0.125	0.697	-0.242	0.232	-0.021	0.987
	PA3350	-0.749	0.004	-0.719	0.006	-0.159	0.575	0.032	0.987
flgM	PA3351	0.706	0.018	0.126	0.656	-0.030	0.831	-0.128	0.855
	PA3352	0.557	0.039	0.001	0.996	-0.560	0.002	-0.088	0.888
	PA3353	-0.177	0.514	-0.217	0.424	-0.243	0.106	-0.245	0.689
wspR	PA3702	-0.367	0.127	-0.122	0.617	0.048	0.711	0.005	0.995
wspF	PA3703	-0.815	0.181	-0.651	0.241	-0.577	0.002	-0.015	0.986
wspE	PA3704	-0.116	0.815	-0.753	0.157	0.022	0.889	0.002	0.999
wspD	PA3705	0.288	0.739	-0.594	0.568	0.000		0.000	

wspC	PA3706	-0.095	0.880	-0.462	0.462	-0.209	0.144	0.050	0.964
wspB	PA3707	-0.290	0.712	-0.340	0.652	-0.346	0.020	0.118	0.858
wspA	PA3708	-0.333	0.201	-0.274	0.301	-0.005	0.989	0.557	0.689
pctC	PA4307	0.033	0.883	0.413	0.074	-1.741	0.002	0.575	0.738
pctB	PA4310	1.475	0.000	0.081	0.753	0.676	0.198	0.567	0.828
rpoN	PA4462	-0.023	0.937	-0.352	0.209	0.086	0.528	-0.100	0.897
pilA	PA4525	1.375	0.000	0.291	0.401	-0.016	0.971	0.458	0.802
clpB	PA4542	1.460	0.000	-0.942	0.003	0.405	0.008	-0.036	0.973
pilS	PA4546	-0.101	0.646	0.065	0.766	-0.149	0.863	-0.297	0.962
pilR	PA4547	0.118	0.615	0.142	0.556	0.185	0.149	-0.175	0.743
cupE4	PA4651	1.266	0.000	-0.129	0.575	-0.712	0.103	0.066	0.982
ctpL	PA4844	-1.036	0.000	0.089	0.685				
motB	PA4953	-0.076	0.749	0.189	0.433	-0.206	0.277	0.049	0.973
motA	PA4954	0.611	0.009	0.155	0.505				
	PA5072	1.263	0.000	0.550	0.022				
algR	PA5261	-0.203	0.483	-0.021	0.944	0.159	0.511	-0.205	0.867
fimS	PA5262	-0.756	0.005	-0.477	0.082				
Antibiotic resistance									
mexR	PA0424	-0.821	0.001	-0.539	0.026	-0.340	0.009	-0.097	0.858
mexA	PA0425	-0.452	0.104	-0.281	0.318	-0.050	0.855	0.136	0.926
mexB	PA0426	-0.539	0.089	-0.707	0.028	0.127	0.587	0.334	0.741
oprM	PA0427	-0.898	0.003	-0.956	0.002	-0.359	0.137	-0.150	0.907
oprD	PA0958	2.230	0.000	0.952	0.001	-0.119	0.648	0.017	0.992
sigX	PA1776	-1.268	0.000	-0.825	0.009	-0.443	0.044	-0.077	0.962
mexY	PA2018	0.981	0.000	-0.345	0.156	1.929	0.001	0.170	0.942
mexX	PA2019	1.365	0.000	-0.161	0.468	1.830	0.000	0.110	0.915
mexZ	PA2020	0.128	0.586	-0.294	0.221	1.183	0.001	0.055	0.973
mexE	PA2493	-0.149	0.538	0.424	0.072				
mexF	PA2494	-0.654	0.013	-0.090	0.726				
oprN	PA2495	-0.371	0.375	-0.251	0.569				
oprP	PA3279	-1.171	0.000	0.013	0.953				
mexG	PA4205	-1.922	0.000	0.150	0.585				
mexH	PA4206	-1.946	0.000	-0.282	0.304	0.007	0.993	1.256	0.561
mexI	PA4207	-1.215	0.000	-0.387	0.244				
opmD	PA4208	-0.429	0.296	-0.418	0.398				
pprA	PA4293	-1.272	0.000	-0.152	0.512				
pprB	PA4296	0.378	0.149	-0.012	0.960	-0.104	0.621	0.320	0.712
oprJ	PA4597	-0.656	0.003	-0.103	0.629				
mexD	PA4598	-0.630	0.004	-0.196	0.369				
mexC	PA4599	0.080	0.751	0.014	0.953				
opmH	PA4974	1.076	0.000	0.028	0.908	1.282	0.001	-0.134	0.903
armZ	PA5471	3.309	0.000	0.003	0.993	2.106	0.000	0.022	0.985
Iron homeostasis									
tonB2	PA0197	2.465	0.000	0.475	0.051				
exbB1	PA0198	2.808	0.000	0.357	0.112				
exbD1	PA0199	1.389	0.000	0.454	0.046				
fiuA	PA0470	-1.061	0.000	-0.266	0.323	-0.268	0.319	-0.615	0.480
fiuR	PA0471	-1.116	0.010	-0.359	0.419	-0.204	0.501	0.150	0.938
fiuI	PA0472	-0.715	0.129	-0.184	0.718	0.648	0.107	-0.207	0.926
bioB	PA0500	0.901	0.002	0.514	0.069	1.286	0.001	0.506	0.492
aprX	PA1245	-0.145	0.729	-1.194	0.007	2.798	0.001	0.452	0.880
aprD	PA1246	-0.512	0.234	-1.617	0.000	-0.099	0.646	0.284	0.743
aprE	PA1247	-0.790	0.306	-1.557	0.041	-0.330	0.341	0.514	0.738
aprF	PA1248	-1.011	0.001	-1.644	0.000	0.270	0.126	0.065	0.962
aprA	PA1249	0.237	0.610	-1.617	0.001	2.755	0.007	0.679	0.869
aprI	PA1250	-0.155	0.537	-0.712	0.005	-1.026	0.001	-0.077	0.940
	PA1271	1.297	0.000	0.234	0.295	-0.023	0.940	0.058	0.973
	PA1365	1.243	0.000	0.424	0.089	-0.034	0.852	-0.226	0.744
	PA2134	-2.533	0.001	-0.474	0.858	-2.533	0.001	-0.474	0.858
pvdA	PA2386	1.310	0.010	0.112	0.827	-0.054	0.862	-0.076	0.973
fpvI	PA2387	-0.430	0.049	-0.318	0.153	-0.447	0.008	-0.001	1.000

fpvR	PA2388	-0.244	0.354	-0.087	0.744	-0.262	0.341	0.163	0.915
pvdT	PA2390	-0.369	0.423	-0.147	0.760	-0.334	0.160	0.065	0.973
opmQ	PA2391	-0.421	0.116	-0.318	0.267	0.646	0.010	-0.024	0.986
pvdP	PA2392	1.416	0.000	0.452	0.175	0.207	0.643	0.436	0.855
pvdN	PA2394	2.033	0.000	0.799	0.014	0.473	0.010	-0.026	0.980
pvdO	PA2395	2.089	0.000	0.925	0.009	-1.797	0.007	-0.242	0.940
pvdF	PA2396	1.726	0.000	0.498	0.177	-0.267	0.222	-0.128	0.915
pvdS	PA2426	0.938	0.006	0.227	0.475	0.370	0.140	0.243	0.855
foxI	PA2466	0.120	0.639	-0.199	0.424	-0.102	0.609	-0.396	0.561
foxR	PA2467	-0.351	0.198	-0.010	0.971	-0.067	0.846	-0.140	0.950
foxI	PA2468	-0.644	0.024	-0.702	0.014				
	PA2469	-1.116	0.000	-0.328	0.451	-0.314	0.178	0.174	0.888
pvdR	PA2807	-0.833	0.008	-0.062	0.821	-2.471	0.000	-0.667	0.470
	PA3268	1.349	0.000	0.445	0.051	0.835	0.002	0.048	0.973
fprA	PA3397	1.320	0.000	0.365	0.261	-0.055	0.794	0.329	0.703
fptA	PA4221	0.603	0.266	-0.023	0.964	1.106	0.006	0.851	0.384
pchI	PA4222	0.000	1.000	0.000	1.000	1.552	0.046	1.672	0.470
pchH	PA4223	0.000	1.000	0.000	1.000	1.836	0.028	1.884	0.428
pchG	PA4224	0.000	1.000	0.000	1.000	2.312	0.004	1.483	0.442
pchF	PA4225	0.000	1.000	0.000	1.000	1.810	0.006	1.050	0.536
pchE	PA4226	0.000	1.000	0.000	1.000	2.441	0.003	1.321	0.470
pchR	PA4227	-0.043	0.898	-0.108	0.744	-0.025	0.905	-0.120	0.908
pchR	PA4227	-0.043	0.898	-0.108	0.744	-0.025	0.905	-0.120	0.908
pchD	PA4228	1.199	0.247	0.039	0.966	1.888	0.001	0.657	0.532
pchD	PA4228	1.199	0.247	0.039	0.966	1.888	0.001	0.657	0.532
pchC	PA4229	1.050	0.655	-0.019	0.970	0.414	0.538	0.403	0.915
pchC	PA4229	1.050	0.655	-0.019	0.970	0.414	0.538	0.403	0.915
pchB	PA4230	0.882	0.641	-0.046	0.979	1.241	0.016	0.986	0.480
pchB	PA4230	0.882	0.641	-0.046	0.979	1.241	0.016	0.986	0.480
pchB	PA4231	0.599	0.505	-0.309	0.731	1.398	0.016	0.562	0.808
pchA	PA4231	0.882	0.641	-0.046	0.979	1.398	0.016	0.562	0.808
feoC	PA4357	-2.061	0.031	-1.145	0.460	-1.425	0.034	-0.642	0.841
feoB	PA4358	-1.972	0.000	-0.533	0.063				
feoA	PA4359	-1.498	0.000	-0.440	0.052	-1.573	0.014	-0.526	0.855
fprB	PA4615	-1.299	0.000	-0.317	0.251	-0.153	0.360	-0.013	0.991
chtA	PA4675	1.693	0.000	0.421	0.077	0.681	0.016	0.070	0.973
fur	PA4764	0.679	0.010	0.109	0.681	0.068	0.557	-0.058	0.938
	PA5505	1.945	0.000	0.618	0.026	-2.467	0.002	-0.109	0.973
tonb1	PA5531	-0.744	0.020	-0.083	0.792	-0.878	0.001	-0.368	0.529
Cell shape defining proteins									
minD	PA3244	1.349	0.000	0.445	0.051	-0.338	0.034	-0.084	0.915
rodA	PA4002	-1.208	0.000	-0.363	0.118				
ftsZ	PA4407	0.528	0.129	-0.351	0.301	-0.072	0.686	-0.224	0.777
spoOJ	PA5562	1.01364	0.000	0.129	0.589	-0.108	0.360	-0.080	0.903
Sulfur metabolism									
cysA	PA0280	5.141	0.000	-0.285	0.195	1.074	0.007	0.745	0.470
ssuB2	PA3347	-0.287	0.255	0.041	0.877	-1.157	0.000	-0.207	0.742
ssuF	PA3441	3.419	0.000	PA3441	2.654	1.353	0.013	1.298	0.381
ssuB	PA3442	4.518	0.000	PA3442	1.495				
ssuC	PA3443	6.198	0.000	PA3443	2.463				
ssuD	PA3444	6.766	0.000	PA3444	3.540	2.519	0.002	1.811	0.262
	PA3445	5.675	0.000	PA3445	3.929	0.130	0.824	1.292	0.470
ssuE	PA3446	5.544	0.000	PA3446	3.060	0.829	0.008	0.122	0.938
	PA3447	1.784	0.000	PA3447	0.499				
	PA3448	2.018	0.000	PA3448	0.999	1.091	0.000	0.324	0.276
iscR	PA3815	-0.672	0.014	-0.099	0.709	0.030	0.888	0.424	0.492
tauD	PA3935	3.989	0.000	1.293	0.000	1.998	0.000	1.273	0.081
tauC	PA3936	4.118	0.000	1.675	0.001				
tauB	PA3937	5.322	0.000	3.023	0.000	2.398	0.003	1.636	0.364
tauA	PA3938	5.042	0.000	3.342	0.000	-0.442	0.443	1.136	0.574
cysD	PA4443	3.754	0.000	2.141	0.000	1.031	0.000	0.331	0.502

Heat shock response									
rpoH	PA0376	1.031	0.002	0.040	0.890	-0.203	0.455	0.191	0.899
rpoD	PA0576	1.125	0.001	0.173	0.578	0.175	0.262	0.082	0.932
	PA1068	1.443	0.000	0.169	0.481	0.863	0.008	0.174	0.903
htpG	PA1596	2.827	0.000	-0.487	0.098	0.278	0.025	-0.044	0.956
ibpA	PA3126	1.987	0.000	-1.318	0.000	0.498	0.034	-0.034	0.981
rpoA	PA4238	1.576	0.000	0.449	0.191	0.428	0.022	0.138	0.868
groES	PA4386	1.554	0.000	-1.203	0.000	0.356	0.011	-0.015	0.985
dnaJ	PA4760	1.491	0.000	-0.784	0.004	0.174	0.557	0.047	0.981
dnaK	PA4761	1.618	0.000	-1.020	0.005	0.269	0.032	-0.006	0.993
grpE	PA4762	2.019	0.000	-0.942	0.000	-0.372	0.047	0.082	0.940
hslV	PA5053	2.442	0.000	-0.803	0.000	0.171	0.360	0.046	0.973
hslU	PA5054	2.231	0.000	-0.732	0.005	0.394	0.018	-0.017	0.986
Redox active proteins and proteins of the oxidative stress response									
coxB	PA0105	-1.249	0.000	-0.208	0.520	-0.380	0.128	-0.185	0.888
ahpF	PA0140	1.375	0.000	0.087	0.713	0.740	0.001	0.000	1.000
cttP	PA0180	0.166	0.524	-0.175	0.507	0.098	0.740	-0.199	0.899
	PA0840	1.096	0.000	0.314	0.150	0.266	0.038	-0.078	0.903
ccoO2	PA1556	-1.590	0.000	0.267	0.242				
ccoN2	PA1557	-1.590	0.000	0.109	0.685				
	PA1856	-1.076	0.000	-0.164	0.478				
	PA2477	-1.179	0.011	-0.328	0.451				
	PA2482	-1.402	0.000	-0.148	0.694	0.419	0.327	-0.036	0.991
	PA3331	2.763	0.000	0.745	0.168	-0.282	0.672	0.180	0.973
fprA	PA3397	1.320	0.000	0.365	0.261	-0.055	0.794	0.329	0.703
finR	PA3398	1.109	0.000	0.039	0.887	0.232	0.044	0.104	0.855
	PA3795	1.160	0.000	0.162	0.536	-0.380	0.118	-0.239	0.853
	PA4061	1.616	0.000	-0.268	0.283	0.615	0.001	-0.049	0.944
	PA4621	-1.343	0.000	0.057	0.843	1.209	0.001	0.157	0.904
grx	PA5129	1.382	0.000	0.402	0.080	-0.382	0.092	-0.109	0.938
Metabolism									
	PA0220	-1.214	0.000	-0.284	-0.284	0.000		0.000	
metK	PA0546	1.891	0.000	0.439	0.232	0.665	0.002	0.202	0.743
	PA1325	6.180	0.000	0.166	0.754	3.667	0.000	-0.086	0.973
ilvA2	PA1326	6.746	0.000	0.451	0.067	2.206	0.000	0.013	0.991
ggt	PA1338	1.371	0.000	-0.020	0.935	0.379	0.076	0.097	0.940
aatJ	PA1339	2.020	0.000	-0.152	0.698	-0.547	0.007	-0.628	0.173
aatM	PA1340	2.176	0.001	-0.281	0.623				
aatP	PA1341	2.596	0.001	0.031	0.963				
aatQ	PA1342	1.901	0.000	0.125	0.677	-1.509	0.003	-0.022	0.993
opdO	PA2113	-1.182	0.000	-0.388	0.116				
aroP1	PA3000	-1.150	0.000	0.086	0.704				
	PA3035	-1.211	0.000	-0.073	0.743	-1.070	0.001	-0.170	0.855
	PA3865	-0.410	0.058	-0.307	0.163	-2.955	0.001	-0.248	0.938
narX	PA3878	-0.923	0.003	-0.216	0.491				
narL	PA3879	-0.563	0.171	-0.001	0.999	-0.698	0.001	-0.214	0.668
	PA3965	1.249	0.000	0.436	0.065	0.088	0.508	-0.153	0.807
	PA4192	4.213	0.000	0.822	0.283				
	PA4193	1.673	0.004	0.214	0.626				
glyA3	PA4602	1.729	0.000	0.520	0.036	0.642	0.003	0.010	0.992
arcD	PA5170	-2.625	0.000	-0.393	0.223	0.374	0.034	-0.242	0.727
crc	PA5332	-0.062	0.807	0.164	0.530	0.093	0.454	-0.074	0.915
Disulfide bond formation									
dsbB	PA0538	0.225	0.308	-0.577	0.012				
dsbD2	PA2478	-0.294	0.445	-0.181	0.650	-1.681	0.005	0.158	0.964
dsbC	PA3737	0.324	0.141	0.406	0.075	-0.133	0.535	-0.014	0.992
trxA	PA5240	0.760	0.008	-0.103	0.717	-1.395	0.000	-0.255	0.492
dsbA	PA5489	0.646	0.021	-0.021	0.938	-1.455	0.001	0.038	0.982
Hypothetical proteins and miscellaneous									
	PA0149	-1.172	0.001	0.157	0.677	0.222	0.357	-0.255	0.841
	PA0200	-2.134	0.000	-0.491	0.031				

	PA0270	-0.473	0.035	-0.751	0.001	-2.768	0.006	-0.601	0.888
dnr	PA0527	-1.495	0.000	-0.500	0.024	-0.202	0.221	-0.084	0.933
	PA0618	0.123	0.775	-0.017	0.972	1.680	0.000	0.088	0.950
	PA0620	0.229	0.494	0.216	0.556	2.613	0.000	0.275	0.861
	PA0622	-0.034	0.910	0.007	0.982	1.267	0.002	-0.018	0.993
	PA0630	-0.521	0.290	0.085	0.878	2.688	0.001	-0.070	0.982
	PA0718	-1.882	0.000	-0.980	0.000	0.000		0.000	
cbpD	PA0852	1.190	0.004	-0.252	0.536	-1.868	0.001	-0.037	0.987
	PA1414	-2.427	0.000	-0.377	0.167	1.234	0.000	-0.045	0.969
anr	PA1544	0.405	0.135	-0.373	0.158	-0.637	0.007	-0.092	0.938
	PA1673	-2.120	0.000	0.178	0.466	-2.178	0.000	-0.477	0.729
modC	PA1861	-1.047	0.000	-0.070	0.776	0.000		0.000	
modB	PA1862	-0.713	0.001	0.171	0.458	0.000		0.000	
modA	PA1863	-0.476	0.043	-0.152	0.511	-2.259	0.001	-0.194	0.944
exaB	PA1983	0.179	0.569	1.497	0.000	-3.154	0.000	-0.097	0.950
	PA2050	1.892	0.001	0.327	0.481	0.000		0.000	
	PA2202	3.856	0.000	0.675	0.005	0.000		0.000	
	PA2274	-2.345	0.000	0.224	0.339	0.000		0.000	
	PA2328	2.829	0.000	0.136	0.810	-0.367	0.474	0.823	0.703
	PA2329	3.357	0.000	0.414	0.517	-0.169	0.322	-0.049	0.973
	PA2565	-1.247	0.011	-0.539	0.340	-0.007	0.967	0.005	0.995
	PA2781	-0.980	0.006	-0.253	0.487	-2.278	0.000	-0.066	0.969
	PA3318	-0.085	0.698	0.074	0.739	-2.291	0.001	-0.660	0.660
	PA3430	-2.045	0.000	1.092	0.001	-0.877	0.029	0.071	0.973
	PA3431	-2.071	0.000	0.361	0.401	0.000		0.000	
	PA3576	-0.355	0.117	-0.551	0.017	-1.901	0.000	0.488	0.030
glpF	PA3581	-1.901	0.000	0.488	0.030	0.000		0.000	
	PA3661	1.151	0.000	1.001	0.001	4.004	0.002	-0.452	0.923
	PA3785	0.632	0.003	0.634	0.009	-2.947	0.000	-0.288	0.899
	PA4063	0.926	0.002	-0.411	0.184	-2.300	0.067	-1.098	0.858
prpL	PA4175	-0.897	0.005	-1.098	0.003	-0.257	0.673	0.548	0.858
olsA	PA4351	-2.166	0.000	-0.460	0.403	0.000		0.000	
	PA4352	-2.188	0.000	-0.388	0.276	-0.729	0.003	0.024	0.985
	PA4364	-1.882	0.000	-0.244	0.376	0.000		0.000	
	PA4523	-2.235	0.000	-0.385	0.275	-0.559	0.002	0.002	0.998
	PA4697	0.354	0.100	-0.031	0.887	-2.409	0.001	-0.180	0.962
	PA5027	-2.300	0.000	-0.741	0.005	0.000		0.000	
	PA5086	-1.154	0.000	-0.552	0.014	-3.088	0.000	-1.481	0.222
	PA5087	-1.133	0.000	-0.383	0.079	0.000		0.000	
	PA5088	-1.129	0.000	-1.198	0.000	-2.205	0.000	-1.478	0.032
	PA5330	-0.538	0.076	0.035	0.912	-2.240	0.001	-0.201	0.944
	PA5359	-0.469	0.067	-0.505	0.052	-2.366	0.000	-0.514	0.689
	PA5475	-2.875	0.000	-0.439	0.107	-1.550	0.001	-0.426	0.741
	PA5481	-2.807	0.001	-0.194	0.950	-2.807	0.001	-0.194	0.950

References

Aendekerk S., Diggle S. P., Song Z., Høiby N., Cornelis P., Williams P. and Cámara M. (2005) The MexGHI-OpmD multidrug efflux pump controls growth, antibiotic susceptibility and virulence in Pseudomonas aeruginosa via 4-quinolone-dependent cell-to-cell communication, *Microbiology*, **151**(4), 1113–1125.

Alhede M., Bjarnsholt T., Jensen P. O., Phipps R. K., Moser C., Christophersen L., Christensen L. D., van Gennip M., Parsek M., Hoiby N., Rasmussen T. B. and Givskov M. (2009) Pseudomonas aeruginosa recognizes and responds aggressively to the presence of polymorphonuclear leukocytes, *Microbiology*, **155**(11), 3500–3508.

Allan B., Linseman M., MacDonald L. A., Lam J. S. and Kropinski A. M. (1988) Heat shock response of Pseudomonas aeruginosa, *Journal Of Bacteriology*, **170**(8), 3668–74.

Almblad H., Harrison J. J., Rybtke M., Groizeleau J., Givskov M., Parsek M. R. and Tolker-Nielsen T. (2015) The Cyclic AMP-Vfr Signaling Pathway in Pseudomonas aeruginosa Is Inhibited by Cyclic Di-GMP, *Journal Of Bacteriology*, **197**(13), 2190–200.

Alteri C. and Mobley H. (2016) The versatile type VI secretion system, *Microbiology Spectrum*, **4**(2).

Anantharajah A., Mingeot-Leclercq M.-P. and Van Bambeke F. (2016) Targeting the Type Three Secretion System in Pseudomonas aeruginosa, *Trends In Pharmacological Sciences*, **37**(9), 734–49.

Anglès F., Castanié-Cornet M.-P., Slama N., Dinclaux M., Cirinesi A.-M., Portais J.-C., Létisse F. and Genevaux P. (2017) Multilevel interaction of the DnaK/DnaJ(HSP70/HSP40) stress-responsive chaperone machine with the central metabolism, *Scientific Reports*, **7**, 41341.

Arevalo-Ferro C., Hentzer M., Reil G., Görg A., Kjelleberg S., Givskov M., Riedel K. and Eberl L. (2003) Identification of quorum-sensing regulated proteins in the opportunistic pathogen Pseudomonas aeruginosa by proteomics. *Environmental Microbiology*, **5**(12), 1350–69.

Arts I. S., Ball G., Leverrier P., Garvis S., Nicolaes V., Vertommen D., Ize B., Tamu Dufe V., Messens J., Voulhoux R. and Collet J.-F. (2013) Dissecting the machinery that introduces disulfide bonds in Pseudomonas aeruginosa, *MBio*, **4**(6), e00912-13.

Aseev L. V, Koledinskaya L. S. and Boni I. V (2016) Regulation of Ribosomal Protein Operons rplM-rpsI, rpmB-rpmG, and rplU-rpmA at the Transcriptional and Translational Levels, *Journal Of Bacteriology*, **198**(18), 2494–502.

Bach T. M. H. and Takagi H. (2013) Properties, metabolisms, and applications of l-proline analogues, *Applied Microbiology And Biotechnology*, **97**(15), 6623–6634.

Bains M., Fernández L. and Hancock R. E. W. (2012) Phosphate starvation promotes swarming motility and cytotoxicity of Pseudomonas aeruginosa, *Applied And Environmental Microbiology*, **78**(18), 6762–8.

Baker P., Whitfield G. B., Hill P. J., Little D. J., Pestrak M. J., Robinson H., Wozniak D. J. and Howell P. L. (2015) Characterization of the Pseudomonas aeruginosa Glycoside Hydrolase PslG Reveals That Its Levels Are Critical for Psl Polysaccharide Biosynthesis and Biofilm Formation, *The Journal Of Biological Chemistry*, **290**(47), 28374–87.

Balasubramanian D., Schneper L., Kumari H. and Mathee K. (2013) A dynamic and intricate regulatory network determines Pseudomonas aeruginosa virulence, *Nucleic Acids Research*, **41**(1), 1–20.

Ball G. G., Durand É., Lazdunski A. and Filloux A. (2002) A novel type II secretion system in Pseudomonas aeruginosa, *Molecular Microbiology*, **43**(2), 475–785.

Banerjee A., Dey S., Chakraborty A., Datta A., Basu A., Chakrabarti S. and Datta S. (2014) Binding mode analysis of a major T3SS translocator protein PopB with its chaperone PcrH from Pseudomonas aeruginosa, *Proteins: Structure, Function, And Bioinformatics*, **82**(12), 3273–3285.

Bardoel B. W., van Kessel K. P. M., van Strijp J. A. G. and Milder F. J. (2012) Inhibition of Pseudomonas aeruginosa Virulence: Characterization of the AprA–AprI Interface and Species Selectivity, *Journal Of Molecular Biology*, **415**(3), 573–583.

Barnes M. R., Gray I. C., Betts M. J. and Russell R. B. (2003) Amino Acid Properties and Consequences of Substitutions, *Bioinformatics For Geneticists*, 289–316.

Basan M., Zhu M., Dai X., Warren M., Sevin D., Wang Y.-P. and Hwa T. (2015) Inflating bacterial cells by increased protein synthesis, *Molecular Systems Biology*, **11**(10), 836–836.

Bastiaansen K. C., van Ulsen P., Wijtmans M., Bitter W. and Llamas M. A. (2015) Self-cleavage of the Pseudomonas aeruginosa Cell-surface Signaling Anti-sigma Factor FoxR Occurs through an N-O Acyl Rearrangement., *The Journal Of Biological Chemistry*, **290**(19), 12237–46.

Baysse C., Cullinane M., Dénervaud V., Burrowes E., Dow J. M., Morrissey J. P., Tam L., Trevors J. T. and O'Gara F. (2005) Modulation of quorum sensing in Pseudomonas aeruginosa through alteration of membrane properties, *Microbiology*, **151**(8), 2529–2542.

Beaume M., Köhler T., Fontana T., Tognon M., Renzoni A. and van Delden C. (2015) Metabolic pathways of Pseudomonas aeruginosa involved in competition with respiratory bacterial pathogens, *Frontiers In Microbiology*, **6**, 321.

Becher A. and Schweizer H. P. (2000) Integration-proficient Pseudomonas aeruginosa vectors for isolation of single-copy chromosomal lacZ and lux gene fusions, *BioTechniques*, **29**(5), 948–50, 952.

Beljantseva J., Kudrin P., Jimmy S., Ehn M., Pohl R., Varik V., Tozawa Y., Shingler V., Tenson T., Rejman D. and Hauryliuk V. (2017) Molecular mutagenesis of ppGpp: turning a RelA activator into an inhibitor, *Scientific Reports*, **7**, 41839.

Benkert B., Quack N., Schreiber K., Jaensch L., Jahn D. and Schobert M. (2008) Nitrate-responsive NarX-NarL represses arginine-mediated induction of the Pseudomonas aeruginosa arginine fermentation arcDABC operon, *Microbiology*, **154**(10), 3053–3060.

Berkmen M. (2012) Production of disulfide-bonded proteins in Escherichia coli, *Protein Expression And Purification*, **82**(1), 240–251.

Bertrand J. J., West J. T. and Engel J. N. (2010) Genetic analysis of the regulation of type IV pilus function by the Chp chemosensory system of Pseudomonas aeruginosa., *Journal Of Bacteriology*, **192**(4), 994–1010.

Bhagirath A. Y., Li Y., Somayajula D., Dadashi M., Badr S. and Duan K. (2016) Cystic fibrosis lung environment and Pseudomonas aeruginosa infection, *BMC Pulmonary Medicine*, **16**(1), 174.

Bhuwan M., Lee H.-J., Peng H.-L. and Chang H.-Y. (2012) Histidine-containing phosphotransfer protein-B (HptB) regulates swarming motility through partner-switching system in Pseudomonas aeruginosa PAO1 strain, *The Journal of Biological Chemistry*, **287**(3), 1903–14.

Bielecki P., Lukat P., Hüsecken K., Dötsch A., Steinmetz H., Hartmann R. W., Müller R. and Häussler S. (2012) Mutation in Elongation Factor G Confers Resistance to the Antibiotic Argyrin in the Opportunistic Pathogen *Pseudomonas aeruginosa*, *ChemBioChem*, **13**(16), 2339–2345.

Blaby-Haas C. E., Furman R., Rodionov D. A., Artsimovitch I. and de Crécy-Lagard V. (2011) Role of a Zn-independent DksA in Zn homeostasis and stringent response, *Molecular Microbiology*, **79**(3), 700–15.

Bleves S., Soscia C., Nogueira-Orlandi P., Lazdunski A. and Filloux A. (2005) Quorum sensing negatively controls type III secretion regulon expression in Pseudomonas aeruginosa PAO1., *Journal Of Bacteriology*, **187**(11), 3898–902.

Blus-Kadosh I., Zilka A., Yerushalmi G. and Banin E. (2013) The effect of pstS and phoB on quorum sensing and swarming motility in Pseudomonas aeruginosa, *PloS One*, **8**(9), e74444.

Bodilis J., Nsigue-Meilo S., Besaury L. and Quillet L. (2012) Variable Copy Number, Intra-Genomic Heterogeneities and Lateral Transfers of the 16*S* rRNA Gene in Pseudomonas, *PLoS ONE*, **7**(4), e35647.

Boonma S., Romsang A., Duang-Nkern J., Atichartpongkul S., Trinachartvanit W., Vattanaviboon P. and Mongkolsuk S. (2017) The FinR-regulated essential gene fprA, encoding ferredoxin NADP+ reductase: Roles in superoxide-mediated stress protection and virulence of Pseudomonas aeruginosa, *PloS One*, **12**(2), e0172071.

Borg A., Holm M., Shiroyama I., Hauryliuk V., Pavlov M., Sanyal S. and Ehrenberg M. (2015) Fusidic acid targets elongation factor G in several stages of translocation on the bacterial ribosome, *The Journal of Biological Chemistry*, **290**(6), 3440–54.

Borlee B. R., Goldman A. D., Murakami K., Samudrala R., Wozniak D. J. and Parsek M. R. (2010) *Pseudomonas aeruginosa* uses a cyclic-di-GMP-regulated adhesin to reinforce the biofilm extracellular matrix, *Molecular Microbiology*, **75**(4), 827–842.

Bouvier B., Cézard C. and Sonnet P. (2015) Selectivity of pyoverdine recognition by the FpvA receptor of Pseudomonas aeruginosa from molecular dynamics simulations, *Physical Chemistry Chemical Physics*, **17**(27), 18022–18034.

Brandel J., Humbert N., Elhabiri M., Schalk I. J., Mislin G. L. A. and Albrecht-Gary A.-M. (2012) Pyochelin, a siderophore of Pseudomonas aeruginosa: Physicochemical characterization of the iron(iii), copper(ii) and zinc(ii) complexes, *Dalton Transactions*, **41**(9), 2820.

Breidenstein E. B. M., de la Fuente-Núñez C. and Hancock R. E. W. (2011) Pseudomonas aeruginosa: all roads lead to resistance, *Trends in Microbiology*, **19**(8), 419–426.

Brickman T. J., Cummings C. A., Liew S.-Y., Relman D. A. and Armstrong S. K. (2011) Transcriptional profiling of the iron starvation response in Bordetella pertussis provides new insights into siderophore utilization and virulence gene expression., *Journal of Bacteriology*, **193**(18), 4798–812.

Broder U. N., Jaeger T. and Jenal U. (2016) LadS is a calcium-responsive kinase that induces acute-to-chronic virulence switch in Pseudomonas aeruginosa, *Nature Microbiology*, **2**, 16184.

Bronstein P. A., Filiatrault M. J., Myers C. R., Rutzke M., Schneider D. J. and Cartinhour S. W. (2008) Global transcriptional responses of Pseudomonas syringae DC3000 to changes in iron bioavailability in vitro, *BMC Microbiology*, **8**(1), 209.

Brown R. (1954) *Composition of scientific words; a manual of methods and a lexicon of materials for the practice of logotechnics,* Volume 1. Smithsonian Institution Press.

Brown T. A. (2002) *Genomics: Chapter 3 Transcriptomes and Proteomes*, American Socitety of Microbiology, 337-356.

de Bruijn F. J. (2016) *Stress and environmental regulation of gene expression and adaptation in bacteria*. Wiley Blackwell.

Brunet Y. R., Bernard C. S., Gavioli M., Lloubès R. and Cascales E. (2011) An Epigenetic Switch Involving Overlapping Fur and DNA Methylation Optimizes Expression of a Type VI Secretion Gene Cluster, *PLoS Genetics*, **7**(7), e1002205.

Brutinel E. D., Vakulskas C. A. and Yahr T. L. (2010) ExsD Inhibits Expression of the Pseudomonas aeruginosa Type III Secretion System by Disrupting ExsA Self-Association and DNA Binding Activity, *Journal of Bacteriology*, **192**(6), 1479–1486.

Burger M., Beacham I. R., Beven C.-A. and Woods R. G. (2001) The aprX–lipA operon of Pseudomonas fluorescens B52: a molecular analysis of metalloprotease and lipase production, *Microbiology*, **147**(2), 345–354.

Burn S. F. (2012) Detection of β-Galactosidase Activity: X-gal Staining, *Methods in Molecular Biology*, 866, 241–250.

Cantin A. M., Hartl D., Konstan M. W. and Chmiel J. F. (2015) Inflammation in cystic fibrosis lung disease: Pathogenesis and therapy, *Journal of Cystic Fibrosis : Official Journal of the European Cystic Fibrosis Society*, **14**(4), 419–30.

Casabona M., Silverman J., Sall K., Boyer F., Coute Y., Poirel J., Grunwald D., Mougous J., Elsen S. and Attree I. (2014) An ABC-transporter and an outer membrane lipoprotein participate in posttranslational activation of type VI secretion in Pseudomonas aeruginosa, *Environmental Microbiology*, **15**(2), 471–486.

Cezairliyan B., Vinayavekhin N., Grenfell-Lee D., Yuen G. J., Saghatelian A. and Ausubel F. M. (2013) Identification of Pseudomonas aeruginosa phenazines that kill Caenorhabditis elegans, *PLoS Pathogens*, **9**(1), e1003101.

Chakraborty R. (2013) *Iron uptake in bacteria with emphasis on E. coli and Pseudomonas*. Springer.

Chakraborty S., Sivaraman J., Leung K. Y. and Mok Y.-K. (2011) Two-component PhoB-PhoR regulatory system and ferric uptake regulator sense phosphate and iron to control virulence genes in type III and VI secretion systems of Edwardsiella tarda, *The Journal Of Biological Chemistry*, **286**(45), 39417–30.

Chen F., Chen C.-C., Riadi L. and Ju L.-K. (2004) Modeling rhl Quorum-Sensing Regulation on Rhamnolipid Production by *Pseudomonas aeruginosa*, *Biotechnology Progress*, **20**(5), 1325–1331.

Chen L., Zou Y., She P. and Wu Y. (2015) Composition, function, and regulation of T6SS in Pseudomonas aeruginosa, *Microbiological Research*, **172**, 19–25.

Chen Y., Wong J., Sun G. W., Liu Y., Tan G.-Y. G. and Gan Y.-H. (2011) Regulation of type VI secretion system during Burkholderia pseudomallei infection., *Infection And Immunity*, **79**(8), 3064–73.

Cho S.-H. and Collet J.-F. (2013) Many roles of the bacterial envelope reducing pathways, *Antioxidants & Redox Signaling*, **18**(13), 1690–8.

Chung J. C. S., Rzhepishevska O., Ramstedt M. and Welch M. (2013) Type III secretion system expression in oxygen-limited Pseudomonas aeruginosa cultures is stimulated by isocitrate lyase activity, *Open Biology*, **3**(1), 120131.

Chung J., Chen T. and Missiakas D. (2000) Transfer of electrons across the cytoplasmic membrane by DsbD, a membrane protein involved in thiol-disulphide exchange and protein folding in the bacterial periplasm, *Molecular Microbiology*, **35**(5), 1099–1109.

Connell S. R., Takemoto C., Wilson D. N., Wang H., Murayama K., Terada T., Shirouzu M., Rost M., Schüler M., Giesebrecht J., Dabrowski M., Mielke T., Fucini P., Yokoyama S. and Spahn C. M. T. (2007) Structural basis for interaction of the ribosome with the switch regions of GTP-bound elongation factors, *Molecular Cell*, **25**(5), 751–64.

Cooley R. B., Smith T. J., Leung W., Tierney V., Borlee B. R., O'Toole G. A. and Sondermann H. (2015) Cyclic Di-GMP-Regulated Periplasmic Proteolysis of a Pseudomonas aeruginosa Type Vb Secretion System Substrate. *Journal of Bacteriology*, **198**(1), 66–76.

Cornelis P. and Dingemans J. (2013) Pseudomonas aeruginosa adapts its iron uptake strategies in function of the type of infections, *Frontiers in Cellular and Infection Microbiology*, **3**, 75.

Cornelis P., Matthijs S. and Van Oeffelen L. (2009) Iron uptake regulation in Pseudomonas aeruginosa, *BioMetals*, **22**(1), 15–22.

Corrigan R. M., Bellows L. E., Wood A. and Gründling A. (2016) ppGpp negatively impacts ribosome assembly affecting growth and antimicrobial tolerance in Gram-positive bacteria, *Proceedings of the National Academy of Sciences of the United States Of America*, **113**(12), E1710-9.

Cuív P. O., Keogh D., Clarke P. and O'Connell M. (2007) FoxB of Pseudomonas aeruginosa functions in the utilization of the xenosiderophores ferrichrome, ferrioxamine B, and schizokinen: evidence for transport redundancy at the inner membrane, *Journal of Bacteriology*, **189**(1), 284–7.

Cunrath O., Gasser V., Hoegy F., Reimmann C., Guillon L. and Schalk I. J. (2015) A cell biological view of the siderophore pyochelin iron uptake pathway in *Pseudomonas aeruginosa*, *Environmental Microbiology*, **17**(1), 171–185.

Cutruzzolà F., Arese M., Ranghino G., van Pouderoyen G., Canters G. and Brunori M. (2002) Pseudomonas aeruginosa cytochrome C(551): probing the role of the hydrophobic patch in electron transfer, *Journal of Inorganic Biochemistry*, **88**(3–4), 353–61.

Dasgupta N., Wolfgang M. C., Goodman A. L., Arora S. K., Jyot J., Lory S. and Ramphal R. (2003) A four-tiered transcriptional regulatory circuit controls flagellar biogenesis in Pseudomonas aeruginosa, *Molecular Microbiology*, **50**(3), 809–824.

Davenport P. W., Griffin J. L. and Welch M. (2015) Quorum Sensing Is Accompanied by Global Metabolic Changes in the Opportunistic Human Pathogen Pseudomonas aeruginosa, *Journal of Bacteriology*, **197**(12), 2072–2082.

Davey M. E., Caiazza N. C. and O'Toole G. A. (2003) Rhamnolipid surfactant production affects biofilm architecture in Pseudomonas aeruginosa PAO1, *Journal of Bacteriology*, **185**(3), 1027–36.

Demarre G., Guérout A.-M., Matsumoto-Mashimo C., Rowe-Magnus D. A., Marlière P. and Mazel D. (2005) A new family of mobilizable suicide plasmids based on broad host range R388 plasmid (IncW) and RP4 plasmid (IncPα) conjugative machineries and their cognate Escherichia coli host strains, *Research in Microbiology*, **156**(2), 245–255.

Dennis J. J. and Zylstra G. J. (1998) Plasposons: modular self-cloning minitransposon derivatives for rapid genetic analysis of gram-negative bacterial genomes, *Applied and Environmental Microbiology*, **64**(7), 2710–5.

Diaz M. R., King J. M. and Yahr T. L. (2011) Intrinsic and Extrinsic Regulation of Type III Secretion Gene Expression in Pseudomonas Aeruginosa, *Frontiers in Microbiology*, **2**, 89.

Diggle S. P., Winzer K., Chhabra S. R., Worrall K. E., Cámara M. and Williams P. (2003) The Pseudomonas aeruginosa quinolone signal molecule overcomes the cell density-dependency of the quorum sensing hierarchy, regulates rhl-dependent genes at the onset of stationary phase and can be produced in the absence of LasR, *Molecular Microbiology*, **50**(1), 29–43.

Diraviam Sriramulu D. (2009) Role of lrp in the Pseudomonas Aeruginosa Small Colony Formation, *Journal of Proteomics & Bioinformatics,* **2**(2), 131–138.

Doi Y. and Arakawa Y. (2007) 16S Ribosomal RNA Methylation: Emerging Resistance Mechanism against Aminoglycosides, *Clinical Infectious Diseases*, **45**(1), 88–94.

Dong T. G., Ho B. T., Yoder-Himes D. R. and Mekalanos J. J. (2013) Identification of T6SS-dependent effector and immunity proteins by Tn-seq in Vibrio cholerae, *Proceedings of the National Academy of Sciences of The United States of America*, **110**(7), 2623–8.

Doyle T. B., Hawkins A. C. and McCarter L. L. (2004) The complex flagellar torque generator of Pseudomonas aeruginosa, *Journal of Bacteriology*, **186**(19), 6341–50.

Du X., Li Y., Zhou Q. and Xu Y. (2015) Regulation of gene expression in Pseudomonas aeruginosa M18 by phenazine-1-carboxylic acid, *Applied Microbiology and Biotechnology*, **99**(2), 813–825.

Durand E., Bernadac A., Ball G., Lazdunski A., Sturgis J. N. and Filloux A. (2003) Type II protein secretion in Pseudomonas aeruginosa: the pseudopilus is a multifibrillar and adhesive structure, *Journal of Bacteriology*, **185**(9), 2749–58.

Edgar R. J., Xu X., Shirley M., Konings A. F., Martin L. W., Ackerley D. F. and Lamont I. L. (2014) Interactions between an anti-sigma protein and two sigma factors that regulate the pyoverdine signaling pathway in Pseudomonas aeruginosa, *BMC Microbiology*, **14**(1), 287.

Elsen S., Efthymiou G., Peteinatos P., Diallinas G., Kyritsis P. and Moulis J.-M. (2010) A bacteria-specific 2[4Fe-4S] ferredoxin is essential in Pseudomonas aeruginosa, *BMC Microbiology*, **10**, 271.

Faure L. M., Llamas M. A., Bastiaansen K. C., de Bentzmann S. and Bigot S. (2013) Phosphate starvation relayed by PhoB activates the expression of the Pseudomonas aeruginosa σvreI ECF factor and its target genes, *Microbiology,* **159**(7), 1315–27.

Fazli M., Almblad H., Rybtke M. L., Givskov M., Eberl L. and Tolker-Nielsen T. (2014) Regulation of biofilm formation in *Pseudomonas* and *Burkholderia* species, *Environmental Microbiology*, **16**(7), 1961–1981.

Ferrández A., Hawkins A. C., Summerfield D. T. and Harwood C. S. (2002) Cluster II che genes from Pseudomonas aeruginosa are required for an optimal chemotactic response, *Journal of Bacteriology*, **184**(16), 4374–83.

Fery-Forgues S. and Lavabre D. (1999) In the Laboratory, *Journal Of Chemical Education*, **76**(9).

Fletcher M. P., Diggle S. P., Crusz S. A., Chhabra S. R., Cámara M. and Williams P. (2007) A dual biosensor for 2-alkyl-4-quinolone quorum-sensing signal molecules, *Environmental Microbiology*, **9**(11), 2683–2693.

Francis V. I., Stevenson E. C. and Porter S. L. (2017) Two-component systems required for virulence in Pseudomonas aeruginosa, *FEMS Microbiology Letters*, **364**(11).

Frangipani E., Visaggio D., Heeb S., Kaever V., Cámara M., Visca P. and Imperi F. (2014) The Gac/Rsm and cyclic-di-GMP signalling networks coordinately regulate iron uptake in *Pseudomonas aeruginosa*, *Environmental Microbiology*, **16**(3), 676–688.

Friedman L. and Kolter R. (2003) Genes involved in matrix formation in Pseudomonas aeruginosa PA14 biofilms, *Molecular Microbiology*, **51**(3), 675–690.

Gad G. F., Mohamed H. A. and Ashour H. M. (2011) Aminoglycoside Resistance Rates, Phenotypes, and Mechanisms of Gram-Negative Bacteria from Infected Patients in Upper Egypt, *PLoS ONE*, **6**(2), e17224.

Ghisaidoobe A. B. T. and Chung S. J. (2014) Intrinsic tryptophan fluorescence in the detection and analysis of proteins: a focus on Förster resonance energy transfer techniques, *International Journal of Molecular Sciences*, **15**(12), 22518–38.

Gicquel G., Bouffartigues E., Bains M., Oxaran V., Rosay T., Lesouhaitier O., Connil N., Bazire A., Maillot O., Bénard M., Cornelis P., Hancock R. E. W., Dufour A., Feuilloley M. G. J., Orange N., Déziel E. and Chevalier S. (2013) The Extra-Cytoplasmic Function Sigma Factor SigX Modulates Biofilm and Virulence-Related Properties in *Pseudomonas aeruginosa*, *PLoS ONE*, **8**(11), e80407.

Giraud C., Bernard C. S., Calderon V., Yang L., Filloux A., Molin S., Fichant G., Bordi C. and de Bentzmann S. (2011) The PprA-PprB two-component system activates CupE, the first non-archetypal *Pseudomonas aeruginosa* chaperone-usher pathway system assembling fimbriae, *Environmental Microbiology*, **13**(3), 666–683.

Gode-Potratz C. J., Chodur D. M. and McCarter L. L. (2010) Calcium and iron regulate swarming and type III secretion in Vibrio parahaemolyticus, *Journal Of Bacteriology*, **192**(22), 6025–38.

Goldová J., Ulrych A., Hercík K. and Branny P. (2011) A eukaryotic-type signalling system of Pseudomonas aeruginosa contributes to oxidative stress resistance, intracellular survival and virulence, *BMC Genomics*, **12**, 437.

Gooderham W. J., Bains M., McPhee J. B., Wiegand I. and Hancock R. E. W. (2008) Induction by cationic antimicrobial peptides and involvement in intrinsic polymyxin and antimicrobial peptide resistance, biofilm formation, and swarming motility of PsrA in Pseudomonas aeruginosa. *Journal of Bacteriology*, **190**(16), 5624–34.

Gottesman S. (2017) Stress Reduction, Bacterial Style, *Journal of Bacteriology*, **199**(20), e00433-17.

Grabowska A. D., Wandel M. P., Łasica A. M., Nesteruk M., Roszczenko P., Wyszyńska A., Godlewska R. and Jagusztyn-Krynicka E. K. (2011) Campylobacter jejuni dsb gene expression is regulated by iron in a Fur-dependent manner and by a translational coupling mechanism, *BMC Microbiology*, **11**(1), 166.

Gray T. M., Arnoys E. J., Blankespoor S., Born T., Jagar R., Everman R., Plowman D., Stair A. and Zhang D. (2008) Destabilizing effect of proline substitutions in two helical regions of T4 lysozyme: Leucine 66 to proline and leucine 91 to proline, *Protein Science*, **5**(4), 742–751.

Green E. R. and Mecsas J. (2016) Bacterial Secretion Systems: An Overview, *Microbiology Spectrum*, **4**(1).

Greipel L., Fischer S., Klockgether J., Dorda M., Mielke S., Wiehlmann L., Cramer N. and Tümmler B. (2016) Molecular Epidemiology of Mutations in Antimicrobial Resistance Loci of Pseudomonas aeruginosa Isolates from Airways of Cystic Fibrosis Patients, *Antimicrobial Agents and Chemotherapy*, **60**(11), 6726–6734.

Grishin A. V, Krivozubov M. S., Karyagina A. S. and Gintsburg A. L. (2015) Pseudomonas Aeruginosa Lectins As Targets for Novel Antibacterials, *Acta Naturae*, **7**(2), 29–41.

Grudniak A. M., Klecha B. and Wolska K. I. (2018) Effects of null mutation of the heat-shock gene *htpG* on the production of virulence factors by *Pseudomonas aeruginosa*, *Future Microbiology*, **13**(1), 69–80.

Guilbaud M., Bruzaud J., Bouffartigues E., Orange N., Guillot A., Aubert-Frambourg A., Monnet V., Herry J-M., Chevalier S. and Bellon-Fontaine M-N. (2017) Proteomic response of *Pseudomonas aeruginosa* PAO1 adhering to solid surfaces, *Frontiers in Microbiology*, **8**, 1465.

Gunesekere I. C., Kahler C. M., Powell D. R., Snyder L. A. S., Saunders N. J., Rood J. I. and Davies J. K. (2006) Comparison of the RpoH-dependent regulon and general stress response in Neisseria gonorrhoeae, *Journal of Bacteriology*, **188**(13), 4769–76.

Güvener Z. T., Tifrea D. F. and Harwood C. S. (2006) Two different *Pseudomonas aeruginosa* chemosensory signal transduction complexes localize to cell poles and form and remould in stationary phase, *Molecular Microbiology*, **61**(1), 106–118.

Ha D.-G., Kuchma S. L. and O'Toole G. A. (2014) Plate-Based Assay for Swarming Motility in Pseudomonas aeruginosa, *Methods in Molecular Biology*, 1149, 67–72.

Ha U.-H., Kim J., Badrane H., Jia J., Baker H. V., Wu D. and Jin S. (2004) An in vivo inducible gene of Pseudomonas aeruginosa encodes an anti-ExsA to suppress the type III secretion system, *Molecular Microbiology*, **54**(2), 307–320.

Hachani A., Lossi N. S., Hamilton A., Jones C., Bleves S., Albesa-Jové D. and Filloux A. (2011) Type VI secretion system in Pseudomonas aeruginosa: secretion and multimerization of VgrG proteins, *The Journal of Biological Chemistry*, **286**(14), 12317–27.

Hannauer M., Yeterian E., Martin L. W., Lamont I. L. and Schalk I. J. (2010) An efflux pump is involved in secretion of newly synthesized siderophore by *Pseudomonas aeruginosa*, *FEBS Letters*, **584**(23), 4751–4755.

Hare N. J., Soe C. Z., Rose B., Harbour C., Codd R., Manos J. and Cordwell S. J. (2012a) Proteomics of *Pseudomonas aeruginosa* Australian Epidemic Strain 1 (AES-1) Cultured under Conditions Mimicking the Cystic Fibrosis Lung Reveals Increased Iron Acquisition via the Siderophore Pyochelin, *Journal Of Proteome Research*, **11**(2), 776–795.

Hare N. J., Solis N., Harmer C., Marzook N. B., Rose B., Harbour C., Crossett B., Manos J. and Cordwell S. (2012b) Proteomic profiling of *Pseduomonas aeruginosa* AES-1R, PAO1 and PA14 reveals potential virulence determinants associated with a transmissible cystic fibrosis-associated strain, *BMC Microbiology*, **12**(1), 16.

Hauser A. R. (2009) The type III secretion system of Pseudomonas aeruginosa: infection by injection, *Nature Reviews Microbiology*, **7**(9), 654–665.

Hay T., Fraud S., Lau C. H.-F., Gilmour C. and Poole K. (2013) Antibiotic Inducibility of the mexXY Multidrug Efflux Operon of Pseudomonas aeruginosa: Involvement of the MexZ Anti-Repressor ArmZ, *PLoS ONE*, **8**(2), e56858.

Heera R., Sivachandran P., Chinni S. V., Mason J., Croft L., Ravichandran M. and Su Yin L. (2015) Efficient extraction of small and large RNAs in bacteria for excellent total RNA sequencing and comprehensive transcriptome analysis, *BMC Research Notes*, **8**(1), 754.

Heinrichs D. E., Young L. and Poole K. (1991) Pyochelin-Mediated Iron Transport in Pseudomonas aeruginosa: Involvement of a High-Molecular-Mass Outer Membrane Protein, *Infection and Immunity*, **59**(10), 3680–3684.

Hoegy F., Mislin G. L. A. and Schalk I. J. (2014) Pyoverdine and Pyochelin Measurements, *Pseudomonas Methods and Protocols*, 293–301.

Høiby N., Ciofu O. and Bjarnsholt T. (2010) Pseudomonas aeruginosa biofilms in cystic fibrosis, *Future Microbiology*, **5**(11), 1663–1674.

Holtkamp W., Wintermeyer W. and Rodnina M. V. (2014) Synchronous tRNA movements during translocation on the ribosome are orchestrated by elongation factor G and GTP hydrolysis, *BioEssays*, **36**(10), 908–918.

Hood R. D., Singh P., Hsu F., Güvener T., Carl M. A., Trinidad R. R. S., Silverman J. M., Ohlson B. B., Hicks K. G., Plemel R. L., Li M., Schwarz S., Wang W. Y., Merz A. J., Goodlett D. R. and Mougous J. D. (2010) A type VI secretion system of Pseudomonas aeruginosa targets a toxin to bacteria, *Cell Host & Microbe*, **7**(1), 25–37.

Horsman S. R., Moore R. A. and Lewenza S. (2012) Calcium Chelation by Alginate Activates the Type III Secretion System in Mucoid Pseudomonas aeruginosa Biofilms, *PLoS ONE*, **7**(10).

Hummerjohann J., Laudenbach S., Rétey J., Leisinger T. and Kertesz M. A. (2000) The sulfur-regulated arylsulfatase gene cluster of Pseudomonas aeruginosa, a new member of the cys regulon, *Journal of Bacteriology*, **182**(7), 2055–8.

Imperi F., Ciccosanti F., Perdomo A. B., Tiburzi F., Mancone C., Alonzi T., Ascenzi P., Piacentini M., Visca P. and Fimia G. M. (2009) Analysis of the periplasmic proteome of Pseudomonas aeruginosa, a metabolically versatile opportunistic pathogen, *Proteomics,* **9**(7), 1901–1915.

Imperi F., Tiburzi F., Fimia G. M. and Visca P. (2010) Transcriptional control of the *pvdS* iron starvation sigma factor gene by the master regulator of sulfur metabolism CysB in *Pseudomonas aeruginosa*, *Environmental Microbiology*, **12**(6), 1630–1642.

Intile P. J., Balzer G. J., Wolfgang M. C. and Yahr T. L. (2015) The RNA Helicase DeaD Stimulates ExsA Translation To Promote Expression of the Pseudomonas aeruginosa Type III Secretion System, *Journal of Bacteriology*, **197**(16), 2664–74.

Intile P. J., Diaz M. R., Urbanowski M. L., Wolfgang M. C. and Yahr T. L. (2014) The AlgZR two-component system recalibrates the RsmAYZ posttranscriptional regulatory system to inhibit expression of the Pseudomonas aeruginosa type III secretion system, *Journal of Bacteriology*, **196**(2), 357–66.

Irie Y., Starkey M., Edwards A. N., Wozniak D. J., Romeo T. and Parsek M. R. (2010) Pseudomonas aeruginosa biofilm matrix polysaccharide Psl is regulated transcriptionally by RpoS and post-transcriptionally by RsmA, *Molecular Microbiology*, **78**(1).

Ithín Maunsell B., Adams C., O ' F., Correspondence G. and O 'gara F. (2017) Complex regulation of AprA metalloprotease in Pseudomonas fluorescens M114: evidence for the involvement of iron, the ECF sigma factor, PbrA and pseudobactin M114 siderophore, *Microbiology*, 152(1), 29-42.

Izoré T., Job V. and Dessen A. (2011) Biogenesis, Regulation, and Targeting of the Type III Secretion System, *Structure*, **19**(5), 603–612.

Johnstone T. C. and Nolan E. M. (2015) Beyond iron: non-classical biological functions of bacterial siderophores., *Dalton Transactions*, **44**(14), 6320–39.

Jones S., Yu B., Bainton N. J., Birdsall M., Bycroft B. W., Chhabra S. R., Cox A. J., Golby P., Reeves P. J. and Stephens S. (1993) The lux autoinducer regulates the production of exoenzyme virulence determinants in Erwinia carotovora and Pseudomonas aeruginosa., *The EMBO Journal*, **12**(6), 2477–82.

Jyot J., Balloy V., Jouvion G., Verma A., Touqui L., Huerre M., Chignard M. and Ramphal R. (2011) Type II secretion system of Pseudomonas aeruginosa: in vivo evidence of a significant role in death due to lung infection, *The Journal of Infectious Diseases*, **203**(10), 1369–77.

Kahlmeter G. and Singh N. (2017) *Global priority list of antibiotic resistant bacteria to guide research, discovery and development of new antibiotics*, World Health Organisation.

Kahlon R. S. (2016) *Pseudomonas : molecular and applied biology*. Springer.

Kang Y., Lunin V. V, Skarina T., Savchenko A., Schurr M. J. and Hoang T. T. (2009) The long-chain fatty acid sensor, PsrA, modulates the expression of rpoS and the type III secretion exsCEBA operon in Pseudomonas aeruginosa, *Molecular Microbiology*, **73**(1), 120–36.

Kanjee U., Ogata K. and Houry W. A. (2012) Direct binding targets of the stringent response alarmone (p)ppGpp, *Molecular Microbiology*, **85**(6), 1029–1043.

Karzai A. W., Susskind M. M. and Sauer R. T. (1999) SmpB, a unique RNA-binding protein essential for the peptide-tagging activity of SsrA (tmRNA), *The EMBO Journal*, **18**(13), 3793–3799.

Kazmierczak B. I., Schniederberend M. and Jain R. (2015) Cross-regulation of Pseudomonas motility systems: the intimate relationship between flagella, pili and virulence, *Current Opinion In Microbiology*, **28**, 78–82.

Keiler K. C. (2015) Mechanisms of ribosome rescue in bacteria, *Nature Reviews Microbiology*, **13**(5), 285–297.

Khalifa A. B. H., Moissenet D., Thien H. V. and Khedher M. (2011) Les facteurs de virulence de *Pseudomonas aeruginosa* : mécanismes et modes de régulations, *Annales De Biologie Clinique*, **69**(4), 393–403.

Kida Y., Higashimoto Y., Inoue H., Shimizu T. and Kuwano K. (2008) A novel secreted protease from Pseudomonas aeruginosa activates NF-κB through protease-activated receptors, *Cellular Microbiology*, **10**(7), 1491–1504.

Kim E.-J. E.-J., Wang W., Deckwer W.-D. and Zeng A.-P. (2005) Expression of the quorum-sensing regulatory protein LasR is strongly affected by iron and oxygen concentrations in cultures of Pseudomonas aeruginosa irrespective of cell density, *Microbiology*, **151**(4), 1127–1138.

Kim H., Lee H. and Shin D. (2012) The FeoA protein is necessary for the FeoB transporter to import ferrous iron, *Biochemical And Biophysical Research Communications*, **423**(4), 733–738.

Kirisits M. J. and Parsek M. R. (2006) Does Pseudomonas aeruginosa use intercellular signalling to build biofilm communities?, *Cellular Microbiology*, **8**(12), 1841–1849.

Klausen M., Heydorn A., Ragas P., Lambertsen L., Aaes-Jørgensen A., Molin S. and Tolker-Nielsen T. (2003) Biofilm formation by Pseudomonas aeruginosa wild type, flagella and type IV pili mutants, *Molecular Microbiology*, **48**(6), 1511–1524.

Kotra L. P., Haddad J. and Mobashery S. (2000) Aminoglycosides: perspectives on mechanisms of action and resistance and strategies to counter resistance, *Antimicrobial Agents And Chemotherapy*, **44**(12), 3249–56.

Kruczek C., Kottapalli K. R., Dissanaike S., Dzvova N., Griswold J. A., Colmer-Hamood J. A. and Hamood A. N. (2016) Major Transcriptome Changes Accompany the Growth of Pseudomonas aeruginosa in Blood from Patients with Severe Thermal Injuries, *PloS One*, **11**(3), e0149229.

Kurushima J., Kuwae A. and Abe A. (2012) Iron starvation regulates the type III secretion system in Bordetella bronchiseptica, *Microbiology and* Immunity, **56**(6), 356–362.

Lambert P. A. (2002) Mechanisms of antibiotic resistance in Pseudomonas aeruginosa, *Journal of the Royal Society of Medicine*, **95**(41), 22–26.

Landry R. M., An D., Hupp J. T., Singh P. K. and Parsek M. R. (2006) Mucin-Pseudomonas aeruginosa interactions promote biofilm formation and antibiotic resistance, *Molecular Microbiology*, **59**(1), 142–151.

Langton Hewer S. C. and Smyth A. R. (1996) Antibiotic strategies for eradicating Pseudomonas aeruginosa in people with cystic fibrosis, in *Cochrane Database Of Systematic Reviews,* (11).

Lau C. K. Y., Krewulak K. D. and Vogel H. J. (2016) Bacterial ferrous iron transport: the Feo system, *FEMS Microbiology Reviews*, **40**(2), 273–298.

Lau G. W., Hassett D. J., Ran H. and Kong F. (2004) The role of pyocyanin in Pseudomonas aeruginosa infection, *Trends in Molecular Medicine*, **10**(12), 599–606.

Laverty G., Gorman S. P. and Gilmore B. F. (2014) Biomolecular Mechanisms of Pseudomonas aeruginosa and Escherichia coli Biofilm Formation, *Pathogens*, **3**(3), 596–632.

Lee J., Wu J., Deng Y., Wang J. J., Wang C., Wang J. J., Chang C., Dong Y., Williams P. and Zhang L.-H. (2013) A cell-cell communication signal integrates quorum sensing and stress response, *Nature Chemical Biology*, **9**(5), 339–343.

Lee J. and Zhang L. (2015) The hierarchy quorum sensing network in Pseudomonas aeruginosa, *Protein & Cell*, **6**(1), 26–41.

LeRoux M., Kirkpatrick R. L., Montauti E. I., Tran B. Q., Peterson S. B., Harding B. N., Whitney J. C., Russell A. B., Traxler B., Goo Y. A., Goodlett D. R., Wiggins P. A. and Mougous J. D. (2015) Kin cell lysis is a danger signal that activates antibacterial pathways of *Pseudomonas aeruginosa*, *ELife*, **4**.

Lewis T. A., Glassing A., Harper J. and Franklin M. J. (2013) Role for ferredoxin:NAD(P)H oxidoreductase (FprA) in sulfate assimilation and siderophore biosynthesis in Pseudomonads, *Journal Of Bacteriology*, **195**(17), 3876–87.

Li W., Trabuco L. G., Schulten K. and Frank J. (2011) Molecular dynamics of EF-G during translocation, *Proteins*, **79**(5), 1478–86.

Liao J. and Sauer K. (2012) The MerR-Like Transcriptional Regulator BrlR Contributes to Pseudomonas aeruginosa Biofilm Tolerance, *Journal of Bacteriology*, **194**(18), 4823–4836.

Lin J., Gagnon M. G., Bulkley D. and Steitz T. A. (2015) Conformational changes of elongation factor G on the ribosome during tRNA translocation, *Cell*, **160**(1–2), 219–27.

Line Lucchetti-Miganeh C., Redelberger D., Chambonnier G. L., Rechenmann F. O., Elsen S., Bordi C., Jeannot K., Attré E I., Plé Siat P. and De Bentzmann S. (2014) Pseudomonas aeruginosa Genome Evolution in Patients and under the Hospital Environment, *Pathogens*, **3**, 309–340.

Lister P. D., Wolter D. J. and Hanson N. D. (2009) Antibacterial-resistant Pseudomonas aeruginosa: clinical impact and complex regulation of chromosomally encoded resistance mechanisms, *Clinical Microbiology Reviews*, **22**(4), 582–610.

Liu Y., Beyer A. and Aebersold R. (2016) On the Dependency of Cellular Protein Levels on mRNA Abundance, *Cell*, **165**, 535–550.

Liu Y., Zhou Q., Wang Y., Liu Z., Dong M., Wang Y., Li X. and Hu D. (2014) Negative pressure wound therapy decreases mortality in a murine model of burn-wound sepsis involving Pseudomonas aeruginosa infection, *PloS One*, **9**(2), e90494.

Livermore D. M. (2002) Multiple Mechanisms of Antimicrobial Resistance in Pseudomonas aeruginosa: Our Worst Nightmare?, *Clinical Infectious Diseases*, **34**(5), 634–640.

Llamas M. A., Mooij M. J., Sparrius M., Vandenbroucke-Grauls C. M. J. E., Ratledge C. and Bitter W. (2007) Characterization of five novel Pseudomonas aeruginosa cell-surface signalling systems, *Molecular Microbiology*, **67**(2), 458–472.

Llamas M. A., Sparrius M., Kloet R., Jiménez C. R., Vandenbroucke-Grauls C. and Bitter W. (2006) The heterologous siderophores ferrioxamine B and ferrichrome activate signaling pathways in Pseudomonas aeruginosa, *Journal of Bacteriology*, **188**(5), 1882–91.

López-Causapé C., Sommer L. M., Cabot G., Rubio R., Ocampo-Sosa A. A., Johansen H. K., Figuerola J., Cantón R., Kidd T. J., Molin S. and Oliver A. (2017) Evolution of the Pseudomonas aeruginosa mutational resistome in an international Cystic Fibrosis clone, *Scientific Reports*, **7**(1), 5555.

Lopez-Medina E., Fan D., Coughlin L. A., Ho E. X., Lamont I. L., Reimmann C., Hooper L. V and Koh A. Y. (2015) Candida albicans Inhibits Pseudomonas aeruginosa Virulence through Suppression of Pyochelin and Pyoverdine Biosynthesis, *PLoS Pathogens*, **11**(8), e1005129.

Lyczak J. B., Cannon C. L. and Pier G. B. (2002) Lung infections associated with cystic fibrosis, *Clinical Microbiology Reviews*, **15**(2), 194–222.

Ma L., Jackson K. D., Landry R. M., Parsek M. R. and Wozniak D. J. (2006) Analysis of Pseudomonas aeruginosa conditional psl variants reveals roles for the psl polysaccharide in adhesion and maintaining biofilm structure postattachment, *Journal of Bacteriology*, **188**(23), 8213–21.

Macvanin M., Ballagi A. and Hughes D. (2004) Fusidic acid-resistant mutants of Salmonella enterica serovar typhimurium have low levels of heme and a reduced rate of respiration and are sensitive to oxidative stress, *Antimicrobial Agents and Chemotherapy*, **48**(10), 3877–83.

Macvanin M., Johanson U., Ehrenberg M. and Hughes D. (2000) Fusidic acid-resistant EF-G perturbs the accumulation of ppGpp, *Molecular Microbiology*, **37**(1), 98–107.

Maiuri L., Raia V. and Kroemer G. (2017) Strategies for the etiological therapy of cystic fibrosis, *Cell Death and Differentiation*, **24**(11), 1825–1844.

Marsden A. E., Intile P. J., Schulmeyer K. H., Simmons-Patterson E. R., Urbanowski M. L., Wolfgang M. C. and Yahr T. L. (2016) Vfr Directly Activates exsA Transcription To Regulate Expression of the Pseudomonas aeruginosa Type III Secretion System, *Journal of Bacteriology*, **198**(9), 1442–50.

Maughan W. P. and Shuman S. (2015) Characterization of 3'-Phosphate RNA Ligase Paralogs RtcB1, RtcB2, and RtcB3 from Myxococcus xanthus Highlights DNA and RNA 5'-Phosphate Capping Activity of RtcB3, *Journal Of Bacteriology*, **197**(22), 3616–24.

McCarthy R. R., Mooij M. J., Reen F. J., Lesouhaitier O. and O'Gara F. (2014) A new regulator of pathogenicity (bvlR) is required for full virulence and tight microcolony formation in Pseudomonas aeruginosa, *Microbiology*, **160**(Pt_7), 1488–1500.

Messenger A. J. and Barclay R. (1983) Bacteria, iron and pathogenicity, *Biochemical Education*, **11**(2), 54–63.

Miethke M. and Marahiel M. A. (2007) Siderophore-based iron acquisition and pathogen control., *Microbiology And Molecular Biology Reviews : MMBR*, **71**(3), 413–51.

Milla C. E., Chmiel J. F., Accurso F. J., VanDevanter D. R., Konstan M. W., Yarranton G., Geller D. E. and KB001 Study Group for the K. S. (2014) Anti-PcrV antibody in cystic fibrosis: a novel approach targeting Pseudomonas aeruginosa airway infection, *Pediatric Pulmonology*, **49**(7), 650–8.

Miller H. K., Kwuan L., Schwiesow L., Bernick D. L., Mettert E., Ramirez H. A., Ragle J. M., Chan P. P., Kiley P. J., Lowe T. M. and Auerbuch V. (2014) IscR is essential for yersinia pseudotuberculosis type III secretion and virulence, *PLoS Pathogens*, **10**(6), e1004194.

Miller J. K., Brantner J. S., Clemons C., Kreider K. L., Milsted A., Wilber P., Yun Y. H., Youngs W. J., Young G., Badawy H. T., Milsted A., Clemons C., Kreider K. L., Wilber P., Young G., Yun Y. H., Wagers P. O. and Youngs W. J. (2014) Mathematical modelling of Pseudomonas aeruginosa biofilm growth and treatment in the cystic fibrosis lung., *Mathematical Medicine And Biology : A Journal Of The IMA*, **31**(2), 179–204.

Minandri F., Imperi F., Frangipani E., Bonchi C., Visaggio D., Facchini M., Pasquali P., Bragonzi A. and Visca P. (2016) Role of Iron Uptake Systems in Pseudomonas aeruginosa Virulence and Airway Infection, *Infection And Immunity*. Edited by S. M. Payne, **84**(8), 2324–2335.

Miura C., Komatsu K., Maejima K., Nijo T., Kitazawa Y., Tomomitsu T., Yusa A., Himeno M., Oshima K. and Namba S. (2015) Functional characterization of the principal sigma factor RpoD of phytoplasmas via an in vitro transcription assay, *Scientific Reports*, **5**(1), 11893.

Mogre A., Sengupta T., Veetil R. T., Ravi P. and Seshasayee A. S. N. (2014) Genomic analysis reveals distinct concentration-dependent evolutionary trajectories for antibiotic resistance in Escherichia coli, *DNA Research : An International Journal for Rapid Publication of Reports on Genes and Genomes*, **21**(6), 711–26.

Morales G., Wiehlmann L., Gudowius P., van Delden C., Tümmler B., Martínez J. L. and Rojo F. (2004) Structure of Pseudomonas aeruginosa populations analyzed by single nucleotide polymorphism and pulsed-field gel electrophoresis genotyping, *Journal of Bacteriology*, **186**(13), 4228–37.

Morita M., Kanemori M., Yanagi H. and Yura T. (1999) Heat-Induced Synthesis of 32 in Escherichia coli: Structural and Functional Dissection of rpoH mRNA Secondary Structure, *Journal of Bacteriology*, **181**(2), 401–410.

Morita Y., Gilmour C., Metcalf D. and Poole K. (2009) Translational control of the antibiotic inducibility of the PA5471 gene required for mexXY multidrug efflux gene expression in Pseudomonas aeruginosa, *Journal of Bacteriology*, **191**(15), 4966–75.

Morita Y., Tomida J. and Kawamura Y. (2012) MexXY multidrug efflux system of Pseudomonas aeruginosa, *Frontiers in Microbiology*, **3**, 408.

Moscoso J. A., Jaeger T., Valentini M., Hui K., Jenal U. and Filloux A. (2014) The Diguanylate Cyclase SadC Is a Central Player in Gac/Rsm-Mediated Biofilm Formation in Pseudomonas aeruginosa, *Journal of Bacteriology*, **196**(23), 4081–4088.

Moscoso J. A., Mikkelsen H., Heeb S., Williams P. and Filloux A. (2011) The Pseudomonas aeruginosa sensor RetS switches Type III and Type VI secretion via c-di-GMP signalling, *Environmental Microbiology*, **13**(12), 3128–3138.

Mougous J. D., Cuff M. E., Raunser S., Shen A., Zhou M., Gifford C. A., Goodman A. L., Joachimiak G., Ordoñez C. L., Lory S., Walz T., Joachimiak A. and Mekalanos J. J. (2006) A virulence locus of Pseudomonas aeruginosa encodes a protein secretion apparatus, *Science*, **312**(5779), 1526–30.

Mowat E., Paterson S., Fothergill J. L., Wright E. A., Ledson M. J., Walshaw M. J., Brockhurst M. A. and Winstanley C. (2011) *Pseudomonas aeruginosa* Population Diversity and Turnover in Cystic Fibrosis Chronic Infections, *American Journal of Respiratory and Critical Care Medicine*, **183**(12), 1674–1679.

Mulcahy H. and Lewenza S. (2011) Magnesium Limitation Is an Environmental Trigger of the Pseudomonas aeruginosa Biofilm Lifestyle, *PLoS ONE*, **6**(8), e23307.

Mulcahy L. R., Isabella V. M. and Lewis K. (2014) Pseudomonas aeruginosa biofilms in disease, *Microbial Ecology*, **68**(1), 1–12.

Musken M., Di Fiore S., Dotsch A., Fischer R. and Haussler S. (2010) Genetic determinants of Pseudomonas aeruginosa biofilm establishment, *Microbiology*, **156**(2), 431–441.

Nguyen A. T., O'Neill M. J., Watts A. M., Robson C. L., Lamont I. L., Wilks A. and Oglesby-Sherrouse A. G. (2014) Adaptation of iron homeostasis pathways by a Pseudomonas aeruginosa pyoverdine mutant in the cystic fibrosis lung, *Journal of Bacteriology*, **196**(12), 2265–76.

Nomura M. (1999) Regulation of ribosome biosynthesis in Escherichia coli and Saccharomyces cerevisiae: diversity and common principles., *Journal Of Bacteriology*, **181**(22), 6857–64. Available at: http://www.ncbi.nlm.nih.gov/pubmed/10559149 (Accessed: 1 March 2018).

Nomura M., Gourse R. and Baughman G. (1984) Regulation of the synthesis of ribosomes and ribosomal components, *Annual Review of* Microbiology, **53**, 75–117.

Norström T., Lannergård J. and Hughes D. (2007) Genetic and phenotypic identification of fusidic acid-resistant mutants with the small-colony-variant phenotype in Staphylococcus aureus., *Antimicrobial Agents And Chemotherapy*, **51**(12), 4438–46.

Nouwens A. S., Beatson S. A., Whitchurch C. B., Walsh B. J., Schweizer H. P., Mattick J. S. and Cordwell S. J. (2003) Proteome analysis of extracellular proteins regulated by the las and rhl quorum sensing systems in Pseudomonas aeruginosa PAO1, *Microbiology*, **149**(5), 1311–1322.

Nyfeler B., Hoepfner D., Palestrant D., Kirby C. A., Whitehead L., Yu R., Deng G., Cauglan R., Woods A., Jones A., Barnes W., Walker J., Gaulis S., Hauy E., Brachmann S., Krastel P., Studer C., Riedl R., Estoppey D., Aust T., Movva N. R., Wang Z., Salcius M., Michaud G., McAllistr G., Murphy L., Tallarico J., Wilson C. J. and Dean C. R., (2012) Identification of elongation factor G as the conserved cellular target of argyrin B., *PloS One*, **7**(9), e42657.

O'Toole G. A. and Kolter R. (1998) Initiation of biofilm formation in Pseudomonas fluorescens WCS365 proceeds via multiple, convergent signalling pathways: a genetic analysis, *Molecular Microbiology*, **28**(3), 449–61.

Ochsner U. A. and Reiser J. (1995) Autoinducer-mediated regulation of rhamnolipid biosurfactant synthesis in Pseudomonas aeruginosa., *Proceedings of the National Academy of Sciences of The United States of America*, **92**(14), 6424–8.

Ochsner U. A., Wilderman P. J., Vasil A. I. and Vasil M. L. (2002) GeneChip® expression analysis of the iron starvation response in Pseudomonas aeruginosa: identification of novel pyoverdine biosynthesis genes, *Molecular Microbiology*, **45**(5), 1277–1287.

Owen E. and Bilton D. (2013) *Annual Data Report 2012: Summary*, UK Cystic Fibrosis.

Ozer E. A., Allen J. P. and Hauser A. R. (2014) Characterization of the core and accessory genomes of Pseudomonas aeruginosa using bioinformatic tools Spine and AGEnt, *BMC Genomics*, **15**(1), 737.

Palmer S. O., Rangel E. Y., Hu Y., Tran A. T. and Bullard J. M. (2013) Two Homologous EF-G Proteins from Pseudomonas aeruginosa Exhibit Distinct Functions, *PLoS ONE*, **8**(11), e80252.

Park A., Murphy K., Krieger J., Brewer D., Taylor P., Habash M. and Cezar M. (2014) A temporal examination of the planktonic and biofilm proteome of whole cell *Pseudomonas aeruginosa* PAO1 using quantitative mass spectrometry, *Molecular and Cellular Proteomics*, **13**, 1095-1105.

Paul B. J., Barker M. M., Ross W., Schneider D. A., Webb C., Foster J. W. and Gourse R. L. (2004) DksA: a critical component of the transcription initiation machinery that potentiates the regulation of rRNA promoters by ppGpp and the initiating NTP, *Cell*, **118**(3), 311–22.

Paulen A., Hoegy F., Roche B., Schalk I. J. and Mislin G. L. A. (2017) Synthesis of conjugates between oxazolidinone antibiotics and a pyochelin analogue, *Bioorganic & Medicinal Chemistry Letters*, **27**(21), 4867–4870.

Pereira S. G., Rosa A. C., Ferreira A. S., Moreira L. M., Proença D. N., Morais P. V. and Cardoso O. (2014) Virulence factors and infection ability of *Pseudomonas aeruginosa* isolates from a hydropathic facility and respiratory infections, *Journal of Applied Microbiology*, **116**(5), 1359–1368.

Pires D. E. V., Ascher D. B. and Blundell T. L. (2014) mCSM: predicting the effects of mutations in proteins using graph-based signatures, *Bioinformatics*, **30**(3), 335–342.

van Der Ploeg J. R., Iwanicka-Nowicka R., Bykowski T., Hryniewicz M. M. and Leisinger T. (1999) The Escherichia coli ssuEADCB gene cluster is required for the utilization of sulfur from aliphatic sulfonates and is regulated by the transcriptional activator Cbl., *The Journal Of Biological Chemistry*, **274**(41), 29358–65.

van der Ploeg J. R., Iwanicka-Nowicka R., Kertesz M. A., Leisinger T. and Hryniewicz M. M. (1997) Involvement of CysB and Cbl regulatory proteins in expression of the tauABCD operon and other sulfate starvation-inducible genes in Escherichia coli., *Journal of Bacteriology*, **179**(24), 7671–8.

Poole K. (2005) Aminoglycoside resistance in Pseudomonas aeruginosa., *Antimicrobial Agents and Chemotherapy*, **49**(2), 479–87.

Potvin E., Sanschagrin F. and Levesque R. C. (2008) Sigma factors in *Pseudomonas aeruginosa*, *FEMS Microbiology Reviews*, **32**(1), 38–55.

Price-Whelan A., Dietrich L. E. P. and Newman D. K. (2007) Pyocyanin alters redox homeostasis and carbon flux through central metabolic pathways in Pseudomonas aeruginosa PA14, *Journal of Bacteriology*, **189**(17), 6372–81.

Prickett M. H., Hauser A. R., McColley S. A., Cullina J., Potter E., Powers C. and Jain M. (2017) Aminoglycoside resistance of Pseudomonas aeruginosa in cystic fibrosis results from convergent evolution in the mexZ gene, *Thorax*, **72**(1), 40–47.

Pukatzki S., Ma A. T., Sturtevant D., Krastins B., Sarracino D., Nelson W. C., Heidelberg J. F. and Mekalanos J. J. (2006) Identification of a conserved bacterial protein secretion system in Vibrio cholerae using the Dictyostelium host model system, *Proceedings of the National Academy of Sciences of the United States Of America*, **103**(5), 1528–33.

Pulcrano G., Iula D. V., Raia V., Rossano F. and Catania M. R. (2012) Different mutations in mucA gene of Pseudomonas aeruginosa mucoid strains in cystic fibrosis patients and their effect on algU gene expression, *New Microbiologica*, **35**, 295–305.

Quecine M. C., Kidarsa T. A., Goebel N. C., Shaffer B. T., Henkels M. D., Zabriskie T. M. and Loper J. E. (2015) An Interspecies Signaling System Mediated by Fusaric Acid Has Parallel Effects on Antifungal Metabolite Production by Pseudomonas protegens Strain Pf-5 and Antibiosis of Fusarium spp., *Applied And Environmental Microbiology*, **82**(5), 1372–82.

Raina M. and Ibba M. (2014) tRNAs as regulators of biological processes, *Frontiers In Genetics*, **5**, 171.

Raineri E., Porcella L., Acquarolo A., Crema L., Albertario F. and Candiani A. (2014) Ventilator-Associated Pneumonia Caused by Pseudomonas aeruginosa in Intensive Care Unit: Epidemiology and Risk Factors, *Journal of Medical Microbiology & Diagnosis*, **3**(3).

Ratjen F. and Döring G. (2003) Cystic fibrosis, *The Lancet*, **361**(9358), 681–689.

Reen F. J., Mooij M. J., Holcombe L. J., McSweeney C. M., McGlacken G. P., Morrissey J. P. and O'Gara F. (2011) The Pseudomonas quinolone signal (PQS), and its precursor HHQ, modulate interspecies and interkingdom behaviour, *FEMS Microbiology Ecology*, **77**(2), 413–428.

Reid T. M. S. and Porter I. A. (1981) An outbreak of otitis externa in competitive swimmers due to Pseudomonas aeruginosa, *The Journal of Hygeine*, **86**(3), 357-62.

Ritchie M. E., Phipson B., Wu D., Hu Y., Law C. W., Shi W. and Smyth G. K. (2015) limma powers differential expression analyses for RNA-sequencing and microarray studies, *Nucleic Acids Research*, **43**(7), e47–e47.

Roche B., Aussel L., Ezraty B., Mandin P., Py B. and Barras F. (2013) Iron/sulfur proteins biogenesis in prokaryotes: Formation, regulation and diversity, *Biochimica Et Biophysica Acta (BBA) - Bioenergetics*, **1827**(3), 455–469.

Rodnina M. V (2016) The ribosome in action: Tuning of translational efficiency and protein folding., *Protein Science : A Publication Of The Protein Society*, **25**(8), 1390–406.

Römling U., Galperin M. Y. and Gomelsky M. (2013) Cyclic di-GMP: the first 25 years of a universal bacterial second messenger., *Microbiology And Molecular Biology Reviews : MMBR*, **77**(1), 1–52.

Romsang A., Dubbs J., Mongkolsuk S. and Bruijn F. J. de (Frans J. de) (2016) *Stress and environmental regulation of gene expression and adaptation in bacteria*. John Wiley & Sons.

Rosenberg J., Müller P., Lentes S., Thiele M. J., Zeigler D. R., Tödter D., Paulus H., Brantl S., Stülke J. and Commichau F. M. (2016) ThrR, a DNA-binding transcription factor involved in controlling threonine biosynthesis in *Bacillus subtilis*, *Molecular Microbiology*, **101**(5), 879–893.

Ruiz J. A., Bernar E. M. and Jung K. (2015) Production of siderophores increases resistance to fusaric acid in Pseudomonas protegens Pf-5., *PloS One*, **10**(1), e0117040.

Sakhtah H., Koyama L., Zhang Y., Morales D. K., Fields B. L., Price-Whelan A., Hogan D. A., Shepard K. and Dietrich L. E. P. (2016) The Pseudomonas aeruginosa efflux pump MexGHI-OpmD transports a natural phenazine that controls gene expression and biofilm development., *Proceedings of the National Academy of Sciences of the United States of America*, **113**(25), E3538-47.

Sakuragi Y. and Kolter R. (2007) Quorum-Sensing Regulation of the Biofilm Matrix Genes (pel) of Pseudomonas aeruginosa, *Journal of Bacteriology*, **189**(14), 5383–5386.

Salsi E., Farah E., Dann J. and Ermolenko D. N. (2014) Following movement of domain IV of elongation factor G during ribosomal translocation, *Proceedings of the National Academy of Sciences*, **111**(42), 15060–15065.

Salsi E., Farah E., Netter Z., Dann J. and Ermolenko D. N. (2015) Movement of elongation factor G between compact and extended conformations, *Journal of Molecular Biology*, **427**(2), 454–67.

Sampedro I., Parales R. E., Krell T. and Hill J. E. (2014) *Pseudomonas* chemotaxis, *FEMS Microbiology Reviews*, **39**(1), 17-46

Schmidt J., Müsken M., Becker T., Magnowska Z., Bertinetti D., Möller S., Zimmermann B., Herberg F. W., Jänsch L. and Häussler S. (2011) The Pseudomonas aeruginosa chemotaxis methyltransferase CheR1 impacts on bacterial surface sampling, *PloS One*, **6**(3), e18184.

Schobert M. and Görisch H. (1999) Cytochrome c550 is an essential component of the quinoprotein ethanol oxidation system in Pseudornonas aeruginosa : cloning and sequencing of the genes encoding cytochrome c550 and an adjacent acetaldehyde dehydrogenase, *Micrcobiology*, **145**, 471–481.

Scott N. E., Hare N. J., White M. Y., Manos J. and Cordwell S. J. (2013) Secretome of Transmissible *Pseudomonas aeruginosa* AES-1R Grown in a Cystic Fibrosis Lung-Like Environment, *Journal of Proteome Research*, **12**(12), 5357–5369.

Sekiya H., Mima T., Morita Y., Kuroda T., Mizushima T. and Tsuchiya T. (2003) Functional cloning and characterization of a multidrug efflux pump, mexHI-opmD, from a Pseudomonas aeruginosa mutant., *Antimicrobial Agents And Chemotherapy*, **47**(9), 2990–2.

Serventi F., Youard Z. A., Murset V., Huwiler S., Bühler D., Richter M., Luchsinger R., Fischer H.-M., Brogioli R., Niederer M. and Hennecke H. (2012) Copper Starvation-inducible Protein for Cytochrome Oxidase Biogenesis in *Bradyrhizobium japonicum*, *Journal of Biological Chemistry*, **287**(46), 38812–38823.

Seyedmohammad S., Fuentealba N. A., Marriott R. A. J., Goetze T. A., Edwardson J. M., Barrera N. P. and Venter H. (2016) Structural model of FeoB, the iron transporter from Pseudomonas aeruginosa, predicts a cysteine lined, GTP-gated pore, *Bioscience Reports*, **36**(2).

Shen D. K., Filopon D., Kuhn L., Polack B. and Toussaint B. (2006) PsrA is a positive transcriptional regulator of the type III secretion system in Pseudomonas aeruginosa, *Infection and Immunity*, **74**(2), 1121–9.

Sheplock R., Recinos D., Mackow N., Dietrich L. and Chander M. (2013) Species-specific residues calibrate SoxR sensitivity to redox-active molecules, *Molecular Microbiology*, **87**(2), 368–381.

Sherlock O., Vejborg R. M. and Klemm P. (2005) The TibA Adhesin/Invasin from Enterotoxigenic Escherichia coli Is Self Recognizing and Induces Bacterial Aggregation and Biofilm Formation, *Infection And Immunity*, **73**(4), 1954–1963.

Shirley M. and Lamont I. L. (2009) Role of TonB1 in pyoverdine-mediated signaling in Pseudomonas aeruginosa., *Journal of Bacteriology*, **191**(18), 5634–40.

Silva Filho L. V. R. F. da, Ferreira F. de A., Reis F. J. C., Britto M. C. A. de, Levy C. E., Clark O., Ribeiro J. D. and Ribeiro J. D. (2013) Pseudomonas aeruginosa infection in patients with cystic fibrosis: scientific evidence regarding clinical impact, diagnosis, and treatment., *Jornal Brasileiro De Pneumologia : Publicacao Oficial Da Sociedade Brasileira De Pneumologia E Tisilogia*, **39**(4), 495–512.

Smyth A. and Elborn J. S. (2008) Exacerbations in cystic fibrosis: 3-Management, *Thorax*, **63**(2), 180–4.

Soto S. M. (2013) Role of efflux pumps in the antibiotic resistance of bacteria embedded in a biofilm, *Virulence*, **4**(3), 223–9.

Southey-Pillig C. J., Davies D. G. and Sauer K. (2005) Characterization of temporal protein production in Pseudomonas aeruginosa biofilms, *Journal of Bacteriology*, **187**(23), 8114–26.

Stapleton F. and Carnt N. (2012) Contact lens-related microbial keratitis: how have epidemiology and genetics helped us with pathogenesis and prophylaxis, *Eye*, **26**(2), 185–93.

Stover C. K., Pham X. Q., Erwin A. L., Mizoguchi S. D., Warrener P., Hickey M. J., Brinkman F., Hufnagle W. O., Kowaliik D. J., Lagrou M., Garber R. L., Goltry L., Tolentino E., Westbrock-Wadman S., Yuan Y., Brody L. L., Coulter S. N., Folger K. R., Kas A., Larbig K., Lim R., Smith K., Spencer D., Wong G. K., Wu Z., Paulsen I. T., Reizer J., Saier M. H., Hancock R. E., Lort S. and Olson M. V. (2000) Complete genome sequence of Pseudomonas aeruginosa PAO1, an opportunistic pathogen, *Nature*, **406**(6799), 959–964.

Sun S., Zhou L., Jin K., Jiang H. and He Y.-W. (2016) Quorum sensing systems differentially regulate the production of phenazine-1-carboxylic acid in the rhizobacterium Pseudomonas aeruginosa PA1201, *Scientific Reports*, **6**, 30352.

Suresh M., Nithya N., Jayasree P. R., Vimal K. P. and Manish Kumar P. R. (2018) Mutational analyses of regulatory genes, mexR, nalC, nalD and mexZ of mexAB-oprM and mexXY operons, in efflux pump hyperexpressing multidrug-resistant clinical isolates of Pseudomonas aeruginosa, *World Journal of Microbiology and Biotechnology*, **34**(6), 83.

Swift S., Karlyshev A. V, Fish L., Durant E. L., Winson M. K., Chhabra S. R., Williams P., Macintyre S. and Stewart G. S. (1997) Quorum sensing in Aeromonas hydrophila and Aeromonas salmonicida: identification of the LuxRI homologs AhyRI and AsaRI and their cognate N-acylhomoserine lactone signal molecules, *Journal of Bacteriology*, **179**(17), 5271–81.

Takase H., Nitanai H., Hoshino K. and Otani T. (2000) Requirement of the Pseudomonas aeruginosa tonB gene for high-affinity iron acquisition and infection, *Infection And Immunity*, **68**(8), 4498–504.

Tarleton J. C. and Ely B. (1991) Isolation and characterization of ilvA, ilvBN, and ilvD mutants of Caulobacter crescentus, *Journal of Bacteriology*, **173**(3), 1259–67.

Taylor P. K., Yeung A. T. Y. and Hancock R. E. W. (2014) Antibiotic resistance in Pseudomonas aeruginosa biofilms: Towards the development of novel anti-biofilm therapies, *Journal of Biotechnology*, **191**, 121–130.

Terzi H. A., Kulah C. and Ciftci İ. H. (2014) The effects of active efflux pumps on antibiotic resistance in Pseudomonas aeruginosa, *World Journal Of Microbiology And Biotechnology*, **30**(10), 2681–2687.

Thompson M. G., Corey B. W., Si Y., Craft D. W. and Zurawski D. V (2012) Antibacterial activities of iron chelators against common nosocomial pathogens., *Antimicrobial Agents And Chemotherapy*, **56**(10), 5419–21.

Tralau T., Vuilleumier S., Thibault C., Campbell B. J., Hart C. A. and Kertesz M. A. (2007) Transcriptomic analysis of the sulfate starvation response of Pseudomonas aeruginosa., *Journal Of Bacteriology*, **189**(19), 6743–50.

Trampari E., Stevenson C. E. M., Little R. H., Wilhelm T., Lawson D. M. and Malone J. G. (2015) Bacterial Rotary Export ATPases Are Allosterically Regulated by the Nucleotide Second Messenger Cyclic-di-GMP, *Journal of Biological Chemistry*, **290**(40), 24470–24483.

Trinh N. T. N., Bilodeau C., Maillé É., Ruffin M., Quintal M.-C., Desrosiers M.-Y., Rousseau S. and Brochiero E. (2015) Deleterious impact of Pseudomonas aeruginosa on cystic fibrosis transmembrane conductance regulator function and rescue in airway epithelial cells, *European Respiratory Journal*, **45**(6).

Tsai A., Uemura S., Johansson M., Puglisi E. V., Marshall R. A., Aitken C. E., Korlach J., Ehrenberg M. and Puglisi J. D. (2013) The impact of aminoglycosides on the dynamics of translation elongation., *Cell Reports*, **3**(2), 497–508.

Tung T. T., Jakobsen T. H., Dao T. T., Fuglsang A. T., Givskov M., Christensen S. B. and Nielsen J. (2017) Fusaric acid and analogues as Gram-negative bacterial quorum sensing inhibitors, *European Journal of Medicinal Chemistry*, **126**, 1011–1020.

Turner K. H., Wessel A. K., Palmer G. C., Murray J. L. and Whiteley M. (2015) Essential genome of Pseudomonas aeruginosa in cystic fibrosis sputum, *Proceedings of the National Academy of Sciences of the United States of America*, **112**(13), 4110–5.

Vakulskas C. A., Pannuri A., Cortés-Selva D., Zere T. R., Ahmer B. M., Babitzke P. and Romeo T. (2014) Global effects of the DEAD-box RNA helicase DeaD (CsdA) on gene expression over a broad range of temperatures, *Molecular Microbiology*, **92**(5), 945–958.

Valentini M., Laventie B.-J., Moscoso J., Jenal U. and Filloux A. (2016) The Diguanylate Cyclase HsbD Intersects with the HptB Regulatory Cascade to Control Pseudomonas aeruginosa Biofilm and Motility, *PLoS Genetics*, **12**(10), e1006354.

Valot B., Guyeux C., Rolland J. Y., Mazouzi K., Bertrand X. and Hocquet D. (2015) What It Takes to Be a Pseudomonas aeruginosa? The Core Genome of the Opportunistic Pathogen Updated., *PLOS ONE*, **10**(5), e0126468.

Vetter I. R. (2014) The Structure of the G Domain of the Ras Superfamily, in *Ras Superfamily Small G Proteins: Biology And Mechanisms 1*, 25–50.

Vogt S. L., Green C., Stevens K. M., Day B., Erickson D. L., Woods D. E. and Storey D. G. (2011) The stringent response is essential for Pseudomonas aeruginosa virulence in the rat lung agar bead and Drosophila melanogaster feeding models of infection, *Infection And Immunity*, **79**(10), 4094–104.

De Vos D., De Chial M., Cochez C., Jansen S., Tümmler B., Meyer J. M. and Cornelis P. (2001) Study of pyoverdine type and production by Pseudomonas aeruginosa isolated from cystic fibrosis patients: prevalence of type II pyoverdine isolates and accumulation of pyoverdine-negative mutations, *Archives Of Microbiology*, **175**(5), 384–8.

Wang S., Liu X., Liu H., Zhang L., Guo Y., Yu S., Wozniak D. J. and Ma L. Z. (2015) The exopolysaccharide Psl-eDNA interaction enables the formation of a biofilm skeleton in *P seudomonas aeruginosa*, *Environmental Microbiology Reports*, **7**(2), 330–340.

Wang Y., Ha U., Zeng L. and Jin S. (2003) Regulation of membrane permeability by a two-component regulatory system in Pseudomonas aeruginosa., *Antimicrobial Agents And Chemotherapy*, **47**(1), 95–101.

Wei Q. and Ma L. (2013) Biofilm Matrix and Its Regulation in Pseudomonas aeruginosa, *International Journal of Molecular Sciences*, **14**(10), 20983–21005.

West S. E. H., Schweizer H. P., Dall C., Sample A. K. and Runyen-Janecky L. J. (1994) Construction of improved Escherichia-Pseudomonas shuttle vectors derived from pUC18/19 and sequence of the region required for their replication in Pseudomonas aeruginosa, *Gene*, **148**(1), 81–86.

Wheeler D. S. and Wong H. R. (2007) Heat shock response and acute lung injury., *Free Radical Biology & Medicine*, **42**(1), 1–14.

Wilderman P. J., Sowa N. A., FitzGerald D. J., FitzGerald P. C., Gottesman S., Ochsner U. A. and Vasil M. L. (2004) Identification of tandem duplicate regulatory small RNAs in Pseudomonas aeruginosa involved in iron homeostasis., *Proceedings Of The National Academy Of Sciences Of The United States Of America*, **101**(26), 9792–7.

Wilderman P. J., Vasil A. I., Johnson Z., Wilson M. J., Cunliffe H. E., Lamont I. L. and Vasil M. L. (2001) Characterization of an endoprotease (PrpL) encoded by a PvdS-regulated gene in Pseudomonas aeruginosa., *Infection And Immunity*, **69**(9), 5385–94.

Wilson D. N. (2014) Ribosomes are the protein-synthesizing factories of the cell. These large macromolecular machines provide the platform on which amino acids are polymerized in a template-dependent fashion to form polypeptide chains, *Nature Publishing Group*, **12**.

Winson M. K., Swift S., Fish L., Throup J. P., Jørgensen F., Chhabra S. R., Bycroft B. W., Williams P. and Stewart G. S. (1998) Construction and analysis of luxCDABE-based plasmid sensors for investigating N-acyl homoserine lactone-mediated quorum sensing., *FEMS Microbiology Letters*, **163**(2), 185–92.

Winsor G. L., Griffiths E. J., Lo R., Dhillon B. K., Shay J. A. and Brinkman F. S. L. (2016) Enhanced annotations and features for comparing thousands of *Pseudomonas* genomes in the Pseudomonas genome database, *Nucleic Acids Research*, **44**(1), 646–653.

Wolfgang M. C., Kulasekara B. R., Liang X., Boyd D., Wu K., Yang Q., Miyada C. G. and Lory S. (2003) Conservation of genome content and virulence determinants among clinical and environmental isolates of Pseudomonas aeruginosa., *Proceedings of the National Academy of Sciences of the United States Of America*, **100**(14), 8484–9.

Yahr T. L., Vallis A. J., Hancock M. K., Barbieri J. T. and Frank D. W. (1998) ExoY, an adenylate cyclase secreted by the Pseudomonas aeruginosa type III system., *Proceedings Of The National Academy Of Sciences Of The United States Of America*, **95**(23), 13899–904.

Yahr T. L. and Wolfgang M. C. (2006) Transcriptional regulation of the Pseudomonas aeruginosa type III secretion system, *Molecular Microbiology*, **62**(3), 631–640.

Yang H., Shan Z., Kim J., Wu W., Lian W., Zeng L., Xing L. and Jin S. (2007) Regulatory role of PopN and its interacting partners in type III secretion of Pseudomonas aeruginosa, *Journal of Bacteriology*, **189**(7), 2599–609.

Yang L., Barken K. B., Skindersoe M. E., Christensen A. B., Givskov M. and Tolker-Nielsen T. (2007) Effects of iron on DNA release and biofilm development by Pseudomonas aeruginosa, *Microbiology*, **153**(5), 1318–1328.

Yanisch-Perron C., Vieira J. and Messing J. (1985) Improved M13 phage cloning vectors and host strains: nucleotide sequences of the M13mp18 and pUC19 vectors, *Gene*, **33**(1), 103–19.

Ye L., Cornelis P., Guillemyn K., Ballet S. and Hammerich O. (2014) Structure revision of N-mercapto-4-formylcarbostyril produced by Pseudomonas fluorescens G308 to 2-(2-hydroxyphenyl)thiazole-4-carbaldehyde [aeruginaldehyde], *Natural Product Communications*, **9**(6), 789–94.

Yeom S., Yeom J. and Park W. (2010) Molecular characterization of FinR, a novel redox-sensing transcriptional regulator in Pseudomonas putida KT2440, *Microbiology*, **156**(5), 1487–1496.

Youard Z. A., Wenner N. and Reimmann C. (2011) Iron acquisition with the natural siderophore enantiomers pyochelin and enantio-pyochelin in Pseudomonas species, *BioMetals*, **24**(3), 513–522.

Zhabokritsky A., Kutky M., Burns L. A., Karran R. A. and Hudak K. A. (2011) RNA toxins: mediators of stress adaptation and pathogen defense, *Wiley Interdisciplinary Reviews: RNA*, **2**(6), 890–903.

Zhang L., Hinz A. J., Nadeau J.-P. and Mah T.-F. (2011) Pseudomonas aeruginosa tssC1 links type VI secretion and biofilm-specific antibiotic resistance, *Journal of Bacteriology*, **193**(19), 5510–3.

Zhao Q. and Poole K. (2000) A second tonB gene in Pseudomonas aeruginosa is linked to the exbB and exbD genes, *FEMS Microbiology Letters*, **184**(1), 127–132.

Zhou J., Lancaster L., Donohue J. P. and Noller H. F. (2014) How the ribosome hands the A-site tRNA to the P site during EF-G-catalyzed translocation, *Science*, **345**(6201), 1188–91.